

Bacterial multi-omics profiling reveals
novel routes to immune evasion
and disease outcome:
Towards targeted therapeutic strategies

Bharathi Sundaresh

A dissertation
submitted to the Faculty of
the department of Biology
in partial fulfillment
of the requirements for the degree of
Doctor of Philosophy

Boston College
Morrissey College of Arts and Sciences
Graduate School

June 2023

Bacterial multi-omics profiling reveals novel routes to
immune evasion and disease outcome:
Towards targeted therapeutic strategies

ABSTRACT

Although vaccines and antibiotics have been historically successful in combating bacterial infections, limited vaccine coverage and the rise of antibiotic resistance emphasize the need to develop alternative, broadly effective, and/or targeted treatment strategies to reduce the health burden of bacterial infections. Rather than relying on therapeutics solely targeting the bacterial pathogen, such as standard antibiotics, therapies that simultaneously focus on host responses are emerging. In this thesis, we propose 'host-informed therapies' (HITs) in two categories: those that aid patients with fully functional immune systems and those that aid patients with perturbed immune processes, as promising alternative or adjunctive treatment strategies for bacterial infections. The host-pathogen interaction during infection is a highly dynamic process between diverse bacterial pathogens and hosts with varying degrees of susceptibility. Systems biology approaches have provided an understanding of host-pathogen parameters globally through the detection of putative biomarkers for diagnosis and identification of critical interactions to discover novel drug targets. However, there remains a gap in understanding bacterial pathogenesis in the context of designing novel host-informed therapies. Here, we use *Streptococcus pneumoniae*, the gram-positive pathogen responsible for the majority of bacterial respiratory tract infections worldwide, as a case study to: (1) Generate a genome-wide map of bacterial immune (complement) evasion targets to design novel host-informed therapies, (2) generate a dual host/pathogen transcriptome map to identify signatures of infection outcome, and (3) validate signatures of bacterial antibiotic tolerance in a mouse lung infection model. Overall, this work exemplifies how systems biology methods can elucidate the intricacies of bacterial pathogenesis but, more importantly, aid in the target identification, validation, and design of antibacterial host-informed therapies.

Thesis Advisor

Tim van Opijnen, PhD, Broad Institute of MIT and Harvard

Thesis Guidance Committee

Michelle Meyer, PhD, Professor, Boston College

Federico Rosconi, PhD, Senior Research Associate, Boston College

John M. Leong, MD, PhD, Professor and Chair, Tufts University School of Medicine

Mara Shainheit, PhD, Associate Director, Clade Therapeutics

Vicki Losick, PhD, Assistant Professor, Boston College

Contents

Chapter 1: Introduction	1
1.1 Summary	2
1.2 The host reponse is integral to disease outcome.....	2
1.3 Challenges in <i>S. pneumoniae</i> treatment	5
1.4 HITs for otherwise healthy individuals	6
1.5 HITs for susceptible hosts with predisposing conditions.....	17
1.6 Overview of this thesis	28
1.7 Glossary.....	29
1.8 References.....	31
Chapter 2: Immune Evasion	41
2.1 Summary	42
2.2 Introduction.....	43
2.3 Results.....	46
2.4 Discussion	61
2.5 Materials and methods.....	64
2.6 Acknowledgements	70
2.7 References.....	71
2.8 Supplemental information.....	75
Chapter 3: Disease Outcome	83
3.1 Summary	84
3.2 Introduction.....	85
3.3 Results.....	88
3.4 Discussion	107
3.5 Materials and methods.....	108
3.6 Acknowledgements	111
3.7 References.....	112
3.8 Supplemental information.....	115

Chapter 4: Antibiotic Tolerance	120
4.1 Summary	121
4.2 Introduction.....	122
4.3 Results.....	125
4.4 Discussion	147
4.5 Materials and methods.....	150
4.6 References.....	160
 Chapter 5: Discussion.....	 167
5.1 Contributions of this work to HIT development.....	168
5.2 Clinical considerations and limitations	170
5.3 Outstanding challenges.....	172
5.5 References.....	173
 Appendix A: Publications, Science Communication, and Awards.....	 174
A.1 Publications	175
A.2 Science communication.....	176
A.3 Awards	178

List of figures

Chapter 1: Introduction

1.1 Overview of host-informed therapeutic strategies to combat pneumococcal pneumonia.....	4
1.2 Host lung damage during pneumococcal pneumonia is a function of the quantitative and qualitative aspects of the host response to <i>S. pneumoniae</i>	7
1.3 Enhancing bacterial clearance by innate immune cells.	14
1.4 Targeting defects in immune defense in susceptible patient populations.	22
1.5 Graphical overview of this thesis.	28

Chapter 2: Immune Evasion

2.1 Bacterial genomic profiling reveals novel routes to complement evasion and targeted therapeutic strategies.....	45
2.2 Overview of a genome-wide screen (Hii-TnSeq) for the identification of bacterial genetic determinants of C3 deposition evasion	49
2.3 Hii-TnSeq reveals both established and novel bacterial C3 deposition evasion factors	50
2.4 Single gene knockouts can individually lead to hyper C3 deposition on the bacterial cell surface, independent of the polysaccharide capsule	53
2.5 <i>S. pneumoniae</i> gene knockouts with a hyper C3 deposition phenotype have a bacterial virulence defect in vivo and an enhanced opsonophagocytic killing ex vivo	56
2.6 <i>S. pneumoniae</i> knockouts with a hyper C3 deposition phenotype are entirely virulent in C3-depleted animals.....	57
2.7 CppA and RrgB, the <i>S. pneumoniae</i> C3-degrading protease and pilus-1 backbone respectively, inhibit C3 deposition and can be targeted with specific therapeutic antibodies....	59
S2.1 Hii-TnSeq analysis and quality control.....	78
S2.2 TIGR4 wildtype and mutant growth data.....	79
S2.3 Representative C3 deposition flow data.....	80
S2.4 Representative capsule quantification flow data.....	81

S2.5 C3 serum titers in complement-depleted mice.....	82
S2.6 <i>S. pneumoniae</i> knockouts with a hyper C3 deposition phenotype are entirely virulent in C3-depleted animals.....	82
 Chapter 3: Disease Outcome	
3.1 Defining lethal and nonlethal infection outcomes	86
3.2 Infection outcomes of <i>S. pneumoniae</i> TIGR4 infection	89
3.3 Infection outcomes of <i>S. pneumoniae</i> PG13 infection	90
3.4 Dual RNA isolation from mouse bronchoalveolar lavage	92
3.5 Summary of dual RNA-Seq library preparation workflow	93
3.6 Summary of dual RNA-Seq data analysis workflow	93
3.7 Mapping of dual RNA-Seq reads	94
3.8 Summary of <i>S. pneumoniae</i> differential transcriptomic analysis.....	95
3.9 Transcriptomic response of <i>S. pneumoniae</i> PG13 under bacteremia and pneumonia infection conditions.....	96
3.10 Subset of significant <i>S. pneumoniae</i> metabolism DEGs	98
3.11 Subset of significant <i>S. pneumoniae</i> transport and cellular community DEGs.....	99
3.12 Summary of <i>M. musculus</i> differential transcriptomic analysis	101
3.13 Comparison of significant <i>M. musculus</i> DE up-regulated genes across infection conditions.....	101
3.14 Gene set enrichment analysis of up-regulated shared, lethal, intermediate, and cleared infection DEGs.....	104
3.15 Overlay of in vivo <i>M. musculus</i> RNA-Seq signatures and published biomarkers of pneumonia.....	105
3.16 GO enrichment network analysis of <i>M. musculus</i> significantly up-regulated DEGs	106
S3.1 <i>S. pneumoniae</i> PG13 infection survival analysis.....	115

S3.2 Pearson correlation threshold of 0.8 applied to all pair-wise comparisons of <i>S. pneumoniae</i> RNA-Seq replicates	116
S3.3 Pearson correlation threshold of 0.8 applied to all pairwise comparisons of <i>M. musculus</i> RNA-Seq replicates	116
S3.4 Mouse DEG enrichment analysis of the lethal infection outcome	117
S3.5 Mouse DEG enrichment analysis of the intermediate infection outcome	118
S3.6 Mouse DEG enrichment analysis of the cleared infection outcome.....	119

Chapter 4: Antibiotic Tolerance

4.1 A genome-wide atlas of negative and positive fitness effects, highlights a multitude of processes that can modulate antibiotic susceptibility	126
4.2 A co-fitness network identifies tight genetic clusters of known and unknown genes and processes	128
4.3 A multitude of options, pathways and processes can simultaneously lead to increased and decreased antibiotic susceptibility	131
4.4 CozEb an integral membrane protein increases antibiotic sensitivity and can be targeted with an antibody	134
4.5 Modulation of the ami transporter decreases sensitivity to many antibiotics.....	137
4.6 Modulation of purine metabolism affects alarmone and ATP synthesis and is linked to changes in ABX sensitivity.....	141
4.7 Decreased antibiotic sensitivity and tolerance can be achieved by modulation of a wide variety of processes	145
4.8 Stop codons are enriched in clinical samples in Tn-Seq predicted tolerome genes	146

Chapter 5: Discussion

5.1 Example HIT strategies proposed in this thesis	169
--	-----

List of tables

Chapter 1: Introduction

1.1 HITs that target excessive inflammation or enhance pathogen clearance during *S. pneumoniae* infection..... 8

1.1 HITs that target defects in host defense in patient populations susceptible to *S. pneumoniae* infection..... 17

Chapter 2: Immune Evasion

2.1 Key resources table 64

S2.1 *S. pneumoniae* strains and knockouts used in this study 75

S2.2 Significantly enriched gene features from Hii-TnSeq..... 76

S2.3 Primers used in this study..... 77

Chapter 3: Disease Outcome

3.1 Clinical score scale for mice infected with *S. pneumoniae* 91

List of abbreviations

AMR	Antimicrobial resistance
BAL	Bronchoalveolar lavage
bp	Base pair
C3	Complement component 3
C5a	Complement component 5a
CDS	Coding sequence
CFU	Colony forming units
CI	Competitive index
CVF	Cobra venom factor
CWSI	Cell wall synthesis inhibitor
DE	Differential expression
DEG	Differentially expressed gene
DSI	DNA synthesis inhibitor
dRNA-Seq	Dual RNA sequencing
Δ Expression	Change in gene expression level
G-CSF	Granulocyte-colony stimulating factor
GM-CSF	Granulocyte-macrophage colony stimulating factor
GO	Gene ontology
Hii-TnSeq	Host-immune-interaction transposon insertion sequencing
HIT	Host-informed therapy
HPI	Hours post-infection
IFA	Incomplete Freund's Adjuvant
IFN	Interferon
IL	Interleukin
IP	Interferon gamma-induced protein
IPD	Invasive pneumococcal disease
KC	Keratinocyte chemoattractant
L2FC	Log ₂ [fold change]
LIF	Leukemia inhibitory factor
MBL	Mannose binding lectin
MCP	Monocyte chemoattractant protein
M-CSF	Macrophage-colony stimulating factor
MDR	Multidrug resistance
MIC	Minimum inhibitory concentration
MIP	Macrophage inflammatory protein
MOA	Mechanism of action
mRNA	Messenger RNA
MT	Mutant strain
ng	Nanogram
NMOK	Neutrophil-mediated opsonophagocytic killing
nt	Nucleotide
OPK	Opsonophagocytic killing
P-adj	Adjusted p-value

PCR	Polymerase chain reaction
PG13	<i>Streptococcus pneumoniae</i> serotype 6C strain PG13
PMN	Polymorphonuclear leukocyte
PSI	Protein synthesis inhibitor
RefSeq	NCBI reference sequence database
RNA-Seq	RNA sequencing
RNS	Reactive nitrogen species
ROS	Reactive oxygen species
rRNA	Ribosomal RNA
RSI	RNA synthesis inhibitor
SCD	Sickle cell disease
scRNA-Seq	Single-cell RNA sequencing
SDMM	Semi-defined minimal medium
SPLiT-Seq	Split Pool Ligation-based Transcriptome sequencing
<i>Spn</i>	<i>Streptococcus pneumoniae</i>
THY	Todd-Hewitt broth with 2% yeast extract
TIGR4	<i>Streptococcus pneumoniae</i> serotype 4 strain TIGR4
TNF	Tumor necrosis factor
Tn-Seq	Transposon insertion sequencing
<i>W</i>	Gene fitness
$\Delta W/dW$	Change in gene fitness
WGS	Whole genome sequencing
WT	Wildtype strain

“Science is a way of thinking much more than it is a body of knowledge.”
- Carl Sagan

Acknowledgements

The past five years have been an adventure. But through it all, I've had amazing people who supported me throughout the PhD, and I can only hope to one day return their kindness.

I would first like to thank my advisor **Tim van Opijnen**, who taught me so much since my first day in the lab. I always left a brainstorming meeting recharged, motivated, and full of new ideas to try at the bench. Tim taught me that science is a creative process, is only possible with collaboration, and to always think big. As a result, I've become a confident, well-rounded scientist, which would have been impossible without Tim's mentorship.

I would also like to acknowledge my thesis guidance committee, **Michelle Meyer, John M. Leong, Mara Shainheit**, and **Vicki Losick**, for their scientific and advisory input throughout the past years.

My PhD would not have been the same without my lab mates. I want to thank **Federico Rosconi** for his mentorship (and friendship) throughout the PhD, especially this past year. Sometimes I think completing the PhD would have been impossible without **Suyen Espinoza**. I found a best friend in a work colleague, and I look forward to being friends with Suyen forever. Not only did **Juance Ortiz-Márquez** have insightful ideas at every lab meeting, but he also always made me laugh, even on the worst days. And I was lucky to briefly work with **Defne Surujon**, but it has been an even greater pleasure to continue to bond over our shared love of plants. I found some of my closest friends in this lab, and I also had the pleasure of working with additional members of the van Opijnen lab, past and present: **Jon Anthony, Karen Zhu, Emily Rudmann, Sophie Bodrog, Bimal Jana, Indu Warriar, Derek Thibault**, and others. Boston College also introduced me to some amazingly supportive friends and colleagues: notably, **İrem Özkan** - thank you for all the laughs and much-needed network of support during grad school.

Thank you to my parents, **Raman and Aparna Sundaresh**, who taught me the importance of hard work and to find the joy in learning. And thank you to my sister, **Tulasi**, whose friendship these past few months has been an enormous boost.

Finally, I would like to thank my fiancé, **Mark Donne**. He has been my rock and biggest cheerleader throughout this journey. He kept me grounded and always believed in me. Mark: you and **Neo** are my family, and I'm so lucky to marry you next year.

1

Introduction:

Host-informed therapies for the treatment of pneumococcal pneumonia

Sections 1.1-1.5 adapted from:

Bharathi Sundaresh*, Shuying (Linda) Xu*, Brian Noonan, Michael K. Mansour,
John M. Leong, and Tim van Opijnen

*Equal co-first author contribution

Cell Trends in Molecular Medicine 27 (10): 971-989
DOI: [10.1016/j.molmed.2021.07.008](https://doi.org/10.1016/j.molmed.2021.07.008)

Author's contributions: B.S. led the writing and research process and made all figures. B.S. and S.X. equally contributed to the discussion, research, and writing of the content. All authors contributed to the writing and reviewed/edited the manuscript before submission.

1.1 Summary

Over the last two decades, traditional antimicrobial strategies have lost efficacy due to a rapid rise in antibiotic resistance and limited success in developing new antibiotics. Rather than relying on therapeutics solely targeting the bacterial pathogen, therapies are emerging that simultaneously focus on host responses. Here, we describe the most promising 'host-informed therapies' (HITs) in two categories: those that aid patients with fully functional immune systems, and those that aid patients with perturbed immune processes. Using *Streptococcus pneumoniae*, the leading cause of bacterial pneumonia, as a case study, we show HITs stand as an attractive option for supplementing infection management. However, to broaden their applicability and design new strategies, targeted research and clinical trials will be essential.

1.2 The host response is integral to disease outcome

The introduction of vaccines and antimicrobials are among the most important strategies that have enabled us to drastically curb the spread and impact of infectious diseases. However, several challenges have impeded their continued efficacy, including the rapid rise of antibiotic resistance, the largely unsuccessful efforts to identify novel classes of antibiotics, and the limited antigenic breadth of vaccines. Rather than relying on therapeutic strategies that solely focus on bacterial killing, growth inhibition, and infection eradication, treatment strategies are emerging that modulate the host, particularly the immune system. These therapies are focused on enhancing the host response and/or defenses against the infection with the potential to significantly improve disease outcome and host health.

The state of the host immune system, which is impacted by numerous factors such as age, genetic predisposition, or coinfection by multiple pathogens, contributes to the

heterogeneity often observed in infection outcomes. Hence, a complementary treatment approach lies in manipulating host immune defenses to promote pathogen clearance while limiting tissue damage. For decades, immune modulation has retained interest among researchers in cancer, autoimmune disorders, and, now more recently, infectious diseases¹⁻³. Therapies specifically designed to account for the state of the host, or, as we term herein, **host-informed therapies** (HITs; see **Glossary**), can be tailored to either intact or perturbed immune processes resulting from unique host susceptibilities to infectious disease.

In this chapter, we discuss HIT strategies using *Streptococcus pneumoniae* (*S. pneumoniae*) as an illustrative benchmark (**Figure 1.1**). *S. pneumoniae* is a global pathogen that can cause life-threatening disease in fully immune competent individuals, but also is notorious for causing particularly severe disease in individuals with specific conditions. We present HIT strategies that could be considered for any infected individual as well as strategies based on specific vulnerabilities to pneumococcal infection, including influenza coinfection, sickle cell disease, and advanced age. Importantly, we discuss HITs that address common infection immunoregulatory pathways and can thus serve as models for promising conjunctive therapies to treat infections beyond those caused by *S. pneumoniae*.

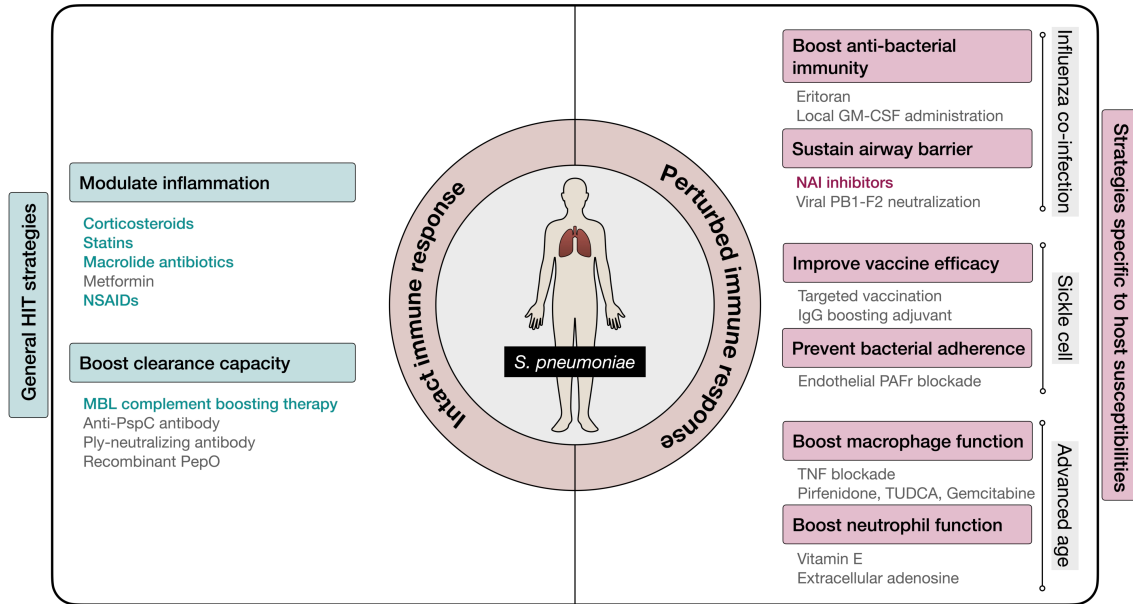


Figure 1.1 | Overview of host-informed therapeutic strategies to combat pneumococcal pneumonia.

HITs against *S. pneumoniae* infections can be tailored to either the intact host immune system (left panels; blue), by targeting excessive lung inflammation and boosting pathogen clearance capacity; or alternatively, they can be aimed at specific perturbed immune responses in infection-susceptible patient populations (right panels; purple), including influenza coinfection, sickle cell disease, and advanced age. HITs used in clinical practice or clinical trials are bolded and colored; others have been validated in preclinical models or are theoretical based on immunological mechanism.

Abbreviations: GM-CSF, granulocyte-macrophage colony-stimulating factor; IgG, immunoglobulin; MBL, mannose binding lectin; NAI, neuraminidase; NSAIDs, non-steroidal anti-inflammatory drugs; PAFr, platelet-activating factor receptor; PepO, endopeptidase O; Ply, pneumolysin; PspC, pneumococcal surface protein C; TNF, tumor necrosis factor; TUDCA, tauroursodeoxycholic acid.

1.3 Challenges in *S. pneumoniae* treatment

S. pneumoniae is commonly found asymptotically colonizing the human nasopharynx, but can cause severe disease including pneumonia, otitis media, meningitis, and sepsis. Since 1977, vaccination has been the cornerstone of pneumococcal disease prevention. However, currently, the two classes of pneumococcal vaccines, the 23-valent **pneumococcal polysaccharide vaccine** (PPSV23) and the pneumococcal vaccines based on **protein-conjugated polysaccharides** (PCV13/ PCV23), only protect against a subset of over 90 different pneumococcal capsular variants (**capsular serotypes**)⁴. Through both the expansion of preexisting non-vaccine pneumococcal serotypes and serotype 'switching' (exchange of capsular polysaccharide genes through transformation), infectious strains not covered by standard vaccination are on the rise⁵. In addition, a worldwide post-vaccination increase in antibiotic resistance frequencies of non-vaccine-type *S. pneumoniae* strains has been reported^{6,7}.

During the 1970s and 1980s, a surge in antibiotic-resistant pneumococci strains was reported⁸. Pneumococci resistant to penicillin (minimum inhibitory concentration of ≥ 0.1 $\mu\text{g/ml}$), erythromycin, and trimethoprim-sulfamethoxazole (TMP-SMX) spread across the world, to Australia, Israel, Spain, Poland, South Africa, and the United States^{9,10}. Tetracycline and chloramphenicol resistance was also identified, as well as fluoroquinolone resistance, although to a relatively low level in comparison¹¹. Multi-drug resistant (MDR) pneumococci, classified as resistant to three or more classes of antimicrobials, were first identified in 1978 via nosocomial transmission¹², and has since been reported in increasing frequency. In the United States today, MDR *S. pneumoniae* is much less common after over 20 years of conjugate vaccine usage, however, the risk remains for acquiring resistant infections in particular populations: the elderly, patients with previous antibiotic use, and patients previously admitted to the hospital in the last year¹³. In 2017, *S. pneumoniae* infections led to over 30,000 outpatient visits in the United States alone, and 30% of cases involved isolates resistant to one or more antibiotics (CDC Pneumococcal Disease^l). Consequently, approximately 2.5 million individuals succumb to pneumonia globally each year, of which an estimated 1.5M specifically

succumb to *S. pneumoniae*, making it the leading bacterial cause of lower respiratory tract infections ¹⁴.

1.4 HITs for otherwise healthy individuals

During pneumococcal pneumonia, pulmonary inflammation orchestrates innate immune cell-mediated responses to *S. pneumoniae*, including cell recruitment, activation, and phagocytic killing, to foster pathogen clearance and prevent systemic spread ¹⁵. However, when faced with *S. pneumoniae*'s immune evasion strategies, these responses can fall short, requiring patients to receive medical intervention to prevent severe infection. Conversely, although inflammation is a required element for bacterial pulmonary clearance, if dysregulated, as manifested by high levels of proinflammatory chemokines and cytokines, upregulated host adhesion molecules, and excessive infiltrating immune cells, the inflammatory response damages alveolar tissue, disrupts the airway barrier, and promotes bacterial dissemination into the bloodstream ¹⁵. As a result, an effective inflammatory response to infection often needs to maintain a balance between host defense and timely return to homeostasis. In mouse models, while early inflammation and rapid immune cell recruitment into the lungs are essential for limiting pulmonary pneumococcal burden ^{16,17}, sustained inflammation and large numbers of pulmonary neutrophils beyond 12 hours post-infection correlate with a greater bacterial burden, more severe systemic infection, and reduced survival ^{18,19}. Indeed, mice that survived infection largely resolved inflammation by 72 hours post-infection ¹⁹. A clinical method to treat the hyper-immune reaction triggered by infection in human patients is extracorporeal approaches, where the patient's blood is removed, and passed through a column containing a material designed to trap molecules or cells. In April 2020, the FDA granted emergency use authorization for the therapeutic apheresis to treat patients 18 or over with confirmed COVID-19 admitted to the intensive care unit with the goal of ameliorating a cytokine storm caused by proinflammatory cytokines ^(NCT04333420II).

Optimal disease recovery from *S. pneumoniae* infection may require both an effective initial acute inflammatory response and rapid resolution of inflammation later in the course of infection. Thus, patients with a fully functional immune system can often benefit

from HIT strategies that boost innate immune cell function or modulate the inflammatory response, which acts in the appropriate manner and timeframe to restore the immune response to the effective range (**Figure 1.2**).

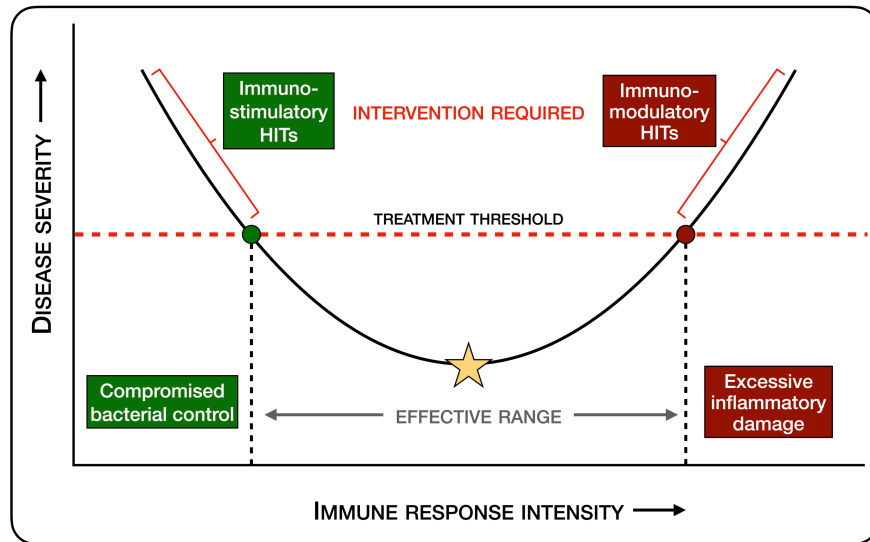


Figure 1.2 | Host lung damage during pneumococcal pneumonia is a function of the quantitative and qualitative aspects of the host response to *S. pneumoniae*.

Clinical disease (pneumococcal pneumonia) occurs at either extreme of the immune response: compromised bacterial control (green) or excessive inflammatory damage (dark red). Conceptually, HITs can be interventions that aim to reduce disease severity by either enhancing (immunostimulatory) or controlling (immunomodulatory) the immune response, to reestablish an effective immune response.

Table 1.1 | HITs that target excessive inflammation or enhance pathogen clearance during *S. pneumoniae* infection

Compromised host response	Target outcome	Drug class	Stage of drug	Reference
Excessive inflammation	Diminish proinflammatory gene expression. Increase anti-inflammatory cytokines.	Corticosteroids (Prednisone)	Clinical practice (For moderate and severe pneumonia)	24-27
	Increase anti-inflammatory cytokines. Activate alveolar macrophages.	Macrolide antibiotics (Azithromycin, Erythromycin)		36,37
	Diminish tissue-destructive inflammation. Reduce acute symptoms (pain, fever, cough).	Nonsteroidal anti-inflammatory drugs		46-48
	Diminish tissue-destructive inflammation. Increase autophagy and lung barrier function.	Statins	Clinical trial (For moderate pneumonia)	29-35
	Decrease proinflammatory cytokines & neuroinflammation. Increase autophagy.	Metformin	Preclinical (For pneumonia and sepsis)	38-43
Ineffective complement response	Boost MBL complement pathway	Recombinant human MBL (rMBL)	Clinical trial	52-55, III
	Target pneumococcal complement evasion factors	PspC-targeted vaccination and/or neutralizing antibody therapy	Preclinical*	59
	Downregulate over-aggressive complement response	C5a-blocking antibody	Clinical trial	II
Diminished autophagic function	Inhibit pneumococcal autophagy evasion	PspC-targeted immunization and/or pneumolysin-neutralizing antibodies	Preclinical*	72,73
Endothelial barrier dysfunction	Inhibit bacterial adhesion	Integrin-targeting antibody, small molecule, or peptide inhibitor	Clinical trial	78,80,81

*Preclinical refers to proposed host-informed therapies validated in mouse models only.

1.4.1 Anti-inflammatory strategies

Anti-inflammatory drugs can supplement traditional antibiotics by curtailing inflammation-related tissue damage during bacterial infection. Of course, inflammation has been a target of multiple drug classes, and by repurposing drugs that have prior safety and regulatory approval, anti-inflammatory strategies can be fast-tracked in clinical trials and implemented in the clinic. Examples of such drugs are listed in **Table 1.1**, and we highlight several in more detail below.

Corticosteroids are a class of broad-spectrum anti-inflammatory agents commonly employed in inflammatory diseases, as well as some infectious diseases as adjuvant therapy, most recently severe COVID-19 ²⁰. The use of corticosteroids such as prednisone is controversial in the treatment of *S. pneumoniae*-related community-acquired pneumonia (CAP) due to limited supporting clinical data and the confounding **antipyretic effect** of these drugs in the absence of bacterial clearance ²¹. The most recent meta-analysis of 9 randomized clinical trials and 6 cohort studies found no evidence of mortality improvement when administering corticosteroids to CAP patients ²². However, in a number of these studies, corticosteroid treatment accelerated time to clinical stability, resulting in shorter hospital stays, decreased duration of intravenous antibiotics, and reduced need for mechanical ventilators ²³. Moreover, studies focusing on patients with severe CAP further corroborate the beneficial role of corticosteroids in patients with a general hyperinflammatory response ²⁴⁻²⁷. In other pulmonary bacterial infections including tuberculosis (TB), caused by the bacterium *Mycobacterium tuberculosis*, broadly acting glucocorticoids such as dexamethasone and prednisone have become standard-of-care HITs in patients with advanced disease ²⁸.

Statins are traditionally prescribed to control cholesterol levels. However, statins can also reduce chronic inflammation by downregulating endothelial cell adhesion molecules, reducing cytokine production, curtailing leukocyte extravasation and improving lung barrier function ²⁹. Consequently, patients on preexisting statin treatment are less likely to develop bacterial sepsis and other complications ³⁰, including secondary cardiovascular conditions ³¹. Furthermore, prior statin use lowers the risk of pneumonia

infection³² and decreases mortality in individuals infected with *S. pneumoniae*³³. Statins seem to prevent *S. pneumoniae* epithelial barrier breach that fosters the progression of acute lung infection to systemic infection, a mechanism that could explain why the beneficial effects of statins do not extend to patients critically ill with severe septicemia^{34,35}. This suggests that patients with less severe forms of pneumonia will likely benefit most from the anti-inflammatory and immunomodulatory effects of the long-term use of statins.

Macrolides can impact the pathogen through its antimicrobial properties, as well as the host through its immunomodulatory activities. Macrolides can promote the production of anti-inflammatory cytokines and the activation of alveolar macrophages, and thereby increase bacterial killing. Preclinical assessments in mice treated with azithromycin show reduced chemokine production and limited pulmonary neutrophil and T cell influx thereby promoting rapid resolution of inflammation³⁶. A meta-analysis of 28 observational studies with critically ill CAP patients demonstrates that macrolides are more effective at reducing mortality in comparison to other non-macrolide antibiotics³⁷. This suggests that patients with severe pneumococcal pneumonia could benefit from macrolide antibiotics not only through their bacteriostatic effects but also through their effect on the immune response.

Metformin is an extensively used repurposed type II diabetes drug, which, in addition to its metabolic effect on gluconeogenesis, reduces inflammation and enhances the immune response against multiple pathogens including *M. tuberculosis*, *Trypanosoma cruzi*, *Trichinella spiralis*, and *Staphylococcus aureus* as shown in human and mouse experiments³⁸⁻⁴¹. In an experimental pneumococcal meningitis model, metformin demonstrates neuroprotective properties by reducing neuroinflammation and meningitis-induced hearing impairment⁴². In animal models of sepsis, metformin ameliorates lipopolysaccharide (LPS)-induced proinflammatory cytokine production and attenuates **endotoxemia**⁴³. Metformin may thus have general efficacy against the aforementioned bacterial species and be of dual benefit in type II diabetic patients who have increased susceptibility to bacterial infections.

In principle, nonsteroidal anti-inflammatory drugs (NSAIDs) can be applied broadly to bacterial infections as antipyretics and analgesics to suppress acute symptoms such as

pain, fever, and cough. However, studies on NSAIDs efficacy in treating pneumonia and lower respiratory tract infections have yielded conflicting results ⁴⁴, with some even reporting an increased risk of complications as an adverse effect of NSAID exposure (specifically ibuprofen) ⁴⁵. On the other hand, studies point to newly discovered antibacterial activities of NSAIDs, making them promising therapeutics to treat bacterial infections ⁴⁶⁻⁴⁸. It has recently been established that the evidence against the use of NSAIDs has not been systematically assessed ⁴⁹. A comprehensive review examining the risk of pneumonia complications in pediatric and adult patients treated with NSAIDs ⁴⁹ indicated that the conclusion of risks of NSAIDs in treating infection could be due to bias intrinsic to small data sets. Altogether, NSAIDs still hold potential and warrant further exploration as a general anti-inflammatory adjuvant therapy for bacterial infections.

While these inflammation-modulatory therapies are promising HITs to treat pneumococcal infection, it is important to keep in mind that return to homeostasis requires the dynamic regulation of inflammation (**Figure 1.2**). On the one hand it is essential to trigger a level of inflammation that is host-protective; on the other hand, immune response intensity should not exceed what is necessary and become destructive to the host, i.e., too little control leads to pathogen escape, while a hyper-response may lead to a hyperinflammatory state and subsequent host damage. Clinical severity, stage of pathogenesis, and infection niche of the bacterial pathogen are all variables that influence treatment efficacy. Anti-inflammatory immunomodulators for *S. pneumoniae* infection appear to foster diverse clinical outcomes, making their regular use in near-term frontline therapy problematic. To solve this challenge, randomized, controlled human clinical trials that better characterize patient phenotypic subpopulations, such as disease severity, infection timeline, and systemic involvement, will help better target the indicated therapies to specific groups and/or disease conditions, with better patient outcomes as a result.

1.4.2 Enhancing innate immunity

S. pneumoniae is predominantly an extracellular pathogen and nasopharyngeal carriage is a prerequisite for disease and transmission. Colonization of the nasopharynx is facilitated by the bacterium's ability to adhere to host cells, subvert clearance by mucociliary flow, and evade mucosal innate and adaptive immunity¹⁵. Intact humoral and cell-mediated immune responses are essential for pathogen killing and prevention of an escalating infection. Persistence and survival of *S. pneumoniae* require the evasion of multiple immune mediators that target extracellular bacteria, including **complement deposition**, opsonophagocytic uptake, and phagocytic killing by both local and recruited phagocytic cells. Engulfed *S. pneumoniae* faces multiple intracellular killing mechanisms, including phagosome maturation, **canonical (non-selective) autophagy**, and a newly discovered process termed **LC3-associated phagocytosis (LAP)**, which combines the molecular machineries of phagocytosis and autophagy to facilitate fusion with lysosomes and degradation of phagocytosed bacteria.

S. pneumoniae has evolved several strategies to evade certain host immune mechanisms. This in turn has prompted the design of several HITs to enhance and trigger the innate immune system to engage in an effective antibacterial response. Below we discuss three such examples: i) complement-targeted therapeutics, ii) autophagy-targeted therapeutics, and iii) bacterial adhesion-targeted therapeutics, which are summarized in **Table 1.1**.

1.4.3 Targeting complement evasion

Opsonization by complement and antibody is one of the most effective mechanisms of *S. pneumoniae* recognition and killing by phagocytic cells. However, like many other pathogenic microorganisms, *S. pneumoniae* can bind to complement regulatory proteins, neutralizing their host protective function⁵⁰. Major complement regulatory proteins targeted by *S. pneumoniae* include: C4BP (co-factor for C4b inactivation), **Factor H** (regulator for alternative pathway C3 convertase decay), and vitronectin (inhibitor of membrane attack complex MAC formation)⁵¹.

One approach is to boost complement, for instance, through targeting the mannose binding lectin (MBL) complement pathway (**Figure 1.3a**). The MBL pathway is an important protective mechanism against *S. pneumoniae* infection as shown through mouse experiments and in human cohorts with genetic MBL deficiencies who are at higher risk of infection ^{52,53}. Recombinant human MBL (rhMBL) was in the process of being tested in a Phase 1B clinical trial for infection-susceptible patients, such as cancer patients undergoing chemotherapy ⁵⁴, before discontinuation in 2009 due to slow clinical trial enrollment and changes in company strategy. While rhMBL did not meet the criteria to move forward in clinical development, it was deemed safe and well-tolerated (NCT00886496III) and has been subsequently explored for the treatment of influenza A ⁵⁵. Similar complement-boosting therapeutics could work as a generalizable strategy in combating other bacterial pathogens with similar immune evasion mechanisms, such as *Borrelia burgdorferi*, *Bordetella pertussis*, and *Staphylococcus aureus* ^{56,57}.

Another approach is to target pneumococcal factors known to compromise complement function. One example of a *S. pneumoniae* surface protein with the ability to bind and neutralize complement regulators is pneumococcal surface protein C (PspC), which functions as both a Factor H- and vitronectin-binding protein ⁵⁸. The surface localization, highly conserved structure, and key role in complement evasion-associated virulence of PspC make it an excellent target for vaccination or targeted neutralizing antibodies (**Figure 1.3a**). For instance, PspC-immunized mice produce antibodies that not only recognize most *S. pneumoniae* clinical isolates, but also decrease Factor H (FH) binding when pre-opsonized in vitro ⁵⁹. Other *S. pneumoniae* surface proteins including pneumococcal surface protein A (PspA) ^{60,61}, pneumococcal histidine triad proteins (Phts) ⁶², and pneumococcal pilus adhesin (RrgA) ⁶³ play an integral role in bacterial virulence and evasion from the complement system, rendering them additional promising targets for similar selective strategies.

Finally, an over-aggressive complement response can be extremely harmful to the host, resulting in pneumonia developing to severe sepsis and septic shock ^{64,65}. The terminal complement pathway effectors C5 and its activated product C5a play a key role in the development of sepsis and the resultant multiorgan failure and high mortality rates. HITs

targeting C5 and C5a can be uniquely beneficial in controlling pneumococcal pneumonia from developing into systemic infection. For example, IFX-1, a monoclonal antibody, was tested in a placebo-controlled, double-blinded study (SCIENS) with 72 patients suffering from early septic organ dysfunction. IFX-1 significantly reduced and effectively blocked C5a in a dose-dependent manner, and positive trends were reported in other clinically relevant endpoints, such as organ dysfunction score (SOFA score), need for ventilator support, and length of stay in the ICU (NCT04333420II).

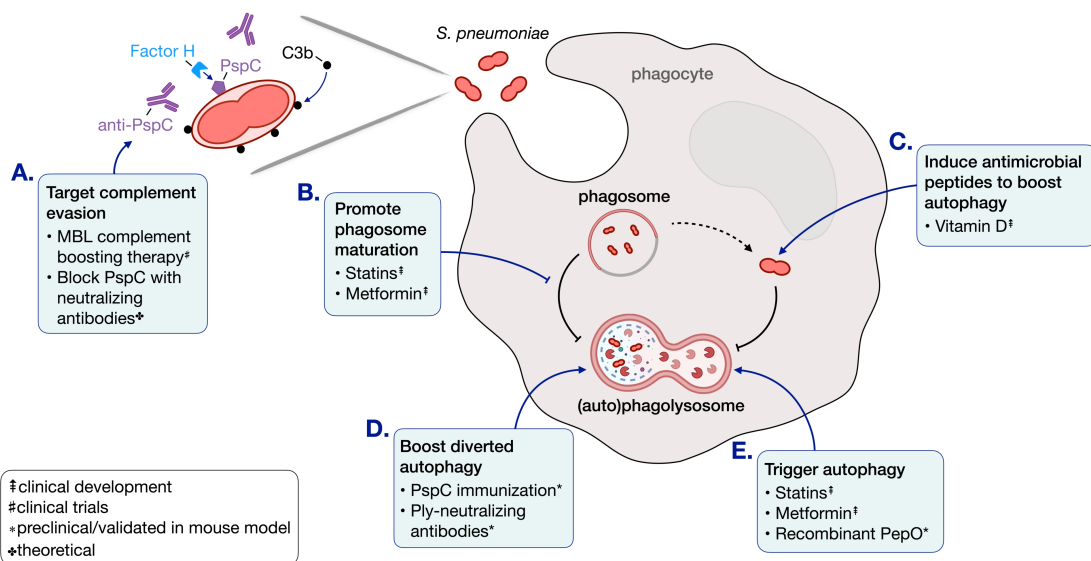


Figure 1.3 | Enhancing bacterial clearance by innate immune cells.

HITs are utilized to enhance and prompt the immune system to effectively engage in an antibacterial response and successfully clear *S. pneumoniae* by phagocytic killing. By targeting *S. pneumoniae* mechanisms of immune evasion, for example, complement evasion and diverted autophagy, effective innate immune response may be reestablished.

Abbreviations: C3b, complement component 3b; MBL, mannose binding lectin; PepO, endopeptidase O; Ply, pneumolysin; PspC, pneumococcal surface protein C.

1.4.4 Enhancing autophagy

During an effective immune response, pneumococci are phagocytosed by host cells such as macrophages and neutrophils and subsequently destroyed. In addition to direct opsonophagocytic killing, other vesicular defense systems, such as autophagy, can be triggered in response to select pathogens and assist with the antimicrobial response. Modulating host autophagy has proven efficacious against several infectious diseases. For instance, in active TB infection, metformin and statins enhance macrophage intracellular autophagic killing of *M. tuberculosis* through LC3 upregulation^{38,66} (**Figure 1.3b**). Similarly, boosting autophagy with vitamin D or with small molecule autophagy inducers (**Figure 1.3c**) improves macrophage killing of *Salmonella enterica* serovar Typhimurium in vitro and in vivo⁶⁷.

Both canonical non-selective autophagy and non-canonical autophagy observed in phagocytic cells (LAP) are vital defense systems against engulfed *S. pneumoniae*, contributing to rapid phagosome delivery to lysosomes and efficient bacterial killing⁶⁸⁻⁷¹. To avoid clearance by these mechanisms, *S. pneumoniae* engages in autophagy evasion strategies when inside the phagosome. In vitro experiments have shown that pneumococcal surface protein PspC diverts *S. pneumoniae* away from the autophagic pathway by causing degradation of autophagy-related key regulator 14 (Atg14)⁷², a key host protein that orchestrates autophagy by promoting the fusion of autophagosomes to lysosomes⁷³. Thus, this diversion strategy could be specifically targeted with PspC antibodies to inhibit the PspC-Atg14 interaction (**Figure 1.3d**). On the other hand, the *S. pneumoniae* pore-forming toxin pneumolysin (Ply) plays a pivotal role in triggering LAP in both nonphagocytic cells and phagocytic cells (macrophages)⁷¹. In dendritic cells, Ply inhibits LC3 recruitment to intracellular *S. pneumoniae*, thus diminishing subsequent lysosomal degradation^{74,75}. A Ply-neutralizing peptide can increase uptake in autophagosomes and reduce intracellular bacterial survival in vitro⁷⁴, and Ply-neutralizing antibodies can protect against pneumococcal pneumonia in mice⁷⁶ (**Figure 1.3d**). Alternatively, autophagy-triggering proteins on the surface of *S. pneumoniae* might be harnessed to boost *S. pneumoniae*-targeted autophagy. For instance, endopeptidase O

(PepO) triggers macrophage autophagy, and recombinant PepO enhances pulmonary bacterial clearance in a mouse model of infection (**Figure 1.3e**)⁷⁷.

1.4.5 Targeting bacterial adhesion

When bacterial infection caused by *S. pneumoniae* becomes systemic, a cascade of immune responses is initiated that can often overload the host. Microvascular dysfunction can occur due to microbial adhesion. The resulting damage to the integrity of the endothelial barrier facilitates bacterial escape to the bloodstream, causing secondary infections that can lead to organ failure, and trigger excessive immune responses that overwhelms the host⁷⁸.

Integrins are non-covalently linked $\alpha\beta$ heterodimers widely expressed on epithelial, endothelial, and immune cell surfaces; they regulate downstream events including cytoskeleton rearrangement, immune mediator secretion, immune cell recruitment, extravasation, and regulating structural integrity⁷⁹. The major surface protein PspC of *S. pneumoniae* has been shown to bind to the plasma protein vitronectin and crosslink the bacterium to the integrin $\alpha V\beta 3$ ⁸⁰. HITs such as antibodies, small molecules, and peptide inhibitors targeting integrins can be utilized to inhibit bacterial binding to endothelial cells⁷⁸. The cyclic peptide integrin $\alpha V\beta 3$ inhibitor, Cilengitide, has shown ex vivo capability of competitively antagonizing bacterial binding to endothelial cells⁸¹. Clinical studies are required to determine if prophylactic use of a drug such as Cilengitide in patients with existing *S. pneumoniae* infection (or a similar bacterial infection) can prevent the development of systemic infection and the subsequent risk of immune cascade dysfunction.

The anti-inflammatory and innate immune cell-boosting approaches described above can be used to treat pneumococcal pneumonia and subsequent systemic infection in patients without predisposing conditions and generally at any stage of infection, as they are less dependent on specific clinical host states. Through epigenetic, transcriptional, and functional reprogramming of innate immune cells, some of these approaches may bring about long lasting and heterologous protection against infection in the form of 'trained' innate immunity. In addition, by targeting immunoregulatory pathways that are

relevant to diverse bacterial infections, these interventions might be generalized to infections beyond pneumococcal pneumonia.

1.5 HITs for susceptible hosts with predisposing conditions

Host susceptibilities can greatly influence therapeutic efficacy, especially when immune responses are perturbed by predisposing conditions. For instance, *S. pneumoniae* can be more lethal in sickle cell anemic patients, elderly individuals, and as a secondary infection following viral influenza. Patients with underlying health conditions can benefit from HIT interventions tailored to their specific susceptibilities. Importantly, some HITs listed in **Table 1.2** are already used in clinical practice, while others are at a range of developmental (preclinical) and research stages.

Table 1.2 | HITs that target defects in host defense in patient populations susceptible to *S. pneumoniae* infection

Host condition	Defect in host defense	Target outcome	Drug class	Stage of drug	Reference
Influenza	Enhanced Type I interferon (IFN-I) antiviral response	Boost antibacterial immunity	Eritoran: limit IFN-I mediated epigenetic modification	Preclinical*	83
			IL-27 blockade: limit IL-10 and increase IL-17	Preclinical*	87,88
	Epithelial damage/exposed subepithelial tissue	Sustain airway barrier function	Neuraminidase inhibitors: limit exposure of epithelial adhesion receptors	Clinical practice	101-103
			Viral PB1-F2 blockade: limit viral induced cell apoptosis	Theoretical	104,105
Sickle cell disease	Diminished vaccine response	Targeted pneumococcal vaccination	Vaccine targets not required for survival in sickle cell hosts (CcpA, PiaA)	Preclinical*	108
			LT-IIb adjuvant: enhance IgG	Theoretical	109

			response to vaccination		
	Chronically activated vascular endothelium	Block host endothelial adhesion molecules	Platelet-activating factor receptor (PAFr) blockade	Preclinical*	110,111

Advanced age	Monocyte-directed inflammation	Decrease monocyte-directed inflammaging	TNF- α blockade: limit premature inflammatory monocytes exit from bone marrow	Preclinical*	116
	Neutrophil-directed inflammation	Decrease neutrophil-directed inflammaging	Vitamin E: limit inflammatory neutrophil recruitment	Preclinical*	119
	Macrophage dysfunction	Decrease macrophage dysfunction	Pirfenidone: enhance macrophage function by increasing mitochondrial ATP production	Preclinical*	121
			Tauroursodeoxycholic acid (TUDCA): enhance NLRP3 inflammasome activation by supporting UPR	Preclinical*	122,123
			Gemcitabine: enhance macrophage UPR and Atg9 activity	Preclinical*	122,123
Neutrophil dysfunction	Decrease neutrophil dysfunction	Extracellular adenosine (EAD): inhibit neutrophil IL-10 production and enhance killing	Preclinical*	19,130, 131	

*Preclinical refers to proposed host-informed therapies validated in mouse models only.

Abbreviations: ATP, adenosine triphosphate; Atg9, autophagy-related protein 9; CppA, C3-degrading protease; EAD, extracellular adenosine; GM-CSF, granulocyte-macrophage colony-stimulating factor; IFN-1, interferon-1; IL-10, interleukin-10; IL-17, interleukin-17; IL-27, interleukin-27; LT-IIb, type II heat-labile enterotoxin b; NLRP3, NLR family pyrin domain containing 3; PAFr, platelet-activating factor receptor; PiaA, pneumococcal iron acquisition protein A; TNF, tumor necrosis factor; TUDCA, tauroursodeoxycholic acid; UPR, unfolded protein response.

1.5.1 Influenza coinfection

Influenza infection is known to increase susceptibility to secondary bacterial pneumonia, which not only presents with higher bacterial burden, but also is associated with higher mortality and morbidity⁸². The increased susceptibility often results from a lingering elevated **Type I interferon (IFN-I) antiviral response**, and virus-induced tissue damage that disrupts the airway barrier. Potential HITs exist that can tackle these two aspects of a viral infection-triggered immune environment.

1.5.1.1 Restoring antibacterial immunity

While beneficial for viral clearance, lingering antiviral immune responses such as IFN-I signaling can dampen immunity against bacteria including *S. pneumoniae*⁸³. During secondary bacterial infections, IFN-I limits chemokine ligand 2 (CCL2)-mediated macrophage recruitment^{84,85}, reduces the phagocytic response, suppresses **T helper 17 (Th17)-mediated immunity**⁸⁶, and promotes lymphocyte exhaustion⁸² (**Figure 1.4a**). Therefore, limiting IFN-I signaling can benefit multiple antibacterial immune responses. However, directly tampering with IFN-I activity may compromise antiviral immunity critical to combat lingering viral infection. Consequently, downstream effectors of IFN-I signaling that cause increased susceptibility to secondary bacterial infections are seen as safer targets for blockade.

In this sense, the **toll-like receptor 4 (TLR4)** antagonist Eritoran is suggested to blunt influenza-induced IFN- β induction and reverse IFN-I mediated epigenetic changes that mediate susceptibility to bacterial infection⁸³. Such epigenetic reprogramming induced by Eritoran breaks the state of 'trained' immune suppression following viral infection, enabling macrophages to react with stronger and more rapid responses when challenged with future bacterial triggers. In mouse models, Eritoran demonstrates long-term protective effects against lethal secondary *S. pneumoniae* infection by rescuing mice from a state of immunosuppression⁸³ (**Figure 1.4a**). Similarly, therapies such as interleukin-27 (IL-27) blockade and recombinant IL-17A specifically restore the $\gamma\delta$ T cell and Th17 cell branches of antibacterial immunity that is dampened downstream of IFN-I

signaling^{87,88}. IL-27 blockade additionally acts by limiting interleukin-10 (IL-10) which inhibits neutrophil recruitment⁸⁹ (**Figure 1.4a**). Both therapies increase resistance to pneumococcal infection following influenza infection in mice⁸⁷. In addition, emerging evidence suggests that various IFN-I subtypes and IFN-I receptors have differential contributions to antiviral immunity and bacterial infection susceptibility. For instance, IFN- α subtypes are immunostimulatory cytokines with strong antiviral activities against influenza virus both in vitro and in vivo⁹⁰. Therefore, by targeting alternative subtypes of IFN-I, an effective antiviral response can be preserved while reducing susceptibility to secondary infection^{91, 92}. Importantly, such a strategy is applicable to secondary pneumonia caused by other bacterial pathogens, such as *S. aureus*, *Haemophilus influenzae*, and *Pseudomonas aeruginosa*.

To note, some inflammatory cytokines are indispensable during infection and coinfection, and should be taken into consideration when postulating cytokine-blockade-dependent therapy options. From this perspective, cytokines such as interleukin-6 (IL-6) surprisingly have a protective function in influenza-*S. pneumoniae* coinfection, since its depletion leads to significantly increased bacterial burdens in mice⁹³. IL-6 been shown to increase expression of acute-phase proteins and mediate both cell homeostasis and phagocytosis, revealing therapeutic value in recombinant IL-6 therapies⁹³. Inversely, secretion of tumor necrosis factor-alpha (TNF- α), leads to an uncontrolled immune response, namely an exaggeration of T cell activity, results in an increase in the inflammatory potential during coinfection and impairment of macrophages' phagocytic activity⁹⁴. Thus, boosting and/or modulating aspects of the inflammatory response during influenza coinfection is a delicate scale to restore immunity to the effective range.

1.5.1.2 Sustaining airway barrier function

IFN-I hampers lung epithelial repair by interfering with epithelial proliferation and differentiation. In addition to IFN-I response-mediated epithelial cell death, influenza infection can promote apoptosis of ciliated cells, slow ciliary beating, and increase prevalence of binding receptors on host epithelium⁹⁵. Damaged epithelium can have large, exposed areas of laminin, type I and IV collagen, fibrin, and fibrinogen deposition,

which encourages *S. pneumoniae* binding to host epithelial cells ^{96,97}. Viral infection also reduces the expression of key epithelial cell junctional complexes, including occludin, claudin-4, and junctional adhesion molecules (JAM), destabilizing junctional barriers ⁹⁸. These events in turn allows *S. pneumoniae* to achieve deep tissue invasion ⁹⁹, which often leads to dissemination to the bloodstream and systemic spread .

Targeting specific influenza virulence factors that promote epithelial barrier breach can reduce secondary pneumococcal complications (**Figure 1.4a**). One such target is **neuraminidase**, a viral sialidase expressed on influenza virus that removes lung sialic acids thereby exposing epithelial receptors for pneumococcal adherence in tracheal, eustachian-tube, and middle-ear epithelium ¹⁰⁰. Neuraminidase inhibitor (NAI)-based antiviral therapies, such as oseltamivir, are commonly prescribed to influenza patients. The prophylactic antiviral effects of NAIs are only significant if administered within the first 48 hours of clinical influenza symptom onset and delayed NAI treatment has no effect on pulmonary viral titer ¹⁰¹. However, oseltamivir effectively prevents secondary *S. pneumoniae* infection, even when treatment is initiated 5 days into viral infection ¹⁰¹⁻¹⁰³. This suggests that despite a persistent viral load, NAI-mediated decrease in epithelial damage alone can be effective in preventing a secondary *S. pneumoniae* insult.

Another theorized target of interest is **PB1-F2**, a proinflammatory viral accessory protein that promotes ciliary epithelial cell apoptosis by inhibiting mitochondrial function. PB1-F2-mediated cell death in the lung increases fibrinogen deposition, inflammatory cell infiltration, and cytokine/chemokine release ¹⁰⁴. Additionally, PB1-F2-mediated cell death may trigger a positive cytokine loop that is amplified by secondary bacterial infection and exacerbate tissue-destructive inflammation leading to lethality. Decreasing PB1-F2 expression (or replacement with C-terminal truncated PB1-F2 proteins lacking mitochondrial localization ability), reduces the severity of secondary bacterial pneumonia in mice. Hence, an antagonist of the PB1-F2 protein that is currently under investigation may have benefits that go beyond its antiviral therapeutic effects ^{104,105}.

Limiting specific signaling modalities downstream of IFN-I and/or targeting tissue-damaging influenza virulence factors (e.g., neuraminidase, PB1-F2) can restore

antibacterial immunity and sustain airway barrier function during influenza infection, respectively. Therefore, HITs that counteract viral activities crippling host antibacterial immunity can be generally applied to prevent the development of serious secondary pulmonary bacterial infections.

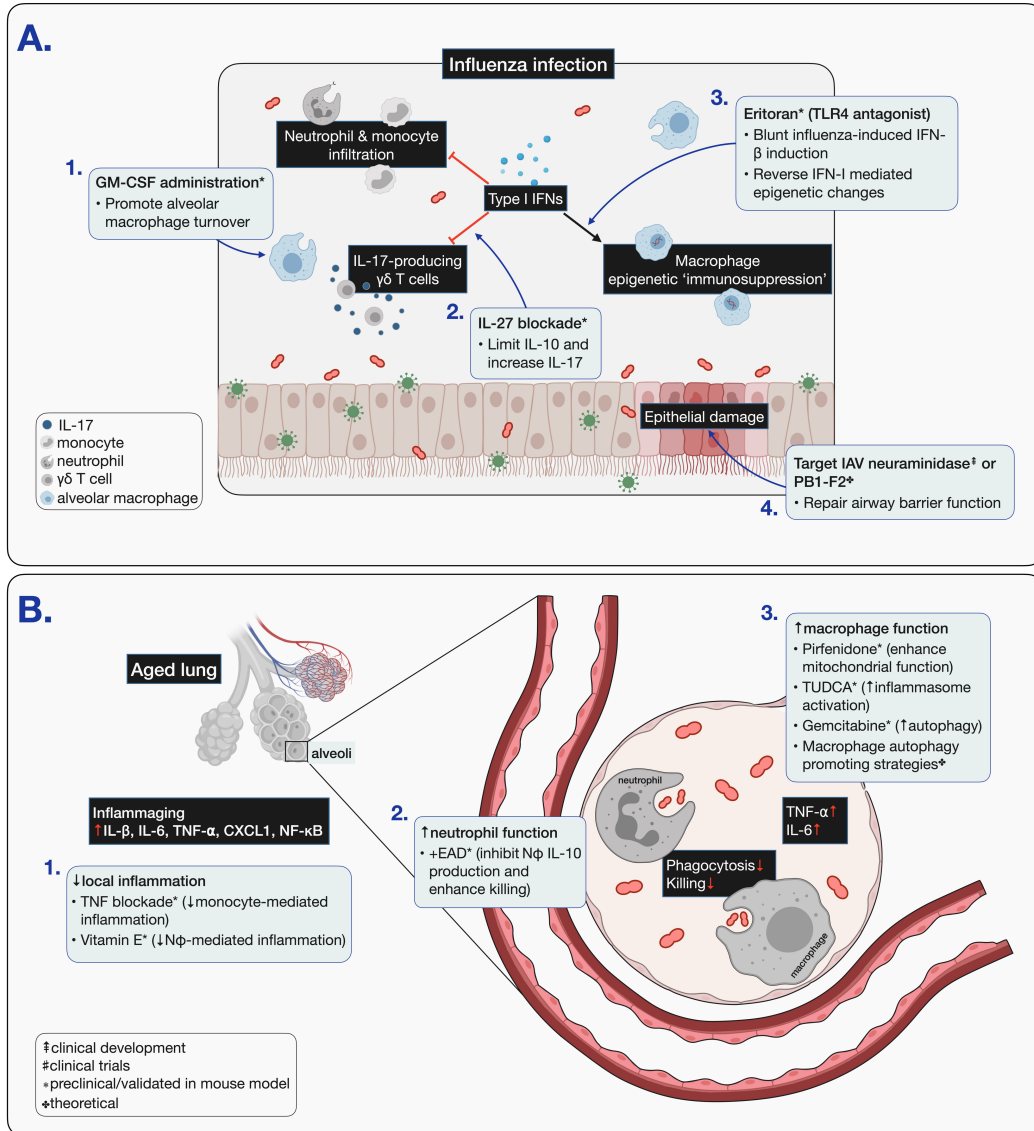


Figure 1.4 | Targeting defects in immune defense in susceptible patient populations.

Panel A. Integral to the immune response to influenza are type 1 interferons (IFN-I), produced following recognition of viral nucleic acids. However, IFN-I signaling can dampen immunity against secondary *S. pneumoniae* infection (and other secondary bacterial infections), resulting in reduced neutrophil and monocyte infiltration, suppressed IL-17 production and Th17-mediated antibacterial immunity, and macrophage epigenetic changes. Our proposed HITs (blue boxes) tackle components of this compromised host antibacterial response by **1.** promoting alveolar macrophage turnover; **2.** limiting IL-10 and increasing IL-17; **3.** blunting influenza-induced IFN- β induction; and **4.** repairing the airway barrier function.

Abbreviations: $\gamma\delta$ T cells, gamma delta T cells; GM-CSF, granulocyte-macrophage colony-stimulating factor; IFN, interferon; IL-10, interleukin-10; IL-17, interleukin-17; IL-27, interleukin-27; TLR4, toll-like receptor 4; IAV, influenza A virus.

Panel B. Immunosenescence and inflammaging impair immune defenses in the elderly. General differences in cell-mediated immunity (immunosenescence) and chronic inflammation (inflammaging) in the elderly compared to the young are marked by red arrows. Levels of inflammatory cytokines become elevated with age at the steady state as well as under infection. Phagocytic cell functions decline with age, resulting in reduced phagocytosis and bacterial killing. We propose multiple host-informed therapies (blue boxes) specific to combating *S. pneumoniae* infection in the elderly to **1.** reduce cell-directed inflammation; **2.** increase neutrophil function; **3.** increase macrophage function.

Abbreviations: CXCL1, C-X-C motif chemokine ligand 1; EAD, extracellular adenosine; IL- β , interleukin-beta; IL-6, interleukin-6; IL-10, interleukin-10; N Φ , neutrophil; NF κ B, nuclear factor kappa-light-chain-enhancer of activated B cells; TNF, tumor necrosis factor; TNF- α , tumor necrosis factor-alpha; TUDCA, tauroursodeoxycholic acid.

1.5.2 Sickle cell disease

Sickle cell disease (SCD) is the most common genetic disorder worldwide and results in the production of structurally abnormal and functionally defective red blood cells. Sickle cell patients, especially children, are highly susceptible to invasive *S. pneumoniae* infection and present with more abrupt and severe manifestations¹⁰⁶. HITs that would benefit this susceptible patient population could be focused on overcoming diminished vaccine responses, and/or chronic endothelial inflammation.

1.5.2.1 SCD-niche targeted pneumococcal vaccination

Protection against pneumococcal infection in the SCD population is largely dependent on vaccination with pneumococcal polysaccharides, which generates protective IgG antibodies that are essential for opsonization, immune recognition, and clearance of pulmonary infections. However, splenic function decreases progressively in SCD, which leads to decreased antibody production and a diminished response to vaccination. To further complicate this problem, pneumococcal vaccines such as PPSV23 which covers 23 serotypes, provide far from exhaustive protection¹⁰⁷.

A murine SCD infection model coupled with transposon-insertion sequencing (Tn-Seq) identified a number of *S. pneumoniae* virulence factors essential in a wild-type mouse with an intact immune system but no longer required for survival in a SCD mouse model¹⁰⁸. These data illustrate the existence of significant differences in host environments, including potential differences in the complement system and nutrient availability (e.g., iron). Importantly, experiments highlight how this can affect vaccine efficacy. For instance, two common pneumococcal vaccine antigens that effectively protect the general population - the complement degrading protease (CpaA) and an iron transporter (PiaA) - show little efficacy in preventing pneumococcal infection in a SCD mouse model¹⁰⁸. Therefore, vaccination strategies for SCD patients can be improved by customization with antigens specifically required for pathogenesis in the SCD host environment. Furthermore, since SCD patients have decreased splenic function and consequently decreased antibody production, adjuvants to promote IgG production can be beneficial. For instance, administering the type II heat-labile enterotoxin (LT-IIb) adjuvant during

pneumococcal vaccination promotes IgG production in mice and is especially effective in protecting against invasive *S. pneumoniae* isolates ¹⁰⁹.

1.5.2.2 Platelet-activating factor receptor (PAFr) blockade

As a result of chronic hypoxia and recurrent infection, SCD patients often suffer from a chronically activated vascular endothelium that expresses a variety of adhesion molecules and surface lectins. **Platelet-activating factor (PAF)** is an endothelial adhesion molecule known to be overexpressed under inflammatory conditions in SCD patients. PAFr is a G protein-coupled receptor that normally binds PAF, but also binds phosphorylcholine, which is part of the pneumococcal cell wall and mimics the bioactive end of PAF. PAFr binding to choline allows for bacterial adhesion and entry into endothelial cells, leading to access to the bloodstream and systemic disease. Blocking PAFr attenuates pneumococcal infection and prolongs host survival in experimental SCD mouse models ¹¹⁰. A PAFr blocking antibody, a blocking peptide, or a receptor antagonist ¹¹¹ in conjunction with antibiotic therapy could thus be a particularly beneficial HIT for SCD patients with pneumococcal infection.

Targeted pneumococcal vaccination strategies and blocking PAFr in SCD patients can provide protection against pneumococcal infection and obstruct bacterial attachment and endothelium entry. Therefore, HITs that target the disrupted mechanisms in SCD patients could protect this uniquely susceptible population from infection.

1.5.3 Impaired immune defenses in the elderly

Infection-related deaths make up one-third of all elderly deaths (aged over 65), and pneumococcal pneumonia ranks in the top 10 causes of infection in this population ¹¹². One reason the elderly succumb to infection at higher rates is age-related changes in the immune system ^{113,114}. This can be generally categorized into **inflammaging**, a chronic elevation of basal and induced inflammation, and **immunosenescence**, a decline in cell-mediated immunity (**Figure 1.4b**).

1.5.3.1 Inflammaging

Inflammation during *S. pneumoniae* infection is enhanced with age, as characterized by increased levels of chemokines and inflammatory cytokines such as TNF- α and decreased anti-inflammatory cytokines such as IL-10^{114, 115}. Specifically, chronic exposure to TNF- α allows for premature monocytes to exit the bone marrow and extravasate to the site of infection during *S. pneumoniae* challenge, leading to increased bacterial burden¹¹⁶. In aged mice, both TNF- α blocking antibodies and charged microsphere-mediated depletion of TNF- α -producing Ly6C+ monocytes show therapeutic potential in combating *S. pneumoniae* infection¹¹⁶ (**Figure 1.4b**).

Vitamin E is an antioxidant with anti-inflammatory functions¹¹⁷. Alpha-tocopherol (α -Toc), the most bioavailable form of Vitamin E, restores immune responses in older adults, specifically in memory T cell-, CD4 T cell-, and antibody-mediated responses. In the context of *S. pneumoniae* infection, α -Toc limits excessive inflammatory neutrophil recruitment to the lung, both by downregulating proinflammatory chemokines and limiting adhesion molecule expression on neutrophils^{118,119} (**Figure 1.4b**). Supplementation of α -Toc in aged mice results in a drastic decrease in *S. pneumoniae* bacterial burden¹¹⁹, suggesting that the elderly population could benefit from Vitamin E supplementation to curtail *S. pneumoniae*-induced neutrophil-mediated inflammatory processes. Importantly, supplementation with α -Toc offers protection against respiratory infections of both viral and bacterial origin in the elderly¹²⁰. This suggests that addressing inflammaging in the elderly can generally decrease infection susceptibility and improve quality of life.

1.5.3.2 Immunosenescence

During aging, oxidative stress and mitochondrial damage accumulation can overwhelm cellular antioxidant capability. In macrophages, this leads to decreased mitochondrial ATP production, defective macrophage activation, and reduced responsiveness to bacterial infection¹²¹. Pirfenidone, an anti-fibrotic drug with antioxidant and anti-

inflammatory properties, enhances mitochondrial and macrophage function in mouse models of *S. pneumoniae* infection, and limits exacerbated inflammatory cell recruitment leading to tissue damage ¹²¹ (**Figure 1.4b**).

Aging also leads to an accumulation of unfolded and misfolded proteins in the endoplasmic reticulum (ER) lumen, inducing an **unfolded protein response (UPR)** that can impair immune signaling. As a result of UPR activity, aged macrophages show defective ‘NLR family pyrin domain containing 3’ (NLRP3) inflammasome activation during *S. pneumoniae* infection ¹²². Enhanced ER stress can also inhibit macrophage response to *S. pneumoniae* through activity of the autophagy-related gene 9 (Atg9a) ¹²³. Treatment with the ER stress-reducing agent tauroursodeoxycholic acid (TUDCA), or with the nucleoside metabolic inhibitor gemcitabine to suppress Atg9a expression, effectively restores bactericidal activity against *S. pneumoniae* in aged macrophages ^{122,123} (**Figure 1.4b**). Therapeutic interventions that promote autophagy may help restore the autophagic response to *S. pneumoniae* in aged macrophages, in contrast to promoting autophagy in otherwise healthy (non-aged) macrophages as described above. Similar strategies can be employed against other autophagy-inducing pathogens that show increased virulence in the elderly, including *Legionella pneumophila*, *Listeria monocytogenes*, and *M. tuberculosis* ¹²⁴⁻¹²⁶.

Neutrophil function is known to decline with age, displaying diminished phagocytosis, reactive oxygen production, neutrophil extracellular trap formation, and chemotaxis ¹²⁷⁻¹²⁹. Upon cellular insult, including pneumococcal infection, ATP is released from cells and metabolized to extracellular adenosine (EAD). EAD is recognized by EAD A1 receptors expressed on neutrophils to regulate intracellular killing required for effective neutrophil-mediated clearance. Pharmacological or genetic driven increase of EAD production (e.g. through inhibition of EAD-degrading adenosine deaminase) rescues age-related neutrophil defects in pneumococcal killing ¹⁹, inhibits IL-10 production ¹³⁰, reduces epithelial PAFr expression, and limits *S. pneumoniae* invasion ¹³¹ (**Figure 1.4b**). Moreover, since the EAD response is also triggered by pathogens other than *S. pneumoniae* ¹³², EAD supplementation may be effective in limiting pathologic inflammation in the context of other bacterial infections in the elderly population.

1.6 Overview of this thesis

In this thesis, we use *Streptococcus pneumoniae*, the gram-positive pathogen responsible for the majority of bacterial respiratory tract infections worldwide, as a case study to:

Chapter 2 | Generate a genome-wide map of bacterial immune (complement) evasion targets and use findings to design novel host-informed therapies.

Chapter 3 | Generate a dual host/pathogen transcriptome map to identify signatures of infection outcome.

Chapter 4 | Validate signatures of bacterial antibiotic resistance/tolerance in a murine lung infection model.

Overall, this work exemplifies how multi-omics methods can elucidate the intricacies of bacterial pathogenesis but, more importantly, aid in the target identification, validation, and rational design of novel antibacterial host-informed therapies.

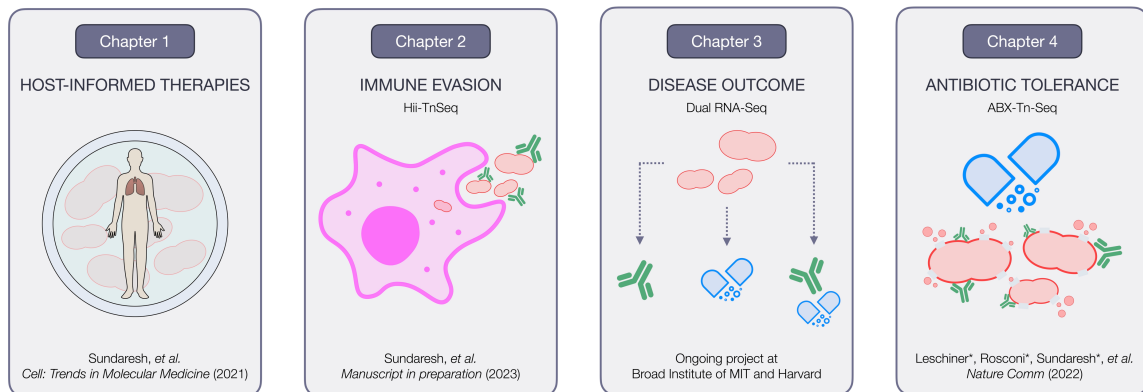


Figure 1.5 | Graphical overview of this thesis.

This thesis seeks to answer two key questions: (1) How does a bacterium escape the host immune response on a phenotypic and transcriptomic level? and (2) What are bacterial and host signatures of an infection on a phenotypic and transcriptomic level? Accomplishments from this thesis contribute to the (1) target identification, validation, and rational design of novel antibacterial host-informed therapies (HITs) and (2) methods to identify bacterial and host markers for application in clinical diagnostics and prognostics.

1.7 Glossary

Term	Definition
Antipyretic effect	A substance that reduces fever, by causing the hypothalamus to override a prostaglandin-induced increase in temperature and the body thereby works to lower overall temperature.
Canonical (non-selective) autophagy	Regulated mechanism of eukaryotic cells that removes unnecessary or dysfunctional components; a well-conserved lysosomal degradation pathway that plays a key role in combatting bacterial infections.
Capsular serotype	<i>S. pneumoniae</i> capsular polysaccharides are composed of repeating units of oligosaccharides. Based on chemical structure, >90 distinct capsular serotypes can be defined.
Complement system	Arm of the immune system that enhances the ability of antibodies and phagocytic cells to clear microbes and damaged cells, promote inflammation, and attack the pathogen cell surface.
Endotoxemia	Systemic inflammation. A lethal proinflammatory condition characterized by high blood levels of TNF- α , IL-1, IL-6, MIF, and other proinflammatory cytokines.
Factor H	155 kDa glycoprotein and member of the regulators of complement activation family and a vital complement control protein.
Host-informed therapy (HIT)	Defined here as existing and proposed therapies specifically designed with the state of the host in mind, tailored to either intact or perturbed immune processes resulting from unique host susceptibilities to bacterial disease.
Neuraminidase	Influenza A virus surface glycoprotein on the virion surface and a main target for host neutralizing antibodies.
PB1-F2	90 amino acid protein expressed in influenza A viruses; implicated in viral pathogenicity including cell death, immunopathology, and induction of host proinflammatory responses.
Immunosenescence	A decline in cell-mediated immunity (i.e., phagocytic cells, such as neutrophils/macrophages) associated with old age.
Inflamming	Chronic elevation of basal and induced inflammation associated with old age.
LC3-associated phagocytosis (LAP)	LAP combines the molecular machinery of phagocytosis with that of autophagy, resulting in LC3-decorated phagosomes or LAPosomes which show enhanced fusion with lysosomes resulting in enhanced killing and degradation of contained pathogens within the LAPosomes.
Opsonization	Molecular mechanism whereby pathogenic molecules, microbes (bacteria/virus/fungi), or apoptotic cells are marked by host antibodies, complement, or other proteins. This "marking" allows recognition and attachment to cell surface receptors on phagocytic or NK cells to facilitate clearance.
Platelet-activating factor (PAF)	Phospholipid activator that mediates leukocyte functions, platelet aggregation and degranulation, and inflammation. PAF is produced by numerous cells involved in host defense, including platelets, endothelial cells, neutrophils, monocytes, and macrophages.
Platelet-activating factor receptor (PAFr)	G-protein coupled receptor which binds platelet-activating factor (PAF).
Pneumococcal polysaccharide vaccine	23-valent pneumococcal polysaccharide vaccine (PPSV23; Pneumovax, Merck) covering 23 <i>S. pneumoniae</i> virulent serotypes; licensed in 1983 and recommended for patients aged 65 years and older or 2-64 years of age with preexisting health conditions such as chronic heart/lung disease, SCD, HIV infection, or immunosuppression.
Pneumococcal protein-conjugated polysaccharide vaccine	Pneumococcal vaccines based on protein-conjugated polysaccharides (PCV13 and PCV23/Prevnar, Pfizer); routinely given to children at 2, 4, 6, and 12-15 months of age, recommended for children and adults 2-64 years of age with certain health conditions, and for all adults 65 years of age and older.

Th17-mediated immunity	Distinguished by the production of interleukin-17 (IL-17), Th17 cells develop from Th progenitors under the influence of a network of inflammatory cytokines, including IL-1, IL-6, and TGF- β . The Th17 response is critical in host defense against extracellular pathogens, particularly bacteria that colonize mucosal surfaces, including <i>S. pneumoniae</i> .
Toll-like receptor 4 (TLR4)	Toll-like receptors (TLRs) are pattern recognition receptors (PRRs), a key component of innate immunity. TLR4 specifically recognizes bacterial lipopolysaccharide (LPS), along with several other components of pathogens and endogenous molecules produced during insult (i.e., tissue damage).
Type I interferon (IFN-I) antiviral response	Pleiotropic cytokines that trigger antiviral states in cells and potentiate adaptive immune responses. Upon induction in the innate immune response, IFN-I triggers the expression of interferon-stimulated genes which upregulate the effector function of immune cells (such as dendritic cells, B cells, T cells) toward the successful clearance of infections.
Unfolded protein response (UPR)	Changes in the function of the endoplasmic reticulum in host cells can result in the accumulation of unfolded/misfolded proteins, referred to as ER stress. ER stress engages the UPR, an adaptive reaction that reduced unfolded protein load to maintain cellular functions and viability.

1.8 References

1. Bucktrout, S.L. et al. (2018) Recent advances in immunotherapies: from infection and autoimmunity, to cancer, and back again. *Genome Med* 10 (1), 79.
2. Kaufmann, S.H.E. et al. (2018) Host-directed therapies for bacterial and viral infections. *Nat Rev Drug Discov* 17 (1), 35-56.
3. Naran, K. et al. (2018) Principles of Immunotherapy: Implications for Treatment Strategies in Cancer and Infectious Diseases. *Front Microbiol* 9, 3158.
4. Masomian, M. et al. (2020) Development of Next Generation Streptococcus pneumoniae Vaccines Conferring Broad Protection. *Vaccines (Basel)* 8 (1).
5. Cremers, A.J. et al. (2015) The post-vaccine microevolution of invasive Streptococcus pneumoniae. *Sci Rep* 5, 14952.
6. Moore, M.R. et al. (2008) Population snapshot of emergent Streptococcus pneumoniae serotype 19A in the United States, 2005. *J Infect Dis* 197 (7), 1016-27.
7. Farrell, D.J. et al. (2007) Increased antimicrobial resistance among nonvaccine serotypes of Streptococcus pneumoniae in the pediatric population after the introduction of 7-valent pneumococcal vaccine in the United States. *Pediatr Infect Dis J* 26 (2), 123-8.
8. Kislak, J.W. et al. (1965) Susceptibility of pneumococci to nine antibiotics. *Am J Med Sci* 250 (3), 261-8.
9. Anderson, P. and Betts, R. (1989) Human adult immunogenicity of protein-coupled pneumococcal capsular antigens of serotypes prevalent in otitis media. *Pediatr Infect Dis J* 8 (1 Suppl), S50-3.
10. Negash, A.A. et al. (2021) Phenotypic and Molecular Characterization of Penicillin and Macrolide-Resistant Streptococcus pneumoniae Serotypes Among Pediatric Patients in Addis Ababa, Ethiopia. *Infect Drug Resist* 14, 1765-1772.
11. Jones, R.N. et al. (2013) Update on antimicrobial susceptibility trends among Streptococcus pneumoniae in the United States: report of ceftaroline activity from the SENTRY Antimicrobial Surveillance Program (1998-2011). *Diagn Microbiol Infect Dis* 75 (1), 107-9.
12. Jacobs, M.R. et al. (1978) Emergence of multiply resistant pneumococci. *N Engl J Med* 299 (14), 735-40.
13. Nava, J.M. et al. (1994) Predictive factors for invasive disease due to penicillin-resistant Streptococcus pneumoniae: a population-based study. *Clin Infect Dis* 19 (5), 884-90.

14. GBD 2019 Diseases and Injuries Collaborators (2020). Global burden of 369 diseases and injuries in 204 countries and territories, 1990-2019: a systematic analysis for the Global Burden of Disease Study 2019. *Lancet* 396, 1204–1222.
15. Weiser, J.N. et al. (2018) *Streptococcus pneumoniae*: transmission, colonization and invasion. *Nat Rev Microbiol* 16 (6), 355-367.
16. Xu, F. et al. (2008) Modulation of the inflammatory response to *Streptococcus pneumoniae* in a model of acute lung tissue infection. *Am J Respir Cell Mol Biol* 39 (5), 522-9.
17. Garvy, B.A. and Harmsen, A.G. (1996) The importance of neutrophils in resistance to pneumococcal pneumonia in adult and neonatal mice. *Inflammation* 20 (5), 499-512.
18. Bhowmick, R. et al. (2013) Systemic disease during *Streptococcus pneumoniae* acute lung infection requires 12-lipoxygenase-dependent inflammation. *J Immunol* 191 (10), 5115-23.
19. Bou Ghanem, E.N. et al. (2015) Extracellular Adenosine Protects against *Streptococcus pneumoniae* Lung Infection by Regulating Pulmonary Neutrophil Recruitment. *PLoS Pathog* 11 (8), e1005126.
20. de Gans, J. et al. (2002) Dexamethasone in adults with bacterial meningitis. *N Engl J Med* 347 (20), 1549-56.
21. Chalmers, J.D. (2016) Corticosteroids for community-acquired pneumonia: a critical view of the evidence. *Eur Respir J* 48 (4), 984-986.
22. Siemieniuk, R.A. et al. (2015) Corticosteroid Therapy for Patients Hospitalized With Community-Acquired Pneumonia: A Systematic Review and Meta-analysis. *Ann Intern Med* 163 (7), 519-28.
23. Blum, C.A. et al. (2015) Adjunct prednisone therapy for patients with community-acquired pneumonia: A multicentre, double-blind, randomised, placebo-controlled trial. *The Lancet*.
24. Torres, A. et al. (2015) Effect of corticosteroids on treatment failure among hospitalized patients with severe community-acquired pneumonia and high inflammatory response: A randomized clinical trial. *JAMA - Journal of the American Medical Association*.
25. Nie, W. et al. (2012) Corticosteroids in the treatment of community-acquired pneumonia in adults: a meta-analysis. *PLoS One* 7 (10), e47926.
26. Confalonieri, M. et al. (2005) Hydrocortisone infusion for severe community-acquired pneumonia: a preliminary randomized study. *Am J Respir Crit Care Med* 171 (3), 242-8.

27. Tagami, T. et al. (2015) Low-dose corticosteroid use and mortality in severe community-acquired pneumonia patients. *Eur Respir J* 45 (2), 463-72.
28. Thwaites, G. et al. (2009) British Infection Society guidelines for the diagnosis and treatment of tuberculosis of the central nervous system in adults and children. *J Infect* 59 (3), 167-87.
29. Troeman, D.P. et al. (2013) The immunomodulatory effects of statins in community-acquired pneumonia: a systematic review. *J Infect* 67 (2), 93-101.
30. Yende, S. et al. (2011) Understanding the potential role of statins in pneumonia and sepsis. *Critical Care Medicine*.
31. Hackam, D.G. et al. (2006) Statins and sepsis in patients with cardiovascular disease: A population-based cohort analysis. *Lancet*.
32. Myles, P.R. et al. (2009) Risk of community-acquired pneumonia and the use of statins, ace inhibitors and gastric acid suppressants: a population-based case-control study. *Pharmacoepidemiol Drug Saf* 18 (4), 269-75.
33. Mortensen, E.M. et al. (2005) The effect of prior statin use on 30-day mortality for patients hospitalized with community-acquired pneumonia. *Respir Res* 6, 82.
34. Thomas, G. et al. (2015) Statin therapy in critically-ill patients with severe sepsis: a review and meta-analysis of randomized clinical trials. *Minerva Anesthesiol* 81 (8), 921-30.
35. Kruger, P. et al. (2013) A multicenter randomized trial of atorvastatin therapy in intensive care patients with severe sepsis. *Am J Respir Crit Care Med* 187 (7), 743-50.
36. Karlström, A. et al. (2011) Toll-like receptor 2 mediates fatal immunopathology in mice during treatment of secondary pneumococcal pneumonia following influenza. *Journal of Infectious Diseases*.
37. Sligl, W.I. et al. (2014) Macrolides and mortality in critically ill patients with community-acquired pneumonia: a systematic review and meta-analysis. *Crit Care Med* 42 (2), 420-32.
38. Yu, X. et al. (2019) Impact of metformin on the risk and treatment outcomes of tuberculosis in diabetics: a systematic review. *BMC Infect Dis* 19 (1), 859.
39. Garnett, J.P. et al. (2013) Metformin reduces airway glucose permeability and hyperglycaemia-induced *Staphylococcus aureus* load independently of effects on blood glucose. *Thorax* 68 (9), 835-45.
40. Othman, A.A. et al. (2016) Atorvastatin and metformin administration modulates experimental *Trichinella spiralis* infection. *Parasitol Int* 65 (2), 105-12.

41. Brima, W. et al. (2015) The brighter (and evolutionarily older) face of the metabolic syndrome: evidence from *Trypanosoma cruzi* infection in CD-1 mice. *Diabetes Metab Res Rev* 31 (4), 346-359.
42. Muri, L. et al. (2019) Metformin mediates neuroprotection and attenuates hearing loss in experimental pneumococcal meningitis. *Journal of Neuroinflammation*.
43. Tsoyi, K. et al. (2011) Metformin inhibits HMGB1 release in LPS-treated RAW 264.7 cells and increases survival rate of endotoxaemic mice. *Br J Pharmacol* 162 (7), 1498-508.
44. Ferrer, M. et al. (1997) Effect of acetylsalicylic acid on pulmonary gas exchange in patients with severe pneumonia: A pilot study. *Chest*.
45. Kotsiou, O.S. et al. (2017) Prehospital NSAIDs use prolong hospitalization in patients with pleuro-pulmonary infection. *Respir Med* 123, 28-33.
46. Smith, C.E. et al. (2017) Non-steroidal Anti-inflammatory Drugs Are Caspase Inhibitors. *Cell Chem Biol* 24 (3), 281-292.
47. Yin, Z. et al. (2014) DNA replication is the target for the antibacterial effects of nonsteroidal anti-inflammatory drugs. *Chem Biol* 21 (4), 481-487.
48. Bernard, G.R. et al. (1997) The effects of ibuprofen on the physiology and survival of patients with sepsis. *New England Journal of Medicine*.
49. Sodhi, M. et al. (2020) Non-steroidal Anti-inflammatory Drugs and the Risk of Pneumonia Complications: A Systematic Review. *Pharmacotherapy* 40 (9), 970-977.
50. Hyams, C. et al. (2010) The *Streptococcus pneumoniae* capsule inhibits complement activity and neutrophil phagocytosis by multiple mechanisms. *Infect Immun* 78 (2), 704-15.
51. Hovingh, E.S. et al. (2016) Hijacking Complement Regulatory Proteins for Bacterial Immune Evasion. *Front Microbiol* 7, 2004.
52. Ali, Y.M. et al. (2012) The lectin pathway of complement activation is a critical component of the innate immune response to pneumococcal infection. *PLoS Pathog* 8 (7), e1002793.
53. Munoz-Almagro, C. et al. (2014) High prevalence of genetically-determined mannose binding lectin deficiency in young children with invasive pneumococcal disease. *Clin Microbiol Infect* 20 (10), O745-52.
54. Petersen, K.A. et al. (2006) Phase I safety, tolerability, and pharmacokinetic study of recombinant human mannan-binding lectin. *J Clin Immunol* 26 (5), 465-75.

55. Guo, J. et al. (2015) Limited effect of recombinant human mannose-binding lectin on the infection of novel influenza A (H7N9) virus in vitro. *Biochem Biophys Res Commun* 458 (1), 77-81.
56. de Gouw, D. et al. (2014) The vaccine potential of *Bordetella pertussis* biofilm-derived membrane proteins. *Emerg Microbes Infect* 3 (8), e58.
57. Stranger-Jones, Y.K. et al. (2006) Vaccine assembly from surface proteins of *Staphylococcus aureus*. *Proc Natl Acad Sci U S A* 103 (45), 16942-7.
58. Pathak, A. et al. (2018) Factor H binding proteins protect division septa on encapsulated *Streptococcus pneumoniae* against complement C3b deposition and amplification. *Nature Communications*.
59. Moreno, A.T. et al. (2012) Cross-reactivity of antipneumococcal surface protein C (PspC) antibodies with different strains and evaluation of inhibition of human complement factor H and secretory IgA binding via PspC. *Clin Vaccine Immunol* 19 (4), 499-507.
60. Nakahashi-Ouchida, R. et al. (2021) A nanogel-based trivalent PspA nasal vaccine protects macaques from intratracheal challenge with pneumococci. *Vaccine* 39 (25), 3353-3364.
61. Chan, W.Y. et al. (2019) A Novel, Multiple-Antigen Pneumococcal Vaccine Protects against Lethal *Streptococcus pneumoniae* Challenge. *Infect Immun* 87 (3).
62. Godfroid, F. et al. (2011) Preclinical evaluation of the Pht proteins as potential cross-protective pneumococcal vaccine antigens. *Infect Immun* 79 (1), 238-45.
63. Day, C.J. et al. (2017) Lectin activity of the pneumococcal pilin proteins. *Sci Rep* 7 (1), 17784.
64. Gerard, C. (2003) Complement C5a in the sepsis syndrome--too much of a good thing? *N Engl J Med* 348 (2), 167-9.
65. Karasu, E. et al. (2019) Targeting Complement Pathways in Polytrauma- and Sepsis-Induced Multiple-Organ Dysfunction. *Front Immunol* 10, 543.
66. Tahir, F. et al. (2020) Anti-tuberculous Effects of Statin Therapy: A Review of Literature. *Cureus* 12 (3), e7404.
67. Nagy, T.A. et al. (2019) Autophagy induction by a small molecule inhibits *Salmonella* survival in macrophages and mice. *Antimicrobial Agents and Chemotherapy* 63 (12).
68. Cole, J. et al. (2021) Pneumolysin Is Responsible for Differential Gene Expression and Modifications in the Epigenetic Landscape of Primary Monocyte Derived Macrophages. *Front Immunol* 12, 573266.

69. Li, P. et al. (2015) *Streptococcus pneumoniae* induces autophagy through the inhibition of the PI3K-I/Akt/mTOR pathway and ROS hypergeneration in A549 cells. *PLoS ONE* 10 (3).
70. Ogawa, M. et al. (2020) *Streptococcus pneumoniae* triggers hierarchical autophagy through reprogramming of LAPosome-like vesicles via NDP52-delocalization. *Communications Biology* 3 (1).
71. Inomata, M. et al. (2020) Macrophage LC3-associated phagocytosis is an immune defense against *Streptococcus pneumoniae* that diminishes with host aging. *Proc Natl Acad Sci U S A* 117 (52), 33561-33569.
72. Shizukuishi, S. et al. (2020) *Streptococcus pneumoniae* hijacks host autophagy by deploying CbpC as a decoy for Atg14 depletion. *EMBO reports*.
73. Diao, J. et al. (2015) ATG14 promotes membrane tethering and fusion of autophagosomes to endolysosomes. *Nature* 520 (7548), 563-6.
74. Subramanian, K. et al. (2020) Mannose receptor-derived peptides neutralize pore-forming toxins and reduce inflammation and development of pneumococcal disease. *EMBO Mol Med*, e12695.
75. Surve, M.V. et al. (2018) Heterogeneity in pneumolysin expression governs the fate of *Streptococcus pneumoniae* during blood-brain barrier trafficking. *PLoS Pathogens* 14 (7).
76. Salha, D. et al. (2012) Neutralizing antibodies elicited by a novel detoxified pneumolysin derivative, PlyD1, provide protection against both pneumococcal infection and lung injury. *Infect Immun* 80 (6), 2212-20.
77. Shu, Z. et al. (2020) *Streptococcus pneumoniae* PepO promotes host anti-infection defense via autophagy in a Toll-like receptor 2/4 dependent manner. *Virulence* 11 (1), 270-282.
78. Nader, D. et al. (2020) A new perspective in sepsis treatment: could RGD-dependent integrins be novel targets? *Drug Discov Today* 25 (12), 2317-2325.
79. Takada, Y. et al. (2007) The integrins. *Genome Biol* 8 (5), 215.
80. Voss, S. et al. (2013) The choline-binding protein PspC of *Streptococcus pneumoniae* interacts with the C-terminal heparin-binding domain of vitronectin. *J Biol Chem* 288 (22), 15614-27.
81. Garcarena, C.D. et al. (2017) Pre-emptive and therapeutic value of blocking bacterial attachment to the endothelial alphaVbeta3 integrin with cilengitide in sepsis. *Crit Care* 21 (1), 246.

82. Blevins, L.K. et al. (2014) Coinfection with *Streptococcus pneumoniae* negatively modulates the size and composition of the ongoing influenza-specific CD8(+) T cell response. *J Immunol* 193 (10), 5076-87.
83. Shirey, K.A. et al. (2019) Influenza “Trains” the host for enhanced susceptibility to secondary bacterial infection. *mBio*.
84. Nakamura, S. et al. (2011) Synergistic stimulation of type I interferons during influenza virus coinfection promotes *Streptococcus pneumoniae* colonization in mice. *Journal of Clinical Investigation*.
85. Shahangian, A. et al. (2009) Type I IFNs mediate development of postinfluenza bacterial pneumonia in mice. *Journal of Clinical Investigation*.
86. Kudva, A. et al. (2011) Influenza A Inhibits Th17-Mediated Host Defense against Bacterial Pneumonia in Mice. *The Journal of Immunology*.
87. Cao, J. et al. (2014) Activation of IL-27 signalling promotes development of postinfluenza pneumococcal pneumonia. *EMBO Molecular Medicine*.
88. Robinson, K.M. et al. (2015) The role of IL-27 in susceptibility to post-influenza *Staphylococcus aureus* pneumonia. *Respiratory Research*.
89. Barthelemy, A. et al. (2017) Influenza A virus-induced release of interleukin-10 inhibits the anti-microbial activities of invariant natural killer T cells during invasive pneumococcal superinfection. *Mucosal Immunol* 10 (2), 460-469.
90. Matos, A.D.R. et al. (2019) Antiviral potential of human IFN- α subtypes against influenza A H3N2 infection in human lung explants reveals subtype-specific activities. *Emerg Microbes Infect* 8 (1), 1763-1776.
91. Shepardson, K.M. et al. (2018) IFNAR2 Is Required for Anti-influenza Immunity and Alters Susceptibility to Post-influenza Bacterial Superinfections. *Front Immunol* 9, 2589.
92. Shepardson, K.M. et al. (2016) Differential Type I Interferon Signaling Is a Master Regulator of Susceptibility to Postinfluenza Bacterial Superinfection. *mBio* 7 (3).
93. Gou, X. et al. (2019) IL-6 During Influenza-*Streptococcus pneumoniae* Co-Infected Pneumonia-A Protector. *Front Immunol* 10, 3102.
94. Small, C.L. et al. (2010) Influenza infection leads to increased susceptibility to subsequent bacterial superinfection by impairing NK cell responses in the lung. *J Immunol* 184 (4), 2048-56.
95. LeMessurier, K.S. et al. (2020) Respiratory Barrier as a Safeguard and Regulator of Defense Against Influenza A Virus and *Streptococcus pneumoniae*. *Front Immunol* 11, 3.

96. Park, S.S. et al. (2021) Streptococcus pneumoniae binds to host GAPDH on dying lung epithelial cells worsening secondary infection following influenza. *Cell Rep* 35 (11), 109267.
97. Talmi-Frank, D. et al. (2016) Extracellular Matrix Proteolysis by MT1-MMP Contributes to Influenza-Related Tissue Damage and Mortality. *Cell Host Microbe* 20 (4), 458-470.
98. Short, K.R. et al. (2016) Influenza virus damages the alveolar barrier by disrupting epithelial cell tight junctions. *European Respiratory Journal*.
99. Peter, A. et al. (2017) Localization and pneumococcal alteration of junction proteins in the human alveolar-capillary compartment. *Histochemistry and Cell Biology*.
100. McCullers, Jonathan A. and Rehg, Jerold E. (2002) Lethal Synergism between Influenza Virus and Streptococcus pneumoniae: Characterization of a Mouse Model and the Role of Platelet-Activating Factor Receptor. *The Journal of Infectious Diseases*.
101. McCullers, Jonathan A. and Bartmess, Kimberly C. (2003) Role of Neuraminidase in Lethal Synergism between Influenza Virus and Streptococcus pneumoniae. *The Journal of Infectious Diseases*.
102. Treanor, J.J. et al. (2000) Efficacy and safety of the oral neuraminidase inhibitor oseltamivir in treating acute influenza: A randomized controlled trial. *Journal of the American Medical Association*.
103. Whitley, R.J. et al. (2001) Oral oseltamivir treatment of influenza in children. *Pediatric Infectious Disease Journal*.
104. McAuley, J.L. et al. (2010) The Effects of Influenza A Virus PB1-F2 Protein on Polymerase Activity Are Strain Specific and Do Not Impact Pathogenesis. *Journal of Virology*.
105. McAuley, J.L. et al. (2007) Expression of the 1918 influenza A virus PB1-F2 enhances the pathogenesis of viral and secondary bacterial pneumonia. *Cell Host Microbe* 2 (4), 240-9.
106. Dayie, N.T.K.D. et al. (2018) Pneumococcal carriage among sickle cell disease patients in Accra, Ghana: Risk factors, serotypes and antibiotic resistance. *PLoS ONE*.
107. Richter, S.S. et al. (2013) Pneumococcal serotypes before and after introduction of conjugate vaccines, United States, 1999-2011(1.). *Emerg Infect Dis* 19 (7), 1074-83.
108. Carter, R. et al. (2014) Genomic analyses of pneumococci from children with sickle cell disease expose host-specific bacterial adaptations and deficits in current interventions. *Cell Host and Microbe*.

109. Greene, C.J. et al. (2016) Novel Strategy To Protect against Influenza Virus-Induced Pneumococcal Disease without Interfering with Commensal Colonization. *Infect Immun* 84 (6), 1693-1703.
110. Miller, Martha L. et al. (2007) Hypersusceptibility to Invasive Pneumococcal Infection in Experimental Sickle Cell Disease Involves Platelet-Activating Factor Receptor. *The Journal of Infectious Diseases*.
111. Hosoki, K. et al. (2012) Staphylococcus aureus directly activates eosinophils via platelet-activating factor receptor. *Journal of Leukocyte Biology*.
112. Brooks, L.R.K. and Mias, G.I. (2018) Streptococcus pneumoniae's Virulence and Host Immunity: Aging, Diagnostics, and Prevention. *Front Immunol* 9, 1366.
113. Weight, C.M. et al. (2021) Insights Into the Effects of Mucosal Epithelial and Innate Immune Dysfunction in Older People on Host Interactions With Streptococcus pneumoniae. *Front Cell Infect Microbiol* 11, 651474.
114. Frasca, D. and Blomberg, B.B. (2016) Inflammaging decreases adaptive and innate immune responses in mice and humans. *Biogerontology* 17 (1), 7-19.
115. Williams, A.E. et al. (2015) Enhanced inflammation in aged mice following infection with Streptococcus pneumoniae is associated with decreased IL-10 and augmented chemokine production. *American Journal of Physiology - Lung Cellular and Molecular Physiology*.
116. Puchta, A. et al. (2016) TNF Drives Monocyte Dysfunction with Age and Results in Impaired Anti-pneumococcal Immunity. *PLoS Pathogens*.
117. Panemangalore, M. and Chung Ja, L. (1992) Evaluation of the indices of retinol and α -tocopherol status in free-living elderly. *Journals of Gerontology*.
118. Bou Ghanem, E.N. et al. (2015) The alpha-tocopherol form of vitamin E reverses age-associated susceptibility to streptococcus pneumoniae lung infection by modulating pulmonary neutrophil recruitment. *J Immunol* 194 (3), 1090-9.
119. Ghanem, E.N.B. et al. (2017) The alpha-tocopherol form of vitamin E boosts elastase activity of human PMNs and their ability to kill streptococcus pneumoniae. *Frontiers in Cellular and Infection Microbiology*.
120. Hemila, H. (2016) Vitamin E administration may decrease the incidence of pneumonia in elderly males. *Clin Interv Aging* 11, 1379-1385.
121. Plataki, M. et al. (2019) Mitochondrial Dysfunction in Aged Macrophages and Lung during Primary Streptococcus pneumoniae Infection is Improved with Pirfenidone. *Sci Rep* 9 (1), 971.

122. Cho, S.J. et al. (2018) NLRP3 inflammasome activation in aged macrophages is diminished during *Streptococcus pneumoniae* infection. *Am J Physiol Lung Cell Mol Physiol* 314 (3), L372-L387.
123. Mitzel, D.N. et al. (2014) Age-enhanced endoplasmic reticulum stress contributes to increased Atg9A inhibition of STING-mediated IFN-beta production during *Streptococcus pneumoniae* infection. *J Immunol* 192 (9), 4273-83.
124. Sopena, N. et al. (2007) Community-acquired legionella pneumonia in elderly patients: characteristics and outcome. *J Am Geriatr Soc* 55 (1), 114-9.
125. Domingo, P. et al. (2013) The spectrum of acute bacterial meningitis in elderly patients. *BMC Infect Dis* 13, 108.
126. Guerra-Laso, J.M. et al. (2013) Macrophages from elders are more permissive to intracellular multiplication of *Mycobacterium tuberculosis*. *Age (Dordr)* 35 (4), 1235-50.
127. Bou Ghanem, E.N. et al. (2018) Nasopharyngeal Exposure to *Streptococcus pneumoniae* Induces Extended Age-Dependent Protection against Pulmonary Infection Mediated by Antibodies and CD138 + Cells. *The Journal of Immunology*.
128. Simell, B. et al. (2011) Aging reduces the functionality of anti-pneumococcal antibodies and the killing of *Streptococcus pneumoniae* by neutrophil phagocytosis. *Vaccine* 29 (10), 1929-34.
129. Wensch, C. et al. (2000) Effect of age on human neutrophil function. *Journal of Leukocyte Biology*.
130. Siwapornchai, N. et al. (2020) Extracellular adenosine enhances the ability of PMNs to kill *Streptococcus pneumoniae* by inhibiting IL-10 production. *J Leukoc Biol*.
131. Bhalla, M. et al. (2020) A1 adenosine receptor signaling reduces *Streptococcus pneumoniae* adherence to pulmonary epithelial cells by targeting expression of platelet-activating factor receptor. *Cell Microbiol* 22 (2), e13141.
132. Barletta, K.E. et al. (2012) Adenosine A(2B) receptor deficiency promotes host defenses against gram-negative bacterial pneumonia. *Am J Respir Crit Care Med* 186 (10), 1044-50.

2

Immune evasion:

Bacterial genomic profiling reveals
novel routes to complement evasion
and targeted therapeutic strategies

Bharathi Sundaresh*, Federico Rosconi, Mara Shainheit, Jason W. Rosch
and Tim van Opijnen

*First author contribution

Manuscript in preparation

Author's contributions: B.S. performed all experiments, data collection, data analysis, data interpretation, and wrote the chapter. B.S. and T.v.O. devised the study. F.R., M.S., J.W.R., and T.v.O. contributed to key conceptual ideas. All authors contributed to manuscript editing before submission.

2.1 Summary

Complement activation is a critical first line of defense against bacterial pathogens. Individuals with complement deficiencies are more sensitive to invasive infections by gram-positive bacteria such as *Streptococcus pneumoniae*. During the innate immune response, bacteria are first opsonized, or marked, for phagocytosis by the major complement protein C3 which triggers recognition and engulfment by neutrophils recruited to the site of infection. Activation of the innate receptors on the surface of neutrophils initiates antimicrobial mechanisms, ultimately destroying the pathogen. *S. pneumoniae* has numerous mechanisms to avoid C3 complement deposition, of which we only possess a limited understanding. Combining an in vitro C3 deposition assay, FACS selection, and Tn-Seq, we developed a robust method, host-immune-interaction-Tn-Seq, or Hii-TnSeq, to obtain a high-resolution, genome-wide understanding of the surface proteins and associated molecular pathways used by the bacterial pathogen to avoid complement deposition. Specifically, we show that *S. pneumoniae* has multiple previously uncharacterized gene products that impede C3 deposition on the bacterial cell surface, including the pilus-1 protein, a putative C3-degrading protease, and the thiamine pyrophosphokinase. In vivo targeted therapeutic studies demonstrate that directed antibodies against two identified proteins reduce the bacterial burden to non-lethal levels. In conclusion, we identified and validated newly identified *S. pneumoniae* surface proteins involved in complement evasion, and we demonstrated that these proteins are suitable targets for developing targeted antimicrobial therapies.

2.2 Introduction

Although vaccines and antibiotics have been historically successful in combating bacterial infections, limited vaccine coverage and the rise of antibiotic resistance emphasize the need to develop alternative strategies to reduce the health burden of bacterial infections. Most pathogenic bacterial species express surface proteins of which a subset is involved in avoiding detection and/or immune clearance by the host. Importantly, their surface localization makes them in principle directly targetable and accessible to immune components. This suggests that if these bacterial proteins could be efficiently targeted, for instance with an antibody-based therapeutic, we could restore bacterial detection by the host immune system, a strategy known as an immunostimulatory host-informed therapy (HIT) ¹⁻⁴.

Bacteria have developed a myriad of mechanisms and strategies to evade host immune machinery and promote their survival and proliferation ⁵. Complement evasion is one of the most common immune evasion strategies ^{6,7}. Complement activation starts through one of three cascade pathways (classical, mannose-lectin, and alternative) that converge at the level of C3 convertase formation and result in the cleavage of the central C3 molecule ⁸. Amplification of C3 deposition occurs via the alternative pathway C3 convertase, which also promotes the formation of C5 convertases directing the cleavage of C5 into C5a and C5b. C5a is a potent anaphylatoxin that recruits inflammatory cells, specifically neutrophils. Following neutrophil arrival, neutrophil-mediated opsonophagocytic killing, or NMOK, is initiated. First, innate receptors on neutrophils' surfaces recognize C3 opsonized bacteria triggering their engulfment, after which antimicrobial factors destroy internalized bacteria in the phagolysosome ^{9,10}. Activation of any of the three complement pathways partially depends on bacterial-encoded surface proteins necessary for mediating the first and critical step of NMOK. Gram-negative and gram-positive pathogens mask their surface antigens with a carbohydrate capsule or alter their surface lipids to avoid complement deposition.

The human bacterial pathogen *Streptococcus pneumoniae*, a major cause of community-acquired pneumonia and mortality, is an excellent example of a bacterial pathogen capable of successfully evading complement. Annually, ~1 million children (<5 years of

age) and ~0.5M immunocompromised individuals (e.g., elderly, patients with primary and secondary immunodeficiencies) succumb to *S. pneumoniae* infections ¹¹, making it an important global pathogen. In industrialized countries, nearly every child experiences an ear infection before the age of 5; approximately 30-50% of which are caused by *S. pneumoniae* ¹². This results in ~25 million medical visits and accounts for ~\$3 billion spent annually on treatments ¹³. *S. pneumoniae* especially remains a threat to patients with complement deficiencies (e.g., multiple myeloma, Sickle Cell Disease) and impaired neutrophil function (e.g., Chediak-Higashi syndrome), but we lack a clear understanding of the interplay between impaired innate immune function and the pathogen. To evade complement attack, *S. pneumoniae* has evolved multiple virulence factors contributing to complement resistance including the thick polysaccharide capsule, PspA and PspC ^{14,15} to inhibit C3 convertase formation and LytA to reduce opsonization by C3b ^{16,17}. While these factors have been identified as contributing to C3 inhibition, we continue to be short of a complete understanding of bacterial proteins involved at the *S. pneumoniae*-C3 interface.

In this study, we use an in vitro C3 deposition assay and FACS enrichment in combination with Tn-Seq ¹⁸ (Host-immune-interaction-Tn-Seq; **Hii-TnSeq**) to generate a genome-wide understanding of complement deposition evasion in *S. pneumoniae* ¹⁹. We benchmark our method and analysis with numerous validations, including in vitro growth and in vitro C3 deposition of single-gene knockout strains. By combining Hii-TnSeq data with in vivo-infection Tn-Seq data, we predict a panel of C3 evasion factors in *S. pneumoniae* and experimentally validate them ex vivo and during an in vivo mouse infection. Most notable novel genetic mechanisms of complement evasion include gene products involved in degradation pathways, bacterial pilus formation, and the thiamine salvage pathway. Finally, treating animals with specific antibodies against identified C3 deposition evasion targets lead to bacterial clearance and faster infection resolution. Our results demonstrate a complete genetic characterization of complement deposition evasion in *S. pneumoniae*, which extends far beyond the polysaccharide capsule. Ultimately, we can combine existing high-throughput screening tools (i.e., Tn-Seq), with key components of the immune system (i.e., complement deposition) to build bacterial genotype-phenotype immune interaction maps (Hii-TnSeq) to develop novel targeted antimicrobial strategies.

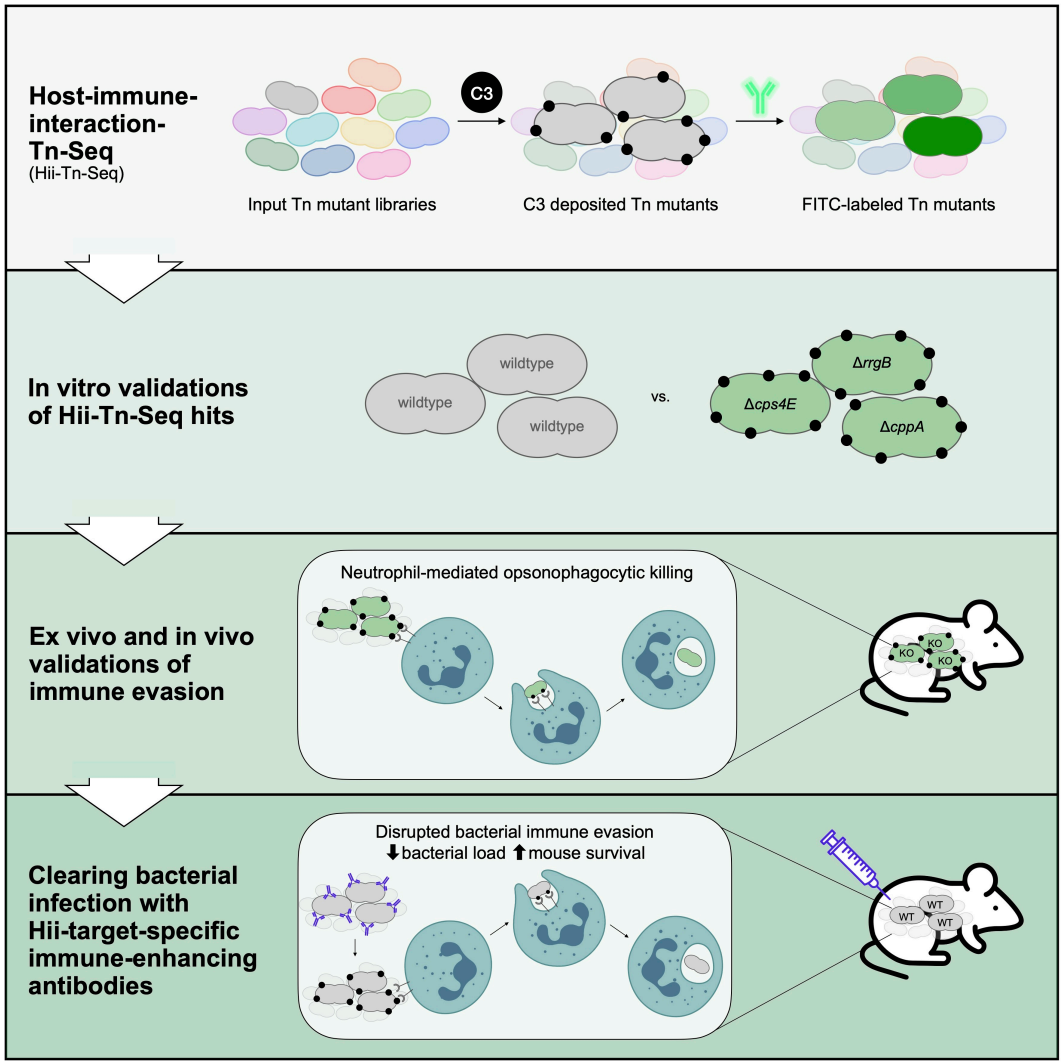


Figure 2.1 | Bacterial genomic profiling reveals novel routes to complement evasion and targeted therapeutic strategies.
 Graphical abstract summarizing Chapter 2.

2.3 Results

2.3.1 A genome-wide view of bacterial C3 deposition reveals novel routes to complement evasion

Previous studies in *S. pneumoniae* identified factors that reduce or inhibit C3 deposition, including the choline-binding proteins PspA, PspC, and LytA²⁰⁻²², and the exoglycosidases NanA, BgA, and StrH^{23,24}. However, understanding how *S. pneumoniae* proteins are mechanistically involved in dampening C3 deposition across the entire genome and multiple strains still needs to be determined. Tn-Seq is a powerful tool that combines transposon (Tn) mutagenesis with Illumina sequencing to rapidly identify all bacterial genes required in a given environment^{18,25}. Similar to previous methods that employed sorting-based enrichment of Tn mutants to screen for a particular phenotype^{26,27}, we hypothesized that Tn-Seq, in combination with a FACS-based C3 deposition assay²⁸⁻³⁰, could generate a genome-wide map of the genetic determinants of C3 deposition evasion in *S. pneumoniae*.

In the first step of the Hii-TnSeq procedure, exponential phase *S. pneumoniae* cultures are challenged to C3 deposition in infant rabbit serum and subsequently incubated with an anti-C3 rabbit FITC-conjugated antibody (**Figure 2.2a**). The obtained percentage of FITC+ cells visualized by flow cytometry is an indirect measure of C3 deposition. *S. pneumoniae*'s polysaccharide capsule works as an effective C3 deposition blocking agent³¹⁻³⁴. In order to validate the procedure, we first tested *S. pneumoniae* TIGR4 (serotype 4, virulent strain) wildtype (WT) and a TIGR4-derived acapsular (Δ Capsule) strain (**Figure 2.2d**). As expected, TIGR4 WT consistently has a low FITC intensity/C3 deposition (with only 5-10% of the cell population FITC+), while acapsular TIGR4 consistently has a high FITC intensity/C3 deposition (70-100% FITC+). For the genome-wide screen, two independently constructed TIGR4 Tn libraries were assayed with this protocol at least six times (technical replicates to account for sample-to-sample variation). Fluorescence-activated cell sorting recognizes C3 deposition on the cell surface of Tn mutants, binning the cells by FITC fluorescence intensity into bin zero, one, two, or three, with bin three containing the Tn mutants with maximum FITC intensity/C3

deposition (**Figure 2.2b**). DNA extracted from the different bins' sorted cells is processed^{18,32}, Illumina sequenced, and analyzed (**Figure 2.2c**).

Using our in-house pipeline, *Aerobio*, sequencing reads mapped to the *S. pneumoniae* TIGR4 genome are used to calculate each Tn mutant's frequency within bins zero, one, two, and three. The frequency ratio between bin three (C3⁺⁺⁺) and bin zero (C3 negative population) estimates the fold enrichment of each mutant. To consider a nonessential gene a potential C3 evasion factor, all or most of the Tn mutants in that gene should be significantly enriched in bin three compared to bin zero (**Figure 2.2e**). Therefore, using the data obtained from Hii-TnSeq, the genes involved in C3 deposition evasion must fulfill two requirements: 1) the calculated average of every mutant's *log*₂ fold change (bin3/bin0) in every gene is over 2.0 (**Figure 2.3a, blue + green points**), and 2) this average is significantly different from the expected non-enriched value (defined as the median of the fold change distribution for every nonessential gene).

Using this conservative approach, we identified 27 genes (hyper-enriched Tn mutants) with a potential role in allowing *S. pneumoniae* to evade C3 deposition and downstream processes such as NMOK (using a mutant *log*₂ fold change over 5.0 to reduce the dataset, **Figure 2.3a, green points**). These genes belong to pathways and processes across all gene functional categories, including but not limited to: amino acid metabolism, capsule/carbohydrate metabolism, DNA repair and editing, folding/sorting/degradation, membrane transport, and of hypothetical/uncharacterized function. We selected a subset of 12 hits (**Figure 2.3b**, SP0084 and SP0470 not pictured) for downstream validations based on at least one of three key features: (1) a previously unpublished association to bacterial C3 complement deposition evasion; (2) localization to the bacterial cell surface as a potential target for a novel antibacterial therapy; (3) requirement for in vivo infection based on previous Tn-Seq datasets^{36,37}. This panel includes the following surface-localized hits: PTS sugar transport IIC (*celB*; SP0250), the backbone of the pilus-1 protein (*rrgB*; SP0463), the putative C3-degrading protease (*cppA*; SP1449), and a methionine ABC transporter (SP1957, SP1958). In addition to surface localized proteins that allow *S. pneumoniae* to evade C3 complement deposition, we found disrupting key intracellular processes can additionally result in a hyper complement deposition phenotype, including a proline dipeptidase (*pepQ*; SP1591) and a thiamine pyrophosphokinase (SP1982).

Finally, exoglycosidases including a putative amylase (*amy*; SP1382) and galactokinase (*galK*; SP1853) were included in the panel, potentially operating by a similar method to NanA, BgA, and StrH^{23,24} and/or involved in polysaccharide capsule biosynthesis. Our comprehensive findings highlight the strength of Hii-TnSeq to generate a genome-wide picture of all bacterial proteins involved in dampening C3 deposition across the bacterial intracellular space, membrane, cell wall, and capsule.

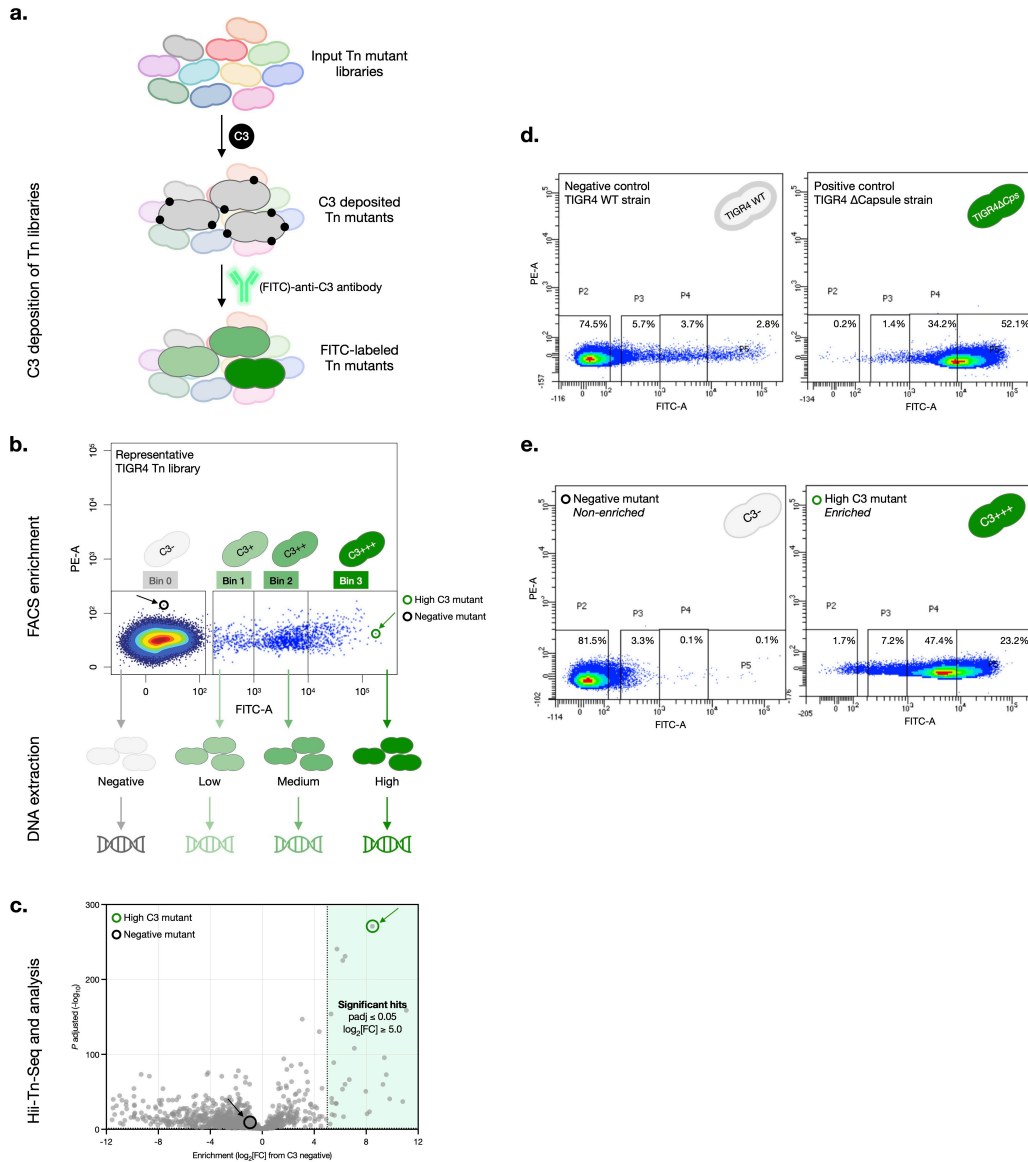


Figure 2.2 | Overview of a genome-wide screen (Hii-TnSeq) for the identification of bacterial genetic determinants of C3 deposition evasion.

a. High-saturation transposon mutant libraries in the *S. pneumoniae* strain TIGR4 are subjected to C3 deposition in infant rabbit serum, labeled with an anti-C3 FITC-conjugated antibody, and screened for their C3 deposition phenotype through FACS. **b.** Mutants are sorted based on FITC intensity (negative, low, medium, or high; a representative library is pictured), after which DNA is extracted from each sorted bin and an additional unsorted input library to prepare Tn-Seq libraries. **c.** After Illumina sequencing, reads are mapped to the *S. pneumoniae* TIGR4 genome to identify the location of transposon insertions within each sorted bin sample ($n=2$ high saturation libraries, each consisting of 6 independent sorts into 4 bins). The number of unique insertions within a gene or feature is compared between negative, low, medium, and high bins to identify potential C3 deposition evasion factors across the *S. pneumoniae* TIGR4 genome. **d.** A representative TIGR4 wildtype (isogenic strain) negative control has 12.2% FITC+ (P3+P4+P5) or a low C3 deposition phenotype; a representative TIGR4 Δ Capsule (isogenic strain) positive control has 87.7% FITC+ (P3+P4+P5) or a hyper C3 deposition phenotype. **e.** A representative negative or *non-enriched* Tn mutant has a low % FITC+ if it were to independently be subjected to the C3 deposition assay, and a representative positive *enriched* Tn mutant alternatively has a high % FITC+.

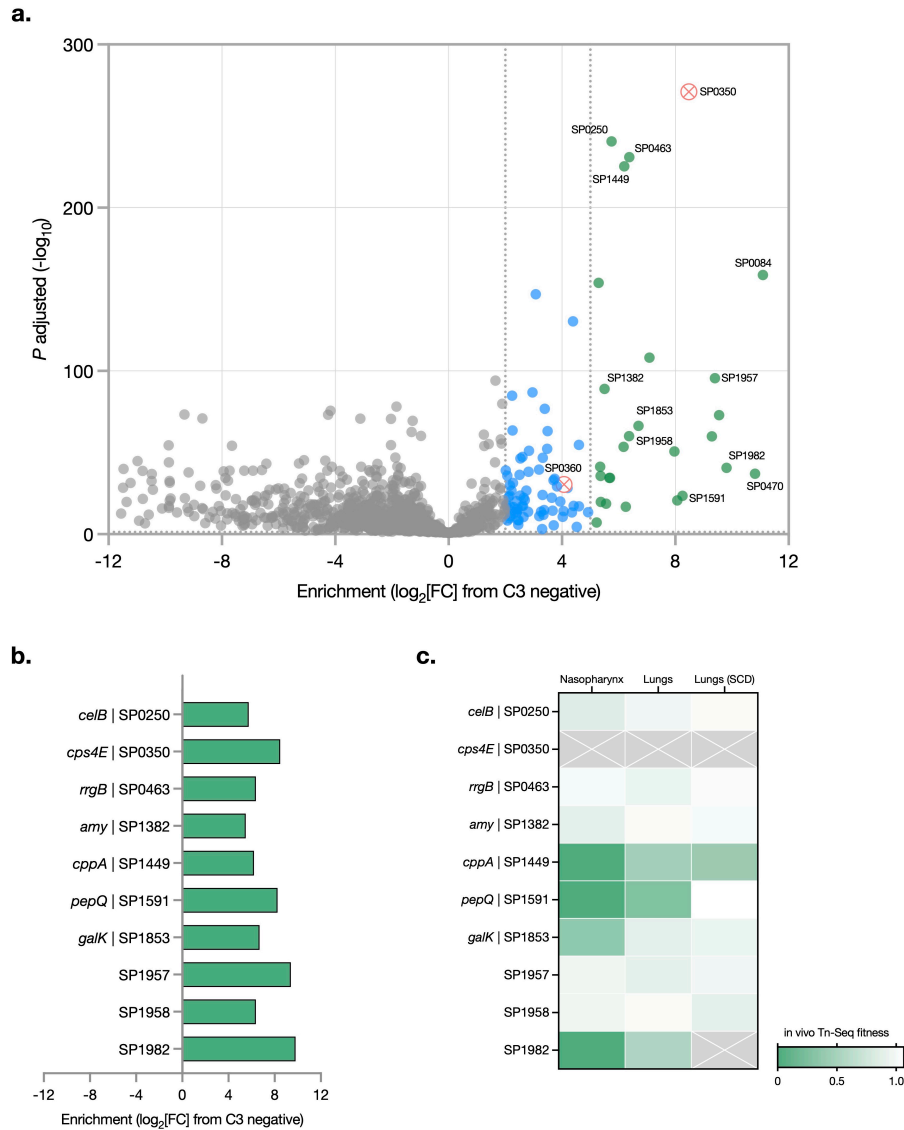


Figure 2.3 | Hii-TnSeq reveals both established and novel bacterial C3 deposition evasion factors.

a. Hii-TnSeq analysis workflow consists of first defining the mean mutant frequency for each gene in each bin, calculating the fold change of each mutant's frequency in bin three (C3+++), compared to bin zero (C3 negative), and assigning statistical significance to each mutant's enrichment value compared to the median of the distribution. Significant enrichment of mutants in bin three (C3+++), samples compared with the bin zero (C3 negative) sorted controls, as determined via multiple unpaired t-tests of [mutant frequency in high bin/mutant frequency in negative bin] compared to the median of the distribution. The first vertical line indicates a \log_2 fold change (FC) of ≥ 2.0 (blue points; enriched mutants) and the second vertical line indicates a \log_2 fold change (FC) of ≥ 5.0 (green points; hyper enriched mutants). Genes whose interruption likely causes acapsular phenotypes are highlighted as red points. **b.** A selected panel of 10 hyper enriched hits, in order of *S. pneumoniae* TIGR4 genome locus tags, with the \log_2 fold change (FC) (enrichment value) shown. **c.** A heatmap overlaying the selected panel of hyper enriched Hii-TnSeq hits with published *S. pneumoniae* TIGR4 Tn-Seq phenotypes in the nasopharynx and lungs of mice^{36,37} and the lungs of a sickle cell disease mouse model⁴⁵. Green indicates a fitness defect when the gene is disrupted, while white indicates no effect on fitness. SCD = sickle cell disease mouse model. Grey indicates gene with no overlaid Tn-Seq data.

2.3.2 Capsule-independent mechanisms contribute to *S. pneumoniae* C3 evasion

Capsule levels influence susceptibility to C3 complement deposition, opsonophagocytosis, and virulence in models of sepsis³¹⁻³⁴. Less encapsulated strains are more susceptible to C3 deposition (as modeled by the TIGR4 acapsular positive control, **Figure 2.2d**) and neutrophil-mediated killing, while more encapsulated strains (as modeled by the TIGR4 wildtype negative control, **Figure 2.2d**) are more resistant to these processes and are also more virulent during systemic (blood) infection. Based on *S. pneumoniae* capsule's crucial interactions with the immune system, it is not surprising we identify the capsule sugar transferase (SP0350), responsible for attaching the first capsule residue to the lipid carrier undecaprenyl phosphate (UP)³⁸, as a C3 complement deposition evasion factor. This finding speaks to the strength of our assay to construct a complete genome-wide map of complement evasion in *S. pneumoniae*, including well established factors.

To benchmark Hii-TnSeq and test whether our data analysis method and identified panel of hits are in fact C3 deposition evasion factors, site-directed knockout strains were constructed in *S. pneumoniae*³⁹ for the panel of twelve selected hits and subjected to the C3 deposition assay (**Figure 2.4a**). *S. pneumoniae* TIGR4 WT and Δ Capsule strains were included as controls and for setting flow cytometry gates (**Figure 2.4b**). Of the twelve constructed strains, ten confirmed the hyper C3 deposition phenotype, with a subset comparable to the TIGR4 Δ Capsule control (**Figure 2.4c**). Two knockouts from our panel, Δ SP0084/hk08 and Δ SP0470/hypothetical protein, did not validate, likely due to (1) polar effects of the *magellan6* transposon, or (2) redundancies in two-component systems (SP0084, the histidine kinase of two-component system 08) across the *S. pneumoniae* genome. The validation experiments of these ten factors highlight that Hii-TnSeq is able to accurately predict a gene's contribution to complement deposition.

As the polysaccharide capsule hinders C3 deposition, the ten validated strains' capsule levels were measured by flow cytometry to assess whether enhanced C3 deposition of the knockout panel was capsule-dependent or independent (**Figure 2.4d**). In this assay, the mean fluorescence intensity for the TIGR4 WT control is approximately 200-fold

higher than that of TIGR4 acapsular cells (**Figure 2.4e**). Aside from the capsule sugar transferase (SP0350) knockout, all the validated strains display a similar capsule expression to TIGR4 WT (**Figure 2.4f**), confirming the knockouts' hyper C3 deposition phenotype was not due to disrupted capsule expression. Overall, Hii-TnSeq identifies novel uncharacterized complement evasion mechanisms that extend beyond the polysaccharide capsule.

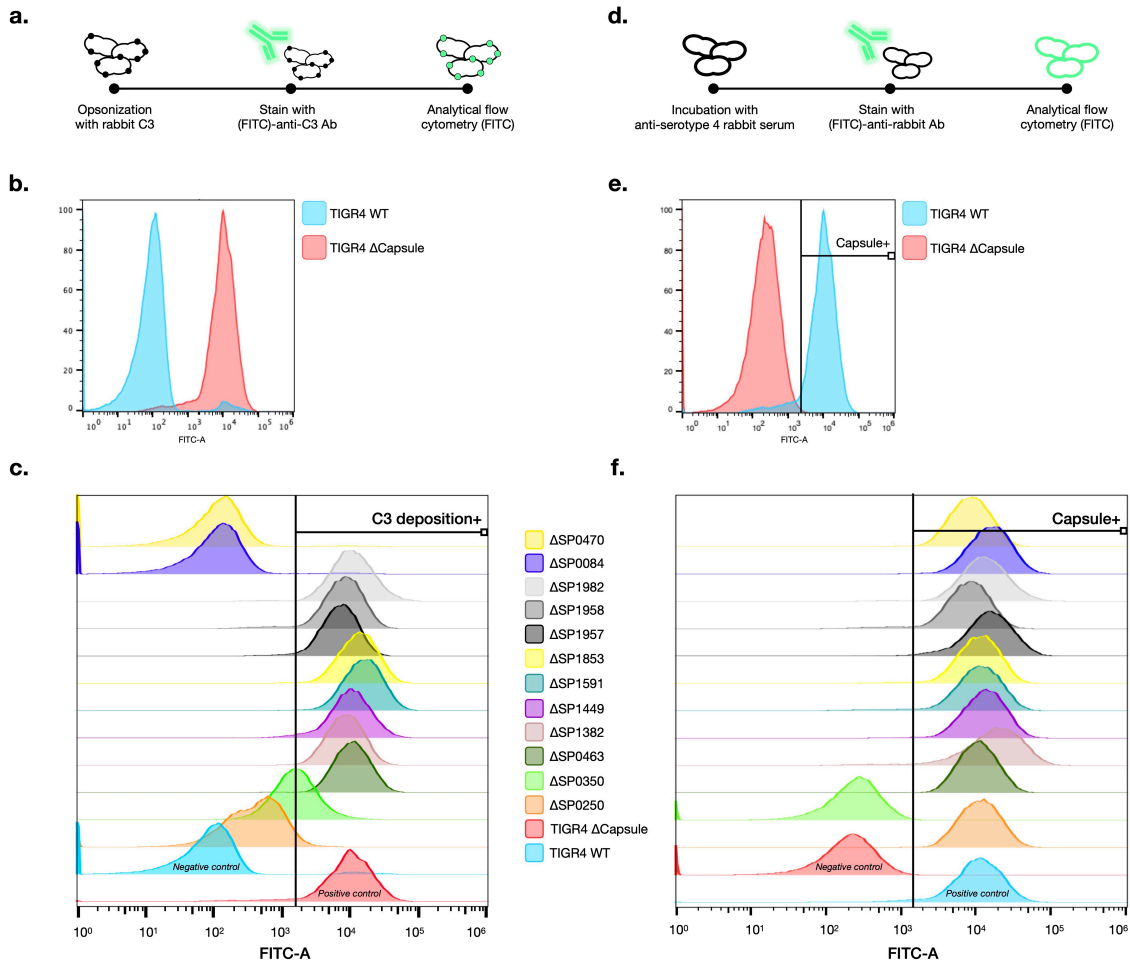


Figure 2.4 | Single gene knockouts can individually lead to hyper C3 deposition on the bacterial cell surface, independent of the polysaccharide capsule.

a. Schematic of C3 deposition assay. **b.** The *S. pneumoniae* TIGR4 wildtype (WT) strain exhibits a low C3 deposition phenotype (~7-10% FITC+), while the TIGR4 acapsular strain (Δ Capsule) exhibits a hyper C3 deposition phenotype (~70-90% FITC+). **c.** Twelve enriched genes, identified by Hii-TnSeq, were selected to construct isogenic single gene knockout strains, and validated by C3 deposition assay and flow cytometry analysis. Ten of twelve strains confirmed to have a hyper C3 deposition phenotype, indicated by a FITC+ shift from TIGR4 wildtype (blue). **d.** Schematic of capsule quantification assay. **e.** Capsule quantification assay by flow cytometry is set up with controls TIGR4 wildtype exhibiting a high capsule phenotype (~100% FITC+), while the TIGR4 Δ Capsule strain exhibits a low capsule phenotype (<10% FITC+). **f.** Ten validated (and two non-validated; SP0084 and SP0470) isogenic single gene knockout strains were assayed for capsule phenotype, all of which had wildtype levels of capsule, aside from Δ cps4E (SP0350), indicating C3 deposition evasion in *S. pneumoniae* extends far beyond the well characterized polysaccharide capsule. Flow cytometry data is representative of three independent experiments, **Supplemental Figures 2.3 and 2.4.**

2.3.3 Ex vivo and in vivo importance of identified C3 evasion factors

The requirement and significance of bacterial factors in vivo are far more complex than during the in vitro C3 deposition assay, which raises the question of whether many of our findings from Hii-TnSeq are important during an active *S. pneumoniae* infection. In vivo Tn-Seq data^{36,37} predicts that (1) Δ SP0250/*celB*, (2) Δ SP0350/*cps4E*, Δ SP0463/*rrgB*, (4) Δ SP1449/*cppA*, (5) Δ SP1591/*pepQ*, (6) Δ SP1957, and (7) Δ SP1982 Tn mutants have a fitness defect in the mouse lungs (**Figure 2.3c**). A mouse pneumonia model to evaluate the phenotype of the seven knockouts (**Figure 2.5a, left panel**) revealed that only Δ SP0463/*rrgB*, Δ SP1449/*cppA*, and Δ SP1982/thiamine pyrophosphokinase have significantly attenuated virulence. Infection with these strains exhibited a lower clinical score and reduced bacterial burden in the lungs (**Figure 2.5b, left panel**); however, only Δ SP1449/*cppA*, and Δ SP1982/thiamine pyrophosphokinase presented significant attenuation in the bloodstream (**Figure 2.5b, right panel**). While Hii-TnSeq is a powerful method to generate a genome-wide map of *S. pneumoniae* complement evasion, C3 deposition performed in vitro may not reflect in vivo phenotypes due to evolved bacterial virulence redundancies across the genome. This rationale could explain the lack of virulence attenuation of Δ SP0250/*celB*, Δ SP1591/*pepQ*, and Δ SP1957 knockouts during a mouse lung infection. The lack of virulence C3-mediated attenuation in mice infected with Δ SP0250/*celB*, Δ SP1591/*pepQ*, and Δ SP1957 could be further explored by performing C3 deposition on *S. pneumoniae* knockout strains harvested from the mouse lung.

To model neutrophil-mediated opsonophagocytic killing (NMOK) ex vivo, the three knockouts with attenuated in vivo virulence plus TIGR4 WT and Δ Capsule strains were opsonized in infant rabbit serum and subsequently incubated with freshly isolated mouse bone marrow neutrophils to determine *S. pneumoniae* survival (**Figure 2.5a, right panel**). The three knockouts (Δ SP0463/*rrgB*, Δ SP1449/*cppA*, and Δ SP1982/thiamine pyrophosphokinase) and the TIGR4 acapsular control displayed a significantly reduced survival compared to the TIGR4 wildtype (**Figure 2.5c**), suggesting these gene products are required in vivo for *S. pneumoniae* to withstand NMOK.

Finally, we further addressed the link between the attenuated knockouts and C3 deposition evasion by infecting complement-depleted animals (complement depletion by cobra venom factor; **Figure 2.6a**). Under these conditions, infection with knockouts Δ SP0463/*rrgB*, Δ SP1449/*cppA*, and Δ SP1982/thiamine pyrophosphokinase resulted in increased bacterial survival compared to TIGR4 WT infection in both the mouse lungs and bloodstream of C3-depleted animals (**Figure 2.6b**). This data further confirms the importance of RrgB, CppA, and the thiamine pyrophosphokinase for *S. pneumoniae* virulence and pathogenesis. Paired with our C3 deposition and opsonophagocytic killing data, we can state that these factors contribute to *S. pneumoniae*'s evasion of complement deposition and clearance in vivo, making them indispensable to the pathogen to cause pneumonia and further complications such as bacteremia.

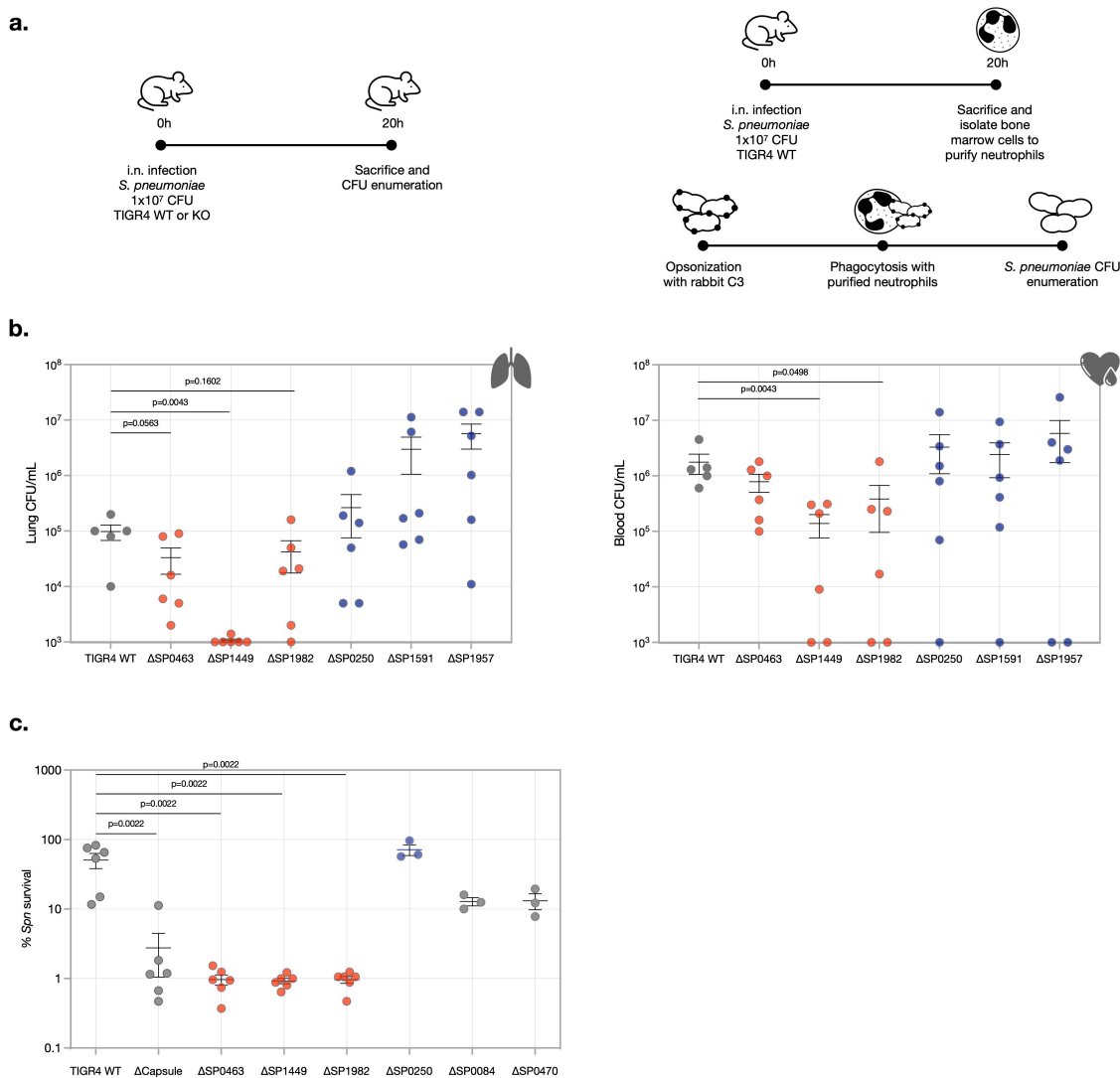


Figure 2.5 | *S. pneumoniae* gene knockouts with a hyper C3 deposition phenotype have a bacterial virulence defect in vivo and an enhanced opsonophagocytic killing ex vivo.

a. Schematic of infection timeline in mice with intact innate immunity (left) and of mouse bone marrow neutrophil purification and functional opsonophagocytic killing assays (right). **b.** Mouse infections with TIGR4 WT or isogenic single gene knockouts (KO) confirm Δ SP0463, Δ SP1449, and Δ SP1982 are less fit as determined by recovered CFU/mL in the lungs (left panel; $n=5-6$ mice/condition; lines represent the mean \pm SEM). Δ SP0463 and Δ SP1982 are less fit to enter and replicate in the bloodstream, as determined by recovered CFU/mL in the blood by cardiac puncture (right panel; $n=5-6$ mice/condition; lines represent the mean \pm SEM). **c.** Percent of *S. pneumoniae* TIGR4 wildtype (WT) or KO strains survival after interaction with bone marrow neutrophils purified from mice intranasally (i.n.) exposed to *S. pneumoniae* TIGR4 WT, opsonized with 10% infant rabbit serum ($n=OPK$ reactions using pooled purified neutrophils isolated from 4 mice/group). Data are pooled from three independent experiments, with colony-forming units (CFU) plated in duplicate or triplicate. Data are displayed as mean \pm SEM. Significance is measured through a two-tailed t-test: * $p<0.01$, ** $p<0.001$, *** $p<0.0001$.

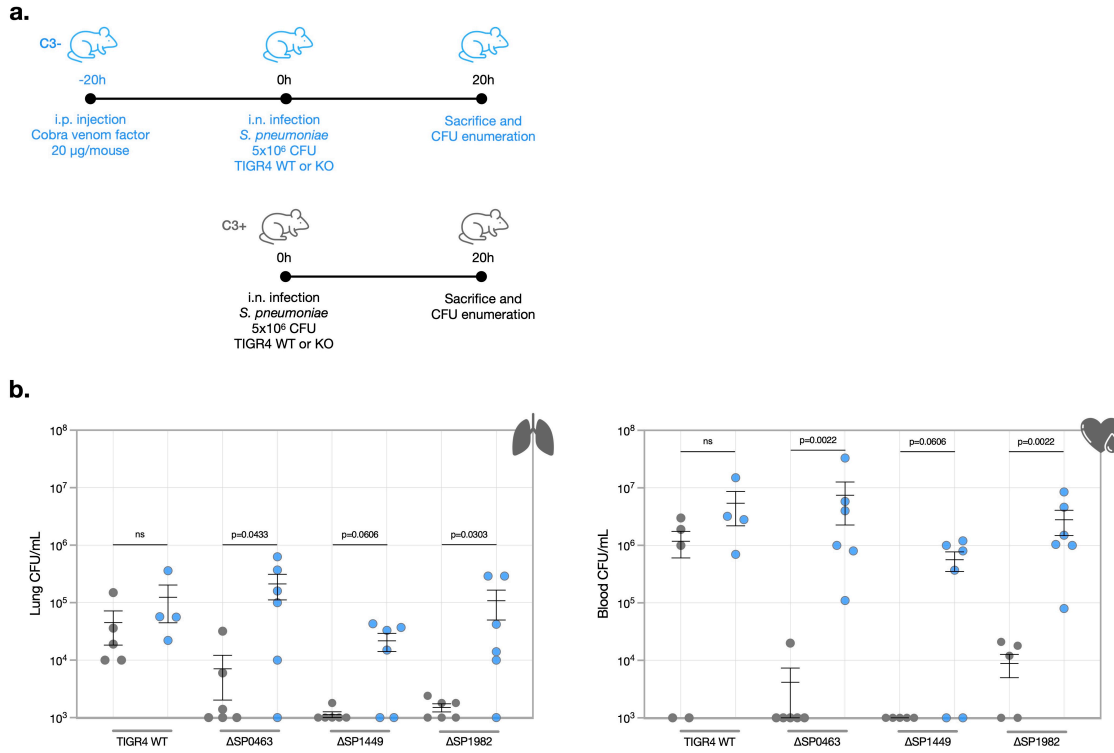


Figure 2.6 | *S. pneumoniae* knockouts with a hyper C3 deposition phenotype are entirely virulent in C3-depleted animals.

a. Schematic of infection timeline in mice with depleted C3 complement by cobra venom factor (CVF, blue) compared to mice with intact innate immunity (grey). **b.** The phenotypes of Δ SP0463, Δ SP1449, and Δ SP1982 in the mouse lungs are rescued in C3-depleted mice, at a lower inoculum dose of 5×10^6 CFU (left panel; $n=4-6$ mice/condition; lines represent the mean \pm SEM). Similarly, the phenotypes of Δ SP0463, Δ SP1449, and Δ SP1982 in the mouse bloodstream are rescued in C3-depleted mice, at a lower inoculum dose of 5×10^6 CFU (right panel; $n=4-6$ mice/condition; lines represent the mean \pm SEM). Significance is measured through a two-tailed t-test: * $p < 0.01$, ** $p < 0.001$, *** $p < 0.0001$.

2.3.4 RrgB and CppA can be therapeutically targeted in vivo with an antibody approach

By identifying bacterial immune evasion targets to restore key immune processes previously escaped by the pathogen, genome-wide immune interaction data has the potential to guide the development of targeted HITs. One strategy is a therapeutic antibody either alone or in combination with the standard-of-care (broad-spectrum antibiotic), similar to the strategy our group previously explored³⁶. Of our validated Hii-TnSeq hits, both RrgB and CppA are suitable targets due to (1) their surface localization prediction; (2) gene disruptions lead to attenuated virulence (**Figure 2.5b**), and (3) they are novel C3 evasion factors. We hypothesize that by specifically targeting their function, we can restore otherwise compromised innate immune processes.

We tested this hypothesis using anti-RrgB or anti-CppA antibodies from rabbits immunized with purified recombinant RrgB and CppA protein products. Mice intranasally challenged with either TIGR4 wildtype, TIGR4 Δ SP0463/RrgB, TIGR4 Δ SP1449/CppA, or PG13, a serotype 6C strain that does not contain RrgB but does contain CppA, were treated with either vehicle (saline), a nonspecific polyclonal rabbit IgG or the target-specific antibody at 1 mg/kg 8 hours post-infection (**Figure 2.7a**). After 24 hours post-infection, the bacterial burden in the lungs and blood of TIGR4 wildtype recovered from animals treated with the control IgG antibody or the vehicle control (saline) were high and similar. However, in the presence of both the RrgB-targeting antibody and the CppA-targeting antibody, the lungs-enumerated CFU is significantly reduced (**Figure 2.7c-d**). RrgB-specific antibody treatment does not reduce the CFU recovered from animals infected with the PG13 strain, whereas the CppA-specific antibody treatment does reduce the CFUs, indicating potential applications of the CppA antibody to additional *S. pneumoniae* clinical strains. Concurrently, separate groups of mice infected with TIGR4 wildtype and treated with either vehicle (saline), the RrgB-targeting antibody, and the CppA-targeting antibody were monitored for symptoms (**Figure 2.7b**). While infection seemed to rebound in mice treated with the RrgB-antibody, possibly due to the high bacterial burden in the bloodstream at 20 hours post-infection (**Figure 2.7c**), treated mice still had longer survival than the untreated group. Strikingly, CppA antibody-treated mice had a significantly longer survival, with 70% of animals completely recovering from *S.*

pneumoniae TIGR4 infection. The data shows that by targeting C3 complement evasion factors such as RrgB or CppA, C3 deposition can be either partially or entirely restored, resulting in downstream NMOK and at least partially reinstated bacterial clearance and improvement of survival outcome.

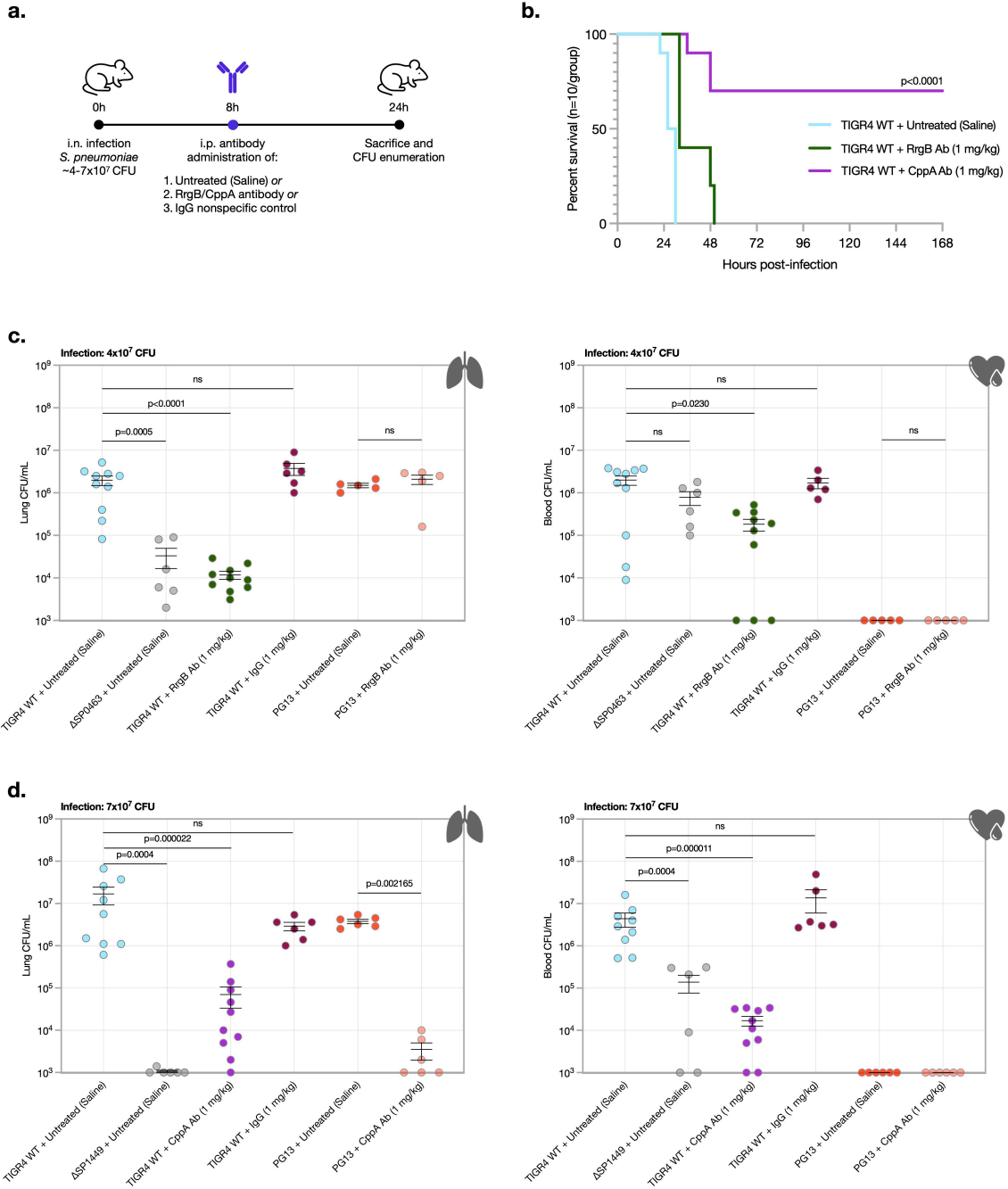


Figure 2.7 | CppA and RrgB, the *S. pneumoniae* C3-degrading protease and pilus-1 backbone respectively, inhibit C3 deposition and can be targeted with specific therapeutic antibodies.

a. Schematic of infection and antibody administration timeline in mice. **b.** Survival analysis of mice with vehicle (saline) treatment, 1.0 mg/kg anti-SP0463 (RrgB) antibody, or 1.0 mg/kg anti-SP1449 (CppA) antibody administered via intraperitoneal (i.p.) injection (n=10/group; Kaplan Meier analysis with Log-rank (Mantel-Cox) test for significance determination). **c.** An in vivo lung infection with TIGR4 WT or Δ SP0463 confirms the knockout is less fit. Challenging WT-infected mice with RrgB-specific antibodies, significantly reduces the recovered CFUs 24-hours post infection in the mouse lungs (left panel) and, in a lesser extent in the bloodstream (right panel). A nonspecific rabbit IgG in the context of TIGR4 WT infection and the RrgB-specific antibody in the context of a *S. pneumoniae* pan-genome (PG) strain (PG13) lacking the RrgB protein but containing the CppA protein confirms antibody specificity. **c.** In vivo lung and blood infection with TIGR4 WT or Δ SP1449 is less fit. Challenging WT-infected mice with CppA-specific antibodies, significantly reduces the recovered CFUs 24-hours post infection in the mouse lungs (left panel) and the bloodstream (right panel) of both TIGR4 and PG13 strains. Significance is measured through a two-tailed t-test: *p<0.01, **p<0.001, ***p<0.0001.

2.4 Discussion

This work shows that Host-immune-interaction-Tn-Seq, or Hii-TnSeq, is a powerful, high-throughput genetic screening platform to pinpoint immune evasion factors. Moreover, it has the potential to be implemented in other genetically tractable bacterial pathogens or assayed in different screenings that mimic key immune conditions. We demonstrate how a subset of our identified hits present *ex vivo* and *in vivo* phenotypes and can be exploited by targeted antimicrobial therapeutic strategies to induce bacterial killing via the immune system. The immune-mediated killing of gram-positive bacteria strongly depends on neutrophils to engulf bacteria via phagocytosis and kill them intracellularly. Complement facilitates this process with C3 binding to the cell surface and stimulating neutrophil-mediated opsonophagocytic killing (NMOK). As a result, pathogenic microbes have developed resistance to complement. *S. pneumoniae* holds a plethora of different mechanisms to resist complement, including the expression of a surface polysaccharide capsule that shields cell surface epitopes³¹, the expression of surface proteins to recruit complement regulatory factors and serum proteases, the secretion of inhibitors to block complement, and minimization of bacterial size²³. In this work, we have extended the list of known pneumococcal C3 evasion mechanisms. Our proof-of-concept studies show that targeting two of these novel C3 evasion factors, RrgB and CppA, offer promising alternative therapeutic strategies aimed at enhancing the immune system against *S. pneumoniae* infection.

Future work with Hii-TnSeq in the context of *S. pneumoniae* and C3 deposition includes fine-tuning the preliminary Hii-TnSeq screen. The flow cytometry strategy of binning cells within bins negative, one, two, and three could introduce artificial boundaries and cause researchers' to preemptively omit phenotypically important findings across the bacterial genome. Instead, we propose a refined approach with three bins/populations: negative, low, and high, with the 'high' bin encompassing both bins two and three of the original strategy described in this chapter (and eliminating the original bin one, that was not used in analyzed data and follow up experiments due to close physical proximity to the C3 negative population). This refined Hii-TnSeq screen would reduce complexities within the data analysis pipeline downstream of sequencing. Furthermore, the Hii-TnSeq dataset includes a subset of Tn mutants with increased resistance to C3 deposition compared to

the median of the distribution (**Figure 2.3a, left points**). Future studies to investigate these phenotypes and link gene disruption to increased complement evasion in vitro are under way.

Diving deeper into novel mechanisms of C3 deposition evasion, *S. pneumoniae* RrgB and CppA have clear established links to bacterial virulence but have never been directly linked to C3 deposition evasion. The *rlrA* pathogenicity islet, containing RrgA/RrgB/RrgC has a varied distribution among *S. pneumoniae* serotypes⁴⁰, and as part of the accessory genome, RrgB is only present in 6 strains of our group's 36-strain pan-genome collection and expressed in only a subset of clinical pneumococcal isolates (~30%)⁴¹. The TIGR4 bacterial surface is covered with multiple copies of the type-1 pilus (P1), decorating the outer cell surface, promoting various interaction scenarios with host proteins during infection. P1 may be impeding C3 deposition and NMOK by one of two modes: (1) decorating its cell surface with additional host factors such as fibrinogen or collagen known to bind RrgB⁴² to evade complement deposition and neutrophil recognition; or (2) P1 directly interacts with complement receptor 3 (CR3) to promote CR3-mediated uptake of *S. pneumoniae* by macrophages and spread of the pathogen from local sites of infection (i.e., the lungs) to the bloodstream⁴³. Contrary to RrgB, CppA, annotated as the *S. pneumoniae* putative C3-degrading protease, is present in all publicly available pneumococcal genomes⁴⁴, is immunogenic in mice and protective against systemic challenge⁴⁵. CppA is required for *S. pneumoniae* fitness in the lungs and blood of wildtype mice³⁷ and required for nasopharyngeal transmission in a ferret model⁴⁵. The direct linkage of C3-degrading activity to CppA has never been established prior to this study, however nearly the entire amino acid sequence of CppA matches to the glyoxalase/bleomycin resistance protein/dihydroxybiphenyl dioxygenase type superfamily of proteins, which contain beta-alpha-beta motifs characteristic of various types of enzymes with affinities for metal ions. The findings from Hii-TnSeq and subsequent validations confirm a role in C3 evasion for both RrgB and CppA and suggest a clear mechanism of action for a targeted therapeutic strategy against either bacterial protein.

While antibiotics have significantly reduced disease occurrence caused by bacteria, we face increasing antimicrobial-resistant (AMR) infections. Alarming, the development of

new antimicrobials lags behind the emergence of resistance. While the development of novel, canonical antimicrobials must continue, other approaches to augment/modulate efficacy are also urgently needed for critical patient populations. Adjunctive therapies targeting immune processes in combination with pathogen-targeted approaches (i.e., antibiotics) hold promise to widely treat bacterial infections. With the advancements in immunophenotyping, biomarkers indicate the exact stage of infection (i.e., by rapid transcriptomic analysis) and allow the monitoring of treatment success or failure. These personalized approaches could give insight into the inflammatory state of infection (hypo- or hyper-) and the application of the appropriate immune-stimulating or -modulating therapeutics. To progress towards implementing such strategies in the clinic, we must first build detailed genetic understandings of how a bacterium interacts with relevant components of the host immune response. While in this study, we only target the RrgB and CppA proteins in *S. pneumoniae* with specific antibodies, similar immune-enhancing drug targets can also be utilized in various other treatment strategies, including but not limited to: (1) an antibiotic and antibody dual approach; (2) an antibody carrying a drug payload or antibody-recruiting moiety; or (3) conjugated nanobodies each targeting a different bacterial surface protein. To further improve the RrgB/CppA-targeting antibody therapeutic strategies, a higher antibody dose or administration in conjunction with a broad-spectrum antibiotic can be pursued. We believe this study is both a case for (re)envisioning the development of antimicrobials and a starting point for building platforms to predict and validate immune-enhancing drug targets.

2.5 Materials and Methods

Table 2.1 | Key resources table

REAGENT or RESOURCE	SOURCE	IDENTIFIER
Serum		
Baby Rabbit Complement	MP Biomedicals	Cat# MP08642961
Type 4 Antisera	Cedarlane	Cat# 16747(SS)
Antibodies		
Goat anti-Rabbit C3 IgG [FITC]	MP Biomedicals	Cat# 0855654
Goat anti-Rabbit IgG [FITC]	Novus Biologicals	Cat# NB120-6009
Anti-RrgB polyclonal antibody	Jason Rosch's lab	N/A
Anti-CppA polyclonal antibody	Jason Rosch's lab	N/A
Bacterial Strains		
<i>S. pneumoniae</i> strain TIGR4	This study	N/A
<i>S. pneumoniae</i> strain PG13	36-strain PG-collection	Rosconi <i>et al.</i> 2022
Chemicals, Peptides, and Recombinant Proteins		
rRrgB	Jason Rosch's lab	N/A
rCppA	Jason Rosch's lab	N/A
Deposited Data		
Tn-Seq reads	This study	NCBI accession pending
Experimental Models: Organisms/Strains		
Swiss Webster mice, adult, female	Charles River Laboratories	N/A
Oligonucleotides		
See Table S4	This study	N/A
Software and Algorithms		
Tn-Seq insert comparison	Tim van Opijnen's lab	https://github.com/jsa-aerial/aerobio
Prism 9	GraphPad	N/A

Ethics statement

All experiments involving animals were performed with prior approval of and in accordance with guidelines of the Boston College Institutional Animal Care and Use Committee (IACUC), under Boston College IACUC approved protocol #2022-008. Laboratory animals are maintained in accordance with the applicable portions of the

Animal Welfare Act and the guidelines prescribed in the DHHS publication, Guide for the Care and Use of Laboratory Animals.

***S. pneumoniae* mouse lung infection**

Infection of mice is achieved by anesthetizing the mice with isoflurane in a BSL-2 procedure room, after which bacteria are delivered by intranasal injection. The suspension contains between 5×10^6 - 2×10^7 bacterial cells in 50 μ L saline. The mice are returned to their cage and given food and water *ad libitum*. The bacteria multiply in the lung and cause pneumonia. At 24 hours post-infection in the case of virulent strains, the mice begin to show initial signs of illness (typically piloerection/ruffled fur). All mice are euthanized at 20-24 hours post-infection (or until the humane endpoint in the case of survival curve analysis) by CO₂ gas asphyxiation followed by vital organ removal. In short, after euthanasia, cardiac puncture is performed. Afterwards, the chest is opened, and the trachea is severed with scissors. 0.5 mL of PBS is injected through tubing into the trachea opening, whereupon the liquid goes up through the nasopharynx and out of the nostrils where the liquid is collected in a 1.5 mL Eppendorf tube. In addition, the lungs are removed and mechanically homogenized in 1 mL of 1X PBS. The nasopharynx effluent, lungs, and blood are serially diluted and plated on blood agar base no. 2 (Sigma-Aldrich) plates supplemented with 5% defibrinated sheep's blood at 37°C in a 5% CO₂ atmosphere for CFU enumeration. Mice were housed with a 12h/12h:dark/light cycle. The room temperature set point was 71 degrees F (± 2 degrees) and the humidity setpoint was 40%.

Mouse bone marrow neutrophil isolations

At 16-24 hours post-infection with 1×10^7 CFU of an intranasal infection of TIGR4 WT, mice are euthanized by CO₂ gas asphyxiation followed by harvesting bone marrow cells from femurs and tibias. Preliminary experiments found the bone marrow neutrophil yield (PMN/mL) was significantly higher from infected mice compared to the bone marrow neutrophil yield from uninfected mice (50-100-fold higher). In short, an incision is made in the mid-abdomen on the ventral side and skin is removed to expose the abdomen and lower extremities. Muscles are removed from both legs using scissors, and acetabulum is dislocated from the hip joint. Separated bones are placed in sterile petri dish containing ice-cold RPMI 1640 1X supplemented with 10% FBS (Gibco) and 1%

penicillin/streptomycin on ice, sterilized, and taken upstairs to the cell culture room for downstream analysis: flushing of bone marrow cells and subsequent purification of neutrophils from bone marrow cells using magnetic bead-based purification (StemCell Research).

Mouse C3 complement depletion

To deplete C3 complement, mice are administered cobra venom factor (CVF; Millipore Sigma) dissolved in buffered saline by intraperitoneal (I.P.) injection at 20-40 µg/animal at 24 hours prior to infectious challenge by *S. pneumoniae*. CVF is a stable anti-complement protein and functionally resembles C3 purified from cobra venom. Mice are monitored during C3 depletion to ensure animals do not develop overt signs of distress or opportunistic infection. To confirm complement depletion induced by CVF treatment, complement activity is determined by the C3 level in the plasma, serum, and BAL fluid by ELISA (Aviva Systems).

***S. pneumoniae* mouse lung infection and antibody administration**

Isoflurane-anesthetized 4-6-week-old female Swiss Webster mice were inoculated intranasally with 10⁷ CFU of wildtype *S. pneumoniae* strain in a volume of 100 µL. Eight hours following the challenge, mice were treated with the vehicle (saline), a control rabbit IgG (InVivoMAb, 1 mg/kg, 100 µL), or anti-SP0463/SP1449 polyclonal rabbit antibody (1 mg/kg, 100 µL). At 16-hours following antibody treatment (24-hours post challenge) mice were euthanized, and lungs and chest cavity blood were removed for quantification of bacteria. Whole lungs were washed twice in PBS, and lung tissue is subsequently homogenized in 1mL PBS. Homogenized lung samples were plated onto blood agar plates for CFU titers.

Bacterial strains and growth conditions

S. pneumoniae strains used in this study are listed in **Supplemental Table 2.1**. Strains were grown on blood agar base no. 2 (Sigma-Aldrich) plates supplemented with 5% defibrinated sheep's blood at 37°C in a 5% CO₂ atmosphere. Liquid cultures were grown statically in THY or semi-defined minimal media (SDMM) at pH 7.3, with 5 µL/mL oxyrase (Oxyrase) and 0.75 µL/mL catalase (Fisher Scientific) at the same incubation conditions as plates. For growth curve assays, strains were grown in THY until an optical density

OD₆₀₀ of ~0.5, pelleted and resuspended in the same volume of phosphate saline buffer (PBS). OD₆₀₀ is adjusted to 0.03 in PBS and 20 µL of this suspension is diluted in 180 µL of different media conditions in wells of flat-bottom 96-well plates. OD₆₀₀ measurements were taken on a BioSpa 8 plate reader (BioTek), and experiments were repeated at least three times on independent days.

Tn-Seq libraries construction

Two independent (high-saturation) transposon libraries, each containing 10,000 to 20,000 insertion mutants, were constructed with transposon Magellan6 as previously described^{18,25,32,35-37}, with the following modifications: (1) transformation reactions were scaled up to 4 mL volume. Transposon mutants were recovered on blood agar base no. 2 plates supplemented with 5% sheep's blood with 200 µg/mL spectinomycin. Library stock cultures were grown several independent times in THY medium supplemented with oxyrase and catalase, gDNA is isolated using the Qiagen DNeasy kit (Qiagen), and Tn-Seq sample preparation and Illumina sequencing were performed as previously described^{18,25,32,35-37}.

C3 deposition assay, fluorescence-activated cell sorting (FACS), and analysis

Two independent libraries are grown to mid-exponential phase (OD₆₀₀ 0.6-0.8) in THY supplemented with oxyrase and catalase (in a minimum of five technical replicates for each), and 10⁸ CFUs are resuspended in Hanks Buffer with Ca²⁺ and Mg²⁺ (Gibco) supplemented with 0.1% gelatin (Fisher Scientific) and subsequently opsonized with 10% infant rabbit serum, free of anti-*S. pneumoniae* antibodies (MP Biomedicals), in a 750 µL total reaction volume and incubated at 37°C for 30 minutes with rolling agitation. The opsonization reactions are stopped on ice for 3 minutes, quenched with Hanks Buffer without Ca²⁺ and Mg²⁺ (Gibco) supplemented with 0.1% gelatin, and pelleted. Samples are stained with 1:200 (FITC)-conjugated goat anti-rabbit C3 antibody (MP Biomedicals) in Hanks Buffer without Ca²⁺ and Mg²⁺ (Gibco) supplemented with 0.1% gelatin, on ice in the dark for 30 minutes. Stained reactions were quenched with Hanks Buffer without Ca²⁺ and Mg²⁺ (Gibco) supplemented with 0.1% gelatin, pelleted, and resuspended in 200 µL 1X PBS. Stained *S. pneumoniae* cells are applied to a BD FACSAria Cell Sorter, and bacteria are collected (minimum 50,000 events) for analysis or a 45-minute sort/sample. FACs bins were determined based on FITC intensity and kept consistent across all

experiments on different days. The following controls are included in each experiment: (1) *S. pneumoniae* wildtype, -serum, -antibody, as a cells only gating control; (2) *S. pneumoniae* wildtype, -serum, +antibody, as an antibody background control; *S. pneumoniae* wildtype, +serum, +antibody, as a 15-20% expected FITC+ control; and (4) *S. pneumoniae* Δ Capsule mutant, +serum, +antibody, as a 90-100% expected FITC+ control. Aliquots of the input population and sorted samples are serially diluted and plated on blood agar base no. 2 (Sigma-Aldrich) plates supplemented with 5% defibrinated sheep's blood at 37°C in a 5% CO₂ atmosphere for CFU enumeration.

Genomic DNA isolation and Tn-Seq

To prepare samples for Tn-Seq, genomic DNA is isolated (Qiagen DNeasy) from bacteria from each FACS selection bin (and input pool) to determine the change in frequency of each Tn insertion in the population. Sample preparation, Illumina preparation, and fitness calculations were done as previously described ^{18,25,32,35-37}.

Site-directed gene deletion construction

Site-directed gene knockouts were constructed by replacing target gene sequences with a chloramphenicol or spectinomycin resistance cassette by homologous recombination as previously described ³⁹. All PCR reactions were performed with Q5 polymerase (NEB). Primers used and knockouts constructed are described in **Supplemental Table 2.3**. Randomly selected colonies were recovered and their gDNA isolated using the Qiagen DNeasy kit (Qiagen). Deletions were confirmed by gDNA isolation, PCR of the 3kb construct, and Sanger sequencing (GeneWiz).

Capsule quantification assay, fluorescence-activated cell sorting (FACS), and analysis

For capsule assays, each *S. pneumoniae* strain is grown to mid-exponential phase (OD₆₀₀ 0.6-0.8) in THY supplemented with oxyrase and catalase, and 250 μ L of culture is pelleted and washed in 1X PBS. Pellets are resuspended in 100 μ L rabbit anti-serotype 4 serum (1:2500, Cedarlane Labs) in PBS and incubated on ice for 30 minutes. Samples are quenched with 500 μ L PBS and centrifuged at 4000 RPM for 5 minutes. Pellets are resuspended in 100 μ L (FITC)-conjugated goat anti-rabbit secondary antibody in PBS and kept on ice in the dark for 30 minutes. Staining reactions are quenched with 500 μ L

PBS, the mixtures are pelleted, resuspended in 200 μ L 1X PBS, and analyzed as previously described. All samples were collected (50,000 events) on a BD FACSAria Cell Sorter or Sony SH800 Flow Cytometer, analyzed, and plotted using FlowJo 10.8.1.

Opsonophagocytic killing assay

Each opsonophagocytic killing assay was conducted on the same day as bone marrow neutrophil (polymorphonuclear leukocyte, PMN) isolation and purification from mice as described above. Briefly, 750 μ L reaction volumes are set up with: 37.5 μ L of 1×10^8 *S. pneumoniae*, 75 μ L infant rabbit serum (MP Biomedicals, 10%), 150 μ L of PMNs (7×10^6 PMN/mL in Hanks Buffer with Ca^{2+} and Mg^{2+} (Gibco) supplemented with 0.1% gelatin (Fisher Scientific)), 487.5 μ L of Hanks Buffer with Ca^{2+} and Mg^{2+} (Gibco) supplemented with 0.1% gelatin (Fisher Scientific). Assays are performed in at least duplicate, and each assay includes a 'no PMN' control. Reactions are incubated at 37°C for 40 minutes with rolling agitation. The OPK reactions are stopped on ice for 3 minutes, and serially diluted and plated on blood agar base no. 2 (Sigma-Aldrich) plates supplemented with 5% defibrinated sheep's blood at 37°C in a 5% CO_2 atmosphere for CFU enumeration. Percent survival is determined by: (CFU/mL of +PMN reaction) / (CFU/mL of -PMN control reaction), and experiments were repeated at least twice on independent days.

Antibody generation and purification

A single rabbit was vaccinated by a commercial vendor (Rockland) with either recombinant SP0463 or SP1449 via the following schedule: rabbit was immunized via intradermal route with 0.1 mg SP0463/SP1449 with Complete Freund's Adjuvant (CFA) followed by an intradermal 0.1 mg booster injection with Incomplete Freund's Adjuvant (IFA) as an adjuvant at day 7, followed by two subcutaneous 0.1 mg booster injections at days 14 and 28 with IFA. Terminal bleed was collected on day 52 following the challenge. SP0463/SP1449 IgG was purified from immunized rabbit serum using protein A magnetic beads (Pierce) according to the manufacturer's specifications.

C3-FACS-Tn-Seq gene enrichment determination

Sequencing analyses are performed with analysis platform *Aerobio* v2.3⁴⁶. Each sample from each bin was sequenced separately, then all the samples from each bin within each library were combined. This gave us the number and location of unique inserts per bin.

The number of insertions per gene were calculated and only insertions with 7 or more reads across samples were included in the analyses.

Calculated mutant frequencies are used to calculate the average \log_2 fold enrichment of a mutant in bin three samples compared to bin zero samples. In short, the enrichment of a single mutant (E_i) is calculated as follows:

$$\log_2 E_i = \frac{(N_i(t_2))}{(N_i(t_1))}$$

in which $N_i(t_1)$ is the mutant frequency in bin zero (C3 negative) and $N_i(t_2)$ is the mutant frequency in bin three (C3+++). The median of the fold change distribution for every nonessential gene is referred to as E_x . T_n mutants in a specified gene are then used to calculate the significance of each gene's contribution to C3 deposition. To determine whether enrichment effects are significantly different between bin three and bin zero, three conditions must be fulfilled: (1) E_i is calculated from at least two independent (high saturation) T_n libraries, each screened in at least triplicate on different days; (2) E_i in every gene is over 5.0; and (3) the difference between E_i and E_x must be significantly different in a one sample t -test with Bonferroni correction for multiple testing, where the degrees of freedom are transposon insertions for *gene i* across biological and technical replicates.

Data visualization and statistics

Figure panels were created with Adobe Illustrator, Apple Keynote, Biorender.com (Boston College full license), and GraphPad Prism 9. Flow cytometric analyses were plotted using FlowJo 10.8.1. Statistical analyses were performed using GraphPad Prism 9 and R 4.2.2.

2.6 Acknowledgements

DNA sequencing was performed at the Boston College Sequencing Core, and flow cytometry was performed at the Boston College Flow Core with the assistance of Patrick Autissier. The authors wish to thank Jon Anthony for running the *Aerobio* sequencing analyses platform, John M. Leong and Michelle Meyer for valuable discussions, Sophie Bodrog for assistance with C3 deposition and OPK assays, and the Boston College Animal Care Facility for animal husbandry. This work was supported by AI110724 and AI148470 to T.v.O., R01 AI171038 to F.R. and J.W.R, and U01 AI124302 to T.v.O. and J.W.R.

2.7 References

1. Sundaresh B, Xu S, Noonan B, Mansour MK, Leong JM, van Opijnen T. Host-informed therapies for the treatment of pneumococcal pneumonia. *Trends Mol Med*. Oct 2021;27(10):971-989. doi:10.1016/j.molmed.2021.07.008
2. Kaufmann SHE, Dorhoi A, Hotchkiss RS, Bartenschlager R. Host-directed therapies for bacterial and viral infections. *Nat Rev Drug Discov*. Jan 2018;17(1):35-56. doi:10.1038/nrd.2017.162
3. Naran K, Nundalall T, Chetty S, Barth S. Principles of Immunotherapy: Implications for Treatment Strategies in Cancer and Infectious Diseases. *Front Microbiol*. 2018;9:3158. doi:10.3389/fmicb.2018.03158
4. Bucktrout SL, Bluestone JA, Ramsdell F. Recent advances in immunotherapies: from infection and autoimmunity, to cancer, and back again. *Genome Med*. Oct 31 2018;10(1):79. doi:10.1186/s13073-018-0588-4
5. Wong J, Choi SYC, Liu R, et al. Potential Therapies for Infectious Diseases Based on Targeting Immune Evasion Mechanisms That Pathogens Have in Common With Cancer Cells. *Front Cell Infect Microbiol*. 2019;9:25. doi:10.3389/fcimb.2019.00025
6. Wonfor T, Li S, Dunphy RW, Macpherson A, van den Elsen J, Laabei M. Novel method for detecting complement C3 deposition on Staphylococcus aureus. *Sci Rep*. Sep 21 2022;12(1):15766. doi:10.1038/s41598-022-20098-7
7. Ermert D, Ram S, Laabei M. The hijackers guide to escaping complement: Lessons learned from pathogens. *Mol Immunol*. Oct 2019;114:49-61. doi:10.1016/j.molimm.2019.07.018
8. Hyams C, Yuste J, Bax K, Camberlein E, Weiser JN, Brown JS. Streptococcus pneumoniae resistance to complement-mediated immunity is dependent on the capsular serotype. *Infect Immun*. Feb 2010;78(2):716-25. doi:10.1128/IAI.01056-09
9. Koppe U, Suttorp N, Opitz B. Recognition of Streptococcus pneumoniae by the innate immune system. *Cell Microbiol*. Apr 2012;14(4):460-6. doi:10.1111/j.1462-5822.2011.01746.x
10. Merle NS, Noe R, Halbwachs-Mecarelli L, Fremeaux-Bacchi V, Roumenina LT. Complement System Part II: Role in Immunity. *Front Immunol*. 2015;6:257. doi:10.3389/fimmu.2015.00257
11. Pneumococcal Disease. (World Health Organization, www.who.int, 2017).
12. Monasta, L., et al. Burden of disease caused by otitis media: systematic review and global estimates. *PLoS One* 7, e36226 (2012).
13. Ear infections and vaccines. (American Academy of Otolaryngology-Head and Neck Surgery, www.entnet.org/content/ears, 2018).

14. Mukerji R, Mirza S, Roche AM, et al. Pneumococcal surface protein A inhibits complement deposition on the pneumococcal surface by competing with the binding of C-reactive protein to cell-surface phosphocholine. *J Immunol*. Dec 1 2012;189(11):5327-35. doi:10.4049/jimmunol.1201967
15. Quin LR, Moore QC, 3rd, McDaniel LS. Pneumolysin, PspA, and PspC contribute to pneumococcal evasion of early innate immune responses during bacteremia in mice. *Infect Immun*. Apr 2007;75(4):2067-70. doi:10.1128/IAI.01727-06
16. Hyams C, Opel S, Hanage W, et al. Effects of *Streptococcus pneumoniae* strain background on complement resistance. *PLoS One*. 2011;6(10):e24581. doi:10.1371/journal.pone.0024581
17. Hyams C, Trzcinski K, Camberlein E, et al. *Streptococcus pneumoniae* capsular serotype invasiveness correlates with the degree of factor H binding and opsonization with C3b/iC3b. *Infect Immun*. Jan 2013;81(1):354-63. doi:10.1128/IAI.00862-12
18. van Opijnen T, Bodi KL, Camilli A. Tn-seq: high-throughput parallel sequencing for fitness and genetic interaction studies in microorganisms. *Nat Methods*. Oct 2009;6(10):767-72. doi:10.1038/nmeth.1377
19. Wahl B, O'Brien KL, Greenbaum A, et al. Burden of *Streptococcus pneumoniae* and *Haemophilus influenzae* type b disease in children in the era of conjugate vaccines: global, regional, and national estimates for 2000-15. *Lancet Glob Health*. Jul 2018;6(7):e744-e757. doi:10.1016/S2214-109X(18)30247-X
20. Kerr AR, Paterson GK, McCluskey J, et al. The contribution of PspC to pneumococcal virulence varies between strains and is accomplished by both complement evasion and complement-independent mechanisms. *Infect Immun*. Sep 2006;74(9):5319-24. doi:10.1128/IAI.00543-06
21. Tu AH, Fulgham RL, McCrory MA, Briles DE, Szalai AJ. Pneumococcal surface protein A inhibits complement activation by *Streptococcus pneumoniae*. *Infect Immun*. Sep 1999;67(9):4720-4. doi:10.1128/IAI.67.9.4720-4724.1999
22. Weiser JN, Ferreira DM, Paton JC. *Streptococcus pneumoniae*: transmission, colonization and invasion. *Nat Rev Microbiol*. Jun 2018;16(6):355-367. doi:10.1038/s41579-018-0001-8
23. Dalia AB, Weiser JN. Minimization of bacterial size allows for complement evasion and is overcome by the agglutinating effect of antibody. *Cell Host Microbe*. Nov 17 2011;10(5):486-96. doi:10.1016/j.chom.2011.09.009
24. Dalia AB, Standish AJ, Weiser JN. Three surface exoglycosidases from *Streptococcus pneumoniae*, NanA, BgaA, and StrH, promote resistance to opsonophagocytic killing by human neutrophils. *Infect Immun*. May 2010;78(5):2108-16. doi:10.1128/IAI.01125-09
25. van Opijnen T, Camilli A. Genome-wide fitness and genetic interactions determined by Tn-seq, a high-throughput massively parallel sequencing method for

microorganisms. *Curr Protoc Microbiol.* Nov 2010;Chapter 1:Unit1E 3. doi:10.1002/9780471729259.mc01e03s19

26. Paulsen IT, Cain AK, Hassan KA. Physical enrichment of transposon mutants from saturation mutant libraries using the TraDISort approach. *Mob Genet Elements.* 2017;7(3):1-7. doi:10.1080/2159256X.2017.1313805

27. Smith LM, Jackson SA, Gardner PP, Fineran PC. SorTn-seq: a high-throughput functional genomics approach to discovering regulators of bacterial gene expression. *Nat Protoc.* Sep 2021;16(9):4382-4418. doi:10.1038/s41596-021-00582-6

28. Shainheit MG, Mule M, Camilli A. The core promoter of the capsule operon of *Streptococcus pneumoniae* is necessary for colonization and invasive disease. *Infect Immun.* Feb 2014;82(2):694-705. doi:10.1128/IAI.01289-13

29. Shainheit MG, Valentino MD, Gilmore MS, Camilli A. Mutations in pneumococcal *cpsE* generated via in vitro serial passaging reveal a potential mechanism of reduced encapsulation utilized by a conjunctival isolate. *J Bacteriol.* May 2015;197(10):1781-91. doi:10.1128/JB.02602-14

30. Nganje CN, Haynes SA, Qabar CM, Lent RC, Bou Ghanem EN, Shainheit MG. PepN is a non-essential, cell wall-localized protein that contributes to neutrophil elastase-mediated killing of *Streptococcus pneumoniae*. *PLoS One.* 2019;14(2):e0211632. doi:10.1371/journal.pone.0211632

31. Geno KA, Gilbert GL, Song JY, et al. Pneumococcal Capsules and Their Types: Past, Present, and Future. *Clin Microbiol Rev.* Jul 2015;28(3):871-99. doi:10.1128/CMR.00024-15

32. Rosconi F, Rudmann E, Li J, et al. A bacterial pan-genome makes gene essentiality strain-dependent and evolvable. *Nat Microbiol.* Oct 2022;7(10):1580-1592. doi:10.1038/s41564-022-01208-7

33. Melin M, Trzcinski K, Meri S, Kayhty H, Vakevainen M. The capsular serotype of *Streptococcus pneumoniae* is more important than the genetic background for resistance to complement. *Infect Immun.* Dec 2010;78(12):5262-70. doi:10.1128/IAI.00740-10

34. Melin M, Jarva H, Siira L, Meri S, Kayhty H, Vakevainen M. *Streptococcus pneumoniae* capsular serotype 19F is more resistant to C3 deposition and less sensitive to opsonophagocytosis than serotype 6B. *Infect Immun.* Feb 2009;77(2):676-84. doi:10.1128/IAI.01186-08

35. Cain AK, Barquist L, Goodman AL, Paulsen IT, Parkhill J, van Opijnen T. A decade of advances in transposon-insertion sequencing. *Nat Rev Genet.* Sep 2020;21(9):526-540. doi:10.1038/s41576-020-0244-x

36. Leshchiner D, Rosconi F, Sundaresh B, et al. A genome-wide atlas of antibiotic susceptibility targets and pathways to tolerance. *Nat Commun.* Jun 7 2022;13(1):3165. doi:10.1038/s41467-022-30967-4

37. van Opijnen T, Camilli A. A fine scale phenotype-genotype virulence map of a bacterial pathogen. *Genome Res.* Dec 2012;22(12):2541-51. doi:10.1101/gr.137430.112
38. Lukose V, Walvoort MTC, Imperiali B. Bacterial phosphoglycosyl transferases: initiators of glycan biosynthesis at the membrane interface. *Glycobiology.* Sep 1 2017;27(9):820-833. doi:10.1093/glycob/cwx064
39. Bricker AL, Camilli A. Transformation of a type 4 encapsulated strain of *Streptococcus pneumoniae*. *FEMS Microbiol Lett.* Mar 15 1999;172(2):131-5. doi:10.1111/j.1574-6968.1999.tb13460.x
40. LeMieux J, Hava DL, Basset A, Camilli A. RrgA and RrgB are components of a multisubunit pilus encoded by the *Streptococcus pneumoniae* rlrA pathogenicity islet. *Infect Immun.* Apr 2006;74(4):2453-6. doi:10.1128/IAI.74.4.2453-2456.2006
41. Ness S, Hilleringmann M. *Streptococcus pneumoniae* Type 1 Pilus - A Multifunctional Tool for Optimized Host Interaction. *Front Microbiol.* 2021;12:615924. doi:10.3389/fmicb.2021.615924
42. Becke TD, Ness S, Kaufmann BK, et al. Pilus-1 Backbone Protein RrgB of *Streptococcus pneumoniae* Binds Collagen I in a Force-Dependent Way. *ACS Nano.* Jun 25 2019;13(6):7155-7165. doi:10.1021/acsnano.9b02587
43. Orrskog S, Rounioja S, Spadafina T, et al. Pilus adhesin RrgA interacts with complement receptor 3, thereby affecting macrophage function and systemic pneumococcal disease. *mBio.* Dec 26 2012;4(1):e00535-12. doi:10.1128/mBio.00535-12
44. Rowe HM, Karlsson E, Echlin H, et al. Bacterial Factors Required for Transmission of *Streptococcus pneumoniae* in Mammalian Hosts. *Cell Host Microbe.* Jun 12 2019;25(6):884-891 e6. doi:10.1016/j.chom.2019.04.012
45. Carter R, Wolf J, van Opijnen T, et al. Genomic analyses of pneumococci from children with sickle cell disease expose host-specific bacterial adaptations and deficits in current interventions. *Cell Host Microbe.* May 14 2014;15(5):587-599. doi:10.1016/j.chom.2014.04.005
46. Anthony, J. S. & van Opijnen, T. A DAG computation server for fully integrated and automated massively parallel sequencing analyses. *GitHub.* <https://github.com/jsa-aerial/aerobio> (2022).

2.8 Supplemental Information

Supplemental Table 2.1 | *S. pneumoniae* strains and knockouts used in this study.

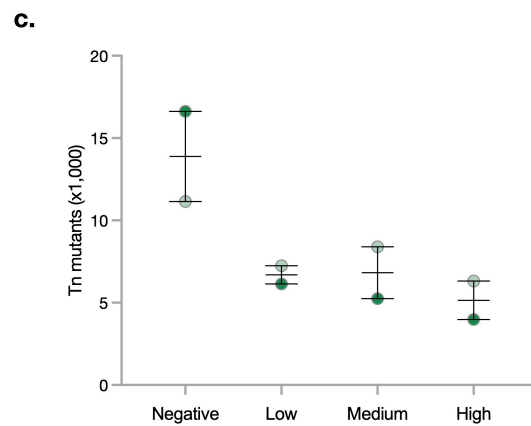
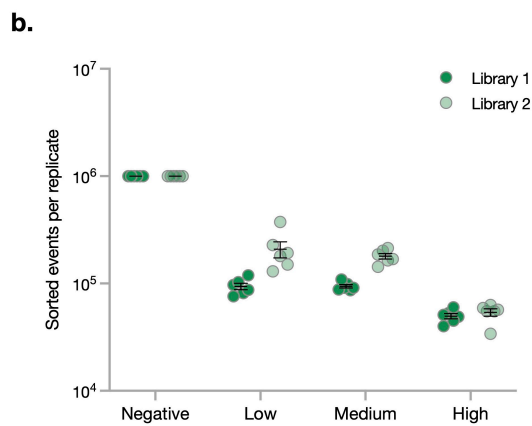
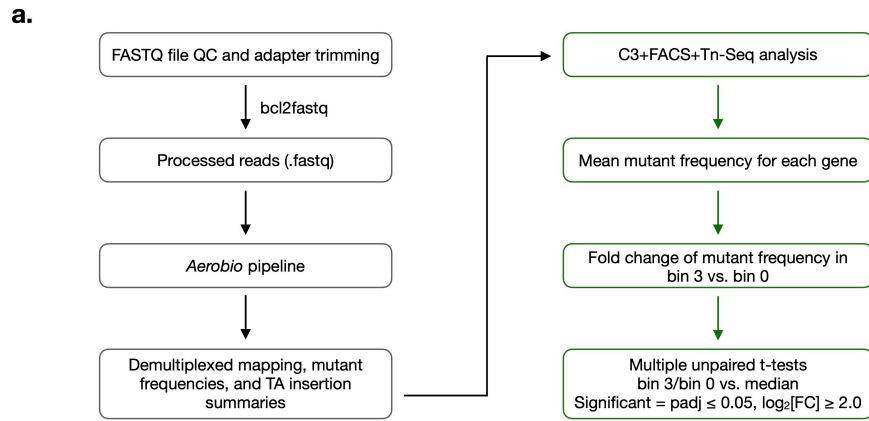
STRAIN	DESCRIPTION	SOURCE
TIGR4	Wild-type serotype 4 encapsulated strain	Laboratory strain
PG13	Wild-type serotype 6C encapsulated strain	Laboratory strain
TIGR4ΔCapsule	Serotype 4 acapsular strain, <i>Cps</i> locus replaced with <i>Spec^R</i> gene (AC2394)	Laboratory strain; Andrew Camilli
TIGR4Δ <i>hk08</i>	Serotype 4 strain with the <i>hk08</i> gene (SP0084) replaced with a <i>Spec^R</i> gene	This work
TIGR4Δ <i>celB</i>	Serotype 4 strain with the <i>celB</i> gene (SP0250) replaced with a <i>Spec^R</i> gene	This work
TIGR4Δ <i>cps4E</i>	Serotype 4 strain with the <i>cps4E</i> gene (SP0350) replaced with a <i>Spec^R</i> gene	This work
TIGR4Δ <i>rrgB</i>	Serotype 4 strain with the <i>rrgB</i> gene (SP0463) replaced with a <i>Spec^R</i> gene	This work
TIGR4ΔSP0470	Serotype 4 strain with the SP0470 gene replaced with a <i>Spec^R</i> gene	This work
TIGR4Δ <i>amy</i>	Serotype 4 strain with the <i>amy</i> gene (SP1382) replaced with a <i>Spec^R</i> gene	This work
TIGR4Δ <i>cppA</i>	Serotype 4 strain with the <i>cppA</i> gene (SP1449) replaced with a <i>Spec^R</i> gene	This work
TIGR4Δ <i>pepQ</i>	Serotype 4 strain with the <i>pepQ</i> gene (SP1591) replaced with a <i>Spec^R</i> gene	This work
TIGR4Δ <i>galK</i>	Serotype 4 strain with the <i>galK</i> gene (SP1853) replaced with a <i>Spec^R</i> gene	This work
TIGR4ΔSP1957	Serotype 4 strain with the SP1957 gene replaced with a <i>Spec^R</i> gene	This work
TIGR4ΔSP1958	Serotype 4 strain with the SP1958 gene replaced with a <i>Spec^R</i> gene	This work
TIGR4ΔSP1982	Serotype 4 strain with the SP1982 gene replaced with a <i>Spec^R</i> gene	This work

Supplemental Table 2.2 | Significantly enriched gene features from Hii-TnSeq. Tn mutants with \log_2 fold change (bin3/bin0) ≥ 5.0 . *P* values are indicated for features in bin 3 samples as compared to the negative control (bin 0).

Gene	Enrichment $\log_2FC(\text{bin3}/\text{bin0})$	Standard deviation	Tn insertions	Adjusted P value
SP_0084	11.0899046	0.96398978	27	0.000001
SP_0470	10.8173557	0.85574103	7	0.000001
SP_1982	9.80749699	0.62909052	8	0.000001
SP_0876	9.54468417	0.965049	15	0.000001
SP_1957	9.4025899	1.04445877	20	0.000001
SP_1115	9.29206041	0.6274053	12	0.000001
SP_0350	8.48262872	0.60972839	56	0.000001
SP_1591	8.25264019	0.88258176	6	0.000001
SP_0164	8.06581935	0.47735574	5	0.000001
SP_2096	7.96524119	1.02397014	13	0.000001
SP_2231	7.09115107	0.93175357	30	0.000001
SP_1853	6.6979729	0.95357159	20	0.000001
SP_0463	6.37917706	0.73219332	67	0.000001
SP_1958	6.37026545	0.9124244	19	0.000001
SP_1602	6.25068983	1.0614597	6	0.000001
SP_1449	6.20093757	0.75622932	68	0.000001
SP_1000	6.17447739	1.00043249	18	0.000001
SP_0250	5.74827177	0.79129814	80	0.000001
SP_0115	5.69762394	0.76009226	12	0.000001
SP_1404	5.67518235	1.0103983	13	0.000001
SP_0256	5.55860681	0.81149921	7	0.000001
SP_1382	5.50029973	0.91562891	33	0.000001
SP_0486	5.3706598	0.58311496	7	0.000001
SP_2067	5.36374827	0.36995368	11	0.000001
SP_1160	5.34831925	0.55580596	14	0.000001
SP_2132	5.29587063	0.72204808	55	0.000001
SP_0617	5.22715606	0.67729021	3	0.000233

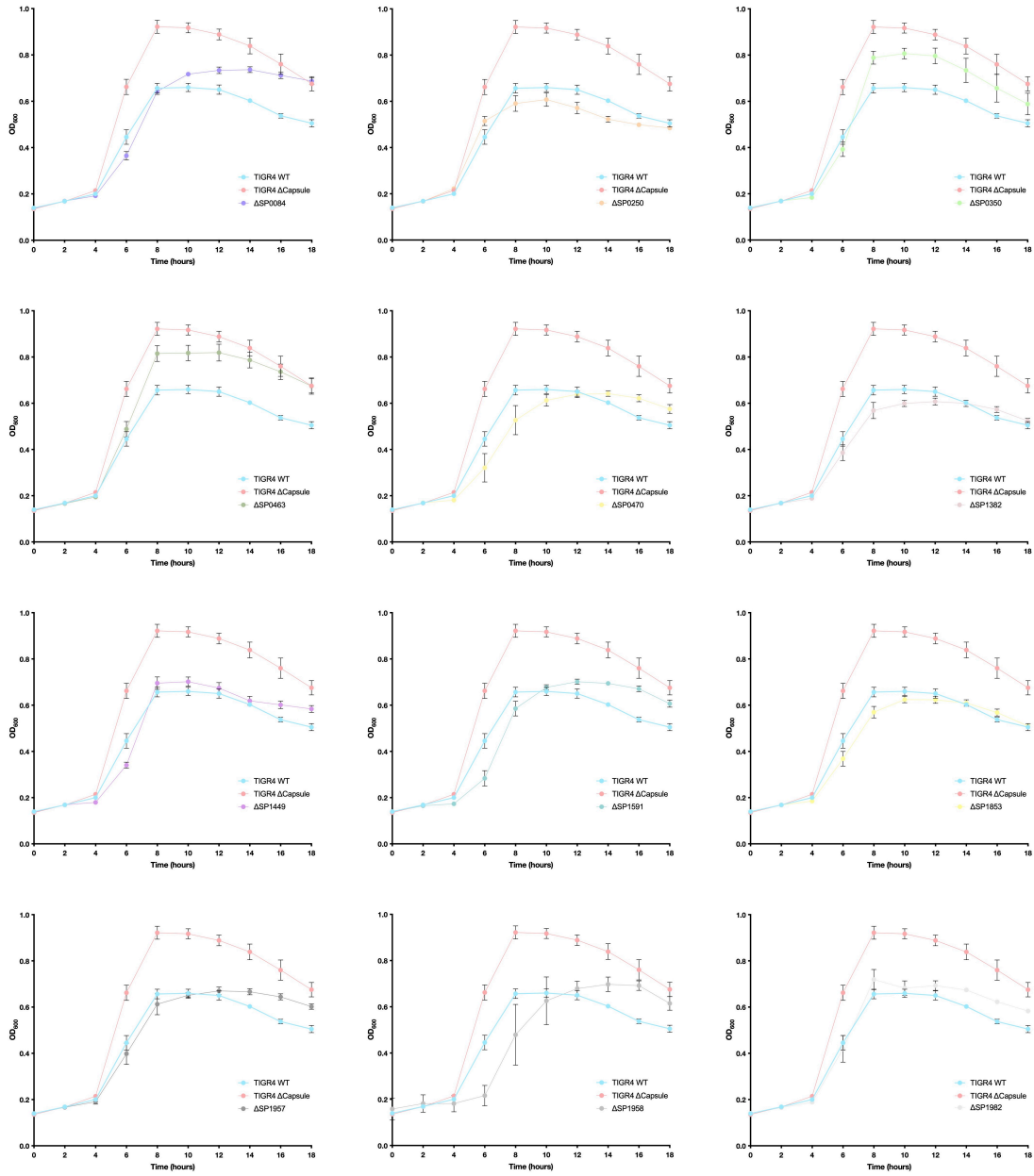
Supplemental Table 2.3 | Primers used in this study. All mutants were constructed in the *S. pneumoniae* strain TIGR4 by homologous recombination ³⁹ with a spectinomycin (SPEC) resistance cassette.

Mutant	F1 primer	SPEC + R1 primer	SPEC + F2 primer	R2 primer	F0 primer	R0 primer
ΔSP_0084	AGATGTCTGA TACGATGATG TC	CGGTATCGAT AAGCTTGATG TTTGTCTCT CGGTTTCTCT A	GGTATCGCT CTTGAAGGAA CCCCTTTACA AATCCAGC	CGCTCACAAT AAGAGAGAA CT	GTTCTGGCG TGACTCCGAT GAA	TAGCAGCCA AGGTGTACT GTTA
ΔSP_0250	TCAAAGTTTA GCTGTTGCTT AC	CGGTATCGAT AAGCTTGATT AATCAAAGAT AGGGCCAAA TC	GGTATCGCT CTTGAAGGA GGTATTTGTG TGTTACTGTT A	AAAGAGAGT GGCCATTAG ATTC	TGACCAAAGT TAAACTGTA GG	TGATTGACTG CGAACCTTAT TA
ΔSP_0350	GCCGACATT AGAAATAGCA CAA	CGGTATCGAT AAGCTTGATT CTATTTCCAT TTGAC	GGTATCGCT CTTGAAGGAT TGGACAATGA AAATAC	CATCTCCTGA AATTGCACCT AT	AGTTCCTCAT CTTGAACTTT TGG	CCTAACTCTC TTTGTCTCTT AA
ΔSP_0463	GGTAGTCGC TTGGAGAATG GAC	CGGTATCGAT AAGCTTGATG ATTTCTCCTT ATTCATATCT C	GGTATCGCT CTTGAAGGG TAAGAGAGAA AGGAGCCAT TG	GAGCTTGGGA GCTCCCATAA ATA	GAATGGTAC GATTACAGAT CCG	CCCCTGTATC TGGCACATC AAT
ΔSP_0470	AAGACACTG CTCAACTTTA CAC	CGGTATCGAT AAGCTTGATG TTTGTATTCT CCATCAAT	GGTATCGCT CTTGAAGGTA TTTGTAGTGG GTAATCCCC	GTCTAAAATC TCTTTATTGG	TATAAGTTCA TCCTCGGAA AAA	AAGATTGTCC TCGATAAGTT CGA
ΔSP_1382	GGAAACATTT ACTTTTTTCC CA	CGGTATCGAT AAGCTTGATA ATGTTTCCTC TTACTTGTC	GGTATCGCT CTTGAAGGTA GCTCATAATA ACCAAGCTA GG	GTCATGAAAA ACCACACTG CGA	GTAATAATAGC AATCATCGAG C	GGCTACTGT GACCAATGTT CAG
ΔSP_1449	TCTCTTTGAT GGCCGTGTC C	CGGTATCGAT AAGCTTGATA AATTCCTCCG TCACTTT	GGTATCGCT CTTGAAGGA GTGGACCAA GATTATTA	ATTGGCCACT CGTTCCTGA C	TCTACCAACG GATGCAAT	CCTTTAAAAA GACCAGTATT TT
ΔSP_1591	CTCAAGACC ATTGAGAATC	CGGTATCGAT AAGCTTGATA TGCTACCTTC TTTCTACCCC T	GGTATCGCT CTTGAAGGA CTATATAGCC CCTATGCTTT C	TATCGAACAC AAGGGAAATT AT	ACTGACATG GACATTCTG A	GAGTTTTCGT TAGATCTTCT TC
ΔSP_1853	GAGGATAGA CCTGTTTGGT C	CGGTATCGAT AAGCTTGATA TGAATTCTCC TTTGACTGTC CG	GGTATCGCT CTTGAAGGTC AAAAGGAGG CTCTATAGTG A	TGCCAAAATC TGCACTGCA GGA	TCAGTCTGGT TCCCAGCAT	TGCTGAAGTC TGATTGTCTC
ΔSP_1957	TGGAAGAGA GAATTCAAAC TAC	CGGTATCGAT AAGCTTGATA TTAACCTCCC TTCAAACAA G	GGTATCGCT CTTGAAGGAA ATCCTTGTTT TTAATTGC	GCTGGAGAA AATGAGATTA T	AAGTGTTAAA TATACCA	GGTCCAGTT CTTGTGGGT GTCA
ΔSP_1958	ACGTGCCATT TTTATCAAAC GC	CGGTATCGAT AAGCTTGATT CTAACTTCCT CTCCATTAT	GGTATCGCT CTTGAAGGAA GAAAACATC TTTATTCCAT G	TTTATCATCA AACCAGATG GTG	TCACATTATT GGATAATATC CAG	GAATGAGAG AACCAGAGG GT
ΔSP_1982	TTATGGGGC AGACAGGTG TT	CGGTATCGAT AAGCTTGATA GGAACCTGC TACAAAACA	GGTATCGCT CTTGAAGGG ATGGAAAGTT TACTTATTC	CGGCACTCT TTTGGATATT AAG	ATGGATTGTG TGGAAGATA GGG	AATTCATCAA TATTGCCAGA

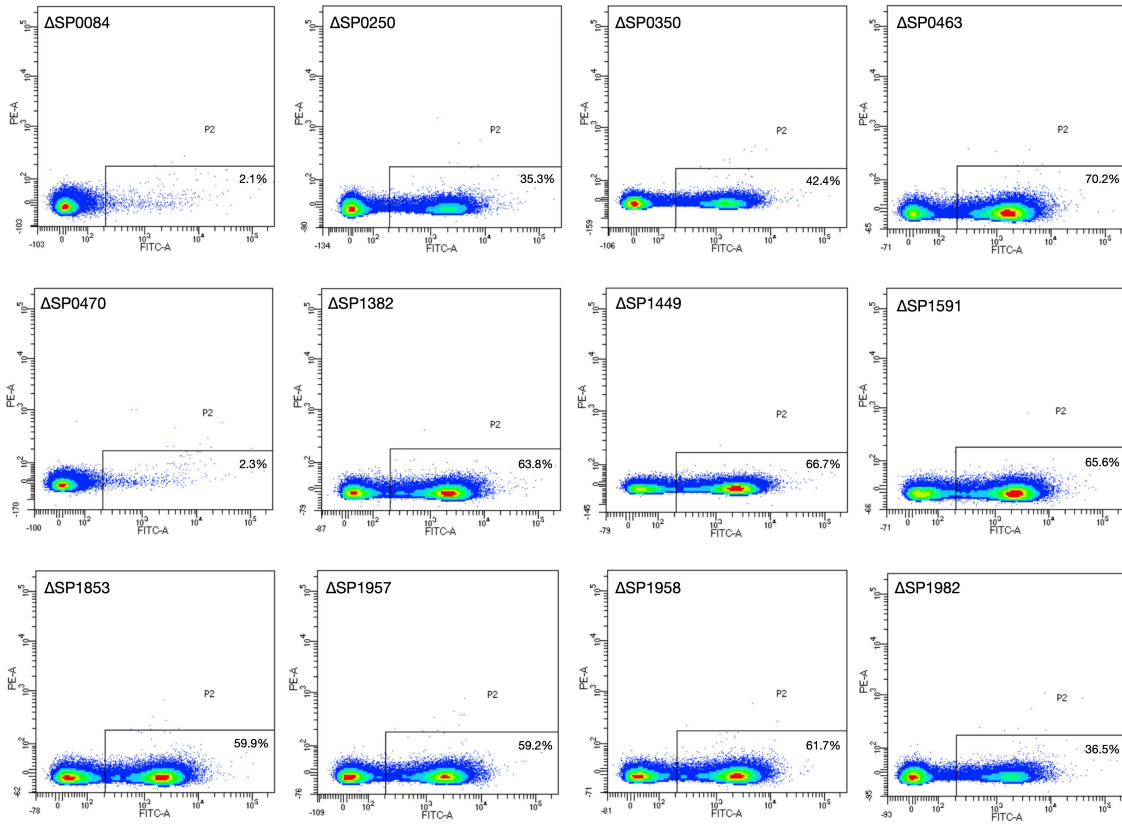


Supplemental Figure 2.1 | Hii-TnSeq analysis and quality control.

a. Hii-TnSeq analysis workflow to identify enriched Tn mutants. **b.** Sorted Hii-TnSeq FITC+ events per replicate, per bin (n=2 libraries, each consisting of 6 independent sorts; lines represent the mean \pm SEM). **c.** Unique Tn mutants observed in each sorted bin (n=2 libraries, each consisting of 6 independent sorts; lines represent the mean \pm SEM).

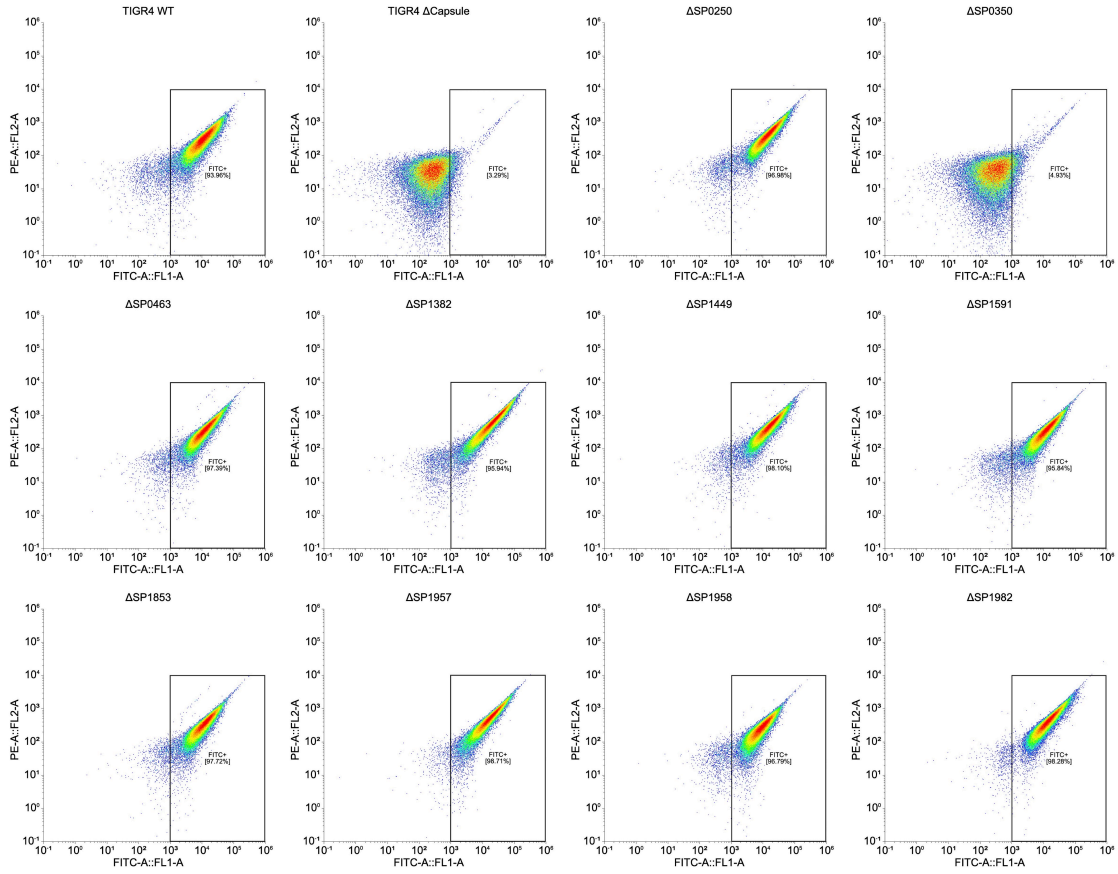


Supplemental Figure 2.2 | TIGR4 wildtype and mutant growth data.
 Growth curve analysis for TIGR4 and derived mutants used in this study in rich media (THY).



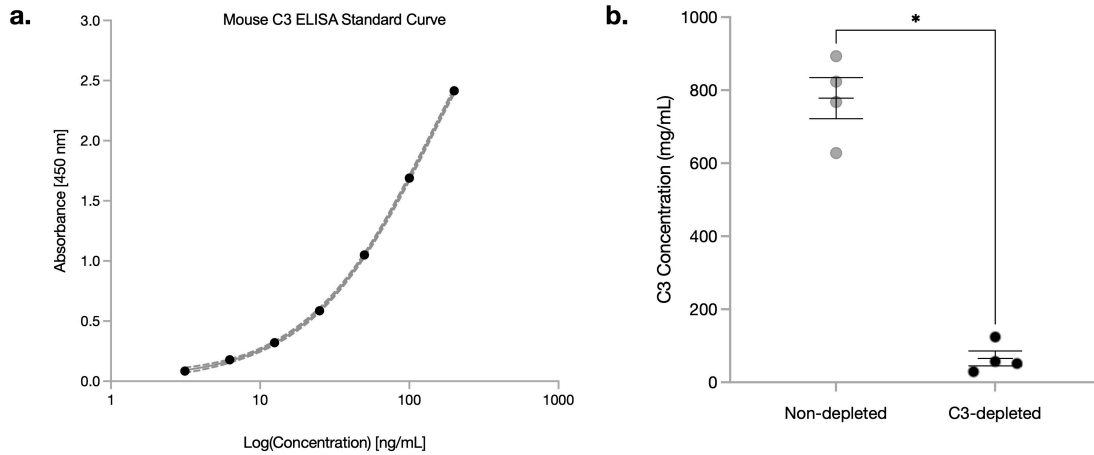
Supplemental Figure 2.3 | Representative C3 deposition flow data.

Flow cytometry output for single gene knockout mutant validations in the C3 deposition assay, analyzed on a BD FACSaria Cell Sorter. %FITC+ is representative of the C3+ phenotype. Flow cytometry data is representative of three independent experiments.



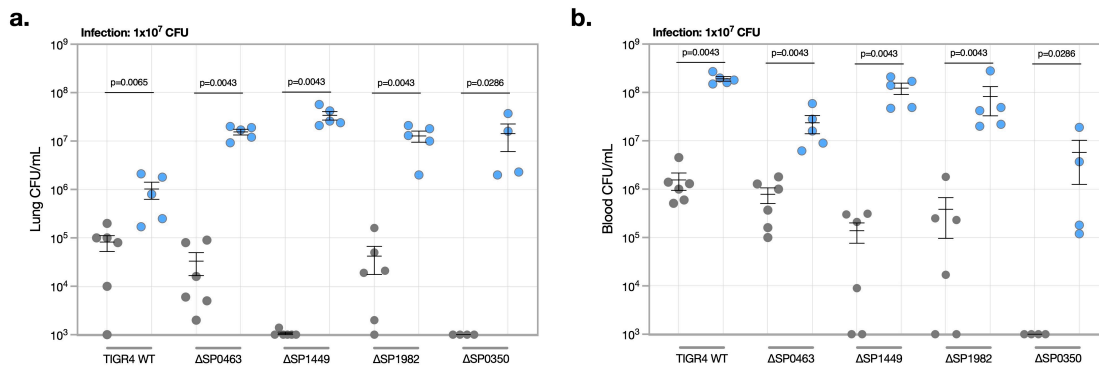
Supplemental Figure 2.4 | Representative capsule quantification flow data.

Flow cytometry output for single gene knockout mutant validations in the capsule quantification assay, analyzed on a Sony SH800 Flow Cytometer. %FITC+ is representative of the Capsule+ phenotype. Flow cytometry data is representative of three independent experiments.



Supplemental Figure 2.5 | C3 serum titers in complement-depleted mice.

Mice depleted of C3 complement by cobra venom factor (CVF) administration by intraperitoneal (I.P.) injection were confirmed to have depleted C3 concentration in serum by ELISA. **a.** Standard curve for serum concentration calculation and **b.** measured C3 concentrations in the serum of non-depleted (untreated) animals and C3-depleted (treated with CVF) animals. Data are displayed as mean \pm SEM. * $p < 0.01$, ** $p < 0.001$, *** $p < 0.0001$, two-tailed t-test.



Supplemental Figure 2.6 | *S. pneumoniae* knockouts with a hyper C3 deposition phenotype are entirely virulent in C3-depleted animals.

Additional infection studies were performed in C3-depleted mice with a higher inoculum dose of 1×10^7 CFU and bacterial burden was determined in the **a.** lungs and **b.** in the bloodstream.

3

Disease outcome:

Identifying signatures of infection outcome
from the dual (host/bacterial)
transcriptome

Bharathi Sundaresh*, Karen (Zeyu) Zhu, and Tim van Opijnen

*First author contribution

Unpublished data, project ongoing at Broad Institute of MIT and Harvard

Author's contributions: B.S. performed all experiments, data collection, data analysis, data interpretation, and wrote the chapter. B.S. and T.v.O. devised the study. K.Z. previously developed methods for dual RNA isolation and dual RNA-Seq library prep.

3.1 Summary

The ability to predict bacterial survival during an active infection has applications in diagnostics, prognostics, and administering tailored antibacterial treatments. Our group has previously shown the transcriptional response to an environmental stress generally distinguishes strains with different survival outcomes in vitro; a strain with survival failure triggers extensive transcriptomic disruption compared to a strain with survival success. The next step is the extension of this model to survival outcomes of pathogenic bacterial strains in vivo during an active infection. To date, dual RNA-Seq has been applied to study the transcriptomes of both the host and the pathogen in cell culture models. While these studies reveal novel responses related to infection, the models lack complexities such as the mammalian innate immune response and nutrient availability of an infection niche. To combat this limitation, we developed a sensitive dual RNA-Seq technique for simultaneously mapping the transcriptomic response for the pathogen and the host in a murine *Streptococcus pneumoniae* infection model during four distinct, confirmed infection scenarios: (1) a lethal, bacteremia infection; (2) an intermediate, pneumonia infection; (3) a nonlethal, cleared infection; and (4) an uninfected host. By mapping both the host (*M. musculus*) and pathogen (*S. pneumoniae*), we discovered transcriptomic signatures specific to each infection scenario. This approach brings us a step closer to personalized diagnostics and prognostics of bacterial infections, with the ultimate goal of deploying highly targeted and patient-specific host-informed therapeutic strategies.

3.2 Introduction

During infection, pathogens trigger the expression of unique genes to ensure their survival and allow replication within the host environment. In turn, the host activates complex immune mechanisms to recognize and kill pathogens. Hence, the simultaneous detection of host and pathogen transcripts during the infection process can provide deeper insights into the host-pathogen interaction than those detected from the host or pathogen alone. Omics technologies provide powerful tools to study bacterial pathogens in their entirety in different experimental set-ups. Specifically, high-throughput transcriptomics can divulge changes in gene expression profiles of both the pathogen and the host cells during infection. In the past five years, dual RNA-Seq (dRNA-Seq) has been applied to study transcriptomes of the host and the pathogen simultaneously in *ex vivo* cell culture models¹⁻², and few studies exist using dRNA-Seq to elucidate host-inherent variability of *S. pneumoniae* infection in vivo³⁻⁶. While these studies have revealed novel responses related to infection, the majority of models used in transcriptomic studies lack components such as the mammalian innate immune response and nutrient availability of an infection micro-environment. Here, we implement the novel method dRNA-Seq in a lung infection murine model mimicking *S. pneumoniae* pneumonia and bacteremia to capture a temporal transcriptomic snapshot in an environment that gives a closer understanding to the pathophysiology of human pneumococcal infection and a better understanding of the host-pathogen duel.

Streptococcus pneumoniae remains a threat to patients with complement deficiencies (e.g., multiple myeloma, Sickle Cell Disease⁷) and impaired neutrophil function (e.g., Chediak-Higashi syndrome⁸), and we lack a clear understanding of the interplay between impaired innate immune function and the pathogen on a transcriptome-wide level. On a simplified level, we hypothesize the dual transcriptomic signature of either the pathogen (*S. pneumoniae*) or the murine host can be utilized as an early predictor for infection outcome: either lethal (**Figure 3.1a**) or nonlethal (**Figure 3.1b**) to the host. However, the factors that regulate the passage of bacteria between different anatomical compartments (i.e., lungs to bloodstream) are unclear. What is known about the *S. pneumoniae*-host interaction are the steps of bacterial invasion facilitating acute pulmonary infection to system disease: evasion of clearance, adherence, endocytosis, paracellular invasion, and

invasion of bloodstream ⁹. *S. pneumoniae* factors integral for the pathogen have been identified at each step, including but not limited to the negatively charged capsular polysaccharide and zinc metalloprotease (ZmpA; IgA1 protease) allowing evasion of host clearance, and pneumococcal surface proteins (ChoP, CbpA) that enable the pneumococcus to traverse the lung epithelium and enter the bloodstream ⁹. What is unknown are how dynamic changes across the bacterial and host transcriptome assist the pathogen to cause a lethal outcome (**Figure 3.1a**) or allow the host to overcome bacterial disease (**Figure 3.1b**).

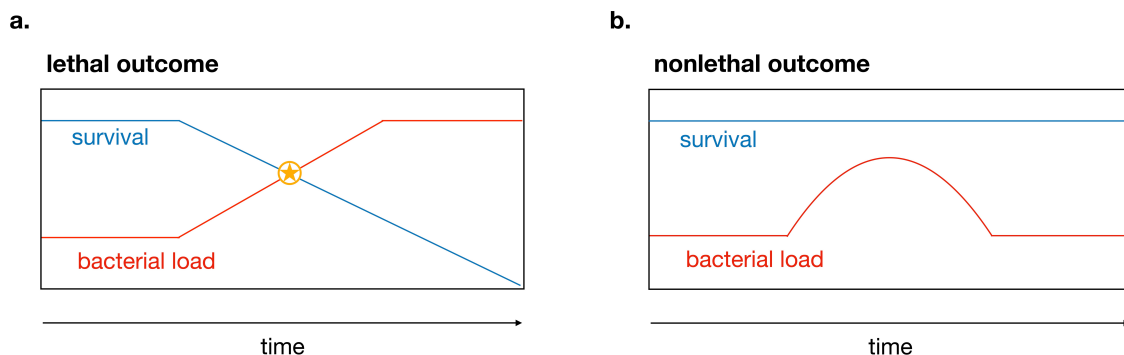


Figure 3.1 | Defining lethal and nonlethal infection outcomes.

a. A lethal outcome of bacterial infection results in a drop in **host survival (blue)**, and an increase in **bacterial load (red)**, while **b.** a nonlethal outcome results in 100% host survival (blue), with the host immune response clearing the bacterial load (red). Star indicates the hypothetical prediction point where a dual RNA-Seq sample's transcriptomic signature allows lethal infection outcome prediction, and therapeutic intervention can be administered to the patient.

In this chapter, we have used an experimental model of infection with *S. pneumoniae* to simultaneously examine the host and bacterial factors involved in the passage of bacteria from the lung to the bloodstream to cause severe infection and bacteremia. We first establish known infection outcomes through a series of preliminary mouse survival experiments and confirm four infection conditions: (1) a lethal, bacteremia infection; (2) an intermediate, pneumonia infection; (3) a nonlethal, cleared infection; and (4) an uninfected host. Consistent with our group's previous observations during in vitro settings ¹⁰, the *S. pneumoniae* transcriptome exhibits a high degree of disruption, defined as a significant portion of the transcriptome significantly differentially expressed, in severe infection conditions (lethal vs. intermediate, lethal vs. cleared) compared to a less severe infection (intermediate vs. cleared). On the contrary, the host transcriptome exhibits a counteracting pattern by triggering an active immune and pro-inflammatory

response across all infection conditions but has signatures specific to: (1) lethal, (2) intermediate, (3) cleared infections. Herein, we present a complete characterization of distinct infection outcomes using the dual transcriptomes of *S. pneumoniae* and a murine host 20 hours-post infection and demonstrate that these responses are characteristic of infection outcome.

3.3 Results

3.3.1. Defining *S. pneumoniae* infection outcomes

To establish the conditions for dRNA-Seq studies, we first required confirmed infection scenarios in a *S. pneumoniae* murine lung infection model, with clear-cut survival predictions. Thus, two variables are established: (1) the strain of *S. pneumoniae*; and (2) the intranasal inoculum dose (CFU). Initially, mice were inoculated with *S. pneumoniae* TIGR4 (serotype 4), a highly virulent strain used in the studies in **Chapters 2 and 4** of this thesis. A dose-range finding study was conducted with mice inoculated with a TIGR4 inoculum ranging from 5×10^5 to 1×10^8 (**Figure 3.2**). Consistent with previous observations, even at a low dose of TIGR4 (i.e., 5×10^5 CFU), a subset of animals succumbs to infection and reaches a clinical score of 5-6 (humane endpoint) (**Table 3.1**) within 24-48 hours (**Figure 3.2a,c**) with a high bacterial burden in the lungs and bloodstream (**Figure 3.2b**). Under the 5×10^5 CFU infection condition, only 60% of mice survived, suggesting even a low dose of TIGR4 will not result in a completely cleared infection. Based on these results, we determined TIGR4 was not a suitable strain for mouse infections with sufficient isolated RNA for downstream dRNA-Seq studies with clear cut infection outcomes.

Based on previous work by our group to analyze virulence across the *S. pneumoniae* pangenome ¹², we selected the strain PG13 ¹³ (serotype 6C) for its high lung transmission (100% animals) and its low blood transmission (<30% animals) at a 1×10^8 CFU inoculum. This pneumonia phenotype without bacteremia allows for (1) a bacteremia infection outcome at a high inoculum dose (PG13, $1-5 \times 10^9$ CFU); (2) a pneumonia infection outcome at an intermediate dose (PG13, 5×10^8 CFU); and (3) a cleared infection outcome (PG13, 1×10^7 CFU) (**Figure 3.3a-c**). Most importantly, all three infection outcomes result in recoverable CFU in the mouse bronchoalveolar lavage (BAL) fluid 20 hours-post infection (**Figure 3.3b**), for dual (host/pathogen) RNA isolation for dual RNA-Seq.

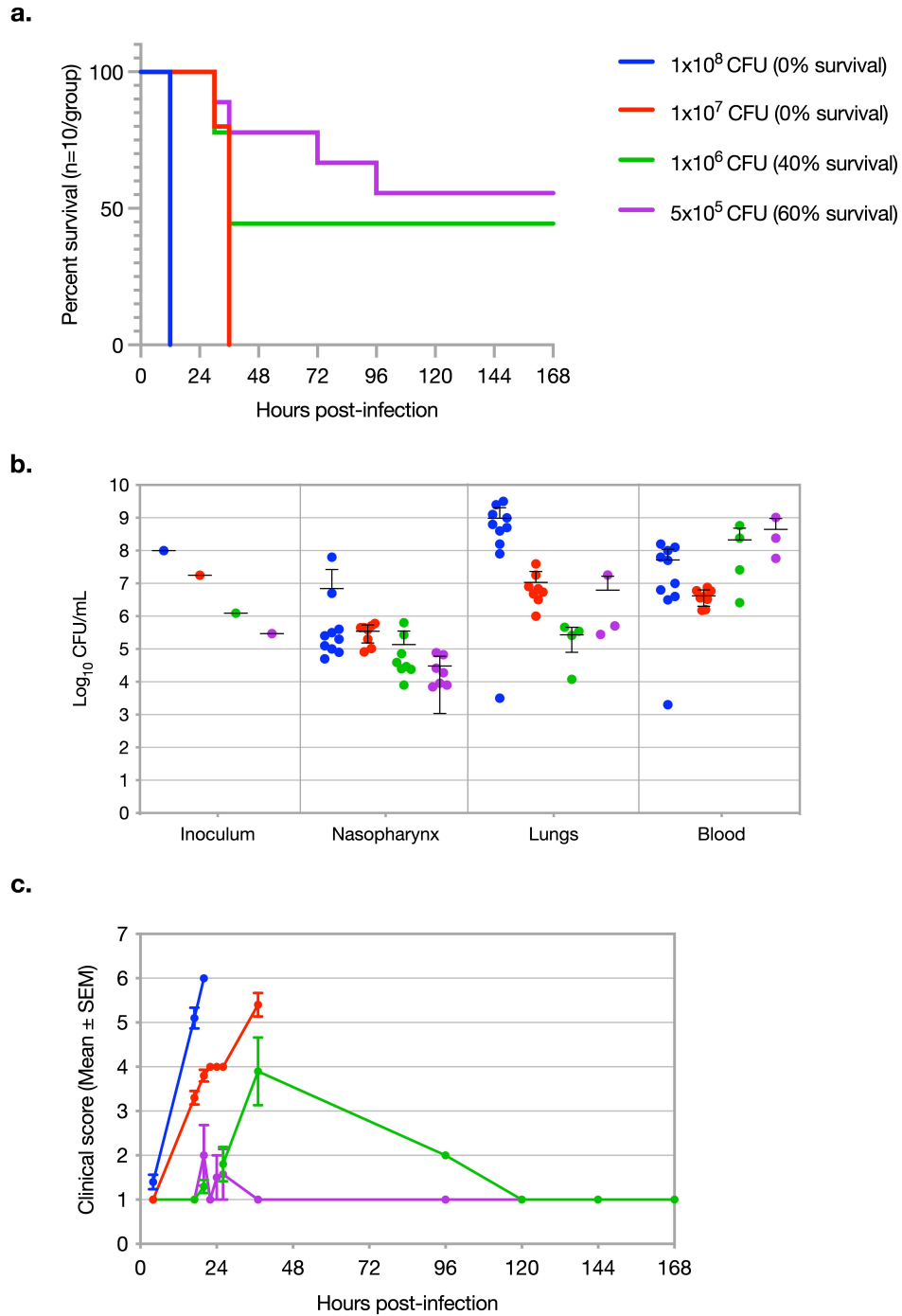


Figure 3.2 | Infection outcomes of *S. pneumoniae* TIGR4 infection.

a. Groups of ten, four- to six-week-old Swiss Webster mice were infected with *S. pneumoniae* TIGR4 (serotype 4) at doses ranging from 5x10⁵ to 1x10⁸ total CFU and monitored for Kaplan Meir survival analysis. **b.** Mice from a. were sacrificed at the humane endpoint (clinical score = 5), and nasopharynx lavage, lung homogenate, and whole blood via cardiac puncture were plated for CFU enumeration. **c.** Clinical score monitoring of mice pre-sacrifice.

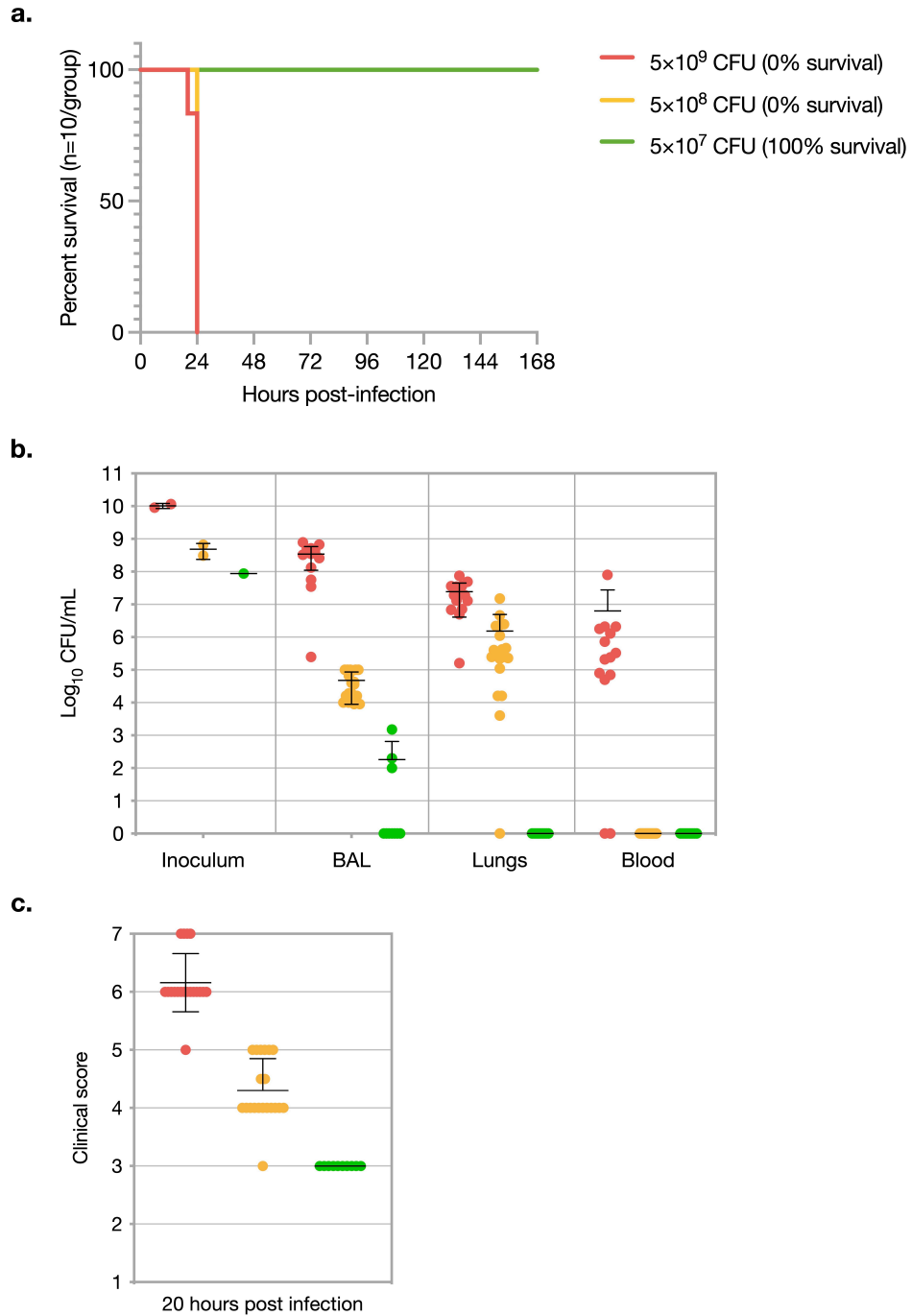


Figure 3.3 | Infection outcomes of *S. pneumoniae* PG13 infection.

a. Groups of ten, four- to six-week-old Swiss Webster mice were infected with *S. pneumoniae* PG13 (serotype 6C) at doses ranging from 5×10^7 to 5×10^9 total CFU and monitored for Kaplan Meir survival analysis. **b.** Mice from were sacrificed 20 hours-post infection, and bronchoalveolar lavage (BAL) for dual RNA-Seq samples, lung homogenate, and whole blood via cardiac puncture were plated for CFU enumeration. **c.** Clinical score of mice pre-sacrifice at dual RNA-Seq experiment's endpoint (20 hours post-infection).

Table 3.1 | Clinical score scale for mice infected with *S. pneumoniae* ¹¹

CLINICAL SCORE	CLINICAL SYMPTOMS
1	Lack of clinical symptoms; healthy animal
2	Slightly hunched animal
3	A hunched animal with starry coat
4	A severely hunched animal with a partial starry coat
5*	A severely hunched animal with a starry coat covering the entire body*
6*	A slightly lethargic animal*
7*	A lethargic animal/moribund*

*Humane endpoint for sacrifice.

3.3.2. Dual RNA isolation and transcriptome profiling

RNA isolations from BAL samples have varying degrees of available material (in nanograms; ng) (**Figure 3.4a**) and quality (**Figure 3.4b**), with most isolations having an RNA integrity (RIN) score ranging from 5.0 – 8.0. Key to the RNA isolation method is: (1) immediate RNA stabilization in *RNAlater* + β -Mercaptoethanol, and (2) prioritizing samples with greater than 4 mL of recovered BAL as starting material. However, RNA yield from BAL samples is relatively low, suggesting BAL RNA should be treated as a low input sample (<100 ng). In this study, total RNA (host+pathogen) from the BAL of each mouse was isolated and subjected to low input strand-specific library preparation (NEBNext Ultra II Directional RNA library prep) and paired-end Illumina sequencing as described in **Figure 3.5** and **Materials and Methods**, which generated an average of 25M total reads per sample.

Sequencing reads were aligned to the murine (GRCm38_mm10) and *S. pneumoniae* PG13 (CP035254; TVO_1901932) genome via STAR ¹⁴ and Bowtie ¹⁵, respectively. Reads mapped to either genome are split and aggregated by featureCounts ¹⁶, and differential expression is calculated with DESeq2 ¹⁷ (**Figure 3.6**). Differential expression comparisons are made between infection conditions and uninfected controls for mouse genes, and between infection conditions and THY broth controls for *S. pneumoniae* genes. Significant differential expression is filtered based on two criteria: $|\log_2\text{FoldChange}| \geq 2.0$ and adjusted p-value (padj) ≤ 0.05 . A comparison of percentages of reads uniquely mapped to the mouse and PG13 genomes showed considerable differences between the three infection conditions (**Figure 3.7a**), notably in the percentage of reads uniquely

mapped to both genomes (**Figure 3.7b**). In the case of three out of four lethal dose replicates, >60% of total reads were assigned to the PG13 genome. In comparison, the intermediate and cleared infection conditions had the majority of reads assigned to the mouse genome. Consistent with a past TIGR4 dual RNA-Seq study in our lab, mouse reads assigned to CDS are low, ranging from 0.5-1M assigned CDS featureCounts per replicate (**Figure 3.7a**). Troubleshooting is underway to increase the mouse reads assigned to CDS either by increasing sequencing depth or optimizing the data analysis workflow. Additionally, and unexpectedly, reads from nonlethal and uninfected replicates were mapped to the PG13 genome. While this could have been due to an experimental contamination during RNA isolation and library prep, the more likely explanation is an issue during data analysis. Moreover, improvements to our analysis workflow are currently in progress.

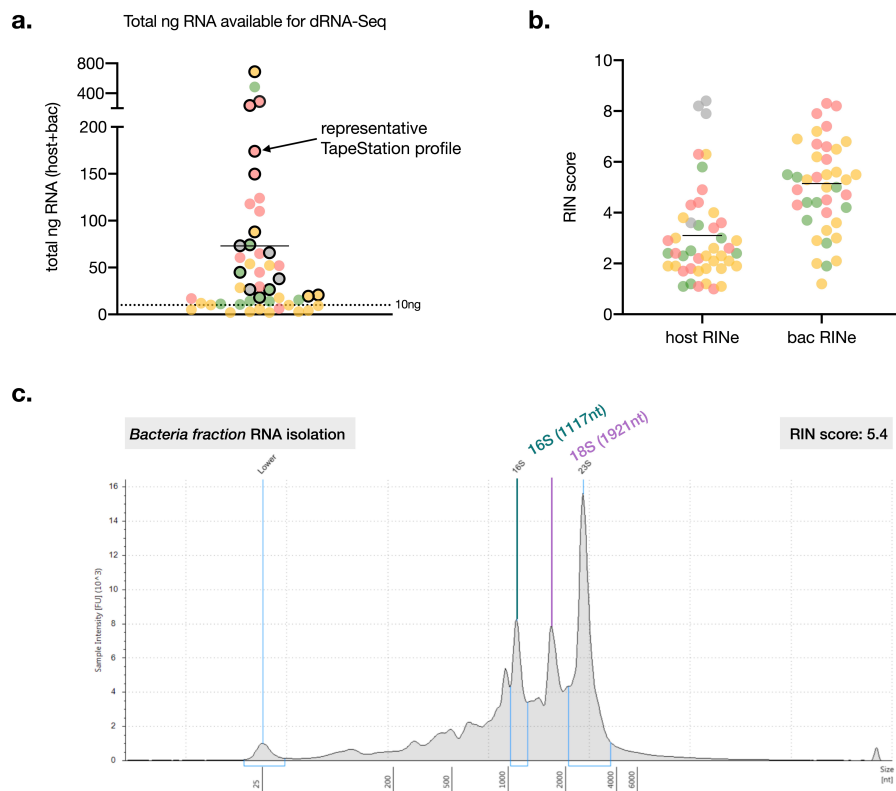


Figure 3.4 | Dual RNA isolation from mouse bronchoalveolar lavage.

a. RNA concentration (outlined points used for dual RNA-Seq study) and **b.** RNA integrity (RIN) score determined by TapeStation 4200 (Agilent) automated electrophoresis system. Each dot represents an independent RNA isolation from a single mouse BAL sample. **c.** A TapeStation trace of the *host fraction* (top) and the *bacteria fraction* (bottom) prior to pooling shows both the prokaryotic 16S rRNA (~1117nt) and the eukaryotic 18S rRNA (~1921nt) peaks in the *bacteria fraction*.

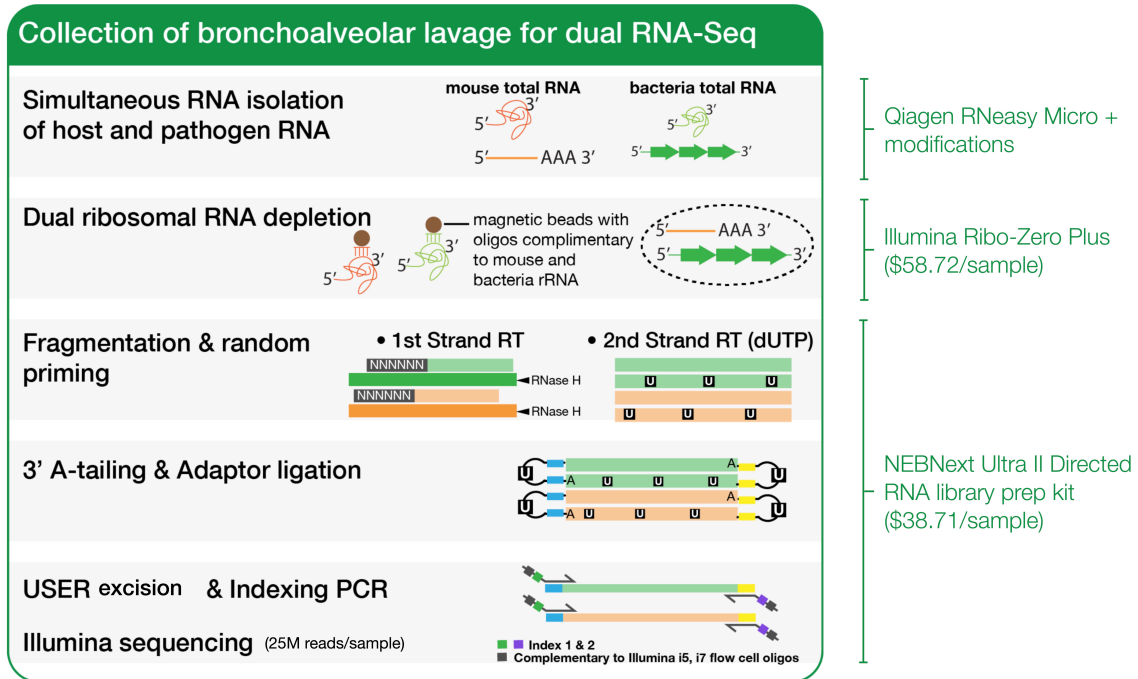


Figure 3.5 | Summary of dual RNA-Seq library preparation workflow.

Total RNA of bacterial and host origin is subjected to ribosomal depletion by Illumina Ribo-Zero Plus. rRNA-depleted and bead cleaned-up RNA is used in the first strand cDNA synthesis with random hexamers, followed by second strand synthesis with dUTP. The double stranded cDNA library is then ligated to adapters containing dUTP in a loop structure. All dUTP are excised by the USER enzyme mix (Uracil DNA glycosylase (UDG) and the DNA glycosylase-lyase Endonuclease VIII) and the single strand cDNA library is size selected and cleaned up with SPRI beads and subjected to an enrichment PCR of 15-18 cycles. *Figure credit: Karen Zhu.*

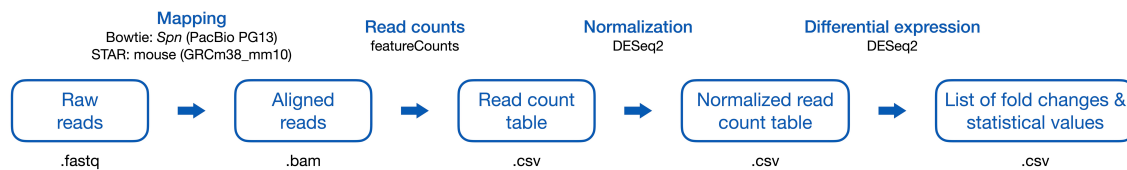


Figure 3.6 | Summary of dual RNA-Seq data analysis workflow.

Sequencing reads are aligned to murine (GRCm38_mm10) and *S. pneumoniae* PG13 (CP035254) and processed, as described in **Materials and Methods**.

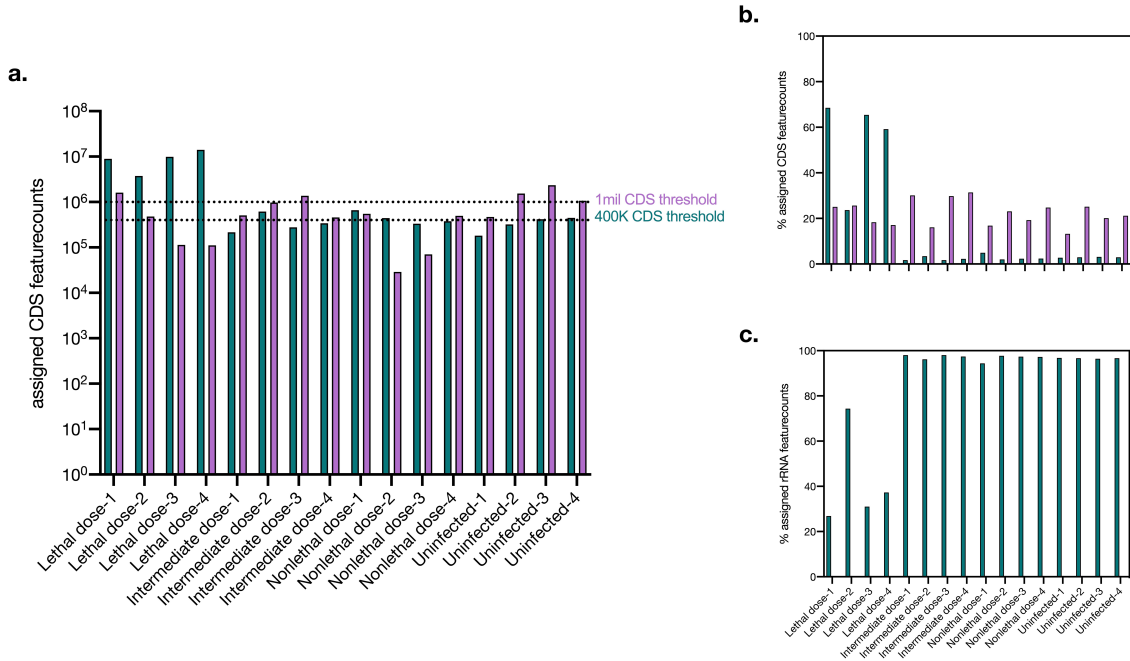


Figure 3.7 | Mapping of dual RNA-Seq reads.

a. Assigned CDS reads (featurecounts) mapped to the mouse genome (purple) and the *S. pneumoniae* PG13 genome (turquoise). **b.** Percentage of reads that are uniquely mapped to the mouse genome (purple) and the *S. pneumoniae* PG13 genome (turquoise). **c.** Percentage of reads that are uniquely mapped to mouse rRNA (purple, <1.0%) and *S. pneumoniae* PG13 rRNA (turquoise). All pairwise sample comparisons of *S. pneumoniae* and mouse RNA-Seq read counts are plotted in **Supplemental Figure 3.2 and 3.3.**

3.3.3. *S. pneumoniae* transcriptomic response across infection conditions

To identify differentially expressed bacterial genes across infection conditions, mRNA-specific reads counts are first compared between in vivo samples and an in vitro broth control, then compared across infection outcomes. On a transcriptome level, genome-wide differential expression is observed under the bacteremia (lethal) vs. cleared infection with 376 DEGs and the bacteremia (lethal) vs. pneumonia (intermediate) infection with 304 DEGs (**Figure 3.8a,b**; with 243 shared DEGs between the two comparisons). The comparison between the intermediate and cleared infection conditions yielded no significant DEGs, due to close similarity between samples. In the case of the comparison in **Figure 3.8c**, the host transcriptome during the cleared infection condition will likely be more illustrative.

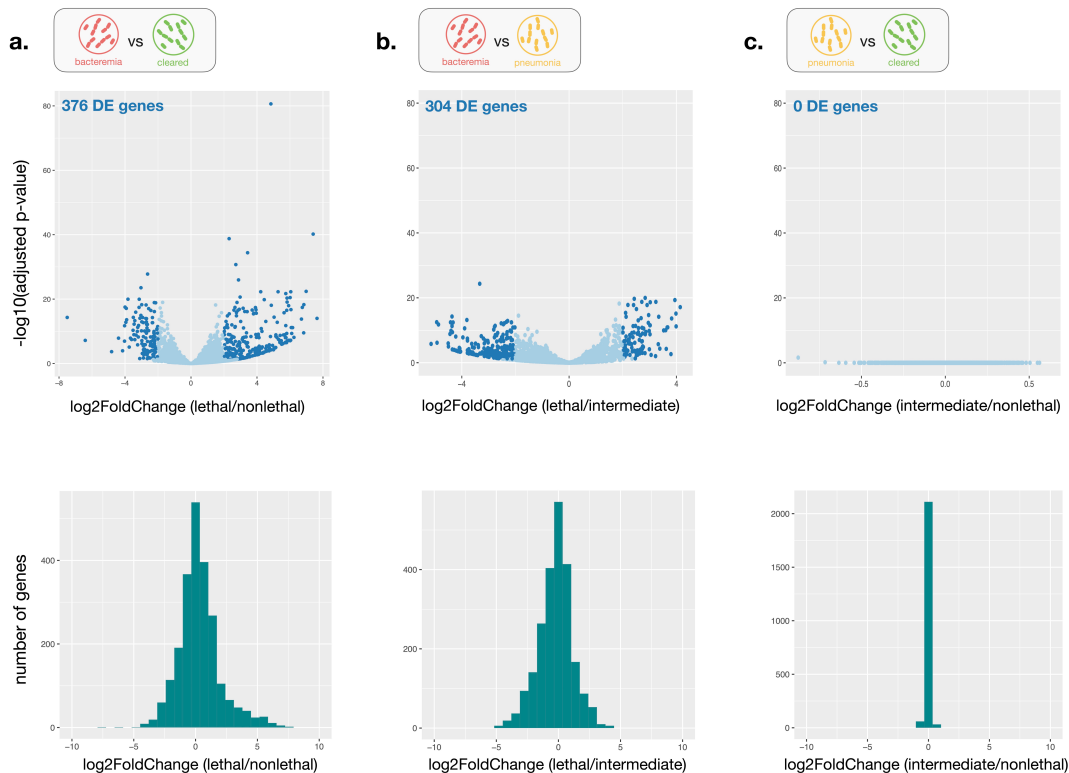


Figure 3.8 | Summary of *S. pneumoniae* differential transcriptomic analysis.

Differentially expressed genes (top) and magnitude of distribution of genome-wide differential expression (bottom) of the bacterial transcriptome with the following comparisons: **a.** lethal infection vs. cleared infection; **b.** lethal infection vs. intermediate infection; **c.** intermediate infection vs. cleared infection. Significant differential expression is filtered based on two criteria: $|\log_2\text{FoldChange}| \geq 2.0$ and adjusted p-value (p_{adj}) ≤ 0.05 .

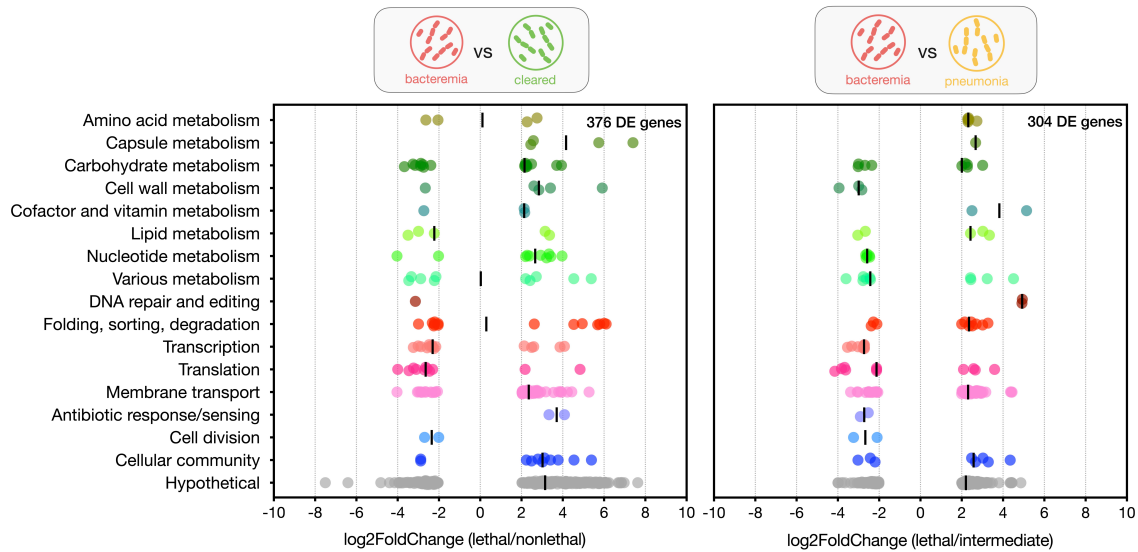


Figure 3.9 | Transcriptomic response of *S. pneumoniae* PG13 under bacteremia and pneumonia infection conditions.

Magnitude distribution of significant (plotted) genome-wide differential expression by gene functional category. Comparisons were made between lethal/cleared infection and lethal/intermediate infection. DEGs with a $|\log_2\text{FoldChange}| \geq 2.0$ and adjusted p-value (p_{adj}) ≤ 0.05 are plotted.

To analyze bacterial DEGs that are both up-regulated and down-regulated, we separated the transcriptomic responses by gene functional category (**Figure 3.9, Figure 3.10, Figure 3.11**). Specific to the bacteremia (lethal) infection outcome is the up-regulation of **capsule genes *cpsC* and *cpsD*** (**Figure 3.10**). Specifically, CpsD (bacterial tyrosine-kinase) localizes at the cell division site and participates in the proper assembly of the capsule¹⁸. CpsC is required for CpsD tyrosine autophosphorylation; a *cpsC*-deletion mutant is rough, and CpsD does not become phosphorylated¹⁹. Mutation of the *cpsD* gene inactivates the ATP-binding site and eliminates capsule production. The capacity to regulate CPS production at the transcriptional, translational, or post-translational level is important for the survival of *S. pneumoniae* in different host environments. The polysaccharide capsule is an established pneumococcal virulence factor (**Chapter 2**), and maximal expression of capsule is essential for systemic virulence as we observed during lethal infection, but the extent of exposure of other important pneumococcal surface structures, such as adhesins, is also influenced by capsular thickness.

Under carbohydrate metabolism, the **surface exoglycosidase beta-galactosidase (BgaC)** was up-regulated across both infection comparisons, suggesting resistance to opsonophagocytosis and de-glycosylation of human glycoconjugates is essential for *S. pneumoniae* to establish a lethal infection outcome ¹⁹. Nearly half of the up-regulated genes are involved in **membrane transport (Figure 3.11a)**, predominately ATP-binding cassettes (ABC) and phosphotransferase system (PTS) transporters for sugars, amino acids, and ions (**Figure 3.11b**). Up-regulated transporters include ATP-binding cassettes (ABC) and phosphotransferase system (PTS) transporters for sugars, amino acids, and ions (**Figure 3.11b**). Several up-regulated carbohydrate metabolism genes are involved in glycolysis, galactose, fructose, and mannose metabolism. Genes in galactose and mannose metabolism have been implicated in the maintenance of colonization and virulence through the control of capsule thickness and quorum sensing ¹⁹.

Competence and bacteriocin genes, two categories of bacterial immunity genes that enhance colonization and outcompete rival microbes within the infection niche are additionally up-regulated. Finally, a notable down-regulated gene across both comparisons is **araD, or L-ribulose-5-phosphate-4-epimerase**, a component of the pentose phosphate pathway. Bacteria utilize arabinose as an energy source by converting it to an intermediate within the pentose phosphate pathway; this suggests *S. pneumoniae* is down-regulating certain energy expenditures during an energy-intensive state of establishing and creating a lethal infection environment within the host lung.

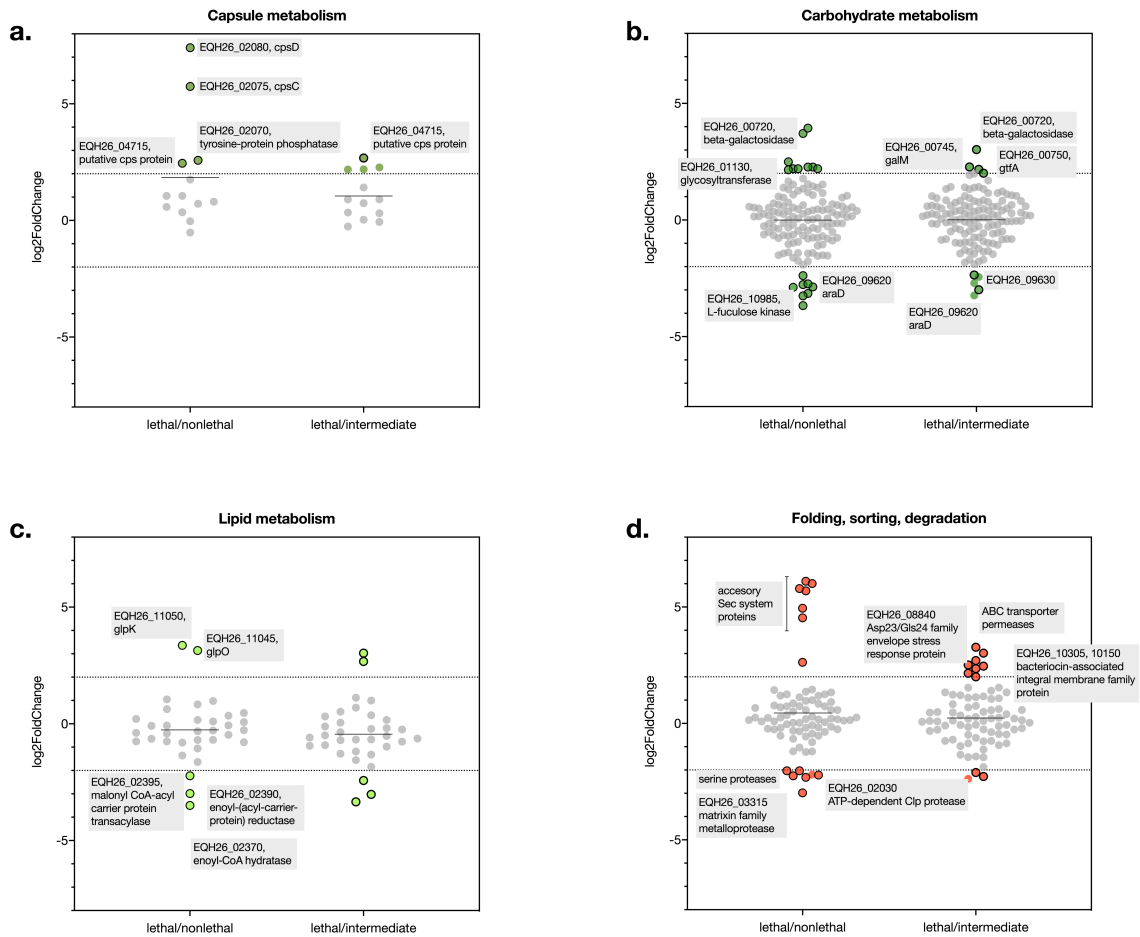


Figure 3.10 | Subset of significant *S. pneumoniae* metabolism DEGs.

Significant DE genes in *S. pneumoniae* **a.** capsule metabolism, **b.** carbohydrate metabolism, **c.** lipid metabolism, and **d.** folding, sorting, degradation gene functional categories. Colored circles (genes) have a $|\log_2\text{FoldChange}| \geq 2.0$, outlined and colored circles have a $|\log_2\text{FoldChange}| \geq 2.0$ and adjusted p-value (padj) ≤ 0.05 .

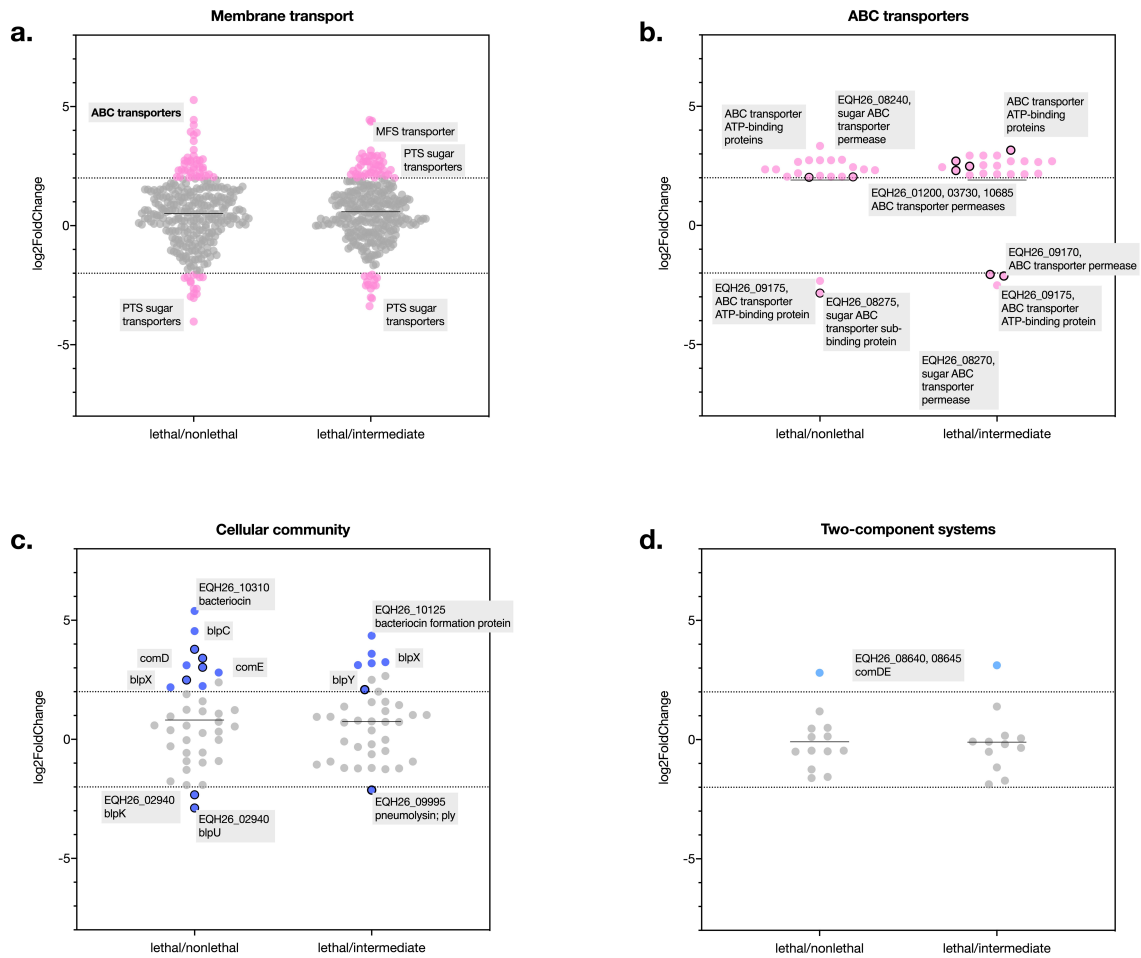


Figure 3.11 | Subset of significant *S. pneumoniae* transport and cellular community DEGs. Significant DE genes in *S. pneumoniae* **a.** membrane transport, **b.** subset of a: ABC transporters, **c.** cellular community, and **d.** subset of c: two-component systems. Colored circles (genes) have a $|\log_2\text{FoldChange}| \geq 2.0$, outlined and colored circles have a $|\log_2\text{FoldChange}| \geq 2.0$ and adjusted p-value (padj) ≤ 0.05 .

3.3.4. Host transcriptomic response across infection conditions

To identify differentially expressed host genes across infection conditions, mRNA-specific reads counts are first compared between mouse infected samples and mouse uninfected controls. Since ENCODE ²⁰ recommends 30M reads per sequencing sample, the low numbers of mouse CDS-specific reads in our samples will likely represent low sequencing depths. We reasoned that although the differential expression of individual genes might not be statistically significant, pathway enrichment patterns in differential expression may provide a higher confidence of our data and identify at least the biological processes, pathways, and molecular functions affected in host cells during *S. pneumoniae* infection. On a transcriptome level, genome-wide differential expression is observed during bacteremia (lethal) infection with 592 DEGs, the pneumonia (intermediate) infection with 418 DEGs, and the cleared infection with 797 DEGs (**Figure 3.12**) with 113 DEGs shared across all three conditions (**Figure 3.13**). Here, we note the largest number of significant DEGs in the cleared vs. uninfected comparison, suggesting the transcriptome of a host that has overcome infection has a chaotic, but notable response that should be further investigated in the context of host-informed therapeutic target discovery and development.

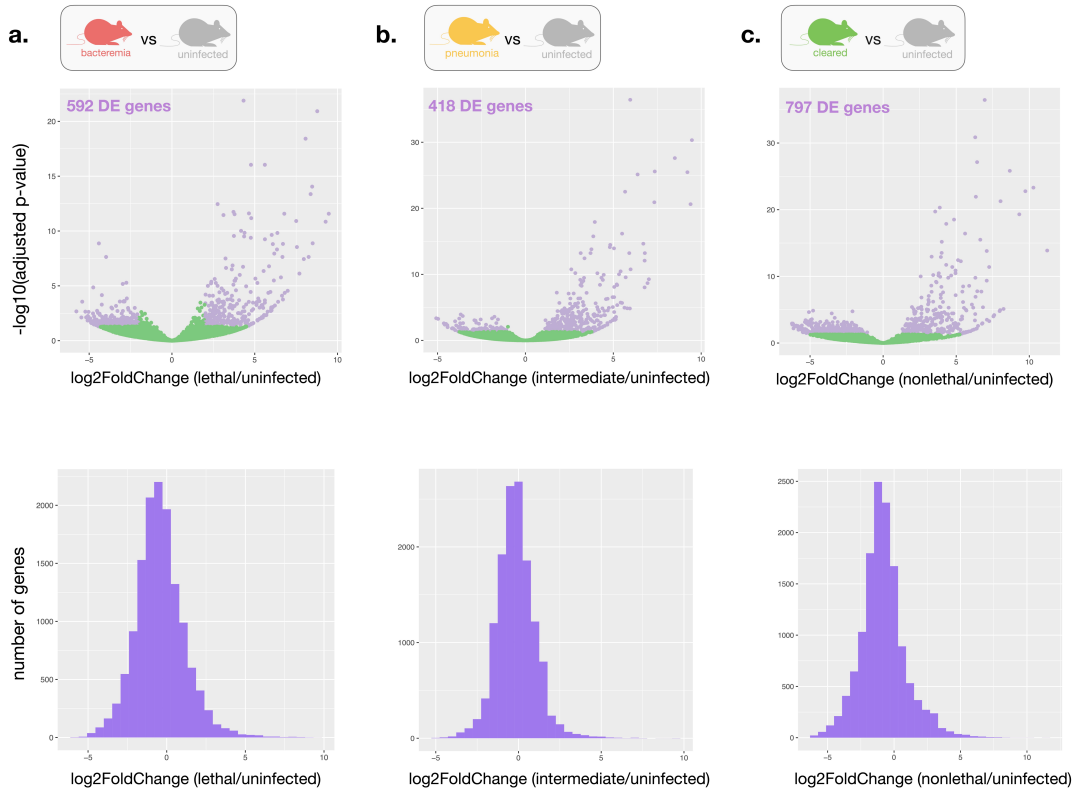


Figure 3.12 | Summary of *M. musculus* differential transcriptomic analysis.

Differentially expressed genes (top) and magnitude of distribution of genome-wide differential expression (bottom) of the host transcriptome with the following comparisons: **a.** lethal infection vs. uninfected; **b.** intermediate infection vs. uninfected; **c.** cleared vs. uninfected. Significant differential expression is filtered based on two criteria: $|\log_2\text{FoldChange}| \geq 2.0$ and adjusted p-value (padj) ≤ 0.05 .

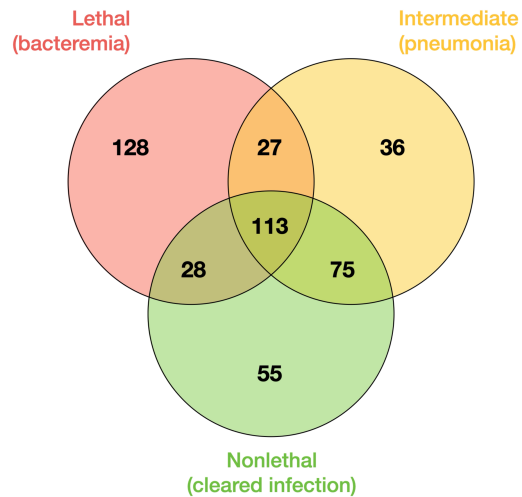


Figure 3.13 | Comparison of significant *M. musculus* DE up-regulated genes across infection conditions.

Venn diagram analysis of genes shared and unique to the three infection scenarios.

Gene Set Enrichment Analysis (GSEA) ²¹ is a computational method to determine whether an *a priori* defined set of genes shows statistically significant, concordant differences between two biological states (e.g., phenotypes). To parse differences across infection conditions, gene set enrichment analysis was first performed on the 113 shared, up-regulated DEGs across the infection scenarios (**Figure 3.14a-b**), then on the unique subsets of DEGs across the lethal, intermediate, and cleared infection scenarios (**Figure 3.14c-e**). GSEA of the 113 shared genes across infection conditions represent innate immune activation across GO Biological Processes (**Figure 3.14a**) and we can confirm mouse BAL is dominated by neutrophils, macrophages, and peripheral blood according to analysis against the ARCHS4 Tissues database (**Figure 3.14b**). The lethal infection outcome (**Figure 3.14c**) is characteristic of **cytokine/chemokine-mediated signaling, regulation of neutrophil chemotaxis, and immune response to bacteria**.

Notably, the **IL-17 signaling pathway** was specifically enriched in the lethal condition. IL-17 family cytokines, such as IL-17A and IL-17F, play important protective roles in the host immune response to variety of bacterial, fungal, parasitic, and viral pathogens ²². The IL-17R signaling and downstream pathways mediate induction of proinflammatory molecules, which participate in the control of pathogens. Characteristic of the host intermediate infection outcome (**Figure 3.14d**) is **DNA damage response processes, and signal transduction by p53**. Numerous *S. pneumoniae* virulence factors, including pneumolysin which was significant up-regulated in only the bacteria intermediate condition (**Figure 3.11c**), affect the lysosomal integrity of host epithelial cells and induce DNA double stranded breaks. Specially, pneumolysin, which is released during bacterial lysis, induces toxic DNA double-stranded breaks in human alveolar epithelial cells, indicated by ATM-dependent phosphorylation of histone H2AX and colocalization with the p53-binding protein ²³.

Ultimately, and perhaps the most compelling, are identification of the host transcriptomic signatures of a cleared infection (**Figure 3.14e**). Pinpointing exact pathways, processes, and proteins responsible for host recovery from bacterial infection has promising implications in the context of host-informed antibacterial therapy development and repurposing existing FDA-approved therapeutics. Notable up-regulated pathways in the

host capable of successfully clearing infection were the **IL-2- and IL-15-mediated signaling pathways**. Specifically, IL-2 is a pleiotropic cytokine known to promote the generation of the complete set of T regulatory cells and to maintain these cells in peripheral tissues ²⁴. IL-2 is produced by CD4⁺ T cells following their activation by antigen-presenting cells (APCs), and it stimulates the proliferation and differentiation of these cells. IL-2 also acts on forkhead box P3-positive (FOXP3⁺) regulatory T cells (Tregs) to maintain them in a functional state, capable of suppressing the development of effector and memory cells ²⁴.

In terms of therapeutic application, IL-2 was initially used to stimulate immune responses to cancer and in HIV-seropositive patients to enhance T cell immunity ²⁴. In neither case was the treatment effective and safe enough to be widely adopted. However, the more recent administration of low-dose IL-2 preferentially expands T-regulatory cells, is clinically approved as a cancer therapy, and is currently under study for several autoimmune conditions ²⁴. In the context of bacterial disease, low-dose IL-2 is under academic investigation for *Staphylococcus aureus* arthritis and shows promise as an adjunctive to antibiotics if administered early during the infection progression ²⁴. There is, however, concern that simply lowering the cytokine dose may not be a consistent or reliable way to selectively manipulate the cellular target of IL-2 in patients. If IL-2 administration activates T-cell responses in patients with both bacterial infection and predisposing disease, it could exacerbate the disease. Conversely, if it induces broad immunosuppression, it may make patients susceptible to additional opportunistic infections (**Chapter 1, Figure 1.2**).

In terms of diagnostic application, many host biomarkers of pneumonia are indicative of inflammation, but not specific to a pathogen of bacterial or viral origin ²⁵. Here, we overlay *in vivo* *M. musculus* dRNA-Seq findings over a panel of published biomarkers of pneumonia (**Figure 3.15**) and find only a subset correlate with our murine model as potential biomarkers for lethal bacterial pneumonia: Interferon- β , Interferon alpha-inducible protein 27, and Interleukin-6.

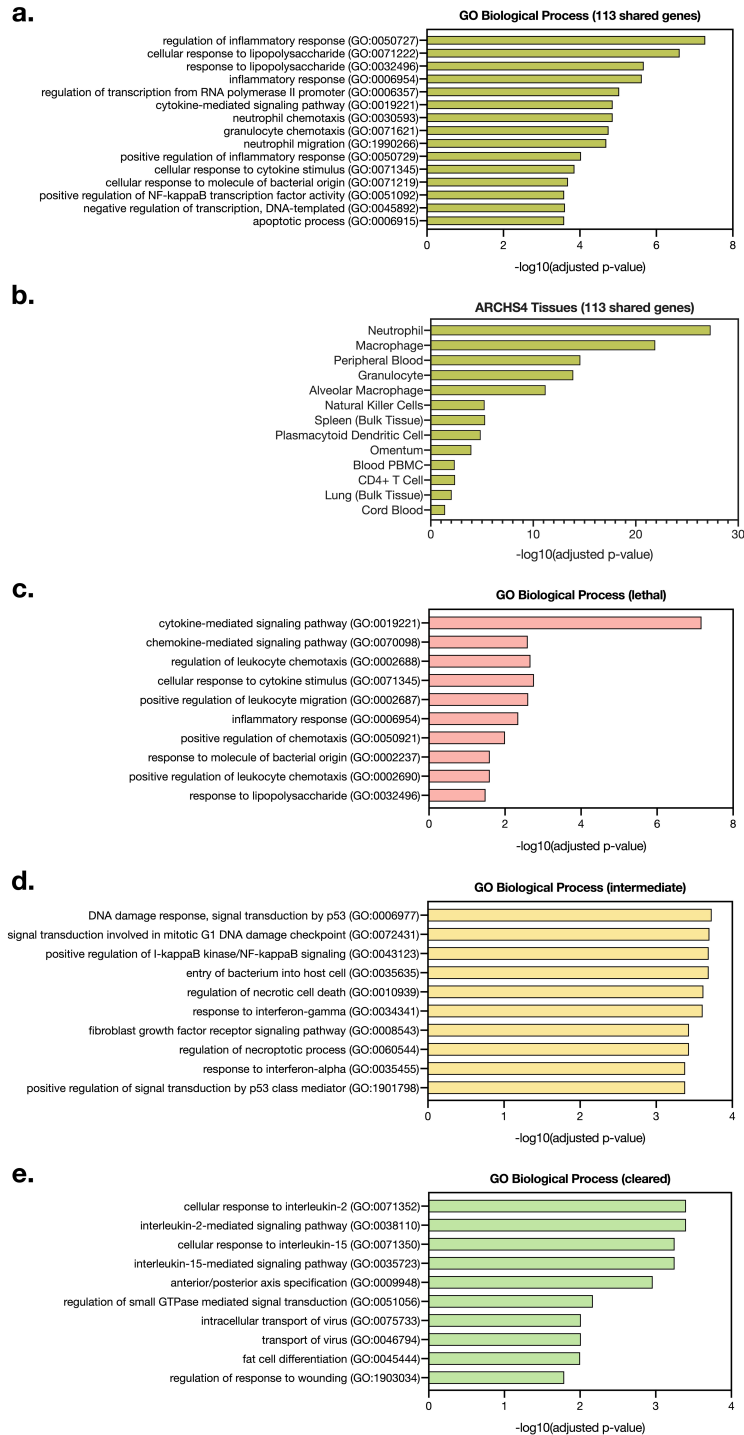


Figure 3.14 | Gene set enrichment analysis of up-regulated shared, lethal, intermediate, and cleared infection DEGs.

a. GO Biological Process gene set enrichment of significant up-regulated DEGs shared across infection conditions. **b.** ARCHS4 Tissues enrichment of significant up-regulated DEGs shared across infection conditions. **c.** GO Biological Process enrichment of significant up-regulated DEGs in lethal condition only. **d.** GO Biological Process enrichment of significant up-regulated DEGs in intermediate condition only. **e.** GO Biological Process gene set enrichment of significant up-regulated DEGs in cleared infection only.

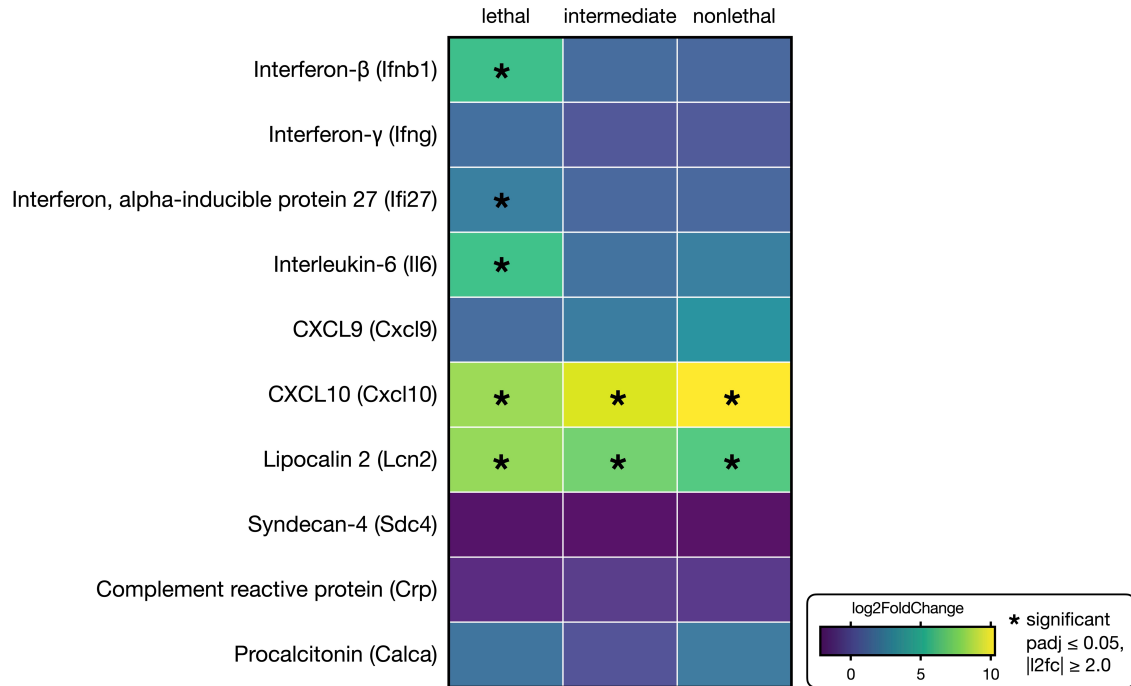


Figure 3.15 | Overlay of in vivo *M. musculus* RNA-Seq signatures and published biomarkers of pneumonia.

A non-exhaustive panel of human pneumonia biomarkers and their corresponding log2foldchange of mouse genes within the dRNA-Seq dataset. * indicates significant differential expression with $|\log_2\text{FoldChange}| \geq 2.0$ and adjusted p-value (padj) ≤ 0.05 .

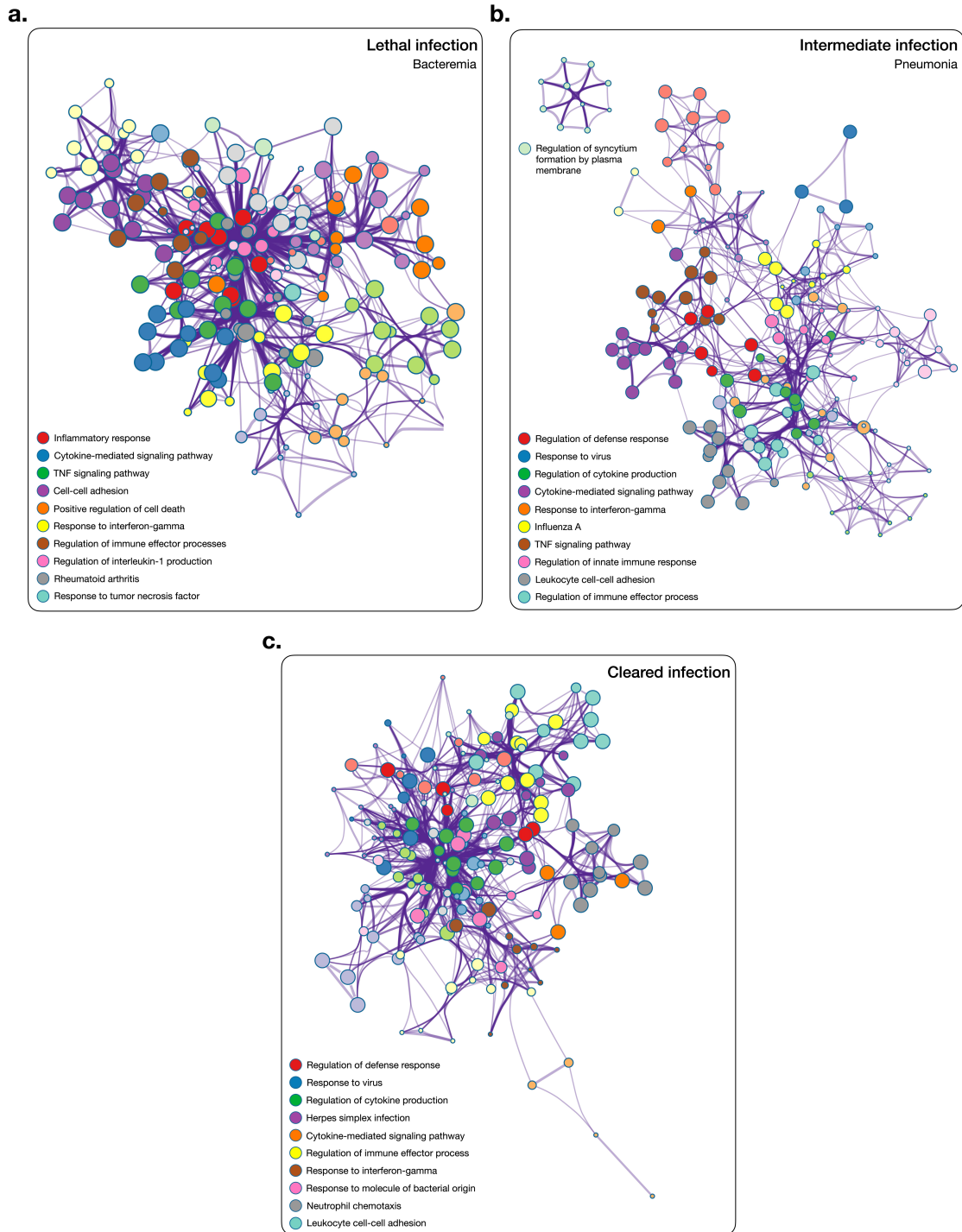


Figure 3.16 | GO enrichment network analysis of *M. musculus* significantly up-regulated DEGs.

Metascape²⁶ was utilized to represent enriched biological pathways in networks, to facilitate the understanding of relationships among biological pathways or processes under the host **a.** lethal infection outcome; **b.** intermediate infection outcome; and **c.** cleared infection outcome. Functionally related terms are grouped into the same cluster, color codes indicate enriched GO term (biological process).

3.4 Discussion

The development of novel antibacterial host-informed therapies relies heavily on our knowledge of the mechanisms of bacterial infection ²⁷⁻²⁹. Therefore, it is crucial to understand how a bacterial infection develops and which bacterial genes are required to infect a host. The use of high-throughput sequencing technologies has unveiled new levels of complexity in the transcriptomic response of pathogens and their hosts during infection. In the last five years, dRNA-Seq has become a leading approach to uncover the intricate relationship between pathogen and host interactions. Hence, dRNA-Seq could be used to define host-pathogen interactions, identify potential biomarkers for infection ³⁰, or tailor personalized host-informed treatment strategies ³¹.

The findings from this study provide several important applications to improving both diagnostics/prognostic and treatment strategies. However, improvements can be made to improve both the robustness of the dRNA-Seq technique and the data resolution. Work at the Innovation Lab for Microbial Phenomics and Systems Analysis (MiPSA) at the Broad Institute of MIT and Harvard is currently underway to extend this project for publication. First, an in-house probe-based rRNA depletion method would be optimal, as the Ribo-Zero Plus kit adds a high expense to the experimental workflow and low specificity to efficiently depleting *S. pneumoniae* rRNA. Second, a single-cell atlas of the host transcriptomic response would add more resolution to the study, which is currently limited by host bulk RNA-Seq and likely losing the complexities of the host response to bacterial infection. Preliminary work took place in our lab exploring the application of SPLiT-Seq ³² (Parse Biosciences), a method that labels the cellular origin of RNA through combinatorial barcoding, and single-cell host RNA-Seq (scRNA-Seq) studies are currently underway to assess both the cell populations within mouse BAL fluid during *S. pneumoniae* infection, and the cell-type-specific transcriptomic signatures. Third, this study is limited with only one timepoint post-infection (20 hours), and a temporal resolution would provide a training model for predictive models, to ultimately predict the host's (mouse) infection outcome. In the future, similar predictive models could be employed to predicting a patient's clinical outcome from a BAL sample to immediately administer the necessary therapeutic interventions.

3.5 Materials and Methods

Bacterial strains and growth conditions

A serotype 6C *S. pneumoniae* strain, PG13, was used in all dRNA-Seq experiments in this chapter. Bacteria were grown on blood agar base no. 2 (Sigma-Aldrich) plates supplemented with 5% defibrinated sheep's blood at 37°C in a 5% CO₂ atmosphere. Liquid cultures were grown statically in THY with 5 µL/mL oxyrase (Oxyrase) and 0.75 µL/mL catalase (Fisher Scientific) at the same incubation conditions as plates. Colony forming units (CFU) of the inoculum and post-infected samples were enumerated by serial dilution and plating on blood agar plates.

Ethics statement

All experiments involving animals were performed with prior approval of and in accordance with guidelines of the Boston College Institutional Animal Care and Use Committee (IACUC), under Boston College IACUC approved protocol #2022-008 or #2019-007. Laboratory animals are maintained in accordance with the applicable portions of the Animal Welfare Act and the guidelines prescribed in the DHHS publication, Guide for the Care and Use of Laboratory Animals.

***S. pneumoniae* mouse lung infection**

Infection of mice is achieved by anesthetizing the mice with isoflurane in a BSL-2 procedure room, after which bacteria are delivered by intranasal injection. The mice are returned to their cage and given food and water *ad libitum*. The bacteria multiply in the lung and cause pneumonia. At 20-24 hours post-infection in the case of virulent strains, the mice begin to show initial signs of illness (typically piloerection/ruffled fur). A clinical score ¹¹ of 1 denoted a lack of clinical signs, a score of 2 indicated a slightly hunched animal, a score of 3 indicated a hunched animal with a starry coat (which refers to a dry hair coat where the hair appears to be standing on end or disturbed, indicating a lack of grooming and poor coetaneous circulation), a score of 4 indicated a severely hunched animal with a starry coat on part of the animal body, a score of 5 indicated a severely hunched animal with a starry coat over the entire body, a score of 6 indicated a slightly lethargic animal, and a score of 7 indicated a lethargic animal. A humane endpoint was set at a clinical score of 5. All mice are euthanized at 24 hours post-infection by CO₂ gas

asphyxiation followed by vital organ removal. In short, after euthanasia, cardiac puncture is performed. Afterwards, the chest is opened, and the trachea is severed with scissors. 0.5 mL of PBS is injected through tubing into the trachea opening, whereupon the liquid goes up through the nasopharynx and out of the nostrils where the liquid is collected in a 1.5 mL Eppendorf tube. In addition, the lungs are removed and mechanically homogenized in 1 mL of 1X PBS. The nasopharynx effluent, lungs, and blood are serially diluted and plated on blood agar base no. 2 (Sigma-Aldrich) plates supplemented with 5% defibrinated sheep's blood at 37°C in a 5% CO₂ atmosphere for CFU enumeration.

Mouse bronchoalveolar lavage

At time points corresponding to experimental design, mice are euthanized by CO₂ gas asphyxiation followed by bronchoalveolar lavage. BAL is performed to collect bacterial cells and compounds secreted into the airspaces (alveoli and bronchial lumen) that can be assessed to determine the degree of pulmonary inflammation (neutrophil influx, cytokine levels, and lung injury). The trachea is first exposed, and forceps are used to pull a 5" strand of silk suture under and through. A 23-gauge x ½" polyethylene catheter is inserted into the trachea and secured with the suture in a single tie. The lavage apparatus (two 1 mL syringes connected to a 4-way stopcock; 1 syringe filled with 1 mL 1X PBS) is then connected to the catheter. Lungs are then slowly filled with 1 mL of 1X PBS, stopcock valve is turned, and the injected lavage fluid is slowly collected, as to not burst the lungs or introduce a vacuum. The injection and collection processes are then repeated for a total of 5 lung washings, resulting in 4-5 mL of collected BAL fluid. BAL fluid is dispensed into 15 mL conical tubes containing 2X volume of *RNAlater* (Invitrogen) + 2% β-Mercaptoethanol. From the BAL fluid, an aliquot (without *RNAlater* + 2% β-Mercaptoethanol) is serially diluted and plated on blood agar base no. 2 (Sigma-Aldrich) plates supplemented with 5% defibrinated sheep's blood at 37°C in a 5% CO₂ atmosphere for CFU enumeration. Each BAL procedure per animal takes about 20-30 minutes to complete.

Dual RNA isolation and purification

Each BAL fluid sample was centrifuged at 1500xg for 10min to separate debris and/or host cells from the rest of the fluid containing bacteria and potentially some host cells, referred to as the *host fraction*. Supernatant was then centrifuged at 4000xg to pellet

bacteria and any remaining host cells, referred to as the *bacteria fraction*. Pelleted cells were lysed with RLT buffer (Qiagen). The bacteria-enriched cell pellets were further lysed by mechanical disruption on a BioSpec Mini-beadbeater-16 (BioSpec) at 4°C. Cell lysates were subjected to a low input RNA isolation using RNeasy Micro kit following the manufacturer's instructions and eluted in 14 µL of diethyl pyrocarbonate (DEPC)-treated water (Qiagen). 1 µL of murine RNase inhibitor was added immediately after elution. RNA isolated from host- and bacteria-enriched cell pellets were run on TapeStation (Agilent) for assessment of RNA integrity and concentration, then pooled together resulting in 26 µL of host + bacteria total RNA.

Library preparation and Illumina sequencing

Prior to ribosomal RNA depletion, each host + bacteria total RNA sample (in 26 µL) was concentrated to a final total volume of 15 µL using Zymo RNA Clean and Concentrator - 5 (Zymo Research) and 1 µL of murine RNase inhibitor was added immediately after elution. Host and bacteria rRNA were depleted using Ribo-Zero Plus rRNA Depletion Kit (Illumina). rRNA-depleted samples were cleaned up using SPRI beads (Agencourt) and subjected to reverse transcription, Illumina-compatible adapter ligation, end repair and PCR enrichment (15-18 cycles) and indexing using NEBNext Ultra II Directional RNA library prep kit and NEBNext multiplex oligos (NEB) following the manufacturer's instructions. 12-16 enriched and indexed libraries were pooled and paired-end sequenced in a single run on an Illumina NextSeq 500 with 150 base pair (bp) reads to ensure a minimum sequencing depth of 25 million reads per sample.

Dual RNA-Seq bioinformatic analysis

RNA-Seq data was processed and analyzed using an in-house developed analysis pipeline, *Aerobio*. In brief, raw reads were demultiplexed, trimmed to 150-bp and quality filtered (96% sequence quality > Q14). Filtered reads are mapped to both *S. pneumoniae* PG13 reference genome (CP035254; TVO_1901932) and mouse reference genome (GRCm38_mm10) using Bowtie ¹⁴ (bacteria) and STAR ¹³ (mouse). For PG13, 1846 out of 2312 genes are functionally characterized/annotated, and PG13 shares 1530 genes with serotype 4 strain TIGR4 used in **Chapters 2 and 4** of this thesis. Reads mapped to either genome is split and aggregated by featureCounts ¹⁵, and differential expression is calculated with DESeq2 ¹⁶. Differential expression comparisons are made between

infection conditions and uninfected controls for mouse genes, and between infection conditions and THY broth controls for *S. pneumoniae* genes. Significant differential expression is filtered based on two criteria: $|\log_2\text{FoldChange}| \geq 2.0$ and adjusted p-value (p_{adj}) ≤ 0.05 .

Gene set enrichment analysis (GSEA) and network generation

Using Metascape²⁶, we first identified all statistically enriched terms (GO/KEGG terms, canonical pathways, hall mark gene sets) and accumulative hypergeometric p-values and enrichment factors were calculated and used for filtering. Remaining significant terms were then hierarchically clustered into a tree based on Kappa-statistical similarities among their gene memberships. Then a kappa score of 0.3 was applied as the threshold to cast the tree into term clusters. We then selected a subset of representative terms from this cluster and converted them into a network layout. More specifically, each term is represented by a circle node, where its size is proportional to the number of input genes fall into that term, and its color represent its cluster identity (i.e., nodes of the same color belong to the same cluster). Terms with a similarity score > 0.3 are linked by an edge (the thickness of the edge represents the similarity score). The network is visualized with Cytoscape 3.1.2 with “force-directed” layout and with edge bundled for clarity. One term from each cluster is selected to have its term description shown as the label.

3.6 Acknowledgements

Illumina sequencing was performed at the Boston College Sequencing Core. The authors wish to thank for Jon Anthony creating the *Aerobio* dual RNA-Seq analysis pipeline, processing, and analyzing Illumina sequencing reads; Federico Rosconi and Juan C. Ortiz-Marquez for valuable discussions, and the Boston College Animal Care Facility for animal husbandry.

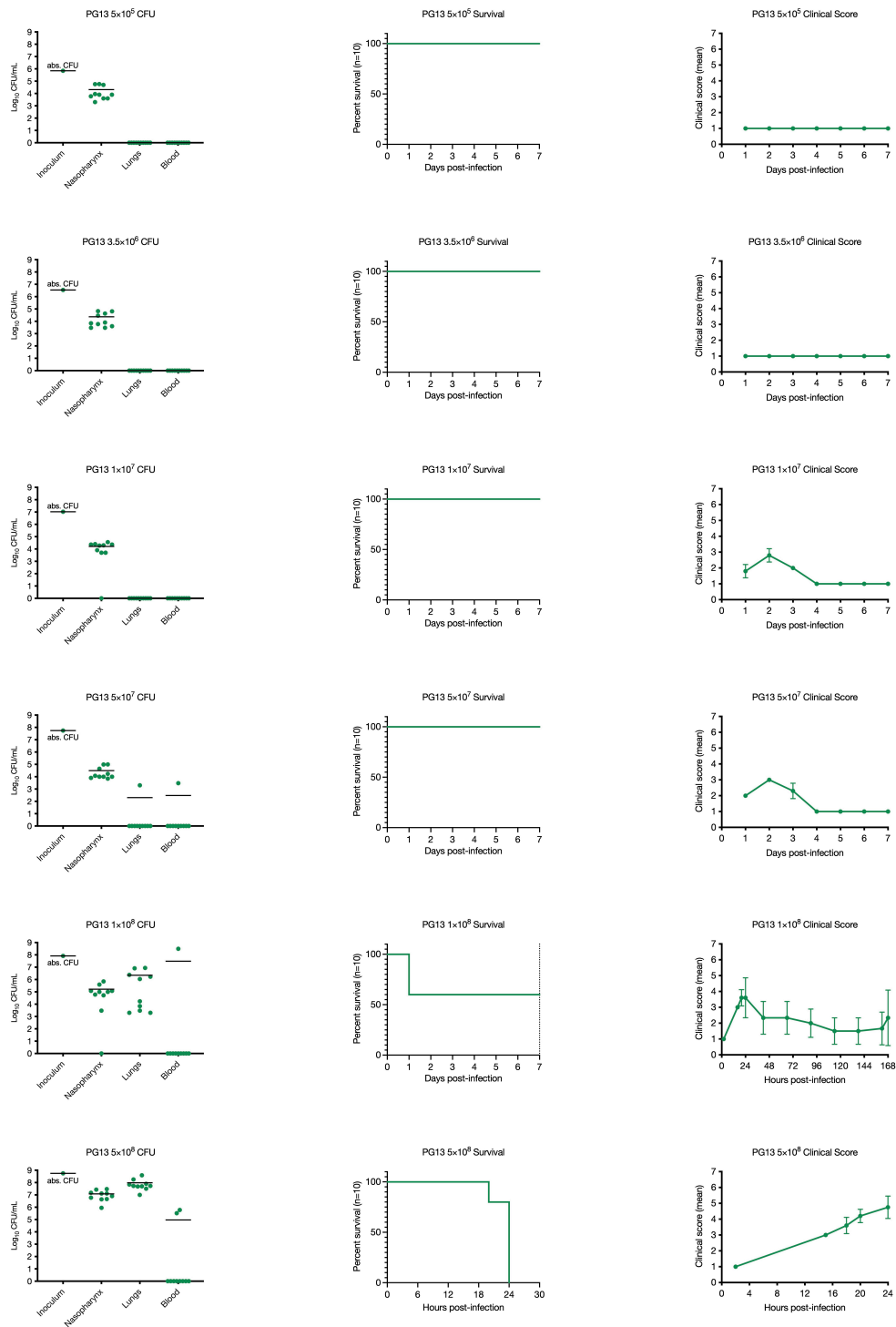
3.7 References

1. Aprianto R, Slager J, Holsappel S, Veening JW. Time-resolved dual RNA-seq reveals extensive rewiring of lung epithelial and pneumococcal transcriptomes during early infection. *Genome Biol.* 2016 Sep 27;17(1):198.
2. Westermann, A.J., Barquist, L., & Vogel, J. Resolving host-pathogen interactions by dual RNA-seq. *PLoS Pathog* 13, e1006033 (2017).
3. Nuss AM, Beckstette M, Pimenova M, Schmöhl C, Opitz W, Pisano F, Heroven AK, Dersch P. Tissue dual RNA-seq allows fast discovery of infection-specific functions and riboregulators shaping host-pathogen transcriptomes. *Proc Natl Acad Sci U S A.* 2017 Jan 31;114(5):E791-E800.
4. Rienksma, R.A., Suarez-Diez, M., Mollenkopf, H.J., Dolganov, G.M., Dorhoi, A., Schoolnik, G.K., Martins Dos Santos, V.A., Kaufmann, S.H., Schaap, P.J., and Gengenbacher, M. Comprehensive insights into transcriptional adaptation of intracellular mycobacteria by microbe-enriched dual RNA sequencing. *BMC Genomics* 16, 34 (2015).
5. Westermann AJ, Förstner KU, Amman F, Barquist L, Chao Y, Schulte LN, Müller L, Reinhardt R, Stadler PF, Vogel J. Dual RNA-seq unveils noncoding RNA functions in host-pathogen interactions. *Nature.* 2016 Jan 28;529(7587):496-501.
6. Ritchie ND, Evans TJ. Dual RNA-seq in *Streptococcus pneumoniae* Infection Reveals Compartmentalized Neutrophil Responses in Lung and Pleural Space. *mSystems.* 2019 Aug 13;4(4):e00216-19.
7. Carter, R., *et al.* Genomic Analyses of Pneumococci from Children with Sickle Cell Disease Expose Host-Specific Bacterial Adaptations and Deficits in Current Interventions. *Cell Host and Microbe* 15, 587-599 (2014).
8. Ganz, T., Metcalf, J.A., Gallin, J.I., Boxer, L.A. & Lehrer, R.I. Microbicidal/cytotoxic proteins of neutrophils are deficient in two disorders: Chediak-Higashi syndrome and "specific" granule deficiency. *J Clin Invest* 82, 552-556 (1988).
9. Weiser JN, Ferreira DM, Paton JC. *Streptococcus pneumoniae*: transmission, colonization and invasion. *Nat Rev Microbiol.* 2018 Jun;16(6):355-367. doi: 10.1038/s41579-018-0001-8.
10. Zhu Z, Surujon D, Ortiz-Marquez JC, Huo W, Isberg RR, Bento J, van Opijnen T. Entropy of a bacterial stress response is a generalizable predictor for fitness and antibiotic sensitivity. *Nat Commun.* 2020 Aug 31;11(1):4365.
11. Jonczyk MS, Escudero L, Sylvius N, Norman M, Henriques-Normark B, Andrew PW. Variation in Inflammatory Response during Pneumococcal Infection Is Influenced by Host-Pathogen Interactions but Associated with Animal Survival. *Infect Immun.* 2016 Mar 24;84(4):894-905.

12. Rosconi, et al., Predicting species-wide virulence for a bacterial pathogen with a large pan-genome. In preparation.
13. Cremers, A. J. et al. The post-vaccine microevolution of invasive *Streptococcus pneumoniae*. *Sci. Rep.* 5, 14952 (2015).
14. Dobin A, Davis CA, Schlesinger F, Drenkow J, Zaleski C, Jha S, Batut P, Chaisson M, Gingeras TR. STAR: ultrafast universal RNA-seq aligner. *Bioinformatics*. 2013 Jan 1;29(1):15-21.
15. Langmead, B., Trapnell, C., Pop, M. *et al.* Ultrafast and memory-efficient alignment of short DNA sequences to the human genome. *Genome Biol* 10, R25 (2009).
16. Liao, Y., Smyth, G.K., & Shi, W. featureCounts: an efficient general purpose program for assigning sequence reads to genomic features. *Bioinformatics* 30, 923-930 (2014).
17. Love, M.I., Huber, W., & Anders, S. Moderated estimation of fold change and dispersion for RNA-seq data with DESeq2. *Genome Biol* 15, 550 (2014).
18. Nourikyan J, Kjos M, Mercy C, Cluzel C, Morlot C, Noirot-Gros MF, Guiral S, Lavergne JP, Veening JW, Grangeasse C. Autophosphorylation of the Bacterial Tyrosine-Kinase CpsD Connects Capsule Synthesis with the Cell Cycle in *Streptococcus pneumoniae*. *PLoS Genet.* 2015 Sep 17;11(9):e1005518.
19. Kadioglu, A., Weiser, J., Paton, J. *et al.* The role of *Streptococcus pneumoniae* virulence factors in host respiratory colonization and disease. *Nat Rev Microbiol* 6, 288–301 (2008).
20. MouseEncodeConsortium, Stamatoyannopoulos, J.A., Snyder, M., Hardison, R., Ren, B., Gingeras, T., Gilbert, D.M., Groudine, M., Bender, M., Kaul, R., Canfield, T., Giste, E., Johnson, A., Zhang, M., Balasundaram, G., Byron, R., Roach, V., Sabo, P.J., Sandstrom, R., Stehling, A.S., Thurman, R.E., Weissman, S.M., Cayting, P., Hariharan, M., Lian, J., Cheng, Y., Landt, S.G., Ma, Z., Wold, B.J., Dekker, J., Crawford, G.E., Keller, C.A., Wu, W., Morrissey, C., Kumar, S.A., Mishra, T., Jain, D., Byraska-Bishop, M., Blankenberg, D., *et al.* (2012). An encyclopedia of mouse DNA elements (Mouse ENCODE). *Genome Biol* 13, 418.
21. Subramanian A, Tamayo P, Mootha VK, Mukherjee S, Ebert BL, Gillette MA, Paulovich A, Pomeroy SL, Golub TR, Lander ES, Mesirov JP. Gene set enrichment analysis: a knowledge-based approach for interpreting genome-wide expression profiles. *Proc Natl Acad Sci U S A.* 2005 Oct 25;102(43):15545-50.
22. Chamoun MN, Blumenthal A, Sullivan MJ, Schembri MA, Ulett GC. Bacterial pathogenesis and interleukin-17: interconnecting mechanisms of immune regulation, host genetics, and microbial virulence that influence severity of infection. *Crit Rev Microbiol.* 2018 Aug;44(4):465-486.

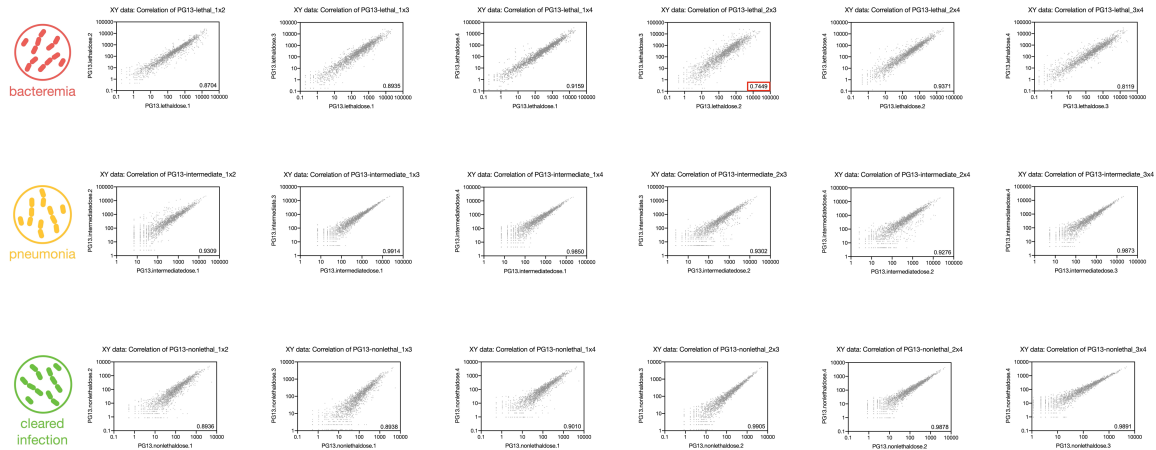
23. Rai, P., He, F., Kwang, J. *et al.* Pneumococcal Pneumolysin Induces DNA Damage and Cell Cycle Arrest. *Sci Rep* 6, 22972 (2016).
24. Bergmann, B., Fei, Y., Jirholt, P. *et al.* Pre-treatment with IL2 gene therapy alleviates *Staphylococcus aureus* arthritis in mice. *BMC Infect Dis* 20, 185 (2020).
25. Savvateeva EN, Rubina AY, Gryadunov DA. Biomarkers of Community-Acquired Pneumonia: A Key to Disease Diagnosis and Management. *Biomed Res Int.* 2019 Apr 30;2019:1701276.
26. Zhou, Y., Zhou, B., Pache, L. *et al.* Metascape provides a biologist-oriented resource for the analysis of systems-level datasets. *Nat Commun* 10, 1523 (2019).
27. Crua Asensio N., Muñoz Giner E., de Groot N.S., Torrent Burgas M. Centrality in the host–pathogen interactome is associated with pathogen fitness during infection. *Nat. Commun.* 2017; 8:14092.
28. de Groot N.S., Torrent Burgas M. A Coordinated Response at The Transcriptome and Interactome Level is Required to Ensure Uropathogenic. *Microorganisms.* 2019; 7:292.
29. Rendón J.M., Lang B., Tartaglia G.G., Burgas M.T. BacFITBase: a database to assess the relevance of bacterial genes during host infection. *Nucleic Acids Res.* 2020; 48:D511–D516.
30. Wolf T., Kammer P., Brunke S., Linde J. Two’s company: studying interspecies relationships with dual RNA-seq. *Curr. Opin. Microbiol.* 2018; 42:7–12.
31. Sundaresh B, Xu S, Noonan B, Mansour MK, Leong JM, van Opijnen T. Host-informed therapies for the treatment of pneumococcal pneumonia. *Trends Mol Med.* Oct 2021;27(10):971-989.
32. Rosenberg AB, Roco CM, Muscat RA, Kuchina A, Sample P, Yao Z, Graybuck LT, Peeler DJ, Mukherjee S, Chen W, Pun SH, Sellers DL, Tasic B, Seelig G. Single-cell profiling of the developing mouse brain and spinal cord with split-pool barcoding. *Science.* 2018 Apr 13;360(6385):176-182.

3.7 Supplemental Information



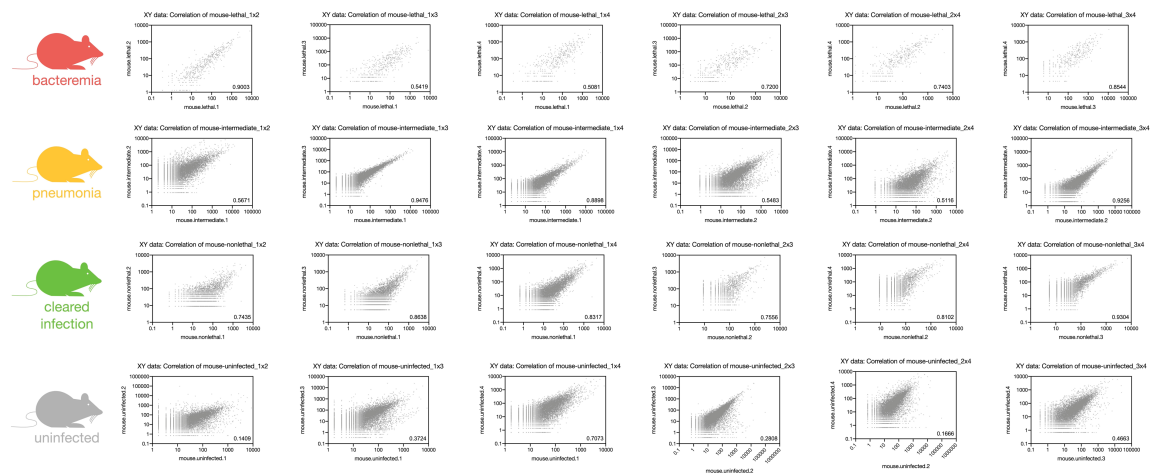
Supplemental Figure 3.1 | *S. pneumoniae* PG13 infection survival analysis.

Mice infected with $5 \times 10^5 - 5 \times 10^8$ *S. pneumoniae* PG13 via intranasal infection were assessed for CFU enumeration in nasopharynx, lungs, and blood at time of sacrifice (left column), Kaplan Meier survival analysis (middle column), and clinical score monitoring (right column). Mean \pm SEM.



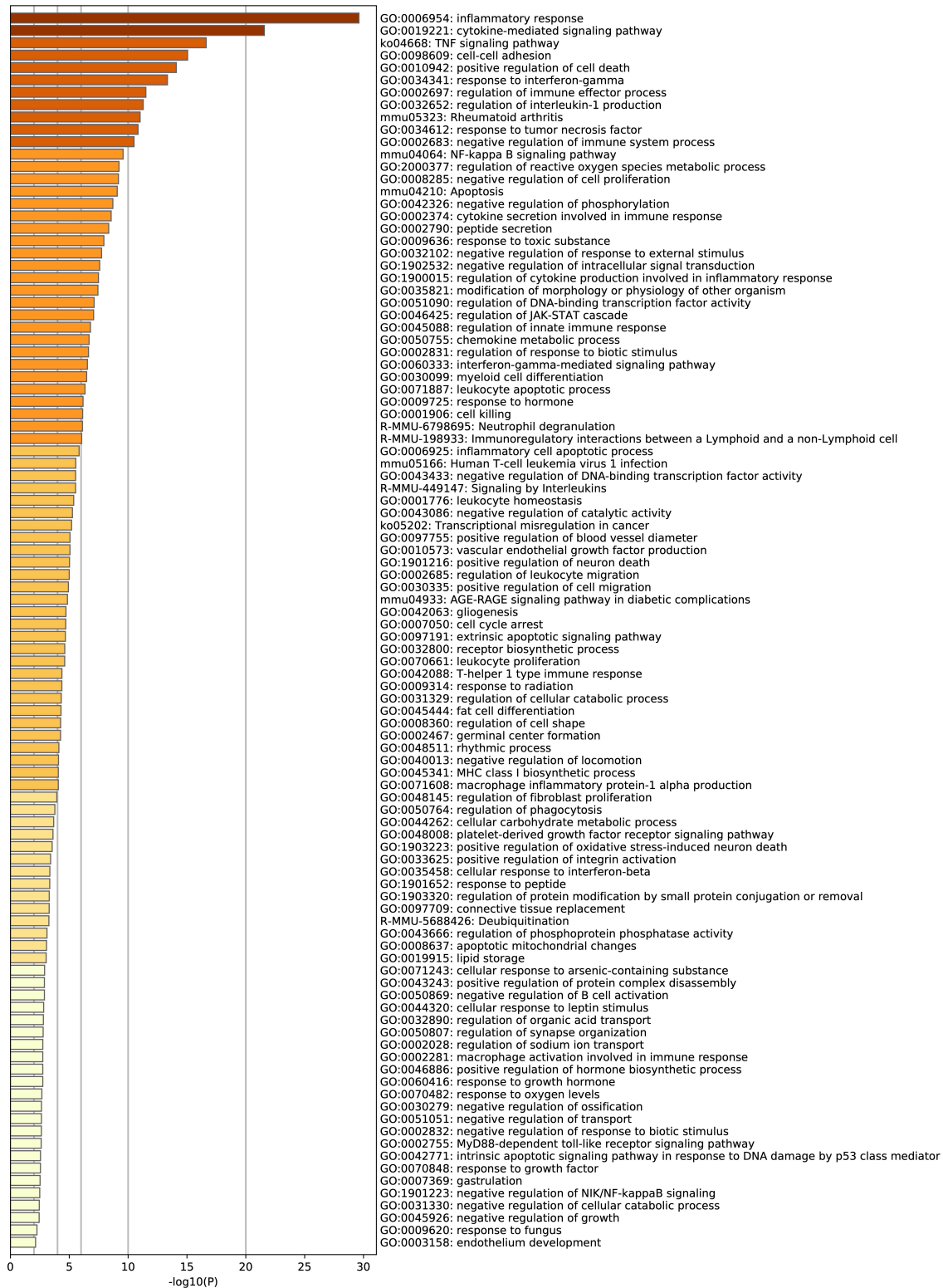
Supplemental Figure 3.2 | Pearson correlation threshold of 0.8 applied to all pair-wise comparisons of *S. pneumoniae* RNA-Seq replicates.

All pairwise sample type comparisons of *S. pneumoniae* RNA-Seq read counts pass a threshold of 0.8, aside from one (PG13.lethaldose.2 x PG13.lethaldose.3) with a Pearson correlation of 0.7449.

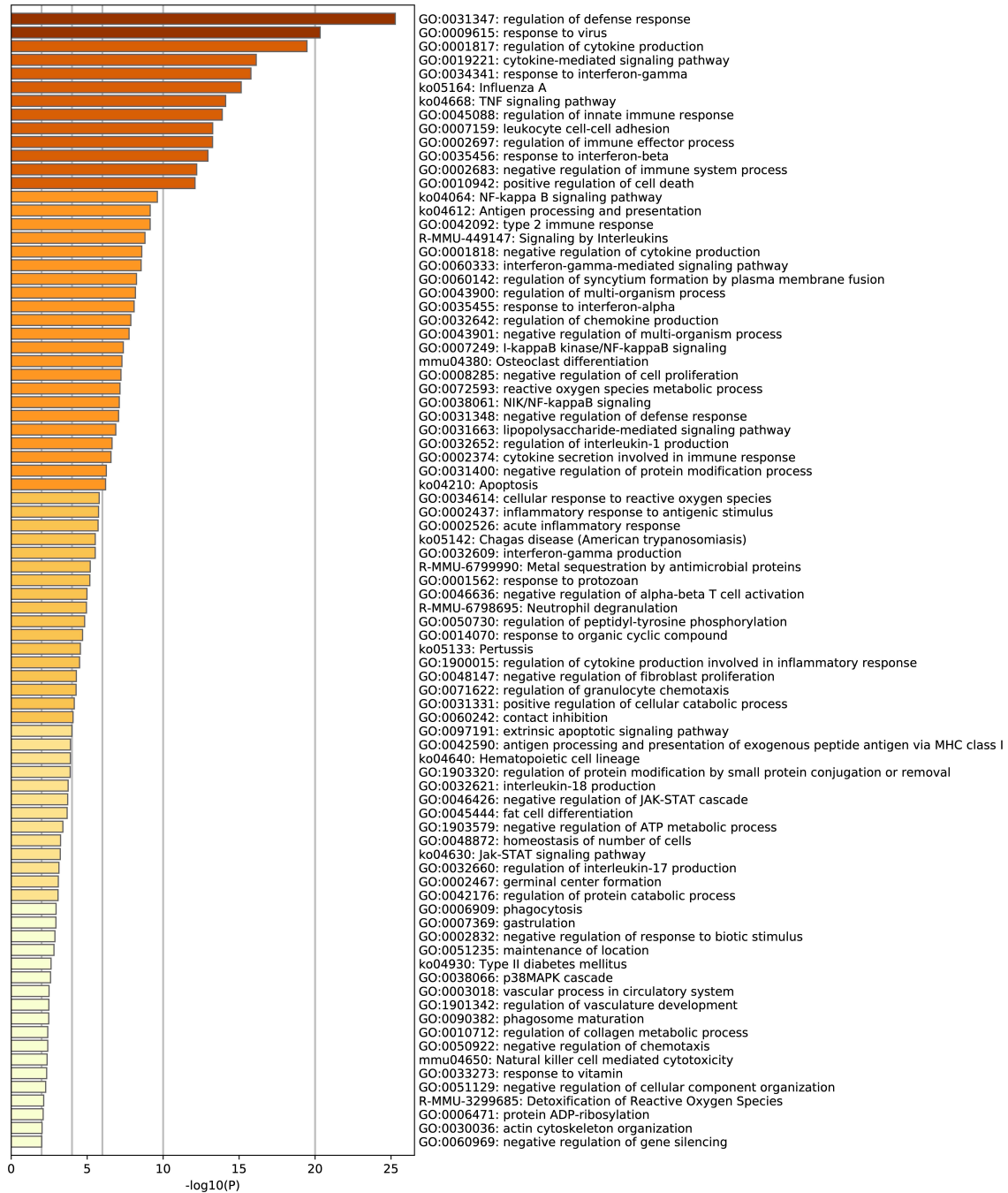


Supplemental Figure 3.3 | Pearson correlation threshold of 0.8 applied to all pairwise comparisons of *M. musculus* RNA-Seq replicates.

Unlike *S. pneumoniae* samples, mouse read counts do not have high correlation between replicates when CDS read counts are low.

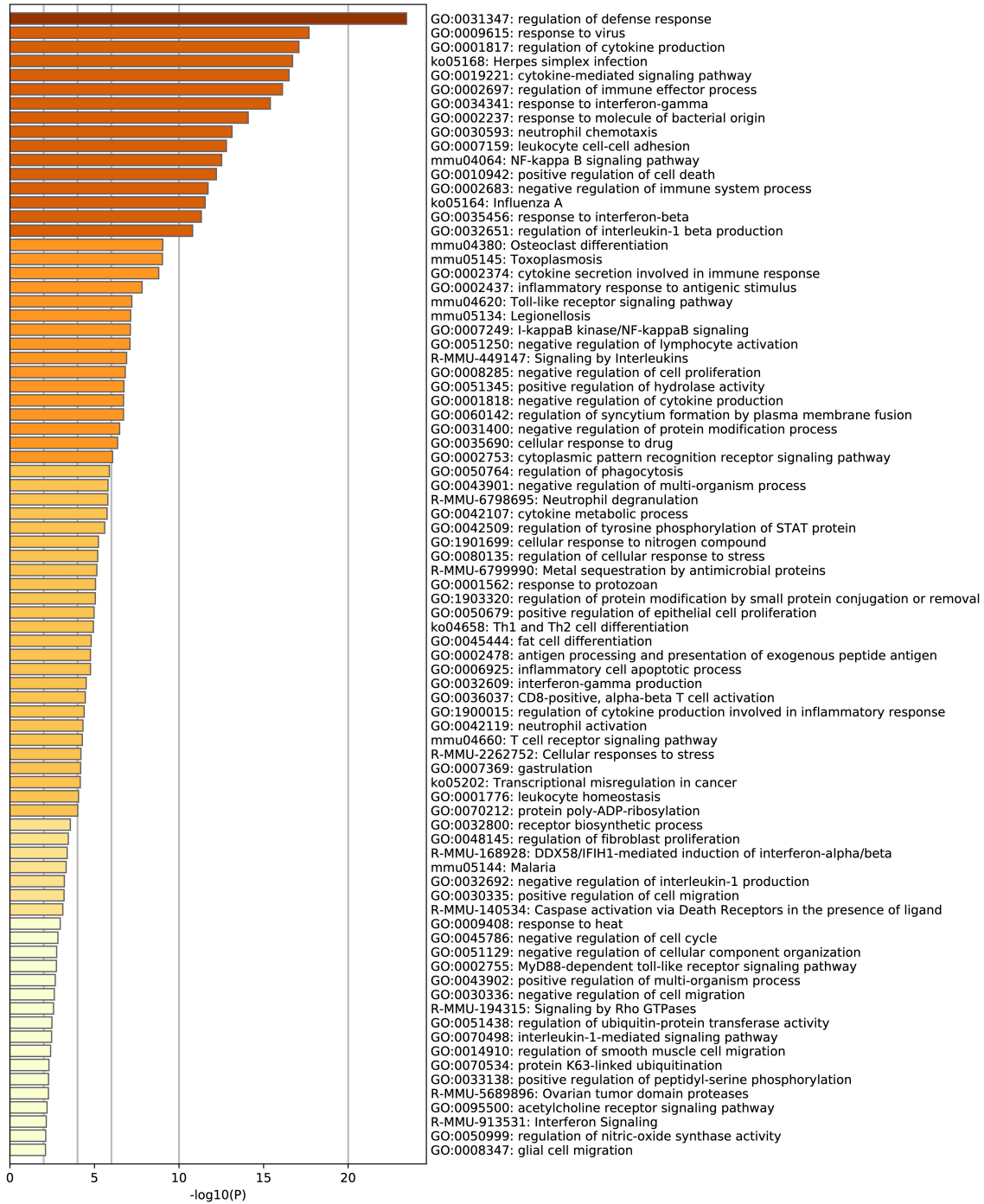


Supplemental Figure 3.4 | Mouse DEG enrichment analysis of the lethal infection outcome.
Lethal/bacteremia condition, 20 hours post-infection.



Supplemental Figure 3.5 | Mouse DEG enrichment analysis of the intermediate infection outcome.

Intermediate/pneumonia condition, 20 hours post-infection.



Supplemental Figure 3.6 | Mouse DEG enrichment analysis of the cleared infection outcome.
Nonlethal/cleared condition, 20 hours post-infection.

4

Antibiotic tolerance: Validating genomic signatures of bacterial antibiotic tolerance during infection

Adapted from:

Dmitry Leshchiner*, Federico Rosconi, Bharathi Sundaresh*, Emily Rudmann*,
Luisa Maria Nieto Ramirez*, Andrew T. Nishimoto, Stephen J. Wood, Bimal Jana,
Noemí Buján, Kaicheng Li, Jianmin Gao, Matthew Frank, Stephanie M. Reeve,
Richard E. Lee, Charles O. Rock, Jason W. Rosch, and Tim van Opijnen

*Equal co-first author contribution

Nature Communications **13** (3165)
DOI: [10.1038/s41467-022-30967-4](https://doi.org/10.1038/s41467-022-30967-4)

Author's contributions: T.v.O. devised the study and wrote the manuscript. E.R, B.S, L.M.N.R, F.R, A.N, S.J.W, B.J, N.B, K.L, J.G, M.F, S.M.R, R.E.L, C.R, J.W.R, and T.v.O. performed wet-lab experiments, data collection and interpretation. D.L. and T.v.O. performed Tn-Seq data analysis, pathway and network construction, analysis, and interpretation. J.W.R. contributed to key conceptual ideas. All authors contributed to manuscript editing and approved the final paper. **Specifically, B.S. significantly contributed to data interpretation, analysis, manuscript writing and editing. B.S. performed all in vivo (mouse) experimental design, experiments, data collection, and interpretation contributing to Figure 4.7 of this thesis and performed all manuscript revision experiments (Supplementary Data 8 addition).**

4.1 Summary

Detailed knowledge on how bacteria evade antibiotics and eventually develop resistance could open avenues for novel therapeutics and diagnostics. It is thereby key to develop a comprehensive genome-wide understanding of how bacteria process antibiotic stress, and how modulation of the involved processes affects their ability to overcome said stress. Here we undertake a comprehensive genetic analysis of how the major human pathogen *Streptococcus pneumoniae* responds to 20 antibiotics. We build a genome-wide atlas of drug susceptibility determinants and generated a genetic interaction network that connects cellular processes and genes of unknown function, which we show can be used as therapeutic targets. Pathway analysis reveals a genome-wide atlas of cellular processes that can make a bacterium less susceptible, and often tolerant, in an antibiotic specific manner. Importantly, modulation of these processes confers fitness benefits during active infections under antibiotic selection. Moreover, screening of sequenced clinical isolates demonstrates that mutations in genes that decrease antibiotic sensitivity and increase tolerance readily evolve and are frequently associated with resistant strains, indicating such mutations could be harbingers for the emergence of antibiotic resistance.

4.2 Introduction

The emergence of antibiotic resistance in bacterial pathogens is a continuously developing complex problem that is only solvable if besides new drugs we also learn to understand the exact (genetic) processes that enable resistance. For instance, new antibiotics and treatment strategies are key to retain the ability to treat resistant infections. However, a comprehensive understanding of how and under which conditions resistance emerges, which genes and pathways contribute to drug sensitivity, and how resistance may be prevented or even taken advantage of, are equally important, as it could make treatments more focused and possibly less dependent on new drugs. For many antibiotics we know which genomic changes can cause resistance. However, it is often not clear how we get there with respect to which evolutionary paths are taken and whether for instance tolerance or lowered drug sensitivity precedes resistance. Interestingly, clinical strains isolated during antibiotic treatment failure may lack known resistance markers and instead contain multiple changes that may have no clear or known role in resistance¹⁻⁵. However, whether these changes play a role or not is often unclear because the distribution of changes that can affect a bacterium's drug sensitivity are largely unknown¹⁻⁷. Therefore, understanding which genes, pathways and processes can contribute to altered drug susceptibility, could help identify genomic changes that not only sensitize bacteria to certain drugs, but desensitize them and may thereby act as precursors for antibiotic escape and/or resistance development.

Resistance emerges primarily through drug target mutations blocking antibiotic lethal action, upregulation of efflux pumps, and the acquisition of drug inactivating enzymes⁷⁻¹³. Importantly, an antibiotic's effects go far beyond the interaction with its direct target. We, and others, have shown that when a bacterium is challenged by an antibiotic, the imposing stress can expand throughout the bacterium and affect and demand the involvement of many different processes^{6,14-17}. For instance, while fluoroquinolones like ciprofloxacin inhibit DNA replication by targeting gyrase and/or topoisomerase, this also triggers double stranded breaks requiring the involvement of DNA repair mechanisms, which in turn requires nucleotide and energy metabolism. Antibiotics can thereby trigger a stress cascade, that with mounting stress increasingly reverberates through the organismal network, until the accumulating stress passes a threshold at which point the

organism succumbs to the pressure ^{15,17}. This explains why mutations in genes or pathways involved in dealing with the downstream (indirect) effects of antibiotic exposure can often make a bacterium more sensitive to a specific antibiotic. Indeed, we have shown for *Streptococcus pneumoniae* and *Acinetobacter baumannii* that, for instance, targeting DNA repair makes bacteria more susceptible to DNA synthesis inhibitors (DSIs) ^{6,16,18}, or targeting the Rod-system and/or Divisome makes *A. baumannii* more sensitive to cell wall synthesis inhibitors (CWSIs)⁶. This means that downstream genes, pathways, and processes can be used as new targets or drug potentiators, either by themselves or in combination with others ^{6,14}. Moreover, in most bacteria, as in any other organism, the majority of genes are of unknown function, it is unclear what role they play in a specific process and/or pathway, or how they are connected within the organismal genomic network. Thus, besides solving gene-function, mapping-out which genes, pathways, and processes are involved in dealing with and overcoming antibiotic-stress, and how they interact with each other, can provide key insights into uncovering new drug targets, or for instance rational combination strategies ⁶.

While identifying off-target genes and pathways that increase drug sensitivity may thus be useful, it is possible that changes in associated processes could, in contrast, just as well reduce the experienced antibiotic stress. Such changes would thereby decrease antibiotic sensitivity and could possibly function as precursors to the emergence of resistance. A possible example of this is tolerance and/or persistence, where a small proportion of cells in a population can be induced by external conditions including nutrient starvation ¹⁹, cell density ²⁰, antibiotic stress ²¹ and stress from the immune system ²² into a cell state that enables them to tolerate high (transient) concentrations of antibiotics. Cell states associated with tolerance include cell dormancy, slow growth, transient expression of efflux pumps, and induction of stress response pathways ^{23,24,25,26}. However, the mechanistic underpinnings of tolerance and decreased antibiotic sensitivity remain largely undefined and possibly differ between bacterial species and vary among antibiotics ²⁷. Moreover, specific mutations can (dramatically) increase the fraction of the surviving population ²⁸⁻³⁰, indicating these tolerant phenotypes have a genetic basis. Lastly, since clinical isolates often carry mutations located outside well-characterized drug targets ^{1-5,31,32}, they could thus be composed of variants with different antibiotic sensitivities. Consequently, such variants with decreased antibiotic sensitivity could

enable antibiotic escape, and/or enable multi-step high-level resistance mutations to evolve as they are given an extended opportunity to emerge ^{25,33-36}. Variants with decreased antibiotic sensitivity may thereby play an important role in antibiotic treatment failure ^{5,37,38}. However, the breadth of possible genetic alterations that can enable (increased) tolerance and/or decrease antibiotic sensitivity are largely unknown, making it unclear how often and probable it is that such variants arise.

In this study we use Tn-Seq in *S. pneumoniae* exposed to 20 antibiotics, 17 additional environments, and two in vivo infection conditions, to generate a genome-wide atlas of drug susceptibility determinants and build a genome-wide interaction network that connects cellular processes and genes of unknown function. We explore several interactions as new leads for gene function, while we show that specific interactions can be used to guide the identification of targets for new antimicrobial strategies. We highlight one such novel target in the membrane, by successfully developing a combinatorial antibiotic-antibody strategy that significantly reduces the bacterial load during an acute mouse lung infection. Furthermore, detailed mapping of antibiotic sensitivity data to pathways and genes with known function suggests a multitude of genome-wide genomic changes exist that can make the bacterium less susceptible and often tolerant to specific antibiotics. We untangle some of the underlying genetic mechanisms and show that decreased susceptibility and tolerance can come from a variety of changes including those in (nucleotide) metabolism, (p)ppGpp and ATP synthesis, transcription, and translation, as well as different types of transport. By further combining in vivo-infection-with antibiotic-Tn-Seq data we predict and experimentally validate that many disruptions may retain their decreased antibiotic sensitivity phenotype in vivo, and thereby outcompete the wildtype in the presence of antibiotics. Moreover, by screening hundreds of clinical isolates we show that changes in genes that can decrease antibiotic sensitivity readily evolve in human patients and are often associated with antibiotic resistance. Consequently, these data highlight the wide array of possibilities that can lead to lowered antibiotic sensitivity and/or tolerance and underscore the importance of understanding the genetics of variants with altered drug susceptibility.

4.3 Results

4.3.1 A genome-wide view of antibiotic sensitivity

To obtain a genome-wide view of the genetic determinants that can modulate antibiotic stress in *S. pneumoniae*, Tn-Seq was employed in the presence of 20 antibiotics (ABXs), representing 9 different ABX groups and four classes including cell wall synthesis inhibitors (CWSIs), DNA synthesis inhibitors (DSIs), protein synthesis inhibitors (PSIs) and an RNA synthesis inhibitor (RSI) (**Figure 4.1a**). Six independent transposon libraries were generated and grown for approximately 8 generations in the absence and presence of an antibiotic at a concentration that reduces growth by approximately 30-50%. Tn-mutant frequencies are determined through Illumina sequencing from the beginning and end of the experiment with high reproducibility between libraries ($R^2 = 0.70-0.90$) which is consistent with previous Tn-Seq experiments^{6,15,16,18,39-42}. Combined with the population expansion during the experiment each mutant's fitness (W_{MT}) is calculated to represent their environment-specific relative growth rate, which means that a mutant with for instance a fitness of 0.5 grows twice as slow as the wild type (WT)^{6,18,39,43,44}. Each gene's antibiotic-specific fitness is statistically compared to baseline fitness without ABXs, and is represented as ΔW ($W_{ABX} - W_{noABX}$) and categorized as: 1) Neutral, $\Delta W = 0$, a mutant's relative growth is similar in the absence and presence of an ABX; 2) Negative, $\Delta W < 0$, a mutant's fitness is significantly lower and thus grows relatively slower in the presence of an ABX; 3) Positive, $\Delta W > 0$, a mutant's fitness is significantly higher and thus grows relatively faster in the presence of an ABX. All antibiotics trigger both positive and negative fitness effects (**Figure 4.1b**), which are distributed across 22 different gene categories (**Figure 4.1c**). Importantly, enrichment analysis shows there are multiple expected patterns, for instance genes involved in DNA-repair are enriched in the presence of fluoroquinolones; cell-wall, peptidoglycan and cell division genes are enriched in β -lactams and glycopeptides; membrane integrity genes in lipopeptides; and transcription and translation in PSIs (**Figure 4.1d**). Additionally, throughout the manuscript we validate a total of 49 predicted genotype x phenotype interactions, which indicates the Tn-Seq data is of high quality and in line with previously shown accuracy^{6,15,16,18,39-42} (**Figure 4.1e**).

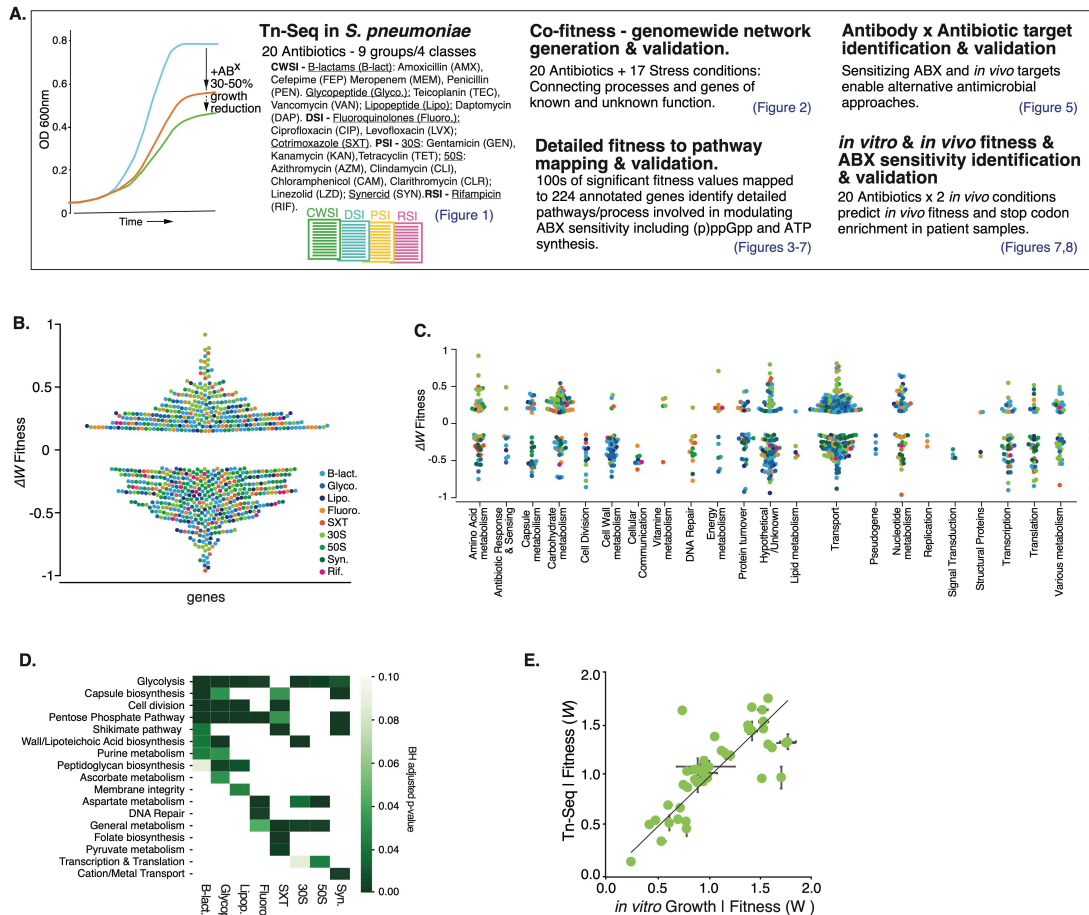


Figure 4.1 | A genome-wide atlas of negative and positive fitness effects, highlights a multitude of processes that can modulate antibiotic susceptibility.

a. Project setup and overview. Tn-Seq is performed with *S. pneumoniae* TIGR4, which is exposed to 20 antibiotics at a concentration that reduces growth by 30-50%. Genome-wide fitness is determined for each condition, suggesting a multitude of options exists to increase as well as decrease antibiotic sensitivity. A co-fitness network is constructed by adding Tn-Seq data from 17 additional conditions, which through a SAFE analysis highlights functional clusters, and connects known and unknown processes. The genome-wide atlas and network are used to develop an antibiotic-antibody combination strategy, and to map out the wide-ranging options that can lead to decreased antibiotic sensitivity *in vitro* and *in vivo* and that are associated with a higher rate of stop-codons in clinical samples. **b.** There are a large number of genetic options that can modulate antibiotic sensitivity; with significant increased ($\Delta W < -0.15$) and decreased sensitivity ($\Delta W > 0.15$) split over all antibiotics almost equally likely. **c.** Additionally, increased and decreased antibiotic sensitivity are distributed across a wide variety of functional categories. **d.** Enrichment analysis shows that some pathways/processes such as glycolysis are relatively often involved in modulating responses to antibiotics, while other processes are more specific. **e.** Validated growth experiments performed throughout the project highlight the Tn-Seq data is of high quality. S.E.M. bars are shown.

4.3.2 Co-fitness interaction networks identify known and unknown genetic relationships

Screens such as Tn-Seq are geared towards highlighting the genetic regions and/or genes that are important under a specific screening condition. With increasing conditions, genes acquire profiles that reflect their involvement/importance in those conditions, where genes with similar profiles indicate having similar and/or shared tasks. Such profiles can thereby help fill gaps in pathways, and/or identify genes and gene-clusters with similar roles. By building a correlation matrix based on each gene's ABX fitness-profile patterns emerge along a similarity range; from genes with highly similar to contrasting profiles. Moreover, to increase statistical power (i.e., more conditions increases the ability to identify more and stronger associations) the ABX dataset was supplemented with previously collected Tn-Seq data from 17 additional non-antibiotic conditions¹⁸. This results in a 1519x1519 gene matrix where positive correlations between genes come from shared phenotypes (i.e., similar profiles), while negative correlations come from opposing phenotypic responses under the same condition (i.e., contrasting profiles). By repeatedly hiding random parts of the data the stability and strength of each correlation is calculated and represented in a stability score. The correlation matrix and stability score are turned into a network, where each node is a gene, and each edge is a correlation coefficient above a threshold (>0.75), which combined with the stability score indicates the strength of the relationship between two genes (**Figure 4.2a**). Spatial Analysis of Functional Enrichment (SAFE)^{45,46} is used to define local neighborhoods within the network, i.e., areas enriched for a specific attribute (e.g., a pathway or functional category), which identifies multiple clusters that represent specific pathways and processes including purine metabolism, cell-wall metabolism, cell division and DNA repair (**Figure 4.2b**). Moreover, the network contains gene-clusters of high connectivity identifying highly related genes including those within the same operon such as the *ami*-operon, an oligo-peptide transporter, the *dlt*-operon which decorates wall and lipoteichoic acids with d-alanine, and the *pst*-operon a phosphate transporter (Fig. 2c, I-III). Besides identifying known relationships, the network also uncovers interaction clusters between genes with known and unknown interactions and function. Several such clusters are highlighted in **Figure 4.2c** (IV-VIII), including genes involved in purine metabolism (further explored below), threonine metabolism, and in secretion of

serine rich repeat proteins (SRRPs), which are important for biofilm formation and virulence ⁴⁷. Importantly, the identification of biologically relevant relationships among (clusters of) genes indicates the data is rich in known and new information.

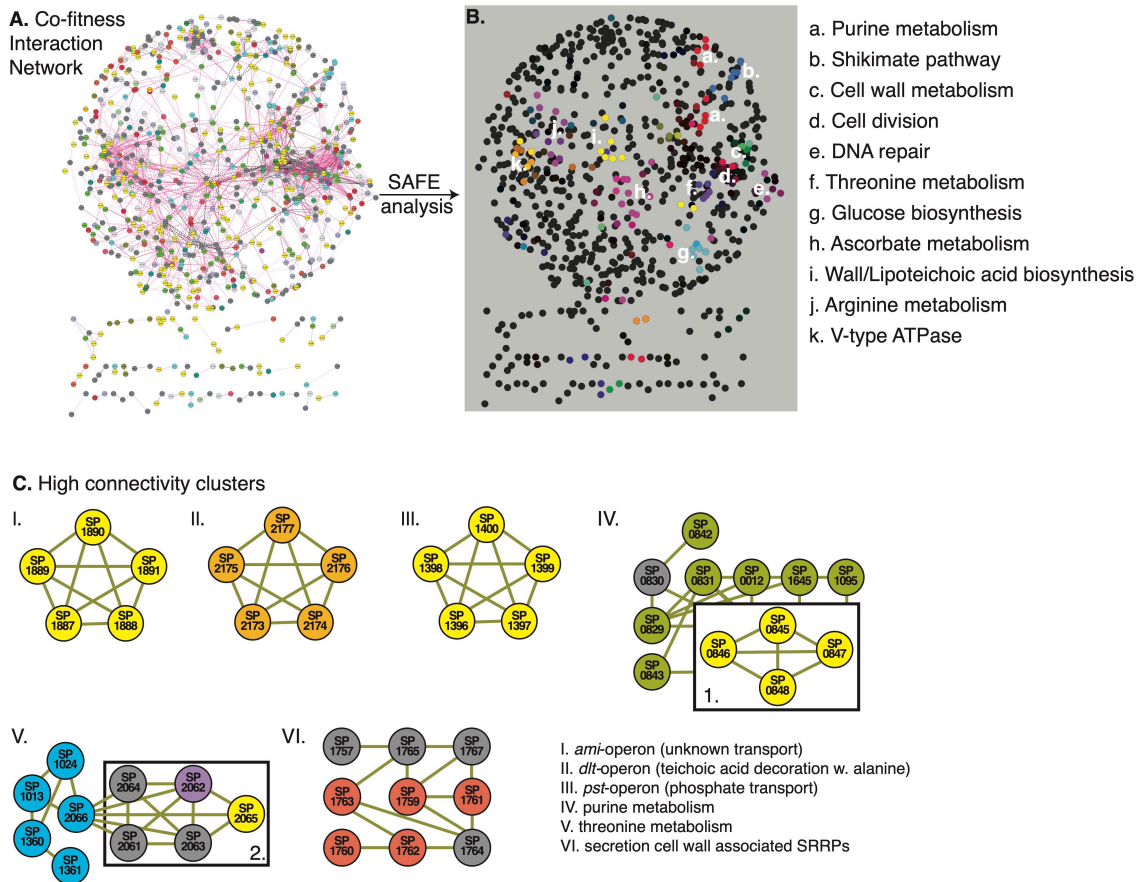


Figure 4.2 | A co-fitness network identifies tight genetic clusters of known and unknown genes and processes.

a. A 1519x1519 gene correlation matrix based on Tn-Seq data from 37 conditions generates a network with genes as nodes, and edges as interactions with a stability score and thresholded correlation >0.75 . The network contains one large, connected component and multiple smaller components placed underneath. **b.** A SAFE analysis identifies at least 11 clusters within the network that represent specific pathways and processes. **c.** The network contains highly connected clusters of smaller groups of genes for instance those within the same operon such as cluster: I. the *ami*-operon; II. the *dlt*-operon; and III. the *pst*-operon. Several additional clusters are highlighted containing annotated and unannotated genes, connected through known and unknown interactions including cluster: IV. containing genes involved in purine metabolism (green nodes) and a putative deoxyribose transporter (yellow; boxed 1.); V. containing genes involved in threonine metabolism (blue) and several genes located as neighbors to SP_2066/*thrC* with unclear functions (boxed 2), including a regulator (SP_2062; purple) and a transporter (SP_2065; yellow); VI. containing genes involved in secretion of serine rich repeat proteins (SRRPs).

4.3.3 Detailed pathway mapping identifies processes that simultaneously increase and decrease drug susceptibility in an antibiotic specific manner

224 genes with a known annotation are present in the data that have at least one significant phenotype in response to an antibiotic, which can be split over 21 functional groups according to a pathway or process they belong to (**Figure 4.3a**). Each group is characterized by having multiple instances of decreased fitness, indicating genes that upon disruption increase sensitivity to one or more antibiotics (negative phenotype). Additionally, each group, except for cell division, also has multiple instances that increase fitness, which is suggestive of genes that upon disruption decrease antibiotic sensitivity (**Figure 4.3a**; positive phenotype). Moreover, each antibiotic group triggers both negative and positive effects (**Figure 4.3b**). Where possible, the 21 functional groups are organized according to a pathway or process they belong to, and each gene is combined with its antibiotic susceptibility profile. This results in an antibiotic susceptibility atlas, which shows on a fine-grained scale, how inhibiting a pathway or process can seemingly simultaneously lead to increased and decreased drug susceptibility in an antibiotic specific manner (**Figure 4.3c**). For instance, in the glycolysis-group, knocking out any of the three genes involved in forming the phosphotransferase (PTS)-system (SP_0282-SP_0284) that imports glucose to generate glucose-6-phosphate (G-6P), has a negative effect on fitness in the presence of 30S and 50S PSIs as well as Synercid (a synergistic combination of two PSIs), while it increases fitness in the presence of all CWSIs (β -lactams, glycopeptides, and daptomycin) and fluoroquinolones. Also, the inhibition of/knocking out SP_0668 (*gki*, glucokinase), an enzyme that converts α -D-Glucose into G-6P, has a positive effect on fitness in all CWSIs and a negative effect in 30S PSIs. In contrast, inhibiting SP_1498 (*pgm*, phosphoglucomutase), the major interconversion enzyme of G-6P and G-1P, has a negative effect on fitness with all antibiotics (**Figure 4.3c**). Additional detailed examples are shown in **Figure 4.3c** for instance for pyruvate metabolism, where inhibiting lactate, or acetaldehyde production increases sensitivity to β -lactams and glycopeptides and decreases sensitivity to 30S PSIs, inhibiting formate production decreases sensitivity to co-trimoxazole and 30S PSIs, and inhibiting acetyl-phosphate production decreases sensitivity to β -lactams, glycopeptides and co-trimoxazole. Within aspartate metabolism a range of changes can be triggered from increased sensitivity to β -lactams, and glycopeptides, to decreased sensitivity to most

other antibiotics. Moreover, the four genes involved in the production of threonine from L-aspartate trigger decreased sensitivity to fluoroquinolones and 30S and 50S PSIs. In the shikimate pathway inhibiting the production of chorismate from phosphoenolpyruvate (PEP) and erythrose-5-phosphate leads to increased sensitivity to β -lactams, co-trimoxazole, and Synercid. Cell division is the only process that upon interference, only generates increased sensitivity, specifically to CWSIs and co-trimoxazole. Interfering with peptidoglycan synthesis also mostly leads to increased sensitivity to CWSIs, as well as to 30S PSIs, while changes to genes that are involved in anchoring proteins to the cell wall (SP_1218 [*srtA*], SP_1833) can decrease sensitivity to CWSIs. Lastly, interfering with protein turnover, for instance through the protease complex ClpCP (SP_2194, SP_0746) and the regulator CtsR (SP_2195), which are generally assumed to be fundamental for responding to stress ^{48,49}, leads to decreased CWSI sensitivity and increased sensitivity to 30S and 50S PSIs (**Figure 4.3c**). Moreover, FtsH (SP_0013), important for clean-up of misfolded proteins from the cell wall, increases sensitivity to 30S PSIs and Synercid, indicating how important protein turnover is especially for surviving 30S PSIs, which can trigger the production of faulty proteins. Most importantly, these data show that, as expected, hundreds of options exist where disruption of a pathway or process leads to increased sensitivity to specific antibiotics. Remarkably, there seem to be almost as many options that can lead to decreased antibiotic sensitivity.

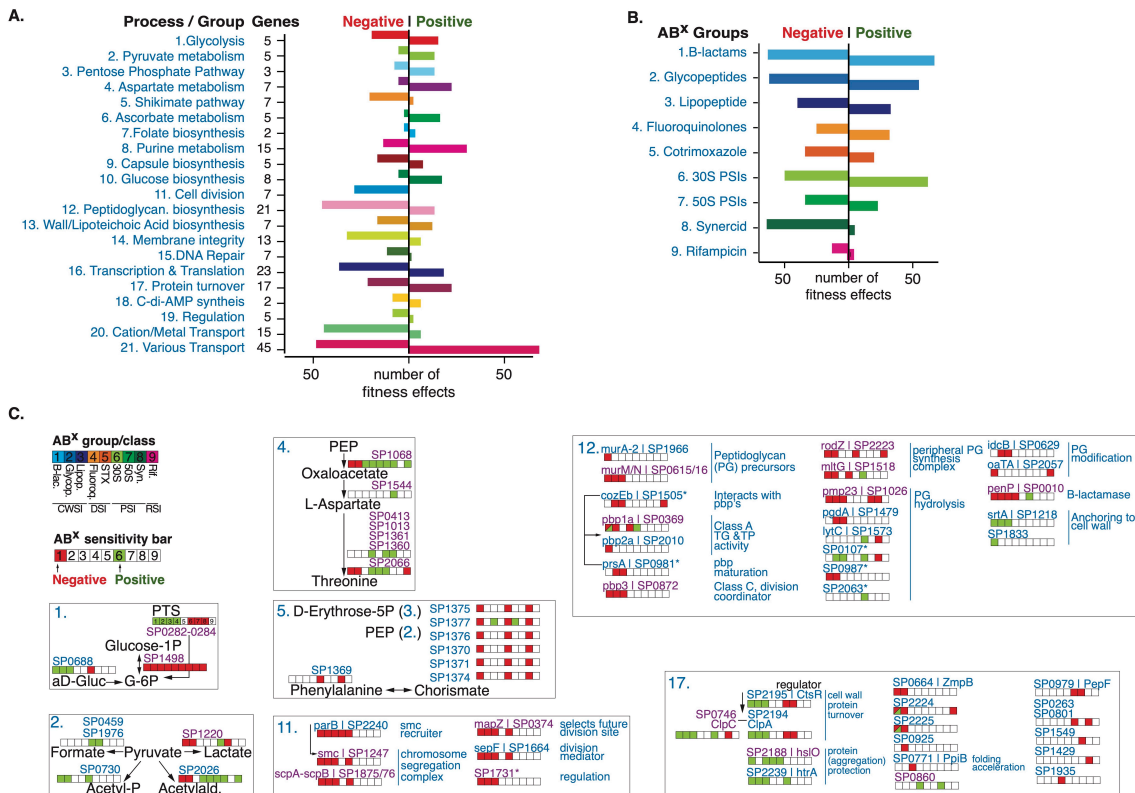


Figure 4.3 | A multitude of options, pathways and processes can simultaneously lead to increased and decreased antibiotic susceptibility.

a. The number of phenotypes scored for each pathway/process. Genes with at least one significant phenotype are split over 21 groups according to a pathway or process they belong to, which highlights how modulation of most pathways can lead to increased (negative phenotype) and decreased (positive phenotype) antibiotic sensitivity. **b.** The number of phenotypes scored for each antibiotic-group. While sensitivity to each antibiotic (group) can be increased by knocking out genes in the genome (negative phenotype), sensitivity can be decreased (positive phenotype) almost as often for most ABXs, except for Synercid, and to a lesser extent rifampicin, where most effects are negative. **c.** Detailed view of 7 out of 21 groups/processes highlighting how modulation of specific targets within each process leads to changes in antibiotic sensitivity. Each group is indicated with a number which is the same as in a. Where possible, genes are ordered according to their place in a process/pathway, and gene numbers (SP_) are combined with gene names and annotation. Each indicated gene is combined with an ‘antibiotic sensitivity bar’ indicating whether disruption leads to increased (red/negative fitness) or decreased (green/positive fitness) sensitivity to a specific or group of antibiotics. When phenotypic responses are the same, multiple genes are indicated with a single bar (e.g., SP0282/SP0283/SP0284 in glycolysis, or SP0413/SP1013/SP1361/SP1360 in Aspartate metabolism). Gene numbers in blue have no effect on growth in the absence of antibiotics when knocked out, while gene numbers in purple have a significant growth defect in the absence of ABXs. Essential genes are not indicated and genes with an asterisk have a partial or tentative annotation that has not been resolved. All 21 groups are listed in Supplemental Figures 2 and 3 in the manuscript published in *Nature Communications*.

4.3.4 *cozEb* encodes a cell division and peptidoglycan synthesis embedded membrane protein that can be critically targeted *in vivo* through an antibody-antibiotic strategy

By identifying targets that (re)sensitize bacteria against existing antibiotics, genome-wide antibiotic susceptibility data have the potential to guide the development of new antimicrobial strategies. One such strategy could be a combined therapeutic antibody-antibiotic approach; the antibody would target a gene-product that is important for sensitivity to one or more antibiotics and ideally the product would be easily accessible for the antibody at the bacterial cell surface. To find suitable candidate targets, Tn-Seq data were filtered for gene-products that, based on a known function or localization prediction, are likely to be present in the cell wall or membrane, and that when disrupted, increase sensitivity to one or more antibiotics. Moreover, it would likely be ideal if the gene is also important for survival *in vivo*. A strong candidate is SP_1505, which in the interaction network is most tightly linked to cell wall metabolism and cell division genes (**Figure 4.4a**). After we previously hypothesized that it may play a role in cell wall integrity¹⁴, it was recently named *cozEb*, with a likely role in organizing peptidoglycan synthesis during cell division⁵⁰, which fits its interaction profile (**Figure 4.4a**). Importantly, the antibiotic Tn-Seq data suggest that disruption creates increased sensitivity to vancomycin and rifampicin, while the product is critical in the presence of daptomycin, which was confirmed through individual growth curves (**Figure 4.4b**). The protein has eight predicted membrane-spanning domains (**Figure 4.4c**), and *in vivo* Tn-Seq predicts it is important for survival in both the nasopharynx and lungs (**Figure 4.4a**). The gene was cloned into an expression plasmid generating an ~30kD product (**Figure 4.4c**), which was used to raise rabbit anti-CozEb antibodies, which were confirmed to be specific for the *cozEb* gene product (**Figure 4.4c**). Potential antibody *in vitro* activity was determined through a bacterial survival assay in the absence and presence of antibodies and either vancomycin or daptomycin. Incubating bacteria with antibodies or daptomycin have no significant effect on bacterial survival, while vancomycin alone at the concentration used slightly reduces the number of surviving bacteria. Moreover, combining the antibody with either vancomycin or daptomycin further reduces the number of surviving bacteria *in vitro* compared to any agent individually (**Figure 4.4d**). To assess whether the antibody-

antibiotic approach works *in vivo*, mice were intranasally challenged with a bacterial inoculum either containing WT or ΔcozEb . Two additional sets of mice were challenged with WT and 8hrs post-infection they were either treated with daptomycin and control IgG-antibody or with daptomycin and CozEb-specific antibody. Mice were sacrificed 24 hrs post-infection, and bacteria in the lungs were enumerated. As predicted by the *in vivo* Tn-Seq data the *cozEb* knockout has a significantly lower fitness in the lungs highlighted by an up to 2.5-log lower bacterial load compared to WT. Importantly, while the WT survives equally well in the presence of the low daptomycin concentration and the control IgG antibody, in the presence of daptomycin and the CozEb-targeting antibody, its survival in the lungs is significantly reduced and resembles that of the *cozEb* knockout (**Figure 4.4e**). This shows that by combining antibiotic and *in vivo* Tn-Seq with gene annotation information, a gene-product can be selected that is central and critical to cell-wall synthesis and cell-division processes. Importantly, due to its presence in the membrane, it is directly targetable with an antibody, thereby sensitizing the bacterium to an antibiotic concentration it is normally not sensitive to.

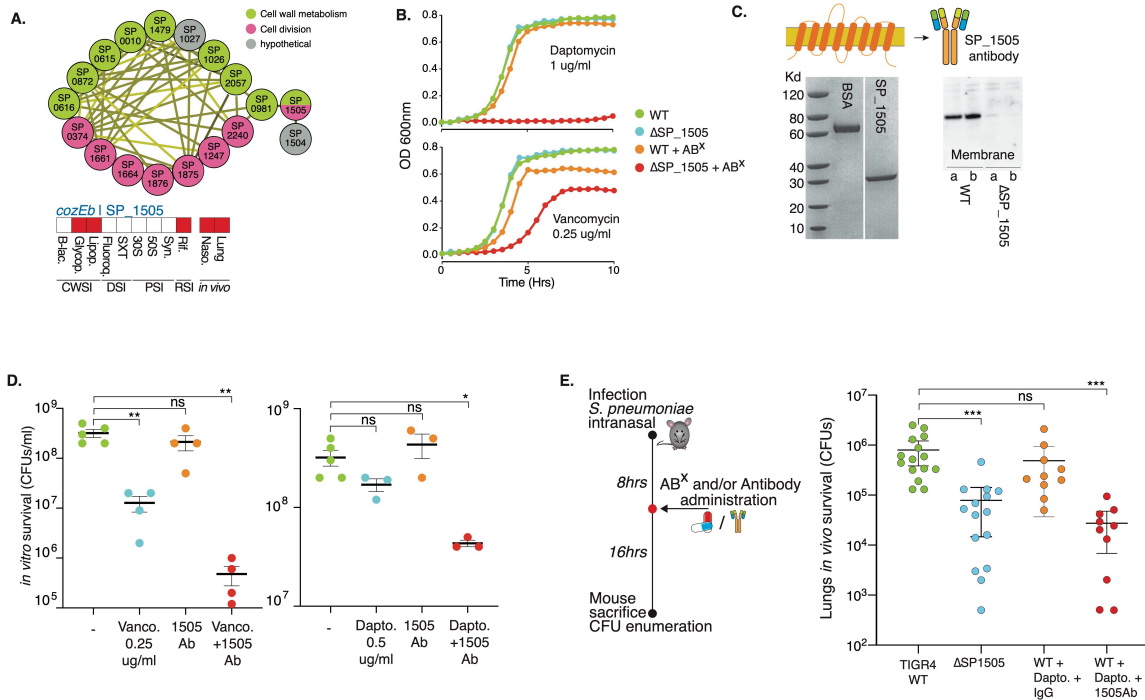


Figure 4.4 | CozEb an integral membrane protein increases antibiotic sensitivity and can be targeted with an antibody.

a. *cozEb*/SP_1505 is tightly clustered with cell division and cell wall metabolism genes, it is predicted to increase sensitivity to glycopeptides and the lipopeptide daptomycin and has a decreased fitness in the mouse lung and nasopharynx. **b.** Reduced relative growth of Δ *cozEb* validates its increased sensitivity to daptomycin and vancomycin. **c.** CozEb has 8 transmembrane domains, which generates a ~30Kd product (BSA is shown as a control). The cloned protein was used to raise antibodies, which proved to be specific for a product in the WT membrane, but does not bind anything in Δ *cozEb*, indicating the antibodies are specific for the membrane protein CozEb. **d.** Incubation of WT for 2hrs with vancomycin (Vanco) or daptomycin (Dapto) and in the presence of CozEb antibody, slightly but significantly decreases bacterial survival. **e.** An *in vivo* lung infection with WT or Δ *cozEb* confirms the mutant is less fit *in vivo*. Challenging the WT with daptomycin and IgG does not affect bacterial survival. In contrast, challenging with daptomycin and CozEb-specific antibodies, significantly reduces the recovered CFUs 24hrs post infection. Significance is measured through an ANOVA with Dunnett correction for multiple testing: * $p < 0.05$, ** $p < 0.01$, *** $p < 0.001$.

4.3.5 The *Ami*-operon encodes an antibiotic importer, and inhibition triggers tolerance

The example above illustrates how negative fitness indicates increased antibiotic sensitivity reflected by reduced relative growth, which can guide the development of (re)sensitizing approaches. In contrast, the occurrences of increased fitness in the dataset indicates that a large number of options exist that can lead to reduced antibiotic sensitivity (**Figure 4.3**). With reduced antibiotic sensitivity to 3 out of 4 antibiotic classes, the *ami*-operon is among genes with the greatest number of positive fitness effects. The operon forms a tight cluster in the interaction network (**Figure 4.3, 4.5a**) and it is annotated as an oligopeptide transporter with no clear function. Two separate knockouts for SP_1888 (*amiE*) and SP_1890 (*amiC*) confirm that increased fitness results in decreased drug sensitivity in the form of increased relative growth in the presence of ciprofloxacin, vancomycin and gentamicin, and increased sensitivity (i.e., decreased relative growth) to Synercid (**Figure 4.5b**). There is limited evidence that the *ami*-transporter may have (some) affinity for at least two different peptides (P1 and P2)⁵¹⁻⁵³. These have been theorized to possibly function as signaling molecules and under certain circumstances may be generated by the bacterium itself⁵¹⁻⁵³. Both peptides were synthesized and while neither peptide affects growth of the WT or knockout mutants in the absence of antibiotics, the WT grows slightly better in the presence of gentamicin and peptide P2, but not P1 (**Figure 4.5b**). This shows that some peptides may, at least partially, inhibit or occupy the *ami*-transporter, and thereby trigger decreased antibiotic sensitivity, in a similar manner as a knockout does. Besides peptides, the *ami*-transporter may be (non-selectively) transporting antibiotics into the cell, which could explain its effect on antibiotic sensitivity. To explore this, bacteria were exposed to ciprofloxacin or kanamycin and the internalized antibiotic concentration was determined through mass spectrometry for WT and both *ami* knockout mutants. In both mutants the amount of internalized ciprofloxacin was significantly lower (~1.7x in $\Delta amiE$, and ~2.3x in $\Delta amiC$), while the kanamycin concentration was found to be significantly lower in $\Delta amiC$ (~2x; **Figure 4.5c**). This shows that a functional *ami*-transporter increases the concentration of fluoroquinolones and 30S PSIs, suggestively by transporting them into the cell, and thereby, due to a higher internal concentration, enhancing the antibiotic's inhibitory

effects on growth. There are multiple examples that transporters can contribute to tolerance^{54,55}, which we recently showed is also the case for the *ade* transporter in *Acinetobacter baumannii*, which contributes to fluoroquinolone tolerance⁷. However, those examples are mostly based on efflux pumps that actively decrease the antibiotic concentration in the cell through upregulation of such pumps. In contrast, with respect to the *ami*-operon it would be the reverse, i.e., inhibition instead of upregulation would lead to tolerance. To explore this possible effect on tolerance, the WT and $\Delta amiE$ were exposed to either 10xMIC of gentamicin or vancomycin over a period of 24hrs. Approximately 1% of the WT population survives 4hrs exposure to gentamicin, while none of the population survives exposure past 8 hrs. The $\Delta amiE$ population displays a slower decline in survival with 1% of the population surviving the first 8hrs (tolerant cells)²⁵. At ~10 hrs the decline ceases and the remaining population (~0.01%) survives at least up to 24hrs, which is representative of a persister fraction²⁵. In contrast, the WT and *amiE* mutant populations decline at similar rates when exposed to vancomycin, showing that inhibition of the *ami*-transporter can lead to tolerance and persistence in an antibiotic specific manner while MICs of gentamicin and vancomycin for WT and $\Delta amiE$ are similar. Importantly, these data show that increased fitness indeed leads to decreased ABX sensitivity, which can translate into at least two phenotypes: increased relative growth and increased survival (i.e., tolerance).

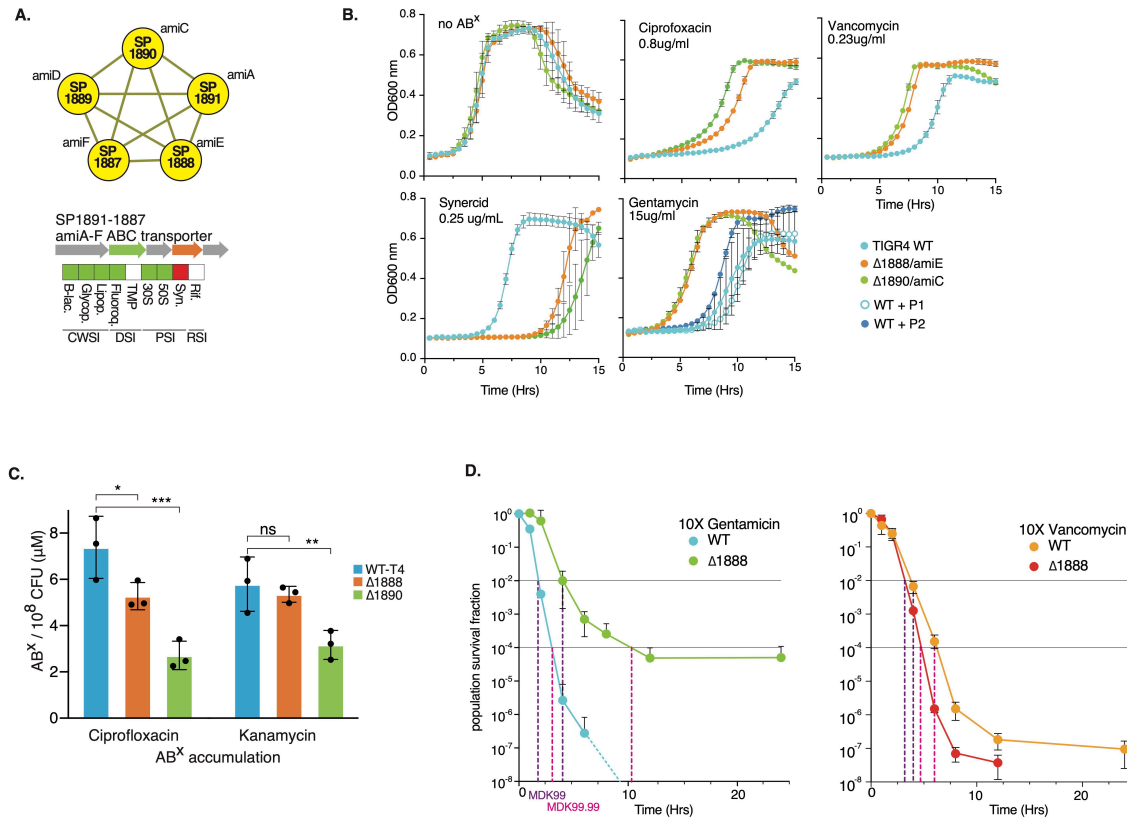


Figure 4.5 | Modulation of the *ami* transporter decreases sensitivity to many antibiotics.

a. The *ami*-operon forms a tight cluster, and upon knockout is predicted to decrease sensitivity to most antibiotics and increase sensitivity to Synercid. **b.** Growth curves of individual knockout mutants of *amiE* and *amiC* validate changes in antibiotic sensitivity, i.e., they show that positive fitness translates into decreased ABX sensitivity and increased relative growth, while negative fitness translates into increased ABX sensitivity and decreased relative growth. Additionally, growth curves suggest the transporter phenotypically responds to peptide P2. **c.** Intracellular antibiotic accumulation analysis shows that the WT strain with an intact transporter reaches a higher intracellular antibiotic concentration, suggesting the transporter is involved in importing antibiotics, explaining why a knockout or occupation with a peptide such as P2, can lead to decreased antibiotic sensitivity. **d.** Besides that modulation of the transporter leads to positive fitness, which translates into decreased ABX sensitivity and increased relative growth in the presence of gentamicin or vancomycin, it also leads to increased survival (i.e., tolerance) to gentamicin, but not vancomycin. Significance is measured through an ANOVA with Dunnett correction for multiple testing: * $p < 0.05$, ** $p < 0.01$, *** $p < 0.001$.

4.3.6 Purine metabolism, (p)ppGpp and ATP production are tightly linked to altered ABX susceptibility and tolerance

Among the 21 functional groups, purine metabolism has some of the largest number of positive fitness effects, mostly with β -lactams and glycopeptides (**Figure 4.3a, 4.6a**). Moreover, two regulators (SP_1821/1979) associated with this pathway decrease sensitivity to β -lactams and/or glycopeptides and two ‘neighboring’ genes with unknown function have either the same (SP_0830), or the opposite effect (SP_1446) on antibiotic sensitivity as their defined neighbor, suggesting they may be involved in the same process as their neighbor (**Figure 4.6a**). Furthermore, the global interaction network positively links an ABC-transporter (SP_0845-0848, **Figure 4.2c, 4.6a**) with multiple genes in this pathway due to their similar profiles. This operon is annotated as a putative deoxyribose-transporter, and to verify whether an interaction exists with purine metabolism, single and double knockouts were created between SP_0846 (the transporter’s ATP binding protein) and SP_0829/*deoB*. Their profiles suggest they do not affect growth in the absence of ABXs and have increased sensitivity to Synercid, which was confirmed with individual growth curves (**Figure 4.6b**). However, when both knockouts are in the same background, their increased sensitivity to Synercid is masked. Thus, as indicated by the network, these results show that the ABC-transporter indeed has a genetic interaction with purine metabolism/salvage but plays an unknown role. Importantly, this confirms that the global network includes valuable interactions that can be explored to uncover functional relationships.

Furthermore, within purine metabolism the alarmone (p)ppGpp is synthesized from GTP and/or GDP. Like other bacterial species, *S. pneumoniae* likely responds to (some) ABXs via induction of the stringent response pathway⁵⁶, in which *relA* (SP_1645) is the key player with both synthetase and hydrolase activity⁵⁷. Additionally, SP_1097 is annotated as a GTP diphosphokinase and may be involved in the synthesis of pppGpp from GTP (**Figure 4.6a**). Our data suggests, and we confirmed for the β -lactam cefepime (**Figure 4.6c**), that when synthesis of the alarmone is inhibited by deletion of *relA*, similar to many other interactions in purine metabolism, this leads to reduced β -lactam and glycopeptide sensitivity manifested by increased relative growth (**Figure 6c**). Moreover, while

SP_1097, as predicted, does not change ABX sensitivity (**Figure 4.6**), a double knockout of *relA*-SP_1097 seems to further decrease sensitivity to cefepime by further increasing relative growth (**Figure 4.6c, Figure 4.7a**). Additionally, besides a change in growth, the single *relA* and double knockout ($\Delta relA$ -SP_1097), also increases tolerance to cefepime by ~1000-fold at 24hrs (**Fig. 4.7b**), without changing the MIC. To understand how *relA* and SP_1097 affect purine metabolism, we used LC/MS to measure (p)ppGpp, ADP, ATP, GDP and GTP. Additionally, we included SP_0831 a purine nucleoside phosphorylase involved in nucleotide salvage, which has the same ABX profile as $\Delta relA$ (**Fig. 4.6a,d**), but should not directly affect (p)ppGpp synthesis. While (p)ppGpp is below the limit of detection during normal growth in any of the strains, as expected $\Delta relA$ and the double mutant $\Delta relA$ -SP_1097 are unable to synthesize the alarmone when exposed to mupirocin, a strong activator of the stringent response (**Figure 4.6e**). In contrast, WT, ΔSP_0831 and ΔSP_1097 synthesize (p)ppGpp upon mupirocin exposure to a similar extent (**Figure 4.6e**). Concerning the di- and trinucleotides in the pathway, upon mupirocin exposure GTP and GDP are significantly reduced in WT, ΔSP_0831 and ΔSP_1097 , likely because they are used for (p)ppGpp synthesis (**Figure 4.6f**). In contrast, while ATP and ADP again remain constant for the $\Delta relA$ mutants, ATP and ADP synthesis are significantly increased upon mupirocin exposure, especially for WT and ΔSP_1097 . This suggests that during activation of the stringent response, synthesis from IMP is directed towards AMP, and not necessarily GMP, at least not enough to replenish GTP and GDP. Additionally, upon mupirocin exposure, ATP only minimally increases for ΔSP_0831 , while it increases over 2-fold for WT and ΔSP_1097 (**Figure 4.6f**). It has been shown for bacteria including *Escherichia coli* and *Staphylococcus aureus* that a decreased ATP concentration can decrease sensitivity to ABXs such as ciprofloxacin⁵⁸. Additionally, in *S. aureus*, (p)ppGpp overexpression has been associated with decreased sensitivity to linezolid⁵⁹. Our data suggests that (p)ppGpp and ATP synthesis may be intrinsically linked, i.e., at least in *S. pneumoniae* the inability to produce the alarmone also results in lowered ATP synthesis, which is associated with a lowered ABX sensitivity to β -lactams and glycopeptides. However, ΔSP_0831 shows that even if (p)ppGpp can be synthesized, modulation of purine metabolism, for instance through the salvage pathway, can result in decreased ATP synthesis, and can lead to lowered ABX sensitivity (i.e., increased relative growth). Importantly, in many bacterial species, alarmone

production is generally assumed to be triggered in response to different types of stress and has been shown to affect a large variety of processes including nucleotide synthesis, lipid metabolism and translation. (p)ppGpp is thereby a ubiquitous stress-signaling molecule that enables bacteria to generate a response that is geared towards overcoming the encountered stress. However, contradictory results between species indicates a possible non-uniformity across bacteria, leaving much to be learned about how the alarmone and the processes it can control fit into the entire organismal (response) network⁵⁶. Our data suggests that the inability (i.e., due to mutations) to generate the alarmone in *S. pneumoniae* in response to β -lactams and glycopeptides is linked to reduced ATP, which under specific circumstances may be an optimal response, as it results in decreased ABX sensitivity translating into increased relative growth and tolerance, and thereby a higher probability to survive the insult (**Figure 4.6c, 4.7a,b**).

4.3.7 There are a multitude of pathways that lead to tolerance in vivo in an antibiotic dependent manner

To further confirm that antibiotic sensitivity can be decreased by inhibiting a variety of processes, knockouts (KOs) were generated for fourteen mutants from 8 different processes. Moreover, an additional goal was to determine what increased fitness (i.e., decreased ABX sensitivity) would look like phenotypically, and thus whether it would translate into increased relative growth and/or tolerance. Of the fourteen mutants with a Tn-Seq predicted increased fitness, thirteen display an increased ability to grow in the presence of an ABX compared to the WT. Moreover, 8 mutants, which inhibit several different processes including different metabolic pathways, transport, and transcription and translation, displayed tolerance, while retaining a similar MIC, and thereby have an increased ability to survive high level exposure to an ABX (5-10xMIC) for at least 24 hours **(Figure 4.7a,b)**. Note that we validated 49 single KO genotype x phenotype associations in this study, with an equal distribution across the entire spectrum of ABX sensitivity **(Figure 4.1e)**. This highlights that our approach uncovered a detailed genome-wide ABX sensitivity Atlas composed of a multitude of genes, pathways, and processes that when modulated can increase and/or decrease ABX sensitivity. The validation experiments highlight that the resulting fitness accurately predicts the relative growth rate of a mutant, which we have previously shown for hundreds of other negative fitness phenotypes ^{6,14-16,18,39-42,44,60-62}. Moreover, it turns out that in the majority of cases, increased fitness not only results in increased relative growth in the presence of an antibiotic, but also tolerance. Thereby, the part of the Atlas that depicts decreased ABX sensitivity (i.e., increased fitness) includes a genome-wide ‘tolerome’, composed of a wide variety of pathways and processes that when modulated trigger tolerance in vitro in an ABX dependent manner.

Obviously, the selection regime in vivo is far more complex and stricter than in a test tube, which raises the question whether many of the options that decrease ABX sensitivity in vitro, including those that increase tolerance, would be available in vivo as well. To explore this, all the Tn-Seq data with a positive fitness in the presence of at least one antibiotic was combined with in vivo Tn-Seq data and filtered for those genes with no or only a small fitness defect predicted in vivo during nasopharynx colonization or lung

infection (**Figure 4.7c**). Two genes were selected that we had confirmed for decreased ABX sensitivity in vitro: **1**) SP_0829/*deoB* synthesizes Ribose-1P and is involved in purine metabolism (**Figure 6a**). $\Delta deoB$ has no effect on in vitro growth in the absence of ABX (**Figure 7a,d**), as predicted it grows better in the presence of cefepime (**Figure 7a,d**), but it does not affect survival/tolerance (**Figure 4.7b**); **2**) SP_1396/*pstA* is the ATP binding protein of a phosphate ABC transporter. $\Delta pstA$ has no effect on in vitro growth (**Figure 4.7a,d**), it has a higher relative growth rate in the presence of meropenem (**Figure 4.7a,d**), and it also increases survival/tolerance (**Figure 7b**). Both mutants were mixed with WT in a 1:1 ratio and used in an in vivo mouse infection competition model as we have done previously¹⁸. Of the infected mice, half were administered antibiotics at 16-hours post infection and were sacrificed 6 hours later to determine the strain's competitive index (CI) (**Figure 4.7e**). Importantly, while both mutants may have a slight disadvantage compared to the WT when colonizing the lung or nasopharynx, their CI increases significantly in the presence of ABXs, leading to increased survival compared to the WT (**Figure 4.7e**). Combining antibiotic- with in vivo Tn-Seq indicates the possibility to predict the existence of a wide-array of possible alterations of specific genes, pathways and processes that can have a beneficial effect in vivo in the presence of antibiotics. Such changes could thereby contribute to escape from antibiotic pressure and even create a path towards the emergence of antibiotic resistance. Importantly, the ability to predict how certain changes affect ABX sensitivity and simultaneously in vivo fitness, could enable new strategies to preemptively prevent treatment failure.

There is possibly significant overlap in the selective pressures a bacterial pathogen would experience in a mouse infection model compared to the human host. This raises the possibility that those gene-disruptions that are predicted by Tn-Seq to lead to decreased antibiotic sensitivity and that simultaneously have no more than a minimal defect in vivo, could also have an advantage in the human host in the presence of ABXs and thereby contribute to ABX escape and/or the emergence of resistance. A premature stop codon most closely reflects the effect a transposon insertion has on a gene, i.e., it disables a gene. We thereby hypothesized that stop codons in certain gene sets predicted by Tn-Seq could be enriched for in antibiotic resistant clinical isolates. To test this hypothesis 4 gene-sets were compiled consisting of those that upon disruption: **1**) decrease

antibiotic sensitivity in at least 1 antibiotic and have no strong defect *in vivo*; **2**) decrease antibiotic sensitivity in at least 1 antibiotic and have a defect *in vivo*; **3**) have little to no effect on antibiotic sensitivity and *in vivo*; **4**) have no effect or increase antibiotic sensitivity and have a defect *in vivo* (**Figure 4.8a,b**). Thousands of strains were selected from the PATRIC^{63,64} database that could be split into a group of co-trimoxazole (SXT) resistant and a group of β -lactam resistant strains, and each group was matched with an equal number of sensitive strains from the database. In all strains in the SXT and β -lactam groups, irrespective of resistant or sensitive status, the number of stop codons in gene sets 1 and 3 are highest, which reflects the Tn-Seq predicted *in vivo* effects, i.e., while gene sets 1 and 3 contain mostly genes with potentially neutral effects, gene sets 2 and 4 contain many genes that are suggested to have a defect *in vivo* when disabled (e.g. with a stop codon) (**Figure 4.8c**). Moreover, SXT resistant isolates in gene set 1 more often contain a stop codon compared to sensitive strains, and in β -lactam resistant isolates this is true for gene-sets 1-3 (**Figure 4.8d**). While these are not ideal comparisons, for instance the entire ABX profile is not clear for many strains, different changes than premature stops could have ABX/*in vivo* modulating effects, strains could have experienced different ABX and/or *in vivo* selective pressures, and genetic changes can be strain-background dependent, it shows that genetic changes that can affect ABX and/or *in vivo* sensitivity, which are predictable with Tn-Seq, readily occur in clinical samples. This in turn underscores that ongoing infections may consist of variants that enable different paths to adjust to or overcoming a challenging host/ABX environment.

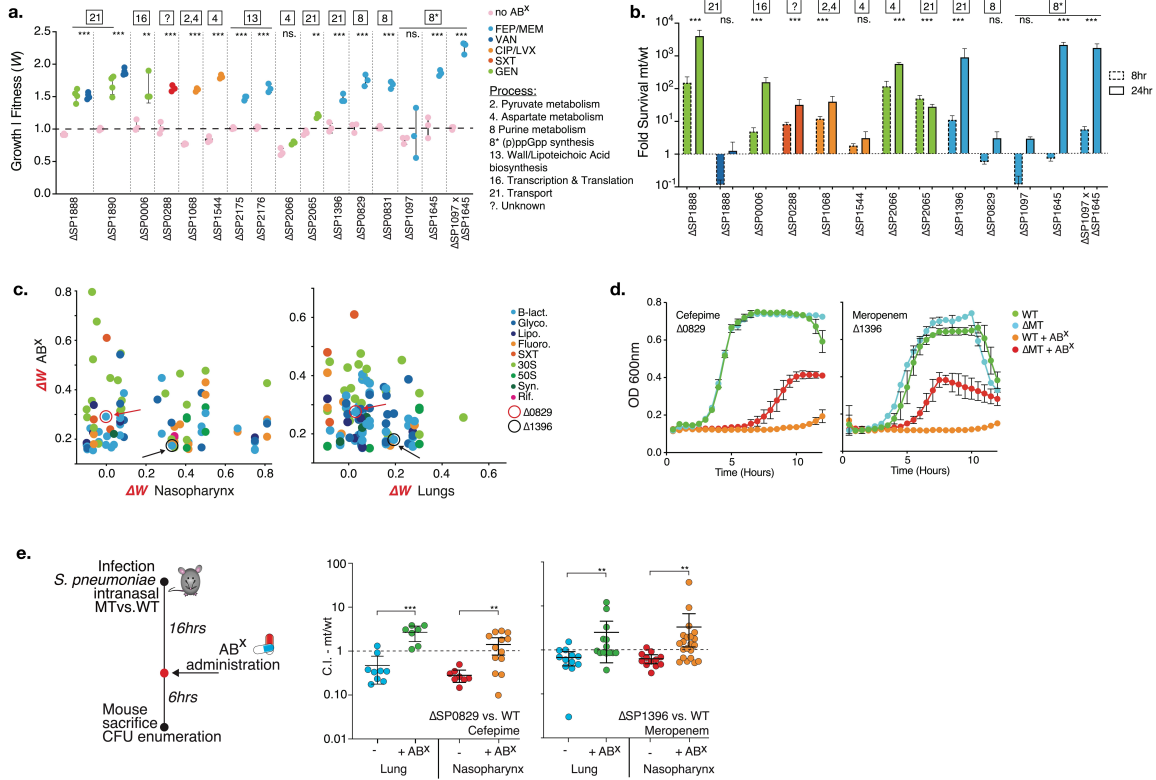


Figure 4.7 | Decreased antibiotic sensitivity and tolerance can be achieved by modulation of a wide variety of processes.

a. Relative growth rates (i.e., fitness) of 16 knockout mutants involved in 7 processes measured in the presence of 7 antibiotics, validate that decreased ABX sensitivity (i.e., increased relative growth) can be achieved by modulating a wide variety of processes. **b.** Significantly increased survival during exposure to 5-10xMIC of an ABX over a 24hr period is observed for 9 out of 12 knockouts. Significance is measured with an ANOVA with Dunnett correction for multiple comparisons: **p<0.01, ***p<0.001. **c.** Tn-Seq data with a positive fitness in the presence of at least one antibiotic (y-axis) is plotted against in vivo Tn-Seq data (x-axis). Note that only in vivo data is shown that is predicted to have no more than a small fitness defect, no fitness defect, or an increased predicted in vivo fitness, either during nasopharynx colonization or lung infection. Circled and indicated with arrows are SP_0829 in red and SP_1396 in black. **d.** In vitro growth curves validate decreased sensitivity (i.e., increased relative growth) to cefepime (SP_0829) and meropenem (SP_1396). **e.** Mice were challenged with WT and MT in a 1:1 ratio of which half received ABX 16hrs post infection (p.i.), and all were sacrificed 24hrs p.i. Displayed are the MT's competitive index (C.I.) in the nasopharynx and lung, and in the presence and absence of cefepime (SP_0829) or meropenem (SP_1396). In all instances, the addition of ABX significantly increases the C.I. of the mutant. Significance is measured with a Mann-Whitney test **p<0.01, ***p<0.001.

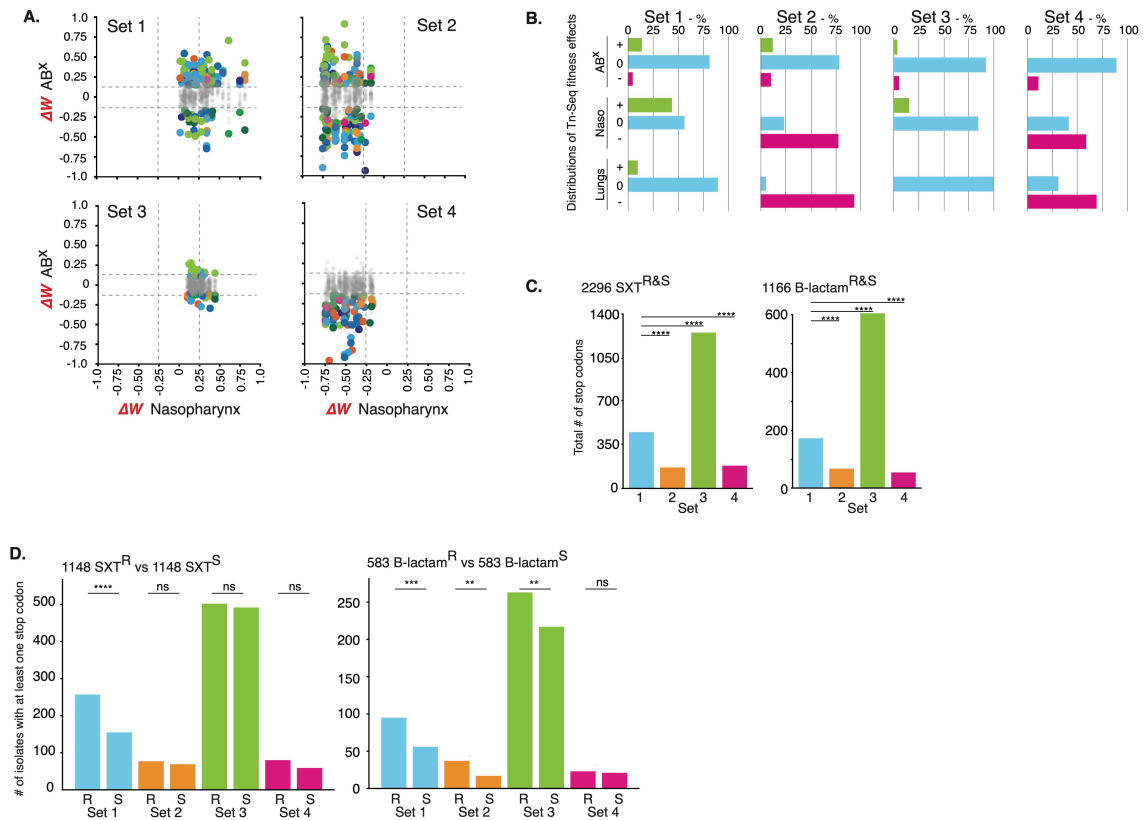


Figure 4.8 | Stop codons are enriched in clinical samples in Tn-Seq predicted tolerome genes.

a. Based on *in vivo* and ABX Tn-Seq data, four gene-sets consisting of 34 genes each were compiled with specific fitness profiles in the presence of antibiotics and *in vivo*. Shown are the *in vivo* effects for nasopharynx, while lung data are depicted in Supplementary Figure 5. ΔW represents the fitness difference of a gene in a specific condition (e.g., an antibiotic, *in vivo*) minus its fitness *in vitro* in rich medium. Dashed lines indicate significance cut-offs, greyed-out dots indicate genes with no significant change in fitness in the presence of antibiotics, colors represent antibiotics and are the same as in **Figure 4.1**. **b.** Detailed distributions for each gene set highlights whether effects in the presence of antibiotics, in the nasopharynx and lungs increase (+), do not affect (0) or decrease (-) relative fitness. Gene set rationales are described in the text. **c.** The total number of stop codons in each gene set for 2296 co-trimoxazole and 1166 β -lactam resistant and sensitive strains. **d.** The number of sensitive and resistant strains with at least one stop codon in a gene in each gene-set. Significance is measured through a Fisher's exact test: ** $p < 0.01$, *** $p < 0.001$, **** $p < 0.0001$.

4.4 Discussion

The emergence and increase in antibiotic resistance among most bacterial pathogens are a continuously developing problem with several important drivers, which include: **1)** a lagging development of new drugs and treatment strategies; **2)** a lack of (rapid) diagnostics and prognostics; and **3)** an incomplete understanding of how antibiotic resistance develops. Moreover, these drivers are inherently connected making it a complex problem to solve. First, the ability of bacteria to evolve resistance elicits an arms-race that requires the development of new drugs and treatment strategies to keep the balance of infection-control tipped in our favor. Thus, while developing new drugs would keep the arms-race in place, the ability to slow or prevent the emergence of resistance could resolve the status quo. Furthermore, even though it is critical to understand how and under which circumstances resistance evolves, the applicability of this knowledge depends on the availability of diagnostics that could inform on the emergence of resistance (precursors) and thereby guide and enable timely, tailored, and targeted treatments. To progress towards a comprehensive understanding of how an infection is developing in the absence or presence of treatment, and how to decide what to do next, we believe that a detailed genetic understanding of how a bacterium deals with and overcomes stress, as well as its genetic potential to achieve this, are key aspects. In this study we contribute to reaching such an understanding by building and exploring a detailed atlas of ABX sensitivities, which highlights how modulation of specific genes, pathways and processes does not only result (as expected) in increased ABX sensitivity, but almost just as often in decreased ABX sensitivity. We show that such an atlas can be used to identify leads for gene function, to uncover the genome's underlying architecture and genetic relationships among genes, for the identification of new drug targets, and the development of new proof-of-principle antimicrobial (ABX sensitizing) strategies. Most importantly, these data identify genome-wide genetic changes that show how modulation of genes, pathways and processes can lead to reduced antibiotic sensitivity (i.e., increased relative growth and tolerance), not only in vitro, but also in vivo. Moreover, we show that mutations that have the potential to trigger the same phenotypes readily occur in patients.

While the primary processes targeted by ABXs are mostly known, this work contributes to the increasing notion that downstream processes, not directly related to the target and which include metabolism, can significantly contribute to antibiotic efficacy^{14,15,18,65-68}. In *E. coli* it has been shown that inhibition of specific steps in purine metabolism can lead to decreased sensitivity to ampicillin and ciprofloxacin, and increased sensitivity to gentamycin⁶⁹. Our data explores a wider set of alterations in purine metabolism in *S. pneumoniae*, which also leads to a wider distribution of changes. However, the overlap with *E. coli* includes decreased sensitivity to β -lactams (an ABX class that includes ampicillin) and we show that inhibition of some reactions in purine metabolism can also lead to decreased sensitivity to fluoroquinolones (an ABX class that includes ciprofloxacin). Additionally, it has been shown for *E. coli* that antibiotic sensitivity to ampicillin and ciprofloxacin can be increased, at least over 4hrs, by supplementing with adenine, but not guanine, which is possibly linked to a reduced ATP demand and synthesis⁶⁹. Our results show that limiting the ability to synthesize adenine, but also guanine, leads to significantly lowered ABX sensitivity to β -lactams and glycopeptides. Moreover, we show that limiting the ability to synthesize adenine, as well as (p)ppGpp, leads to lowered ATP synthesis. The association between decreased ATP synthesis/availability and decreased sensitivity and/or tolerance to antibiotics including β -lactams, glycopeptides and fluoroquinolones has now been shown for a variety of Gram-positive and -negative organisms^{35,58,70,71}. While this suggests that low ATP demand/synthesis/availability may be at the root of a general mechanism that leads to decreased sensitivity to some antibiotics, our genome-wide atlas shows that decreased ABX sensitivity and tolerance to β -lactams, and glycopeptides can be triggered by alterations to pathways and processes other than those directly related to ATP synthesis, which include parts of glycolysis, pyruvate, ascorbate, glucose and purine metabolism, protein turnover and c-di-AMP synthesis. While it is possible that many of these alterations do affect ATP demand, availability and/or synthesis, it is likely that they trigger a much more complex and varied set of changes. Importantly, the full extent of signals and (genetic) alterations that can lead to decreased ABX sensitivity, including tolerance, remain mechanistically poorly understood^{25,34}. This also means that it remains unclear whether there are common denominators or universal rules that are applicable across strains and species^{7,25,34,35,58,70,71}. Different (computational) approaches are being explored

to build such a comprehensive understanding^{6,15,17,69,72,73}, however, unequivocally more genome-wide data from more species remain needed. Thereby, the genome-wide insights we present here are helping build a rationale to measure and model this complexity. One goal of such models would be to obtain a detailed understanding and ability to predict how alterations to specific processes affect responses to ABXs and thereby drive changes in sensitivity^{15,17,25,34,69}. Lastly, these detailed data on reduced antibiotic sensitivities also suggest that more potential routes to ABX-escape, and eventually resistance, may exist than assumed. We believe these data are thereby both an argument and potential starting point for a platform to predict clinically relevant mutations and determinants of antibiotic resistance and/or tolerance. Consequently, they underscore the importance of understanding the genetics of variants with altered drug susceptibility, as their genetics makes them diagnostically identifiable and trackable, while their often-associated collateral sensitivities to other ABXs or drugs could make them targetable.

4.5 Materials and Methods

Bacterial culturing, growth curves and tolerance experiments

Experiments were performed with *S. pneumoniae* strain TIGR4 (NCBI Reference Sequence: NC_003028.3). TIGR4 is a serotype 4 strain that was originally isolated from a patient from Norway with Invasive Pneumococcal Disease (IPD) ^{74,75}. All 'SP_' gene numbers in the tables and figures are according to the TIGR4 genome. Single gene knockouts were constructed by replacing the coding sequence with a chloramphenicol and/or spectinomycin resistance cassette as described previously ^{18,39,40}. *S. pneumoniae* was grown on sheep's blood agar plates or statically in THY, C+Y or semi-defined minimal media at pH 7.3, with 5 µl/ml Oxyrase (Oxyrase, Inc), at 37°C in a 5% CO₂ atmosphere ¹⁵. Where appropriate, cultures and blood plates contained 4 µg/ml chloramphenicol (Cm) and/or 200 µg/ml spectinomycin (Spec). Single strain growth assays were performed three times using 96-well plates by taking OD₆₀₀ measurements on a Tecan Infinite 200 PRO plate reader or BioSpa 8 (BioTek). Growth curves are fitted to an exponential growth equation to calculate their doubling time. WT doubling time is divided by a mutant's (MT) doubling time to represent each mutant's fitness (i.e., relative growth rate; $WT_{\text{doubling time}} / MT_{\text{doubling time}} = W_{\text{mutant}}$), making it directly comparable to Tn-Seq fitness ^{14,15,18,39-41,44,60,62,76,77}. Tolerance experiments were performed by exposing exponentially growing bacteria to 5-10xMIC of an antibiotic. Samples were taken at different time-points over a 24hr period, washed with PBS and plated on blood-agar for enumeration. The number of surviving bacteria at different time points are divided by the starting population to determine the surviving proportion at each time point. The proportion of surviving MT bacteria are divided by the proportion of surviving WT bacteria to determine the fold survival (MT/WT) at each time point as depicted in **Figure 4.7b**.

Tn-Seq experiments, fitness (*W*) and enrichment analyses

Six independent transposon libraries, each containing ~10,000 insertion mutants, were constructed with transposon Magellan6 in WT-T4 as described previously ^{14,18,39,77}. Selection experiments were conducted in rich medium with glucose as a carbon source in the presence or absence of 20 different antibiotics at a concentration that slows growth by ~30-50%. Libraries are grown in ~10ml medium (wo/w ABX), from a starting OD₆₀₀ of ~0.003 (~40,000 CFU/ml) up to an OD₆₀₀ of ~0.3-0.6 (~1.10⁷ CFU/ml), representing ~7-8

generations. Sample preparation, Illumina sequencing, and fitness calculations were done as described ^{14,18,39,44,60,77}. In short, fitness of a single mutant (W_i) is calculated by comparing the fold expansion of the mutant to the fold expansion of the population and is determined by the following exponential growth equation we previously developed ^{18,39,60}.

$$W_i = \frac{\ln(N_i(t_2) \times d / N_i(t_1))}{\ln((1 - N_i(t_2)) \times d / (1 - N_i(t_1)))}$$

in which $N_i(t_1)$ and $N_i(t_2)$ are the mutant frequency at the beginning and end of the experiment respectively and d is the population expansion. All of the insertions in a specified region or gene are then used to calculate the average fitness and standard deviation of the gene knockout in question. The advantage of using this approach is that W_i represents the actual growth rate per generation, which makes fitness independent of time and enables comparisons between conditions. To determine whether fitness effects are significantly different between conditions three requirements have to be fulfilled: 1) W_i is calculated from at least three data points, 2) the difference in fitness between the presence and absence of antibiotic has to be larger than 15% (thus $W_i - W_j < -0.15$ or > 0.15), and 3) the difference in fitness has to be significantly different in a one sample t -test with Bonferroni correction for multiple testing ^{18,39,60}. Importantly, we have previously validated that a mutant's Tn-Seq fitness is indeed directly related to its relative growth rate, which means that a mutant with for instance a Tn-Seq fitness of 0.5 grows twice as slow as the WT. In this study we show that fitness is also directly related to a mutant's relative growth rate, where negative fitness indicates increased ABX sensitivity and a decreased relative growth, while positive fitness indicates decreased ABX sensitivity and increased relative growth. Moreover, while Tn-Seq selection is performed under ABX pressure during growth for 7-8 generations we find here that positive fitness in many cases also leads to increased survival, i.e., tolerance, highlighting that this phenotype can be efficiently untangled through our approach.

In multiple figures ΔW ($W_{ABX} - W_{noABX}$) is displayed, which means that each gene's antibiotic-specific fitness is statistically compared to baseline fitness without ABXs. ΔW thereby indicates a gene's antibiotic-specific fitness effect which can be categorized as: **1) Neutral**, $\Delta W = 0$, a mutant's relative growth is similar in the absence and presence of an ABX; **2) Negative**, $\Delta W < 0$, a mutant's fitness is significantly lower and thus grows

relatively slower in the presence of an ABX; **3)** Positive, $\Delta W > 0$, a mutant's fitness is significantly higher and thus grows relatively faster in the presence of an ABX. For instance, if a gene knockout's $\Delta W = 0.25$, it means that its relative growth rate is ~25% higher in the presence of an ABX than in the absence of the ABX.

To determine whether a particular process or pathway is specifically involved in responding to an antibiotic-group, a hypergeometric test was performed to test for enrichment. The distribution of significant genes within each process was compared to the distribution of the pathways in the overall genome. A p-value and Benjamini-Hochberg adjusted p-value were calculated for each process and antibiotic group, where an adjusted p-value below 5% is considered to identify statistical enrichment.

Determination of minimum inhibitory concentration (MIC)

MICs were determined as previously described¹⁷. In short, 1×10^5 CFU of mid-exponential bacteria in 100 μL are diluted with fresh medium containing a single antibiotic to achieve the following concentration gradients and increments: Ciprofloxacin gradient 0.4-1.8 $\mu\text{g/mL}$ with 0.1 $\mu\text{g/mL}$ increments; Cefepime 0.0175-0.03 $\mu\text{g/mL}$ with 0.0025 $\mu\text{g/mL}$ increments; Gentamicin 17-39.5 $\mu\text{g/mL}$ with 2.5 $\mu\text{g/mL}$ increments; Meropenem 0.006-0.02 $\mu\text{g/mL}$ with 0.002 $\mu\text{g/mL}$ increments; co-trimoxazole 4.5-10 $\mu\text{g/mL}$ with 0.5 $\mu\text{g/mL}$ increments; vancomycin 0.12-0.32 $\mu\text{g/mL}$ with 0.04 $\mu\text{g/mL}$ increments. Each concentration was tested in triplicate in 96-well plates. MICs were monitored on a Tecan Infinite 200 PRO plate reader or BioSpa 8 (BioTek) at 37°C for 12 hours. MIC is determined as the lowest concentration that abolishes bacterial growth.

Co-fitness network construction and SAFE analysis

A gene x condition matrix was constructed to identify correlating fitness profiles and built a co-fitness network. The matrix is based on 20 antibiotic conditions from experiments performed here, supplemented with 17 conditions¹⁸. The additional conditions consist of Sucrose, Fructose, Cellobiose, Raffinose, Sialic Acid, Galactose, Mannose, Maltose, GlcNac, Bipyridyl, transformation, hydrogen-peroxide, methyl-methane sulfonate, pH6, temperature, Norfloxacin. Genes with missing data were removed resulting in a 1519 gene x 37 condition matrix. Genes and conditions were correlated using a Pearson's correlation coefficient and a Spearman's correlation coefficient. Resulting in two

1519x1519, gene vs gene matrices. A significance cutoff was applied and correlations ≥ 0.75 were retained and used as edges to build a co-fitness network consisting of 1519 genes and 2399 edges. An edge-weighted spring embedded layout was applied with Cytoscape ⁷⁸, with the absolute correlation value as the edge weight. This results in a network with several major clusters and multiple genes unconnected to the main network. A stability test was performed to determine the robustness and quality of each edge in the network by building a correlation matrix from partial data. 30 conditions were selected 100 times to build a correlation matrix and using the same cutoff criteria a co-fitness matrix was compiled. Every edge with a correlation value above the threshold was assigned a 1 and every edge below the cut-off 0. This resulted in 100 binary matrices which were then summated, resulting in every gene vs gene interaction being assigned a stability score with a value N out of 100. A SAFE (Spatial Analysis of Functional Enrichment) analysis ^{45,46} on the co-fitness network was performed with Cytoscape. A SAFE analysis is geared towards defining local neighborhoods for each node within a network and calculates an enrichment score for every functional attribute. It then highlights the areas that are the most enriched for that attribute. Attributes were assigned by merging KEGG ⁷⁹ pathway annotation and available functional category annotations, which covers 94% of the genes within the network. The distance threshold was set to the 1st percentile of the map-weighted distance, the Jaccard similarity index was set to 0.5, and nodes in different landscapes were retained.

CozEb (SP1505) cloning and protein expression

Cloning and expression of SP_1505 was undertaken commercially (Genscript). Codon-optimized SP_1505 was cloned into pET28a with a C-terminal His-tag. *E. coli* BL21 (DE3) was transformed with recombinant plasmid. A single colony was inoculated into LB medium containing kanamycin; cultures were incubated at 37°C at 200 rpm and IPTG was introduced for induction. SDS-PAGE and Western blot were used to monitor the expression. Protein was purified from 1L batch culture in Terrific Broth. Cells were harvested by centrifugation, cell pellets were lysed by sonication, and supernatant after centrifugation was kept for future purifications. SP_1505 protein was obtained by three-step purification using Ni column, Superdex 200 column and Q Sepharose. Fractions were pooled and dialyzed followed by 0.22 μm filter sterilization. Protein was initially analyzed by SDS-PAGE and Western blot by using standard protocols for molecular

weight and purity measurements. The primary antibody for Western blot is Mouse-anti-His mAb (GenScript, Cat.No.A00186). The concentration was determined by BCA protein assay with BSA as a standard. Final protein product was stored in 50 mM Tris-HCl, 150 mM NaCl, 10% Glycerol, 0.2% DDM, pH 8.0 and stored at -80°C.

CozEb (SP1505) antibody generation, purification, and quantification

A single rabbit was vaccinated by a commercial vendor (Rockland) with recombinant SP_1505 via the following schedule. Rabbit was immunized via intradermal route with 0.1 mgs SP_1505 with Complete Freund's Adjuvant (CFA) followed by an intradermal 0.1 mg booster injection with Incomplete Freund's Adjuvant IFA as an adjuvant at day 7, followed by two subcutaneous 0.1 mg booster injections at days 14 and 28 with IFA. Terminal bleed was collected on day 52 following challenge. SP_1505 IgG was purified from immunized rabbit serum using protein G resin and columns (Pierce) according to manufacturer specifications. Following purification, antibody was concentrated using 10,000 MWCO centrifugal filters (Millipore) and was dialyzed three times against PBS in a 3.5kDa Slide-A-Lyzer dialysis cassette (Thermo Scientific). Antibody specificity was determined by Western Blot using the parental wild-type and corresponding deletion mutants.

Cell fractionation, TCA precipitation, and Western Blot

Strains were grown in Todd-Hewitt broth to OD 0.4. Following this, cells were fractionated as previously described⁸⁰. Briefly, 2mL of culture was centrifuged at maximum speed. The pellet was resuspended in cell wall digestion buffer [1x Protease inhibitor cocktail (Roche), 300U/uL mutanolysin, 1mg/mL lysozyme in a 30% sucrose-10mM Tris (pH 7.5) buffer with 20mM MgCl₂ and 20mM MES (pH 6.5)] and incubated at 37°C for 60 minutes. After centrifugation, the supernatant containing the cell wall was saved. Pelleted protoplasts were snap frozen in a dry ice ethanol bath, then treated with MgCl₂, CaCl₂, DNase I (Qiagen), and RNase A (Roche) in 50mM Tris buffer (pH 7.5) with 20mM HEPES (pH 8.0), 20mM NaCl, and 1mM DTT with protease inhibitors. The pellet was incubated on ice for one hour, then spun at max speed for 30 minutes at 4°C. The supernatant, which contained the cytoplasmic fraction, and the pellet, which contained the membrane fraction, were saved. 100% TCA was added to the samples so that the final concentration of TCA was 20%. Samples were incubated on ice for 30 min, then centrifuged at full

speed at 4°C to pellet precipitated protein. The TCA supernatant was aspirated, and the pellet was washed twice with 100% acetone, then air-dried at 95°C for 1 minute. Pellets were resuspended in NuPage LDS sample buffer (Thermo Scientific) and boiled at 100°C for 10 minutes. Samples were loaded into NuPage SDS-PAGE gels (Thermo Scientific) and transferred to nitrocellulose membranes using the XCell Sure-Lock mini-cell electrophoresis system (Thermo Scientific). Nitrocellulose membranes were blocked overnight in 5% NFDM and treated with primary antibody against SP_1505 at a concentration of 1:500. After washing, membranes were treated with secondary antibody goat anti-rabbit IgG-HRP (Bio-Rad) at a concentration of 1:3000. Membranes were developed using the SuperSignal West Dura Extended Duration Substrate (Thermo Scientific) and were visualized using a BioRad ChemiDoc MP imaging system.

Antibiotic-antibody targeted in vitro bacterial survival

Bacteria were inoculated from TSA plates into C+Y media, at OD 0.4, culture was split into 1 mL aliquots and treated with vancomycin (0.25 µg/ml) or daptomycin (0.5 µg/ml). For antibody treatment, strains were grown in C+Y media until OD 0.3. At this time, samples were treated with SP_1505 antibody or control rabbit IgG antibody (Sigma) at concentrations indicated in figure legends, incubated for 30 minutes, followed by antibiotic treatment. At 4hrs post antibiotic addition samples were plated for bacterial enumeration.

Antibiotic-antibody mouse challenge

Isoflurane-anesthetized 7-week-old female BALB/c mice were inoculated intranasally with 10⁶ CFU of wild type pneumococcal cells in a volume of 100 µL. Eight hours following the challenge mice were treated with vehicle (Plasmalyte), vancomycin (0.25 mg/kg), daptomycin (2.5mg/kg), a-SP_1505 antibody (100 µL), and control rabbit IgG. At 16 hours following antibody/antibiotic treatment (24hr post-challenge) mice were euthanized, and lungs and chest cavity blood were removed for quantification of bacteria. Whole lungs were washed twice in PBS, and lung tissue was subsequently homogenized in 1 mL PBS. Homogenized lung samples were centrifuged at 300xg, and bacteria-containing supernatant was plated onto Neomycin-containing blood agar plates for CFU titers.

Peptide production

Peptide P1 (Ser-Asn-Gly-Leu-Asp-Val-Gly-Lys-Ala-Asp) and peptide P2 (Ala-Lys-Thr-Ile-Lys-Ile-Thr-Gln-Thr-Arg) were synthesized on a preloaded Wang resin using the standard Fmoc/tBu chemistry for peptide synthesis. All coupling reactions were carried out in DMF using HBTU as the coupling reagent, 0.4 N-Methyl Morpholine in DMF as base. After each coupling, deprotection of the Fmoc group was done by using 20% piperidine in DMF. After completion of synthesis, peptides were cleaved from resin using TFA and purified using RP-HPLC. The integrity and purity of the peptides were confirmed using LC-MS.

Antibiotic accumulation

Antibiotic accumulation was determined as previously described⁸¹. *S. pneumoniae* were grown in THY to OD 0.6. Cells were pelleted, washed twice in PBS, and resuspended in 3.5mL PBS. 1 mL of cells were incubated with 50 μ M antibiotic for 10 minutes at 37°C. Following incubation, 800 μ L of drugged cells were spun (3min, 13,000xg) through 700 μ L of a 9:1 mix of AR20 and high temperature silicon oils (cooled to -80°C), after which the supernatant of silicone oil and free compound were carefully removed. For lysis, pelleted cells were resuspended in 200 μ L dH₂O and lysed via bead beating (3x 15s at 5m/s). Debris was pelleted (10' at 20,000xg) and 100 μ L of supernatant was removed and saved. Cell debris was resuspended in the remaining 50 μ L dH₂O and mixed with 200 μ L methanol. Potential cell debris was pellet again and 150 μ L of the methanol extract was mixed with the 200 μ L dH₂O supernatant from the previous step. The extract was pelleted one final time (10' at 20,000xg) before being filtered (0.22 μ m).

Samples were analyzed with a Waters Acquity M Class series UPLC system and Xevo G2 QTOF tandem MS/MS with Zspray. 100nl of extract was separated using a Phenomenex Kinetex 2.6 μ m XB-C18, 100Å (300 μ m \times 150mm) column with solvent A, 0.1% formic acid in water, and solvent B, 0.1% formic acid in acetonitrile. The inlet method utilized a flow rate of 8 μ lmin⁻¹ with the following gradient: 0–4min, 99.9% solvent A and 0.1% solvent B; 4–5min, 10% solvent A and 90% solvent B; 5–6min, 99.9% solvent A and 0.1% solvent B. Tandem mass spectra were acquired with the following conditions: Ciprofloxacin: CV:20, CE:25, m/z ion: 333.14. \rightarrow 245.11; Kanamycin: CV:40, CE:20, m/z ion: 485.25 \rightarrow 163.11. High-resolution spectra were calibrated by co-infusion of 2ngml⁻¹

leucine enkephalin lockspray (Waters). Data were quantified using Waters MassLynx software where the AUC was determined by integrating the corresponding daughter peak of the parent compound. Concentrations of the unknown compounds were determined by the linear fit of the corresponding standard curve. Concentrations are reported as the average of three biological replicates.

(p)ppGpp induction and LC/MS analysis

S. pneumoniae strains were grown at 37°C in 10 mL ThyB to an OD of ~0.5. Cultures were split into 5 mL aliquots for mupirocin-treated versus untreated controls. To induce the stringent response and ppGpp production, mupirocin was added in a final concentration of 25 µg/mL and incubated at 37°C for 30 minutes. Cells were centrifuged at 6000× g for 5', supernatant was discarded, and cell pellets were frozen at -80 °C. For LC/MS analysis cell pellets were resuspended in 2 ml cold methanol, and 150 pmol of [¹³C₁₀]-GTP (Sigma) was added and incubated at -80 °C for 30 minutes. Samples were centrifuged at 4000xg for 10', and the supernatant was removed and dried overnight in a Savant Speedvac Concentrator SPD 1010 (Thermo Fisher). Samples were analyzed using a Shimadzu Prominence UFLC attached to a QTrap 4500 equipped with a Turbo V ion source (Sciex). Samples (5 µL) were injected onto a SeQuant ZIC-cHILIC, 3 µm, 2.1 x 150 mm column at 30 °C (Millipore) using a flow rate of 0.3 ml/min. Solvent A was 25 mM ammonium acetate, and Solvent B was 75% acetonitrile + 25 mM ammonium acetate. The HPLC program was the following: starting solvent mixture of 0% A/100% B, 0 to 2 min isocratic with 100% B; 2 to 4 min linear gradient to 85% B; 4 to 17 min linear gradient to 65% B; 17 to 22 min isocratic with 65% B; 22 to 25 min linear gradient to 100% B; 25 to 30 min isocratic with 100% B. The QTrap 4500 was operated in the negative mode, and the ion source parameters were: ion spray voltage, -4500 V; curtain gas, 30 psi; temperature, 400 °C; collision gas, medium; ion source gas 1, 20 psi; ion source gas 2, 35 psi; declustering potential, -40 V; and collision energy, -40 V. The MRM transitions are: ppGpp, 602.0/159.0; pppGpp, 682.0/159.0, and [¹³C₁₀]-GTP, 522.0/159.0. [¹³C₁₀]-GTP was used as the internal standard. The system was controlled by the Analyst software (Sciex) and analyzed with MultiQuant™ 3.0.2 software (Sciex). Peaks corresponding to ppGpp and pppGpp were quantified relative to the internal standard. The limit of detection for ppGpp and pppGpp is 5 pmol, and for GTP, GDP, ATP and ADP 0.05pmol.

In vivo mouse competition experiment with and without antibiotics

Groups of at least 12 outbred 4-6-week-old Swiss Webster mice (Taconic Inc.,) were anesthetized by isoflurane inhalation and challenged intranasally (i.n.) with 50 μ l, $\sim 1.5 \times 10^7$ CFU, bacterial suspension in 1X PBS. Each bacterial suspension contained a 1:1 mixture of *S. pneumoniae* TIGR4 wildtype and Δ SP_0829 or Δ SP_1396. The challenge dose was always confirmed by serial dilution and plating on blood agar plates. Infected mice receiving antibiotic treatment were administered either 1 mg/kg cefepime (WTvs Δ SP_0829) or 10 mg/kg meropenem (WTvs Δ SP_1396) 16 hours post-bacterial challenge by intraperitoneal (i.p.) injection. Antibiotic dosing was previously determined to reduce bacterial loads 10-100-fold in vivo. Mice were euthanized by CO₂ asphyxiation at 6 hours post-antibiotic administration (or 22 hours post-bacterial challenge). Blood by cardiac puncture, nasopharynx lavage, and total homogenized lungs were collected from each animal to determine bacterial burden by serial dilution and plating blood agar plates as previously described¹⁸. Mouse experiments were approved under the Boston College IACUC approved protocol 2019-007-01.

Clinical-strain stop-codon analysis

Four gene-sets were compiled to test for the differential occurrence of stop-codons in patient samples. Each gene-set consists of 34 genes and are defined as: **Set 1** consists of genes that when disrupted lead to a significant decrease in antibiotic sensitivity in the presence of at least one antibiotic (*in vitro* ABx fitness positive), and have no fitness defect in lung and nasopharynx (*in vivo* neutral or positive); **Set 2** consists of genes that when disrupted lead to a significant decrease in antibiotic sensitivity in the presence of at least one antibiotic (*in vitro* ABx fitness positive), and have a significant fitness defect in lung and nasopharynx (*in vivo* fitness negative); **Set 3** consists of genes that when disrupted have no fitness benefit in any of the antibiotics (*in vitro* ABx fitness neutral), but with a significant fitness benefit in lung and nasopharynx (*in vivo* fitness positive); **Set 4** consists of genes that have decreased fitness in the presence of antibiotics (*in vitro* ABx fitness negative), and that have a significant fitness defect of >15% in lung and nasopharynx (*in vivo* fitness negative). The PATRIC database was screened for antibiotic resistant *S. pneumoniae* isolates. There is a potential risk that isolates in the database are clonally related, which could mean that multiple isolates would contain exactly the same sequence and for instance the same stop codon, which could bias the analysis. To

reduce this potential bias candidate isolates were limited to those belonging to a different MLST type. While this considerably reduced the number of potential isolates, we were able to collect 533 β -lactam resistant and 1147 co-trimoxazole resistant strains. Moreover, an equal number of non-resistant strains were compiled. From each genome, gene sequences were extracted that match those from each of the 4 gene-sets. Each gene was scanned for premature stop codons occurring in the first 90% of a gene. For each gene-set the number of strains with at least one stop codon in the gene-set were recorded, as well as the total number of stop-codons in all genes in a set. To test for differences in the number of isolates containing a stop codon within (susceptible vs. resistant) and between sets a Fisher's exact test was performed.

Manuscript supplemental information

All supplemental figures, tables, and raw data can be accessed through the published manuscript: [10.1038/s41467-022-30967-4](https://doi.org/10.1038/s41467-022-30967-4).

4.6 References

1. Honsa, E. S. *et al.* RelA Mutant *Enterococcus faecium* with Multiantibiotic Tolerance Arising in an Immunocompromised Host. *mBio* **8**, doi:10.1128/mBio.02124-16 (2017).
2. Band, V. I. *et al.* Antibiotic failure mediated by a resistant subpopulation in *Enterobacter cloacae*. *Nat Microbiol* **1**, 16053, doi:10.1038/nmicrobiol.2016.53 (2016).
3. Band, V. I. *et al.* Antibiotic combinations that exploit heteroresistance to multiple drugs effectively control infection. *Nat Microbiol* **4**, 1627-1635, doi:10.1038/s41564-019-0480-z (2019).
4. Nicoloff, H., Hjort, K., Levin, B. R. & Andersson, D. I. The high prevalence of antibiotic heteroresistance in pathogenic bacteria is mainly caused by gene amplification. *Nat Microbiol* **4**, 504-514, doi:10.1038/s41564-018-0342-0 (2019).
5. Michiels, J. E., Van den Bergh, B., Verstraeten, N. & Michiels, J. Molecular mechanisms and clinical implications of bacterial persistence. *Drug resistance updates : reviews and commentaries in antimicrobial and anticancer chemotherapy* **29**, 76-89, doi:10.1016/j.drug.2016.10.002 (2016).
6. Geisinger, E. *et al.* Antibiotic susceptibility signatures identify potential antimicrobial targets in the *Acinetobacter baumannii* cell envelope. *Nat Commun* **11**, 4522, doi:10.1038/s41467-020-18301-2 (2020).
7. Huo, W. *et al.* Immunosuppression broadens evolutionary pathways to treatment failure during *Acinetobacter baumannii* pneumonia. *bioRxiv* doi.org/10.1101/2021.04.07.438861 (2021).
8. Ma, C., Yang, X. & Lewis, P. J. Bacterial Transcription as a Target for Antibacterial Drug Development. *Microbiol Mol Biol Rev* **80**, 139-160, doi:10.1128/MMBR.00055-15 (2016).
9. Wood, S. *et al.* in *The Pangenome: Diversity, Dynamics and Evolution of Genomes* (eds H. Tettelin & D. Medini) 169-202 (2020).
10. Gillings, M. R., Paulsen, I. T. & Tetu, S. G. Genomics and the evolution of antibiotic resistance. *Ann N Y Acad Sci* **1388**, 92-107, doi:10.1111/nyas.13268 (2017).
11. McKeegan, K. S., Borges-Walmsley, M. I. & Walmsley, A. R. Microbial and viral drug resistance mechanisms. *Trends in microbiology* **10**, S8-14 (2002).
12. Walsh, C. Molecular mechanisms that confer antibacterial drug resistance. *Nature* **406**, 775-781 (2000).
13. Wright, G. D. Mechanisms of resistance to antibiotics. *Current opinion in chemical biology* **7**, 563-569 (2003).

14. van Opijnen, T., Dedrick, S. & Bento, J. Strain Dependent Genetic Networks for Antibiotic-Sensitivity in a Bacterial Pathogen with a Large Pan-Genome. *PLoS pathogens* **12**, e1005869, doi:10.1371/journal.ppat.1005869 (2016).
15. Jensen, P. A., Zhu, Z. & van Opijnen, T. Antibiotics Disrupt Coordination between Transcriptional and Phenotypic Stress Responses in Pathogenic Bacteria. *Cell Rep* **20**, 1705-1716, doi:10.1016/j.celrep.2017.07.062 (2017).
16. Geisinger, E. *et al.* The landscape of intrinsic and evolved fluoroquinolone resistance in *Acinetobacter baumannii* includes suppression of drug-induced prophage replication. *bioRxiv* (2018).
17. Zhu, Z. *et al.* Entropy of a bacterial stress response is a generalizable predictor for fitness and antibiotic sensitivity. *Nat Commun* **11**, 4365, doi:10.1038/s41467-020-18134-z (2020).
18. van Opijnen, T. & Camilli, A. A fine scale phenotype-genotype virulence map of a bacterial pathogen. *Genome Res* **22**, 2541-2551, doi:10.1101/gr.137430.112 (2012).
19. Gutierrez, A. *et al.* Understanding and Sensitizing Density-Dependent Persistence to Quinolone Antibiotics. *Molecular cell* **68**, 1147-1154 e1143, doi:10.1016/j.molcel.2017.11.012 (2017).
20. Vega, N. M., Allison, K. R., Khalil, A. S. & Collins, J. J. Signaling-mediated bacterial persister formation. *Nat Chem Biol* **8**, 431-433, doi:10.1038/nchembio.915 (2012).
21. Dorr, T., Vulic, M. & Lewis, K. Ciprofloxacin causes persister formation by inducing the TisB toxin in *Escherichia coli*. *PLoS biology* **8**, e1000317, doi:10.1371/journal.pbio.1000317 (2010).
22. Helaine, S. *et al.* Internalization of *Salmonella* by macrophages induces formation of nonreplicating persisters. *Science* **343**, 204-208, doi:10.1126/science.1244705 (2014).
23. Balaban, N. Q., Merrin, J., Chait, R., Kowalik, L. & Leibler, S. Bacterial persistence as a phenotypic switch. *Science* **305**, 1622-1625, doi:10.1126/science.1099390 (2004).
24. Lewis, K. Persister cells, dormancy and infectious disease. *Nature reviews. Microbiology* **5**, 48-56, doi:10.1038/nrmicro1557 (2007).
25. Brauner, A., Fridman, O., Gefen, O. & Balaban, N. Q. Distinguishing between resistance, tolerance and persistence to antibiotic treatment. *Nature reviews. Microbiology* **14**, 320-330, doi:10.1038/nrmicro.2016.34 (2016).
26. Nandakumar, M., Nathan, C. & Rhee, K. Y. Isocitrate lyase mediates broad antibiotic tolerance in *Mycobacterium tuberculosis*. *Nat Commun* **5**, 4306, doi:10.1038/ncomms5306 (2014).

27. Trastoy, R. *et al.* Mechanisms of Bacterial Tolerance and Persistence in the Gastrointestinal and Respiratory Environments. *Clinical microbiology reviews* **31**, doi:10.1128/CMR.00023-18 (2018).
28. Moyed, H. S. & Bertrand, K. P. hipA, a newly recognized gene of Escherichia coli K-12 that affects frequency of persistence after inhibition of murein synthesis. *Journal of bacteriology* **155**, 768-775, doi:10.1128/jb.155.2.768-775.1983 (1983).
29. Schumacher, M. A. *et al.* HipBA-promoter structures reveal the basis of heritable multidrug tolerance. *Nature* **524**, 59-64, doi:10.1038/nature14662 (2015).
30. Pontes, M. H. & Groisman, E. A. A Physiological Basis for Nonheritable Antibiotic Resistance. *mBio* **11**, doi:10.1128/mBio.00817-20 (2020).
31. Saroj, S. D., Clemmer, K. M., Bonomo, R. A. & Rather, P. N. Novel mechanism for fluoroquinolone resistance in Acinetobacter baumannii. *Antimicrobial agents and chemotherapy* **56**, 4955-4957, doi:10.1128/AAC.00739-12 (2012).
32. Guerillot, R. *et al.* Convergent Evolution Driven by Rifampin Exacerbates the Global Burden of Drug-Resistant Staphylococcus aureus. *mSphere* **3**, doi:10.1128/mSphere.00550-17 (2018).
33. Levin-Reisman, I. *et al.* Antibiotic tolerance facilitates the evolution of resistance. *Science* **355**, 826-830, doi:10.1126/science.aaj2191 (2017).
34. Balaban, N. Q. & Liu, J. in *Persister Cells and Infectious Disease* (ed K. Lewis) Ch. 1, 1-18 (Springer, 2019).
35. Lewis, K. (Springer, Cham, 2019).
36. Liu, J., Gefen, O., Ronin, I., Bar-Meir, M. & Balaban, N. Q. Effect of tolerance on the evolution of antibiotic resistance under drug combinations. *Science* **367**, 200-204, doi:10.1126/science.aay3041 (2020).
37. Van den Bergh, B., Fauvart, M. & Michiels, J. Formation, physiology, ecology, evolution and clinical importance of bacterial persisters. *FEMS microbiology reviews* **41**, 219-251, doi:10.1093/femsre/fux001 (2017).
38. Fisher, R. A., Gollan, B. & Helaine, S. Persistent bacterial infections and persister cells. *Nature reviews. Microbiology* **15**, 453-464, doi:10.1038/nrmicro.2017.42 (2017).
39. van Opijnen, T., Bodi, K. L. & Camilli, A. Tn-seq: high-throughput parallel sequencing for fitness and genetic interaction studies in microorganisms. *Nat Methods* **6**, 767-772, doi:10.1038/nmeth.1377 (2009).
40. Mann, B. *et al.* Control of virulence by small RNAs in Streptococcus pneumoniae. *PLoS pathogens* **8**, e1002788, doi:10.1371/journal.ppat.1002788 (2012).

41. Carter, R. *et al.* Genomic Analyses of Pneumococci from Children with Sickle Cell Disease Expose Host-Specific Bacterial Adaptations and Deficits in Current Interventions. *Cell Host and Microbe* **15**, 587-599, doi:papers://58864D70-D09B-4A16-B641-1A3EEB7FE0BA/Paper/p22252 (2014).
42. Thibault, D. *et al.* Droplet Tn-Seq combines microfluidics with Tn-Seq for identifying complex single-cell phenotypes. *Nat Commun* **10**, 5729, doi:10.1038/s41467-019-13719-9 (2019).
43. McCoy, K. M., Antonio, M. L. & van Opijnen, T. MAGenTA: a Galaxy implemented tool for complete Tn-Seq analysis and data visualization. *Bioinformatics* **33**, 2781-2783, doi:10.1093/bioinformatics/btx320 (2017).
44. van Opijnen, T. & Levin, H. L. Transposon Insertion Sequencing, a Global Measure of Gene Function. *Annu Rev Genet*, doi:10.1146/annurev-genet-112618-043838 (2020).
45. Costanzo, M. *et al.* A global genetic interaction network maps a wiring diagram of cellular function. *Science* **353**, doi:10.1126/science.aaf1420 (2016).
46. Baryshnikova, A. Systematic Functional Annotation and Visualization of Biological Networks. *Cell Syst* **2**, 412-421, doi:10.1016/j.cels.2016.04.014 (2016).
47. Rose, L. *et al.* Antibodies against PsrP, a novel *Streptococcus pneumoniae* adhesin, block adhesion and protect mice against pneumococcal challenge. *The Journal of infectious diseases* **198**, 375-383, doi:10.1086/589775 (2008).
48. Derre, I., Rapoport, G. & Msadek, T. CtsR, a novel regulator of stress and heat shock response, controls *clp* and molecular chaperone gene expression in gram-positive bacteria. *Molecular microbiology* **31**, 117-131, doi:10.1046/j.1365-2958.1999.01152.x (1999).
49. Ibrahim, Y. M., Kerr, A. R., Silva, N. A. & Mitchell, T. J. Contribution of the ATP-dependent protease ClpCP to the autolysis and virulence of *Streptococcus pneumoniae*. *Infection and immunity* **73**, 730-740, doi:10.1128/IAI.73.2.730-740.2005 (2005).
50. Stamsås, R. M. *et al.* A CozE homologue contributes to cell size homeostasis of *Streptococcus pneumoniae*. *mBio in press* (2020).
51. Hoover, S. E. *et al.* A new quorum-sensing system (TprA/PhrA) for *Streptococcus pneumoniae* D39 that regulates a lantibiotic biosynthesis gene cluster. *Molecular microbiology* **97**, 229-243, doi:10.1111/mmi.13029 (2015).
52. Nasher, F., Heller, M. & Hathaway, L. J. *Streptococcus pneumoniae* Proteins AmiA, AliA, and AliB Bind Peptides Found in Ribosomal Proteins of Other Bacterial Species. *Frontiers in microbiology* **8**, 2688, doi:10.3389/fmicb.2017.02688 (2017).
53. Nasher, F. *et al.* Peptide Ligands of AmiA, AliA, and AliB Proteins Determine Pneumococcal Phenotype. *Frontiers in microbiology* **9**, 3013, doi:10.3389/fmicb.2018.03013 (2018).

54. Pu, Y. *et al.* Enhanced Efflux Activity Facilitates Drug Tolerance in Dormant Bacterial Cells. *Molecular cell* **62**, 284-294, doi:10.1016/j.molcel.2016.03.035 (2016).
55. El Meouche, I. & Dunlop, M. J. Heterogeneity in efflux pump expression predisposes antibiotic-resistant cells to mutation. *Science* **362**, 686-690, doi:10.1126/science.aar7981 (2018).
56. Irving, S. E., Choudhury, N. R. & Corrigan, R. M. The stringent response and physiological roles of (pp)pGpp in bacteria. *Nature reviews. Microbiology* **19**, 256-271, doi:10.1038/s41579-020-00470-y (2021).
57. Kazmierczak, K. M., Wayne, K. J., Rechtsteiner, A. & Winkler, M. E. Roles of rel(Spn) in stringent response, global regulation and virulence of serotype 2 *Streptococcus pneumoniae* D39. *Molecular microbiology* **72**, 590-611, doi:10.1111/j.1365-2958.2009.06669.x (2009).
58. Conlon, B. P. *et al.* Persister formation in *Staphylococcus aureus* is associated with ATP depletion. *Nat Microbiol* **1**, 16051, doi:10.1038/nmicrobiol.2016.51 (2016).
59. Gao, W. *et al.* Two novel point mutations in clinical *Staphylococcus aureus* reduce linezolid susceptibility and switch on the stringent response to promote persistent infection. *PLoS pathogens* **6**, e1000944, doi:10.1371/journal.ppat.1000944 (2010).
60. van Opijnen, T. & Camilli, A. Transposon insertion sequencing: a new tool for systems-level analysis of microorganisms. *Nature reviews. Microbiology* **11**, 435-442, doi:10.1038/nrmicro3033 (2013).
61. Rowe, H. M. *et al.* Bacterial Factors Required for Transmission of *Streptococcus pneumoniae* in Mammalian Hosts. *Cell Host Microbe* **25**, 884-891 e886, doi:10.1016/j.chom.2019.04.012 (2019).
62. Cain, A. K. *et al.* A decade of advances in transposon-insertion sequencing. *Nat Rev Genet* **21**, 526-540, doi:10.1038/s41576-020-0244-x (2020).
63. Gillespie, J. J. *et al.* PATRIC: the comprehensive bacterial bioinformatics resource with a focus on human pathogenic species. *Infection and immunity* **79**, 4286-4298 (2011).
64. Wattam, A. R. *et al.* Improvements to PATRIC, the all-bacterial Bioinformatics Database and Analysis Resource Center. *Nucleic Acids Res* **45**, D535-D542, doi:10.1093/nar/gkw1017 (2017).
65. Yang, J. H., Bening, S. C. & Collins, J. J. Antibiotic efficacy-context matters. *Curr Opin Microbiol* **39**, 73-80, doi:10.1016/j.mib.2017.09.002 (2017).
66. Kohanski, M. A., Dwyer, D. J., Hayete, B., Lawrence, C. A. & Collins, J. J. A common mechanism of cellular death induced by bactericidal antibiotics. *Cell* **130**, 797-810, doi:10.1016/j.cell.2007.06.049 (2007).

67. Dwyer, D. J., Collins, J. J. & Walker, G. C. Unraveling the physiological complexities of antibiotic lethality. *Annu Rev Pharmacol Toxicol* **55**, 313-332, doi:10.1146/annurev-pharmtox-010814-124712 (2015).
68. Belenky, P. *et al.* Bactericidal Antibiotics Induce Toxic Metabolic Perturbations that Lead to Cellular Damage. *Cell Rep* **13**, 968-980, doi:10.1016/j.celrep.2015.09.059 (2015).
69. Yang, J. H. *et al.* A White-Box Machine Learning Approach for Revealing Antibiotic Mechanisms of Action. *Cell* **177**, 1649-1661 e1649, doi:10.1016/j.cell.2019.04.016 (2019).
70. Lewis, K. & Shan, Y. Why tolerance invites resistance. *Science* **355**, 796, doi:10.1126/science.aam7926 (2017).
71. Shan, Y. *et al.* ATP-Dependent Persister Formation in Escherichia coli. *mBio* **8**, doi:10.1128/mBio.02267-16 (2017).
72. Erickson, K. E., Winkler, J. D., Nguyen, D. T., Gill, R. T. & Chatterjee, A. The Tolerome: A Database of Transcriptome-Level Contributions to Diverse Escherichia coli Resistance and Tolerance Phenotypes. *ACS Synth Biol* **6**, 2302-2315, doi:10.1021/acssynbio.7b00235 (2017).
73. Bhattacharyya, R. P. *et al.* Simultaneous detection of genotype and phenotype enables rapid and accurate antibiotic susceptibility determination. *Nature medicine* **25**, 1858-1864, doi:10.1038/s41591-019-0650-9 (2019).
74. Aaberge, I. S., Eng, J., Lermak, G. & Løvik, M. Virulence of Streptococcus pneumoniae in mice: a standardized method for preparation and frozen storage of the experimental bacterial inoculum. *Microbial pathogenesis* **18**, 141-152 (1995).
75. Tettelin, H. Complete Genome Sequence of a Virulent Isolate of Streptococcus pneumoniae. *Science* **293**, 498-506, doi:10.1126/science.1061217 (2001).
76. van Opijnen, T. & Camilli, A. Genome-wide fitness and genetic interactions determined by Tn-seq, a high-throughput massively parallel sequencing method for microorganisms. *Curr Protoc Microbiol* **Chapter 1**, Unit1E.3, doi:10.1002/9780471729259.mc01e03s19 (2010).
77. van Opijnen, T., Lazinski, D. W. & Camilli, A. Genome-Wide Fitness and Genetic Interactions Determined by Tn-seq, a High-Throughput Massively Parallel Sequencing Method for Microorganisms. *Curr Protoc Microbiol* **36**, 1E 3 1-24, doi:10.1002/9780471729259.mc01e03s36 (2015).
78. Shannon, P. Cytoscape: A Software Environment for Integrated Models of Biomolecular Interaction Networks. *Genome Research* **13**, 2498-2504, doi:10.1101/gr.1239303 (2003).

79. Kanehisa, M., Goto, S., Furumichi, M., Tanabe, M. & Hirakawa, M. KEGG for representation and analysis of molecular networks involving diseases and drugs. *Nucleic acids research* **38**, D355-360 (2010).
80. Price, K. E. & Camilli, A. Pneumolysin localizes to the cell wall of *Streptococcus pneumoniae*. *Journal of bacteriology* **191**, 2163-2168, doi:10.1128/JB.01489-08 (2009).
81. Richter, M. F. *et al.* Predictive compound accumulation rules yield a broad-spectrum antibiotic. *Nature* **545**, 299-304, doi:10.1038/nature22308 (2017).

5

Discussion:

The future of antibacterial
host-informed therapies

5.1 Contributions of this work to HIT development

The current treatment against most bacterial infections is a cocktail of broad-spectrum antibiotics, empirically administered to hospitalized patients, in a mostly *one size fits all* approach. This often leads to treatment failure with infection recurrence, while driving increasing rates of antibiotic resistance (2.8 million infections per year in the U.S. ¹). Antibiotic resistance and treatment failure are thereby driving a largely ignored crisis of growing proportions with millions of casualties and untreatable infections every year. Moreover, these approaches are not customized to patients with or without preexisting conditions.

Complementing bacterial infection management with host-informed therapies, or HITs, presents a customizable strategy for patients with and without preexisting conditions ². HITs hold promise in curtailing inflammatory damage, redirecting disrupted immune mechanisms, and in targeting specific immunodeficiencies in infection-susceptible patient populations. Patients without predisposing conditions to pneumococcal pneumonia can benefit from HIT strategies such as repurposed anti-inflammatory drugs and/or those targeted towards *S. pneumoniae* virulence factors that ordinarily thwart the host's innate immune response. Patients with predisposing conditions to pneumococcal pneumonia, such as an influenza coinfection, sickle cell disease, and old age, benefit from personalized approaches that address the specific immunological mechanism at play. For example, it is vital to address both the elevated Type I interferon (IFN-I) antiviral response and virus-induced tissue damage when treating an influenza-*S. pneumoniae* coinfection. Importantly, because many HITs target common infection immunoregulatory pathways, they can be generalizable to different bacterial pathogens.

In this thesis, we demonstrate the usefulness of multi-omics methods to elucidate the intricacies of bacterial pathogenesis and aid in the target identification, validation, and rational design of novel antibacterial host-informed therapies, or HITs. In **Chapter 1**, we introduce the concept of HITs to treat pneumococcal pneumonia in both the general patient population and in patients with predisposing susceptibilities to bacterial infection. In **Chapter 2**, we generate a genome-wide map (using Hii-TnSeq) of bacterial immune (complement) evasion targets and use findings to design preliminary novel HIT strategies.

In **Chapter 3**, we establish the dual RNA-Seq method to generate a dual host/pathogen transcriptomic map to identify signatures of infection outcome to inform the development of future prognostic markers. And finally, in **Chapter 4**, we validate signatures of bacterial antibiotic resistance and tolerance in a murine lung infection model. This thesis provides the field with in vivo findings pertaining to: *S. pneumoniae* immune evasion, host/*S. pneumoniae* determinants of disease outcome, and genetic signatures *S. pneumoniae* antibiotic tolerance. Furthermore, the novel -omics methods outlined in this thesis are generalizable to all culturable bacterial pathogens (Chapter 2: Hii-TnSeq; Chapter 3: dual RNA-Seq; Chapter 4: antibiotic-Tn-Seq and validation), paving the road for translationally-focused microbial systems research to inform the development of alternative antimicrobial treatment strategies.

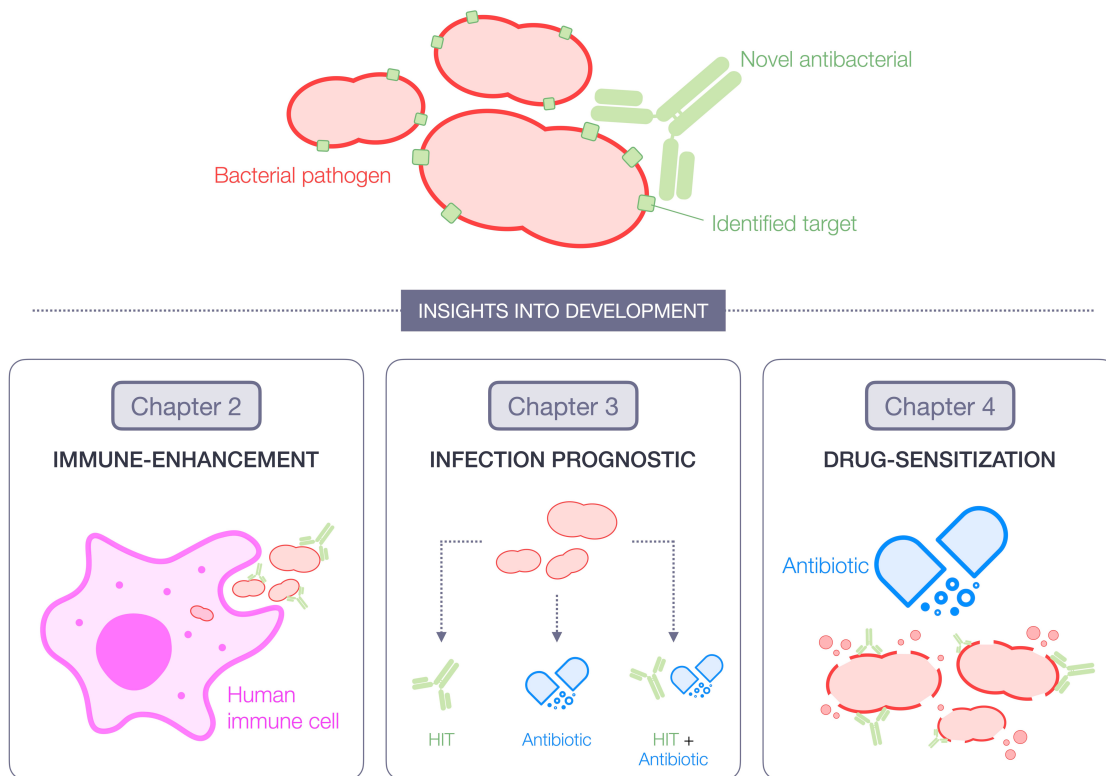


Figure 5.1 | Example HIT strategies proposed in this thesis.

Based on the research presented in this thesis, antibacterial therapeutic targets can be identified using methods such as Hii-TnSeq (**Chapter 2**) or antibiotic-Tn-Seq (**Chapter 4**), leading to therapeutic strategies that either enhance immunity that was otherwise evaded by bacteria or (re)sensitize bacteria to antibiotics. Methods such as dual RNA-Seq (**Chapter 3**) can be deployed as an infection prognostic, to design personalized therapeutic strategies, for example a HIT alone, an antibiotic alone, or a HIT + antibiotic combinatorial approach.

5.2 Clinical considerations and limitations

Although promising, there are important challenges to the implementation and development of novel HITs. Due to challenges in the antibiotic market, novel HITs will require the combined effort of clinical researchers, drug developers, and government-based economic incentivization for appropriate testing, clinical implementation, and drug approval.

5.2.1 Perspectives on Chapter 2

The global therapeutic monoclonal antibody market was valued at approximately US \$115.2 billion in 2018 and is expected to generate revenue of \$300 billion by 2025³. Thus, the market for therapeutic antibody drugs has experienced explosive growth as new drugs have been approved for treating various human diseases, including many cancers, autoimmune, and metabolic diseases. However, therapeutic monoclonal antibodies are much more expensive to produce compared to small-molecule antibiotics, resulting in a significantly higher cost of treatment to the patient. Thus, nanobodies, or the smallest functional single-domain antibodies, offer advantages of high stability, high hydrophilicity, but most importantly cost-effective expression and modification⁴, and have high potential as targeted HITs for infectious diseases.

In contrast to direct-acting small-molecule antibiotics with often predictable pharmacokinetic/pharmacodynamic relationships, HITs are more complex, and their effects are intrinsically more difficult to predict as they depend on the drug's interaction with the host and subsequent downstream events within the complex host immune system. In the clinic setting, the practical use and success of HITs will partially depend on delivery. While oral, intravenous, or intramuscular routes can enable therapeutic serum concentrations, these modalities may not ensure a sustained drug concentration in the target tissue. Particle-based drug packaging systems may therefore be required for a more immune cell-targeted delivery platform. Importantly, it is difficult to comprehensively evaluate these effects and risks in preclinical animal models as the genomic responses in such models often poorly mimic human inflammation⁵. Therefore,

widespread implementation of HITs will rely on multicenter, randomized clinical trials with defined patient cohorts to test safety and efficacy.

5.2.2 Perspectives on Chapter 3

Due to the complexity of the host response and the dramatic changes that can occur within hours of widespread infection, rapid diagnostic tools to assess immune and organ function are needed to help determine the appropriate HIT intervention. Additionally, HITs that stimulate/boost compromised immunity are associated with excessive inflammation risks that can lead to cytokine storm or systemic inflammatory syndrome ⁶. The clinical observation of host immune dysfunction remains a poorly understood although well-recognized cause of increased disease burden and tissue destruction. The ability to recognize, risk-stratify, and immune-modulate host immunity using HITs represents a high yield, unmet clinical need. With the advancements in immunophenotyping, biomarkers can be used to indicate the exact stage of infection (ex. by transcriptomic analysis such as dual RNA-Seq) and allow the monitoring of treatment success or failure. These personalized approaches could give insight into hypo- or hyper-inflammatory state of infection, and the application of the appropriate immunotherapy. Identifying host susceptibilities to bacterial infection that require personalized approaches will instruct the application of the appropriate adjunct HITs as we previously suggested for *S. pneumoniae* infection, that minimize any off-target effects.

5.2.3 Perspectives on Chapter 4

Adjunctive therapies for inflammation, in combination with pathogen-targeted approaches (i.e., antibiotics) are applicable to bacterial infections. Furthermore, in the case of serious bacterial infections, clinical studies of HITs combined with, for instance, an antibiotic, would be required to show a clear advantage over the standard-of-care (antibiotic alone). Despite these challenges, successful HIT development and implementation could lead to promising adjunctive therapies to treat severe bacterial infections.

5.3 Outstanding challenges

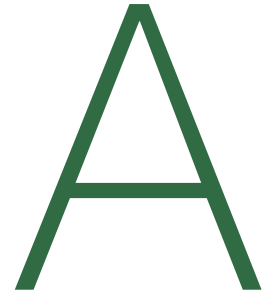
Numerous outstanding challenges remain in the field of novel antibacterial HIT development and implementation:

- 1) Establishing generalizability of efficacious treatments across all bacterial pathogens.
- 2) Establishing antibacterial treatment personalization, depending on the patient's immune state.
- 3) Preventing side effects (inflammation) when utilizing immunostimulatory HITs.
- 4) Employing rapid and relatively inexpensive diagnostics and prognostics to deliver the appropriate HITs.

It is clear there is a clinical need to revolutionize how bacterial infections are currently treated and as this field evolves, answers will be established to these key challenges. The work presented in this thesis extensively contributes to this field, by offering systems-level methods and novel findings to inform the target identification, validation, and design of antibacterial host-informed therapies.

5.5 References

1. CDC. Antibiotic Resistance Threats in the United States, 2019. Atlanta, GA: U.S. Department of Health and Human Services, CDC; 2019
2. Sundaresh B, Xu S, Noonan B, Mansour MK, Leong JM, van Opijnen T. Host-informed therapies for the treatment of pneumococcal pneumonia. *Trends Mol Med*. Oct 2021;27(10):971-989. doi:10.1016/j.molmed.2021.07.008
3. Lu, RM., Hwang, YC., Liu, IJ. *et al.* Development of therapeutic antibodies for the treatment of diseases. *J Biomed Sci* **27**, 1 (2020). <https://doi.org/10.1186/s12929-019-0592-z>.
4. Mei Y, Chen Y, Sivaccumar JP, An Z, Xia N, Luo W. Research progress and applications of nanobody in human infectious diseases. *Front Pharmacol*. 2022 Aug 12;13:963978.
5. Seok, J. *et al.* (2013) Genomic responses in mouse models poorly mimic human inflammatory diseases. *Proc Natl Acad Sci U S A* 110 (9), 3507-12.
6. Pinsky, M.R. *et al.* (1993) Serum cytokine levels in human septic shock. Relation to multiple-system organ failure and mortality. *Chest* 103 (2), 565-75.



Appendix A:
Publications, science communication,
and awards

1. Publications

A.1.1 Publications in van Opijnen lab

Sundaresh B*, Rosconi F, Shainheit M, Rosch JW, van Opijnen T. Bacterial genomic profiling reveals novel routes to complement evasion and targeted therapeutic strategies. *In preparation for September 2023 submission.*

(*: first author contribution)

Lyu Y, Yang F, **Sundaresh B**, Rosconi F, van Opijnen T, Gao, J. Covalent inhibition of a host-pathogen protein-protein interaction curbs the virulence of *Streptococcus pneumoniae*. *In preparation.*

Jewel D, Kelemen RE, Huang RL, Zhu Z, **Sundaresh B**, Malley K, van Opijnen T, Chatterjee A. Optimized virus-assisted directed evolution in mammalian cells yields a hyperefficient pyrrolysyl tRNA for noncanonical amino acid mutagenesis. *Under review.*

Jewel D, Kelemen RE, Huang RL, Zhu Z, **Sundaresh B**, Cao X, Malley K, Huang Z, Pasha M, Anthony J, van Opijnen T, Chatterjee A. Virus-assisted directed evolution of enhanced suppressor tRNAs in mammalian cells. *Nat Methods.* 2023 Jan;20(1):95-103. doi: 10.1038/s41592-022-01706-w.

Leshchiner D*, Rosconi F*, **Sundaresh B***, Rudmann E*, Ramirez LMN*, Nishimoto AT, Wood SJ, Jana B, Buján N, Li K, Gao J, Frank M, Reeve SM, Lee RE, Rock CO, Rosch JW, van Opijnen T. A genome-wide atlas of antibiotic susceptibility targets and pathways to tolerance. *Nat Commun.* 2022 Jun 7;13(1):3165. doi: 10.1038/s41467-022-30967-4.

(*: equal first author contribution)

Sundaresh B*, Xu S*, Noonan B, Mansour MK, Leong JM, van Opijnen T. Host-informed therapies for the treatment of pneumococcal pneumonia. *Trends Mol Med.* 2021 Oct;27(10):971-989. doi: 10.1016/j.molmed.2021.07.008.

(*: equal first author contribution)

A.1.2 Publications during lab rotations

Girdhar K, Soto M, Huang Q, Orliaguet L, Cederquist C, **Sundaresh B**, Hu J, Figura M, Raisingani A, Canfora EE, Dirice E, Fujisaka S, Goossens GH, Blaak EE, Kulkarni RN, Kahn CR, Altindis E. Gut Microbiota Regulate Pancreatic Growth, Exocrine Function, and Gut Hormones. *Diabetes.* 2022 May 1;71(5):945-960. doi: 10.2337/db21-0382.

Dedrick S, **Sundaresh B**, Huang Q, Brady C, Yoo T, Cronin C, Rudnicki C, Flood M, Momeni B, Ludvigsson J, Altindis E. The Role of Gut Microbiota and Environmental Factors in Type 1 Diabetes Pathogenesis. *Front Endocrinol (Lausanne).* 2020 Feb 26;11:78. doi: 10.3389/fendo.2020.00078.

2. Science communication

A.2.1 Oral presentations

June 2023	Pitch, “Immunobac Therapeutics.” Women in Bio: BIO 2023 Pitch, Boston, MA.
May 2023	Pitch, “Immunobac Therapeutics.” MassChallenge Round 2, Boston, MA.
April 2023	Talk, “Bacterial genomic profiling reveals novel routes to immune evasion and targeted therapeutic strategies.” Invited Speaker at Boston College Schiller Institute Graduate Student Colloquium Series, Chestnut Hill, MA.
March 2023	Pitch, “Immunobac Therapeutics.” TiE Boston, Cambridge, MA.
December 2022	Talk, “Genomic profiling reveals novel routes to immune evasion in <i>Streptococcus pneumoniae</i> .” Boston College Data Club, Chestnut Hill, MA.
October 2022	Pitch, “Immunobac Therapeutics.” The Engine Blueprint Program, Cambridge, MA.
October 2022	Pitch, “Immunobac Therapeutics.” MIT I-Corps, Cambridge, MA.
August 2022	Talk, “Genomic profiling reveals novel routes to complement evasion in <i>Streptococcus pneumoniae</i> .” Gordon Research Conference: Streptococcal Biology, Newry, ME.
May 2022	Pitch, “Immunobac Therapeutics.” Nucleate Activator, Cambridge, MA.
December 2021	Talk, “Genomic profiling reveals novel routes to complement evasion in <i>Streptococcus pneumoniae</i> .” Boston College Data Club, Chestnut Hill, MA.
June 2021	Talk, “Genome-wide identification of <i>Streptococcus pneumoniae</i> proteins implicated in C3 complement evasion: Identifying targets for novel host-informed therapies.” Boston Bacterial Meeting, Virtual.

- March 2021 Talk, “Genome-wide characterization of *Streptococcus pneumoniae* proteins interacting with C3 complement.”
Boston College Data Club, Chestnut Hill, MA.
- March 2021 Talk, “Designing host-informed therapies for the treatment of bacterial pneumonia.”
Invited Speaker at Jianmin Gao Lab Group Meeting, Virtual.
- January 2021 Talk, “Identifying signatures of disease outcome by monitoring the host and bacterial transcriptome.”
Boston College Graduate Admissions Open House, Virtual.
- November 2020 Talk, “Genetic approaches for the development of host-directed therapeutics.”
Boston College Graduate Genetics Course, Chestnut Hill, MA.
- September 2020 Talk, “Rapid detection and outcome predictions of infectious disease.”
NIH NIAID Systems Biology Annual Meeting, Virtual.
- July 2020 Flash Talk, “Dissecting the *Streptococcus pneumoniae*-complement interface through a systems-biology approach.”
Boston Bacterial Meeting, Virtual.

A.2.2 Poster presentations

- June 2023 “Bacterial genomic profiling reveals novel routes to complement evasion and targeted therapeutic strategies.”
Boston Bacterial Meeting, Cambridge, MA.
- August 2022 “Genomic profiling reveals novel routes to complement evasion in *Streptococcus pneumoniae*.”
Gordon Research Conference: Streptococcal Biology, Newry, ME.
- June 2022 “Genomic profiling reveals novel routes to complement evasion in *Streptococcus pneumoniae*.”
Boston Bacterial Meeting, Cambridge, MA.
- April 2021 “Genome-wide characterization of *Streptococcus pneumoniae* proteins interacting with C3 complement.” Cold Spring Harbor Systems Immunology Meeting, Virtual.

3. Awards

April 2023	MassChallenge Round 2 Finalist and Accepted to Early-Stage Accelerator Program (top 100 teams, >1000 submissions).
January 2023	Y Combinator Finalist.
August 2022	Forbes 30 under 30 Nominee, Healthcare.
August 2022	Selected Poster for Trainee Talk (top 8 abstracts, >100 submissions). Gordon Research Conference: Streptococcal Biology, Newry, ME.
May 2022	Activator Accelerator Program Finalist. Nucleate, Boston, MA.
June 2021	Selected Abstract for Live Talk (top 22 abstracts, >100 submissions). Boston Bacterial Meeting, Virtual.
July 2020	Flash Talk Award (top 4, >150 submissions). Boston Bacterial Meeting, Virtual.
May 2019	Boston College Donald K. White Teaching Excellence Award (top 4 teaching assistants/year). Boston College, Chestnut Hill, MA.
November 2018	1 st Place Pitch, Healthcare Innovation and Commercialization Course. Harvard Medical School, Boston, MA.